

MODELING OF ABSORPTION HEAT PUMPS:  
SOLAR APPLICATIONS EMPLOYING CHEMICAL STORAGE AND  
STEADY-STATE MODELING WITH A COMPARISON TO EXPERIMENTS

by

Mark Owen McLinden

A thesis submitted in partial fulfillment of the  
requirements for the degree of

Doctor of Philosophy  
(Chemical Engineering)

at the  
UNIVERSITY OF WISCONSIN-MADISON

1984

MODELING OF ABSORPTION HEAT PUMPS:  
SOLAR APPLICATIONS EMPLOYING CHEMICAL STORAGE AND  
STEADY-STATE MODELING WITH A COMPARISON TO EXPERIMENTS

Mark Owen McLinden

Under the supervision of Associate Professor Sanford A. Klein  
and Professor John A. Duffie

This work develops simulation models for absorption heat pumps (AHPs) with the goal of enabling a more analytical approach to their study and design. A continuous, liquid absorbent AHP with chemical storage is modeled using mass and energy balances and assuming mass transfer equilibrium. This model is used with the TRNSYS program to simulate the performance of an AHP in a residential solar-driven heating and cooling system. For the three U.S. climates investigated, an AHP using the NaSCN-NH<sub>3</sub> chemical system provides significant non-purchased energy to the load. Compared to a conventional solar system, the heating performance of the AHP system is better at low collector areas but the cooling performance is slightly lower. The performance is generally improved by increasing the storage mass or thermal capacitance of the system. The two alternate control strategies studied were of little advantage.

The steady-state and cyclic testing of a prototype gas-fired ammonia-water AHP in an environmental chamber is described; measurements include temperatures, pressures, absorbent concentrations, flow rates and heat flows. The coefficient of performance and heating

capacity depend most strongly on ambient temperature; varying the load water temperature and flow rate has lesser effects. The performance of the unit is sensitive to refrigerant charge, with the optimum charge varying with ambient temperature. This AHP shows a significant performance degradation in cyclic operation.

A modular, steady-state simulation program for absorption heat pumps is developed and validated with experimental data. The model utilizes an analysis of the refrigerant and absorbent inventory to set the system pressures. Property relations are supplied as separate subroutines. The rectifier, condenser, evaporator, and refrigerant heat exchanger are modeled with a general N-stream heat exchanger component employing a finite difference formulation. The analyzer is treated as a series of equilibrium stages. An analysis of simultaneous heat and mass transfer is applied to each row of the falling-film absorber. The agreement between experiments and simulations is generally good, although several needed refinements to the model are identified. A factorial design is carried out to investigate the performance sensitivity to design parameters.

## ACKNOWLEDGEMENTS

One cannot complete a task such as the one represented by this thesis without the support and assistance of many others. Most of all I would like to thank my advisors in this project, Professors Sanford Klein and John Duffie. Sandy's unfailing enthusiasm for the project and his belief in me made it much easier to keep plugging away at those times when it seemed like the light at the end of the tunnel was actually an oncoming train. Jack's broader perspective was invaluable and his ability to keep things afloat in the always uncertain area of research funding enabled the project (and I) to survive. Together, they gave me the freedom to learn and pursue my own ideas but they always steered me back on course when I started to wander. Professors Duffie and Klein, along with Professors John Mitchell and William Beckman, also deserve credit for the stimulating yet relaxed atmosphere that exists at the UW Solar Energy Laboratory.

I am extremely appreciative of the opportunity to do experimental work at the National Bureau of Standards. Although everyone in the Building Equipment Division was very helpful, I would especially like to thank Reinhard Radermacher for all of his help and my past (and future) group leader David Didion for turning a fledgling experimentalist loose in the absorption lab.

I would like to thank my colleagues in the Solar Lab for their willingness to exchange ideas and help out when the Univac was

yielding only IGDM and DQO errors. But more importantly, thanks for your friendship over the course of the years. One could not hope for a better group of people to work with.

To all of my friends, but especially Bob, Daryl, Kim, Mick, Bob, Bill and Susie, thanks for helping me keep my perspective and giving me a chance to occasionally clear my mind of things associated with research. To my parents, I owe so much to you; thank you for getting me started on the right track.

Finally, I would like to acknowledge the organizations that funded the various phases of this endeavor. Thanks to the Department of Energy's Office of Conservation and Solar Energy, Oak Ridge National Lab (with funds from DOE), and the Graduate School and Chemical Engineering Department of the University of Wisconsin. The fellowship support of the Wisconsin Alumni Research Foundation and the Department of Chemical Engineering's Schulte Fellowship is sincerely appreciated.

## TABLE OF CONTENTS

ABSTRACT . . . . .	ii
ACKNOWLEDGEMENTS . . . . .	iv
LIST OF FIGURES . . . . .	xii
LIST OF TABLES . . . . .	xv
NOMENCLATURE . . . . .	xviii
SUMMARY . . . . .	1
CHAPTER 1 INTRODUCTION . . . . .	8
1.1 Concept of the Absorption Heat Pump . . . . .	8
1.2 Heat-driven Heat Pumps . . . . .	8
1.2.1 Performance of heat-driven heat pumps . . . . .	9
1.2.2 Heat pump driven by a heat engine . . . . .	11
1.3 Thermochemical Devices . . . . .	14
1.4 Absorption Heat Pumps . . . . .	17
1.4.1 Cycle description and variations . . . . .	17
1.4.2 Historical perspective . . . . .	21
1.4.3 Chemical systems for absorption heat pumps . . . . .	23
1.4.4 Applications for absorption heat pumps . . . . .	26
1.5 Objectives . . . . .	27
CHAPTER 2 SIMULATION OF ABSORPTION HEAT PUMPS WITH CHEMICAL STORAGE IN SOLAR ENERGY SYSTEMS . . . . .	29
2.1 Solar Energy Applications of AHPs With Chemical Storage . . . . .	29

2.2	Review of Solar Absorption Heat Pump Work . . . . .	31
2.2.1	AHPs with thermal energy storage . . . . .	31
2.2.2	Solid absorbent AHP systems . . . . .	35
2.2.3	Liquid absorbent systems . . . . .	37
2.2.4	Absorbent suspended in an inert solvent . . . . .	39
2.2.5	Modeling of AHPs with chemical energy storage . . . . .	40
2.2.6	Previous work by author . . . . .	43
2.3	Transient Simulation and the TRNSYS program . . . . .	45
2.4	Description of Simulated System . . . . .	47
2.5	Transient Simulation Model . . . . .	51
2.5.1	Absorption heat pump component . . . . .	51
2.5.2	Heating and cooling load model . . . . .	58
2.5.3	Control strategy . . . . .	58
2.5.4	Conventional solar heating and cooling system . . . . .	61
2.6	System Simulations--Results and Discussion . . . . .	62
2.6.1	Effects of collector area and storage mass . . . . .	62
2.6.2	Effects of climate . . . . .	68
2.6.3	Effects of storage mass and additional thermal capacitance . . . . .	72
2.6.4	Effects of chemical system . . . . .	78
2.6.5	Effects of heat exchanger effectiveness . . . . .	81
2.6.6	Effects of alternate control strategies . . . . .	82
2.7	Summary and Conclusions for Solar AHP Systems . . . . .	86

CHAPTER 3	EXPERIMENTAL INVESTIGATION OF AN ABSORPTION HEAT PUMP . . . . .	88
3.1	Description of the AHP . . . . .	88
3.2	Test Facility . . . . .	94
3.2.1	Environmental chamber . . . . .	94
3.2.2	Load water system . . . . .	96
3.2.3	Instrumentation . . . . .	97
3.3	Test Procedure . . . . .	99
3.3.1	Steady-state tests . . . . .	99
3.3.2	Absorbent solution sampling . . . . .	100
3.3.3	Cyclic tests . . . . .	101
3.4	Steady-State Test Results . . . . .	103
3.4.1	Overall performance tests . . . . .	103
3.4.2	Cycle investigation tests . . . . .	107
3.4.3	Component analysis . . . . .	112
3.5	Cyclic Performance of the Absorption Heat Pump . . .	115
3.5.1	Cyclic test results . . . . .	115
3.5.2	Cyclic performance considering the effects of load . . . . .	121
3.5.3	Frost accumulation test . . . . .	123
3.6	Summary and Conclusions for the Experimental Investigation . . . . .	123

CHAPTER 4	STEADY-STATE MODELING OF ABSORPTION HEAT PUMPS . . .	125
4.1	Review of Existing Absorption heat pump models . . . .	125
4.1.1	Koenig, et al. . . . .	125
4.1.2	A.D. Little Company . . . . .	127
4.1.3	Anand, et al. . . . .	128
4.1.4	Vliet, et al. . . . .	129
4.1.5	Grossman, et al. . . . .	132
4.1.6	Other absorption heat pump models . . . . .	135
4.1.7	Synopsis of existing AHP models . . . . .	137
4.2	Characterization of System . . . . .	137
4.3	Steady-State Modeling Techniques . . . . .	145
4.4	Steady-State Absorption Heat Pump Model . . . . .	147
4.5	Component Descriptions . . . . .	150
4.5.1	Generator . . . . .	150
4.5.2	Analyzer . . . . .	154
4.5.3	General N-stream heat exchanger . . . . .	158
4.5.4	Falling-film absorber . . . . .	168
4.5.5	Throttle valves . . . . .	177
4.5.6	Solution pump . . . . .	179
4.5.7	Stream mixer/vapor-liquid separator . . . . .	181
4.5.8	Convergence component . . . . .	183

4.6	Simulation of the Prototype AHP . . . . .	189
4.6.1	Cycle representation . . . . .	189
4.6.2	Iteration sequence . . . . .	191
4.6.3	Estimation of heat pump parameters . . . . .	193
4.7	Comparison with Steady-State Experimental Data . . .	197
4.8	Sensitivity Study of an Absorption Heat Pump . . . .	206
4.9	Inventory Analysis and Pressure Iteration . . . . .	214
4.10	Summary and Conclusions for the Steady-State Modeling of Absorption Heat Pumps . . . . .	223
CHAPTER 5	CONCLUSIONS AND RECOMMENDATIONS . . . . .	226
APPENDIX A	USER DOCUMENTATION FOR TRNSYS COMPONENTS . . . . .	230
A.1	Absorption Heat Pump Subsystem . . . . .	230
A.2	AHP Controller Component . . . . .	235
A.3	Heat Exchange Switching Component . . . . .	239
APPENDIX B	USER DOCUMENTATION FOR STEADY-STATE AHP SIMULATION PROGRAM . . . . .	242
B.1	Simulation Deck . . . . .	242
B.2	Component Specifications . . . . .	248
B.2.1	Type 1 generator . . . . .	249
B.2.2	Type 2 falling-film absorber . . . . .	250
B.2.3	Type 3 pump . . . . .	252
B.2.4	Type 4 throttle . . . . .	253
B.2.5	Type 5 general N-stream heat exchanger . . . .	254

B.2.6	Type 6 analyzer . . . . .	257
B.2.7	Type 7 flow mixer/stream splitter . . . . .	258
B.2.8	Types 8 and 9 . . . . .	258
B.2.9	Type 10 convergence component . . . . .	259
B.3	Example Simulation Deck and Program Output . . . . .	260
APPENDIX C	PROPERTY RELATIONS . . . . .	264
C.1	Sodium Thiocyanate-Ammonia System . . . . .	264
C.1.1	Empirical property relations . . . . .	264
C.1.2	Subroutine TMIXU . . . . .	267
C.2	Ammonia-Water System . . . . .	268
C.2.1	Pressure-temperature-composition behavior . . . . .	271
C.2.2	Enthalpy . . . . .	274
C.2.3	Specific volume . . . . .	275
C.2.4	Subroutine YT . . . . .	276
C.2.5	Table interpolation for P-T-x behavior . . . . .	278
APPENDIX D	TEST DATA FOR THE PROTOTYPE ABSORPTION HEAT PUMP . . . . .	280
D.1	Overall Performance Steady-State Tests . . . . .	285
D.2	Cyclic Tests . . . . .	296
D.3	Cycle Investigation Tests . . . . .	302
APPENDIX E	COMPUTER PROGRAMS . . . . .	318
REFERENCES	. . . . .	322

LIST OF FIGURES

Figure		Page
1-1	Operation of a heat-driven heat pump to produce high temperature heat . . . . .	10
1-2	Operation of a heat-driven heat pump to upgrade low temperature heat . . . . .	10
1-3	Carnot analysis of a heat-driven heat pump . . . . .	12
1-4	Carnot COPs for a heat-driven heat pump for a load temperature of 20 C . . . . .	13
1-5	The basic absorption heat pump cycle . . . . .	18
1-6	Continuous absorption heat pump cycle incorporating chemical energy storage . . . . .	22
2-1	Solar-powered absorption chiller with hot-side thermal energy storage . . . . .	32
2-2	Absorption heat pump with combined condenser/refrigerant storage tank and absorber/absorbent storage tank . . . . .	48
2-3	Absorption heat pump solar heating and cooling system . . . . .	50
2-4	Relationship between condenser temperature and generator concentration and temperature for the NaSCN-NH <sub>3</sub> chemical system . . . . .	54
2-5	Effect of collector area and storage mass on seasonal F <sub>NP</sub> for AHP system in Columbia . . . . .	65
2-6	Effect of collector area on seasonal F <sub>NP</sub> for conventional solar heating and cooling system in Columbia . . . . .	67
2-7	Effect of collector area on seasonal F <sub>NP</sub> for AHP system in Madison . . . . .	69
2-8	Effect of collector area on seasonal F <sub>NP</sub> for AHP system in Fort Worth . . . . .	70

Figure	Page
2-9 Monthly average diurnal distribution of heat rejected to ambient during August in Columbia for varying thermal capacitance added to storage tanks; chemical mass = 100 kg	75
2-10 Monthly average diurnal distribution of heat rejected to ambient during August in Columbia for varying thermal capacitance added to storage tanks; chemical mass = 500 kg	76
2-11 Monthly average diurnal distribution of heat extracted from ambient during January in Columbia for varying thermal capacitance added to storage tanks; chemical mass = 500 kg . . . . .	79
3-1 Schematic of the Arkla prototype absorption heat pump, including location of instrumentation . . . . .	90
3-2 Heat pump test facility at the National Bureau of Standards . . . . .	95
3-3 Coefficient of performance and heating capacity for the Arkla AHP as a function of ambient temperature . . . . .	104
3-4 Effect on COP of varying inlet load water temperature for three ambient temperatures . . . . .	106
3-5 COP of the Arkla AHP as a function of ambient temperature and relative refrigerant charge . . . . .	113
3-6 Cyclic performance of the Arkla AHP in terms of part load and heating load factors for two cycling rates . . . . .	118
3-7 Heating capacity and evaporator inlet and outlet temperatures as a function of time for a cyclic test with a 50 percent burner on time . . . . .	119
3-8 Assumed heating load and calculated cyclic COP for the Arkla AHP as a function of ambient temperature . . . . .	122
4-1 Schematic for the characterization of the absorption heat pump cycle . . . . .	139
4-2 Overall structure of the steady-state simulation program .	149
4-3 Schematic representation of the generator model . . . . .	153
4-4 Modeling of the analyzer with equilibrium stages . . . . .	155

Figure	Page
4-5	General N-stream heat exchanger component schematic . . . . . 158
4-6	Behavior of the unmodified fourth-order Runge-Kutta integration for the solution of an evaporator node nearing saturation . . . . . 164
4-7	Falling film absorber component schematic . . . . . 169
4-8	Flowrate-pressure drop behavior as a function of outlet quality for the condenser throttle . . . . . 180
4-9	Schematic representation of the stream mixer/vapor-liquid separator model . . . . . 182
4-10	Recyclic information loops and the location of the convergence component in a simulation . . . . . 184
4-11	Geometric interpretation of the Wegstein and successive substitution iteration methods . . . . . 186
4-12	Simulation schematic for the Arkla prototype absorption heat pump . . . . . 190
4-13	Iteration sequence for the simulation of the Arkla AHP . . . . . 192
4-14	Measured and simulated cycle COPs for the Arkla AHP as a function of ambient temperature . . . . . 198
4-15	Contours of constant inventory as functions of low and high side system pressures calculated for the Arkla AHP at an ambient temperature of -9 C . . . . . 222
A-1	Schematic representation of the TRNSYS absorption heat pump subsystem component . . . . . 231

LIST OF TABLES

Table	Page
2-1 Summary of property relations needed for the TRNSYS AHP model . . . . .	52
2-2 Fixed parameters for the solar AHP simulation . . . . .	63
2-3 Average collector and refrigerant tank temperature, absorbent tank concentration, collector efficiency, COP, tank losses and load for the base case simulation (Columbia, 1000 kg chemical storage, 25 m <sup>2</sup> collector) . . .	66
2-4 Effect of location and collector area on fraction non-purchased energy, load, and non-purchased energy delivered to the load for systems with 1000 kg chemical storage . . .	71
2-5 Effect of chemical storage mass and additional thermal capacitance on $F_{NP}$ for AHP system in Columbia (August results) <sup>NP</sup> . . . . .	74
2-6 Effect of additional thermal capacitance on $F_{NP}$ , absorbent tank concentration and collected energy for AHP system in Columbia (January results; chemical storage mass = 500 kg) . . . . .	78
2-7 Average collector temperature and efficiency, COP and fraction non-purchased energy for sulfuric acid-water AHP with 25 m <sup>2</sup> collector and 1000 kg chemical storage . . .	80
2-8 Effect of heat exchanger effectiveness on $F_{NP}$ and the ratio of the heats of condensation and absorption for AHP system in Columbia (seasonal results) . . . . .	81
2-9 Effect of not supplying auxiliary energy through the heat pump on absorbent tank concentration, collector temperature, collected and auxiliary energy and $F_{NP}$ for system in Columbia . . . . .	83
2-10 Effect of generator bypass control option and collector type on $F_{NP}$ , collected energy, and collector operating time for system in Columbia . . . . .	85

Table	Page
3-1 Effect of varying load water flow on the COP and heating capacity of the Arkla AHP for two ambient temperatures . . .	107
3-2 Effects of varying condenser and absorber flows on system pressures, concentrations, and COP . . . . .	108
3-3 System pressures and concentrations, and evaporator conditions for varying refrigerant charges and ambient temperatures . . . . .	111
3-4 Conditions of streams in the absorption cycle for an ambient temperature of 8.6 C, standard load water conditions, and original refrigerant charge . . . . .	116
3-5 Measured and calculated heat flows for the components of the Arkla AHP . . . . .	116
4-1 Summary of property relations referenced by the steady-state simulation model . . . . .	151
4-2 Comparison of heat flows for a condenser simulated with Euler and second and fourth order Runge-Kutta integrations for varying numbers of nodes . . . . .	167
4-3 Primary component parameters for the simulation of the Arkla absorption heat pump . . . . .	194
4-4 System pressures and measured and simulated COPs and stream temperatures for varying ambient temperatures . . .	200
4-5 Simulated stream qualities and concentrations, refrigerant mass flow rate, and heat flows for varying ambient temperatures . . . . .	203
4-6 Comparison of measured and simulated compositions, heat flows, and refrigerant mass flow rate for tests at two ambient temperatures . . . . .	205
4-7 System pressures, COP, change in COP from standard load water conditions, and simulated solution compositions and heat of evaporation for varying inlet load water temperature at three ambient temperatures . . . . .	207
4-8 Main effects for factorial analysis of the Arkla AHP . . .	211

Table	Page
4-9 Main effects and interactions for second factorial analysis of the Arkla AHP . . . . .	215
4-10 Refrigerant and absorbent inventories for varying ambient temperatures calculated using measured system pressures in the simulation . . . . .	217
4-11 Distribution of refrigerant and absorbent inventory within the absorption cycle calculated for an ambient temperature of -8 C . . . . .	218
4-12 Iterations in pressure and resulting refrigerant and absorbent inventories for an ambient temperature of -9 C; input inventories calculated for system pressures of 0.246 and 2.101 MPa . . . . .	220
C-1 Correlation coefficients for the polynomial fits of liquid and vapor enthalpy for the NaSCN-NH <sub>3</sub> chemical system . . .	265
C-2 Dimensionless coefficients for the Schultz equation of state for ammonia-water mixtures . . . . .	270
D-1 Summary of ambient and load water conditions for the overall performance steady-state tests of the Arkla AHP . .	282
D-2 Summary of cycle times and load water conditions for the cyclic testing of the Arkla AHP . . . . .	283
D-3 Summary of ambient and load water conditions and relative refrigerant charge for the steady-state cycle investigation tests of the Arkla AHP . . . . .	284
E-1 TRNSYS components and related computer programs for the modeling of an absorption heat pump with chemical storage .	319
E-2 Computer programs comprising the steady-state absorption heat pump simulation program . . . . .	320

## NOMENCLATURE

This list contains the symbols used in the main body of this thesis. Symbols appearing in the Appendices are defined as they first appear.

A	area
A, B	general chemical species
AHP	absorption heat pump
b, d	constants for linearization of vapor-liquid equilibrium data
$C_d$	orifice discharge coefficient
COP	coefficient of performance
$C_p$	heat capacity
CPU	central processing unit of computer
$C_1, C_2$	constants for the empirical throttle relationship, Equation [4-89]
det	determinate defined by [4-104]
$\dot{E}_{elec}$	electric energy input
f, g	general (unspecified) functions
$F_{NP}$	fraction of load met by non-purchased energy
$F_R$	collector heat removal factor
g	acceleration of gravity
$G_T$	solar irradiance on collector plane
h	specific enthalpy
hc	heat transfer coefficient

k	thermal conductivity
Ka	phase transition criteria defined by [4-52]
$L_{Ap}$	percent absorption length defined by Reference (91)
Le	Lewis number
m	mass in component or system
$\dot{m}$	mass flow rate
MAX	maximum function
( $\dot{m}C$ )	capacitance rate through a heat exchanger
N	total number of streams, nodes or stages
P	pressure
PLF	part load factor
Q	integrated heat flow
$\dot{Q}$	heat transfer rate
$\dot{q}_m$	vapor absorption flux in absorber
$q_n$	acceleration parameter for Wegstein iteration
$\dot{q}_{wall}$	heat flux at tube wall in absorber
$R_f$	heat transfer resistance due to fouling
R-K	Runge-Kutta integration
RMS	root mean square
$r_\alpha$	heat of absorption
s	slope for Wegstein iteration defined by [4-99]
s.a.	strong absorbent
sim	simulation results
t	time

T	temperature
test	experimental results
$T_s$	surface (interfacial) temperature in absorber
$t_0$	start of cycle
$t_1$	cycle time at which burner shuts off
$t_2$	cycle time at which heat pump shuts off
u	velocity
U	overall heat transfer coefficient
UA	overall heat transfer coefficient-area product
$U_L$	collector loss coefficient
v	specific volume
V	volume of component
$\dot{v}$	volumetric flow rate
vap	(refrigerant) vapor
w.a.	weak absorbent
x	mass concentration
$x_0$	inlet refrigerant concentration to absorber tube
x, y	general variables for discussion of iteration
y	equilibrium vapor quality
z	position variable
$z_s$	position of phase transformation
$\alpha$	thermal diffusivity
$\beta$	slope (from horizontal)
$\gamma$	dimensionless parameter defined by [4-52]

$\Gamma$	flow rate per unit plate width
$\Gamma_h$	heating load factor
$\delta$	film thickness
$\Delta\text{COP}$	change in COP relative to standard conditions
$\Delta P$	pressure drop
$\Delta t$	time step
$\Delta T$	temperature difference or change
$\epsilon$	heat exchanger effectiveness
$\eta$	efficiency
$\eta_{\text{bypass}}$	collector efficiency for heat "bypassing" generator
$\eta_{\text{gen}}$	collector efficiency for heat supplied to generator
$\theta$	parameter defined by [4-71]
$\mu$	viscosity
$\rho$	density
$\tau$	time, length of cycle
$(\tau\alpha)$	collector transmittance-absorptance product
$\omega$	uncertainty in a quantity

#### Subscripts

a, abs	absorber or absorbent
A/C	air conditioning
amb	ambient
anal	analyzer
aux	auxiliary heat source

avg	average
col	collector
c, cond	condenser
cross	cross flow stream in heat exchanger
cyc	cyclic operation
cycle	considering absorption cycle only
eq	equilibrium composition
e, evap	evaporator
fin	extended surface in heat exchanger
flue hx	flue gas heat exchanger
g, gen	generator
g-a	heat exchanger between generator and absorber
gas	natural gas input
heating	heating operation
high	high temperature heat
hx	heat exchange stream
i, j	current iteration, row, stage, or node
ij	quantity from stream i to stream j
in	inlet to node or component
ins	inside of heat exchange tube
liq	liquid solution or liquid portion
lm	log mean average
load	load heat exchanger or heat exchange stream
loss	heat loss to surroundings

low	low temperature heat
med	medium temperature heat
min	minimum capacitance rate in heat exchanger
N	last stage or node
NP	non-purchased energy
o	outside area, orifice
out	outlet of node or component
pump	solution pump
r, ref	refrigerant
sat	saturated liquid or vapor
set	set point
ss	steady-state operation
t	heat exchange tube in absorber
tot	total in tank or system
vap	refrigerant vapor
w	wall of heat exchange tube
1-28	state points defined by system diagram



## SUMMARY

This thesis is concerned with the modeling of absorption heat pumps (AHPs). Currently, absorption machines are designed more by a combination of art and cut-and-try methods than by scientific analysis. This work develops the capability to model AHPs, enabling a more analytical approach to their study and design. This research consisted of three major parts: the modeling of absorption heat pumps with chemical energy storage in a solar space heating and cooling application; the testing of a prototype, fuel-fired AHP designed for a residential heating application; and the development of a modular, steady-state absorption heat pump simulation program and its application to the prototype AHP.

The absorption heat pump cycle, through reversible absorption processes, uses the thermodynamic availability of a high temperature heat input to upgrade the temperature of a lower quality heat input. In Chapter 1, the theoretical limits to the performance of an absorption heat pump are presented and the AHP is discussed in the context of a larger group of related thermochemical and heat pumping devices. The operation of the basic AHP cycle is presented, along with variations on the basic cycle. Chemical energy storage within the absorption cycle can be obtained by separately storing the refrigerant and absorbent. Storage would be useful in an application with an intermittent heat source. The properties required of an

absorbent-refrigerant pair are considered. Finally in Chapter 1, the present and potential applications of absorption heat pumps are discussed.

Because of its ability to combine energy storage and heat-driven heat pumping and air conditioning in a single device, the AHP has potential applications in solar energy systems. Chapter 2 begins with a discussion of the characteristics of AHPs in this application and a review of solar AHP work.

The nature of a solar-driven AHP with chemical storage necessitates a transient simulation over a heating or cooling season. These simulations were carried out using the modular simulation program TRNSYS. The absorption heat pump modeled is a continuous, liquid absorbent system with a combined condenser/refrigerant storage tank and an absorber/absorbent storage tank. This configuration has the ability to store thermal energy by raising the temperature of the tank contents.

The absorption heat pump model developed for use with TRNSYS is based on mass and energy balances written around various parts of the cycle. Property relationships are supplied as separate subroutines, making the model independent of chemical system. The major assumptions employed in the model are: the reaction rates are controlled by heat transfer resistances; the capacitance of the generator and evaporator are negligible compared to those of the storage tanks; all vessels are fully mixed; and the absorbent is nonvolatile. Thus, this model represents a best-case approach in

several respects. Chapter 2 continues with a detailed presentation of the AHP model and a description of the control strategies and load model.

Simulations using this model have shown that a solar-driven AHP system can supply a significant fraction of a residential space heating and cooling load with non-purchased energy in the three U.S. climates studied. The AHP system delivered a significant amount of non-purchased energy at zero collector area (because of auxiliary energy supplied through the heat pump) but at higher collector areas, the performance of the AHP and conventional solar heating systems approached each other. In the cooling season, the AHP system produced a lower solar fraction than a solar-fired lithium bromide-water absorption chiller with hot water storage.

The collector temperatures necessary to operate the AHP were high and thus high-performance collectors (such as evacuated tubes) were required for effective solar operation. Adding thermal capacitance and additional chemical storage mass to the cycle had the effect of leveling out the diurnal distribution of the heat exchange with ambient and in most cases increased the fraction of non-purchased energy supplied to the load. Two alternative heating season control strategies (in addition to the baseline strategy) were investigated in the Columbia, Missouri, climate and found to be of little advantage.

In the second phase of research, a prototype gas-fired, ammonia-water absorption heat pump developed by Arkla Industries was tested at the National Bureau of Standards in order to obtain data for

comparison to the simulation model. Chapter 3 describes the operation of the heat pump, the instrumentation installed, and the procedures for the steady-state and cyclic tests which were carried out in an environmental chamber.

The coefficient of performance (COP) and heating capacity depended most strongly on ambient temperature and ranged from 0.81 (including burner losses and electric input) and 12.0 kW at -21 C to 1.14 and 15.9 kW at 16 C; the COP and capacity tended towards constant values at the extremes of ambient temperature. Lower inlet load water temperatures resulted in slightly higher COPs, especially at lower ambient temperatures. The performance of the heat pump was sensitive to refrigerant charge. A higher charge resulted in higher COPs at high ambient temperatures but lower COPs at low temperatures; a lower charge resulted in a more nearly constant COP. The measured heat flows agreed well with those calculated using measured absorbent concentrations, strong absorbent flow rate, and system temperatures. The prototype AHP showed a significant performance degradation in cyclic operation. Although the steady-state COP was greater than unity for ambient temperatures above -5 C, the cyclic COP calculated for a representative application had a maximum of 0.94 at -3 C.

The final phase of the research was the development of a steady-state absorption heat pump model. Chapter 4 begins with a review of the AHP models in the literature. A shortcoming of the existing AHP models is the need to input or make assumptions about a number of system states (e.g., pressures or compositions). A number

of these models are also quite specific to a given machine. The goals of the model developed here were to be as general and flexible as possible and to not require assumptions about system states.

An exercise identifying the total number of unknowns in an absorption cycle and the relationships available to solve for them showed that an analysis of the absorbent and refrigerant inventory is necessary to fully specify the system. A modular, steady-state simulation program for AHPs was developed incorporating an inventory analysis in an outermost iteration loop to set the low and high side pressures. A modular simulation approach was felt to be more consistent with the goal of a general model than a simultaneous (equation-based) approach. Property relationships were supplied as separate subroutines.

The models formulated for the various components in the cycle neglected pressure drops and heat losses to the surroundings. The generator was treated as a fully-mixed tank with known heat input. The analyzer was modeled as a series of equilibrium stages, with the heat transfer in each stage treated with a constant heat transfer coefficient. A general N-stream heat exchanger component was developed and used for the rectifier, condenser, evaporator and refrigerant and flue gas heat exchangers. This model divided the heat exchanger into nodes and employed a fourth order Runge-Kutta solution of the differential equation describing the heat flow between streams. Local heat transfer coefficients were supplied by a separate subroutine. The falling-film absorber model applied an analysis of

combined heat and mass transfer for vapor absorption into a laminar film to each row of heat exchange tubes. The throttle valve model used an empirical fit of experimental flow rate and pressure drop data to a functional form applicable to homogeneous flow through a sharp-edged orifice. The option of specifying both pressure drop and flow rate was also implemented. The solution pump component modeled both constant volumetric and mass flow rate devices. Finally, a separate component for the convergence of tear streams was developed.

Chapter 4 continues with a comparison of experimental and simulation results. The qualitative behavior of the simulated COPs as a function of ambient temperature agrees well with experimental values. The simulated values of COP were consistently high (by 0.10 to 0.18 for varying ambient temperatures); this difference is at least partially due to not considering heat losses to the surroundings or pressure drops through components in the model. Simulated system temperatures, compositions, and heat flows were also in generally good agreement with experimental values. The model correctly predicted the trends resulting from changing load water temperature.

A factorial design investigating the effects of 15 operating and design variables on the heating COP was carried out. The factors of ambient temperature, low and high side pressure, generator heat input and condenser and evaporator areas had effects on COP of 0.071, -0.072, 0.063, -0.035, 0.056 and 0.055, respectively (for a change of 7 C in temperature, and changes of  $\pm$  5 percent in pressures and heat input, and  $\pm$  20 percent in heat exchanger areas relative to the base

values). Similar changes in the other heat exchanger areas and the solution pump, and throttle valve parameters had effects on COP of less than 0.01.

The use of the inventory relationships to iterate for the low and high side system pressures was not successful and thus experimentally measured pressures were used in the simulations of the Arkla AHP. The iteration for pressures did not reliably converge because of oversimplifications in the modeling of the inventory of components with changing liquid and vapor volumes and the inability of the two-variable secant method to converge for the non-linear inventory functions. However, the usefulness of the inventory analysis was demonstrated and the general trends between system pressures and the calculated ammonia inventory corresponded with the experimentally observed behavior.

In Chapter 5, general conclusions pertaining to absorption heat pumps are presented and recommendations for further study are made. Because of equipment and safety considerations, it is felt that solar-driven AHPs with chemical storage will not be practical in residential or commercial applications. Thus it is recommended that further modeling efforts be directed at more promising applications for AHPs. The performance of the prototype AHP tested was disappointing, but fuel-fired AHPs in general show promise. The steady-state simulation model would be suitable for a detailed investigation of the absorption cycle or the design of AHPs. The further development of this model is recommended.

## CHAPTER 1

### INTRODUCTION

This thesis is concerned with the modeling of absorption heat pumps (AHPs). This chapter places AHPs in the context of a larger group of thermochemical and heat pumping devices. The basic absorption cycle is described along with possible variations. Finally, an overview of the objectives of this thesis and the organization of the subsequent chapters are presented.

#### 1.1 Concept of the Absorption Heat Pump

An absorption heat pump is a device which, through reversible absorption processes, uses the thermodynamic availability of a high temperature heat input to extract heat from a low temperature heat source and upgrade its temperature. Absorption heat pumps can be considered as a member of a larger group of thermochemical devices. These devices utilize reversible chemical reactions and their accompanying heat effects to store, transport or pump energy (1,2). An absorption heat pump is also one type of heat-driven heat pump.

#### 1.2 Heat-driven Heat Pumps

Heat-driven heat pumps are devices which upgrade the temperature of some low to moderate temperature heat input. In contrast to a vapor compression heat pump, however, they are powered by a heat input and not by the input of mechanical work.

There are two fundamental ways of operating a heat-driven heat pump. One method (shown in Figure 1-1) is to produce a quantity of high temperature heat from a larger input of moderate temperature heat. A heat pump operating in this manner might be used in an industrial process to recover part of the energy presently wasted in some process stream.

The other method of operation (shown in Figure 1-2), and the one that this work will focus on, is to use the thermodynamic availability of a high temperature heat input to extract heat from a low temperature heat source. This type of device could be used as a heat-operated refrigerator or air conditioner or as a heat pump in an application where a moderate temperature heating load is met by a high temperature heat source.

### 1.2.1 Performance of heat-driven heat pumps

The performance of a heat pump extracting heat from a low temperature heat source is measured in terms of its coefficient of performance (COP). The COP is defined as the ratio of the desired energy flow to the "high quality" energy (as opposed to "low quality" or low temperature heat from an ambient source) that is input to the device. In a heating application:

$$\text{COP}_{\text{heating}} = \dot{Q}_{\text{med}} / \dot{Q}_{\text{high}} \quad [1-1]$$

and in an air conditioning or refrigeration application:

$$\text{COP}_{\text{A/C}} = \dot{Q}_{\text{low}} / \dot{Q}_{\text{high}} \quad [1-2]$$

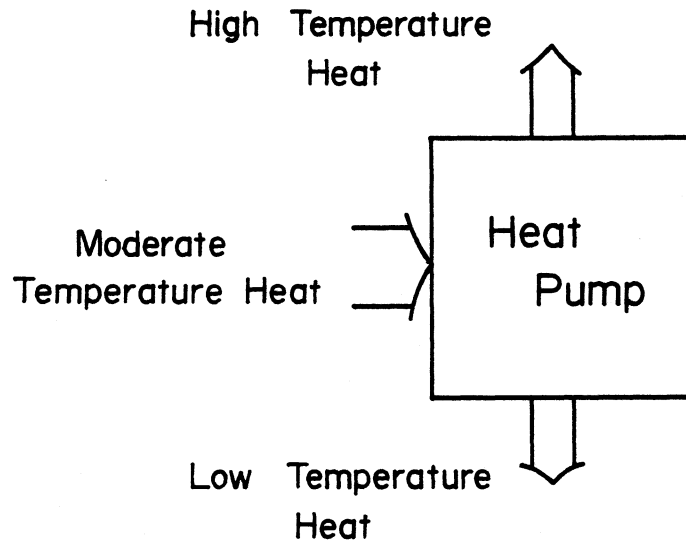


Figure 1-1 Operation of a heat-driven heat pump to produce high temperature heat

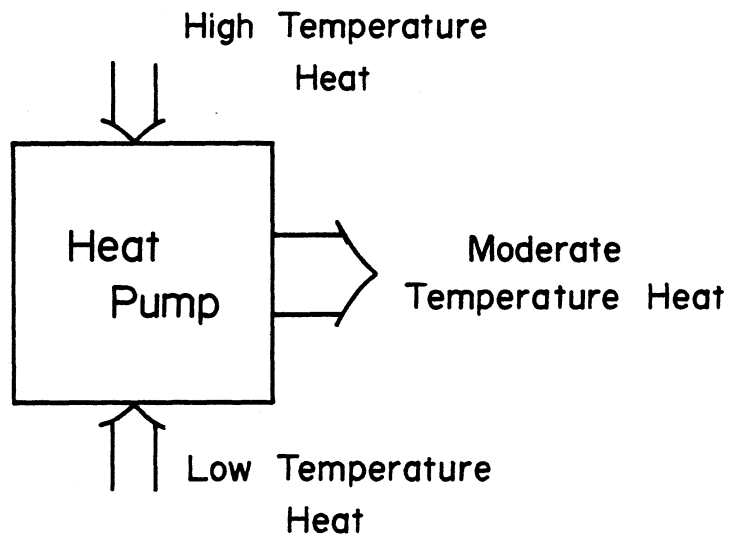


Figure 1-2 Operation of a heat-driven heat pump to upgrade low temperature heat

where  $\dot{Q}_{low}$ ,  $\dot{Q}_{med}$  and  $\dot{Q}_{high}$  are the low, medium and high temperature heat flows shown in Figure 1-2.

The maximum COP of a heat-driven heat pump is limited by the second law of thermodynamics and can be computed by conceptually connecting a Carnot heat engine with a Carnot heat pump as shown in Figure 1-3. This analysis yields the following expressions for heating and air conditioning COPs:

$$COP_{heating} = \frac{T_{med} (T_{high} - T_{low})}{T_{high} (T_{med} - T_{low})} \quad [1-3]$$

$$COP_{A/C} = \frac{T_{med} (T_{high} - T_{low})}{T_{high} (T_{med} - T_{low})} - 1 \quad [1-4]$$

Equation [1-3] is plotted in Figure 1-4 for a value of  $T_{med}$  of 20 C (i.e., the temperature of a space heating load). Even though it represents an upper limit, this figure indicated the tremendous improvement in overall energy efficiency that is possible by using a heat-driven heat pump in a heating application presently met by a high temperature heat source. An example would be space heating where a need for heat at 20 C is met by burning oil or natural gas with a flame temperature of well over 1000 C. (Here the low temperature heat source might be ambient air.)

### 1.2.2 Heat pump driven by a heat engine

One way to achieve the overall effect of a heat-driven heat pump is to drive a vapor compression heat pump with a heat engine. This

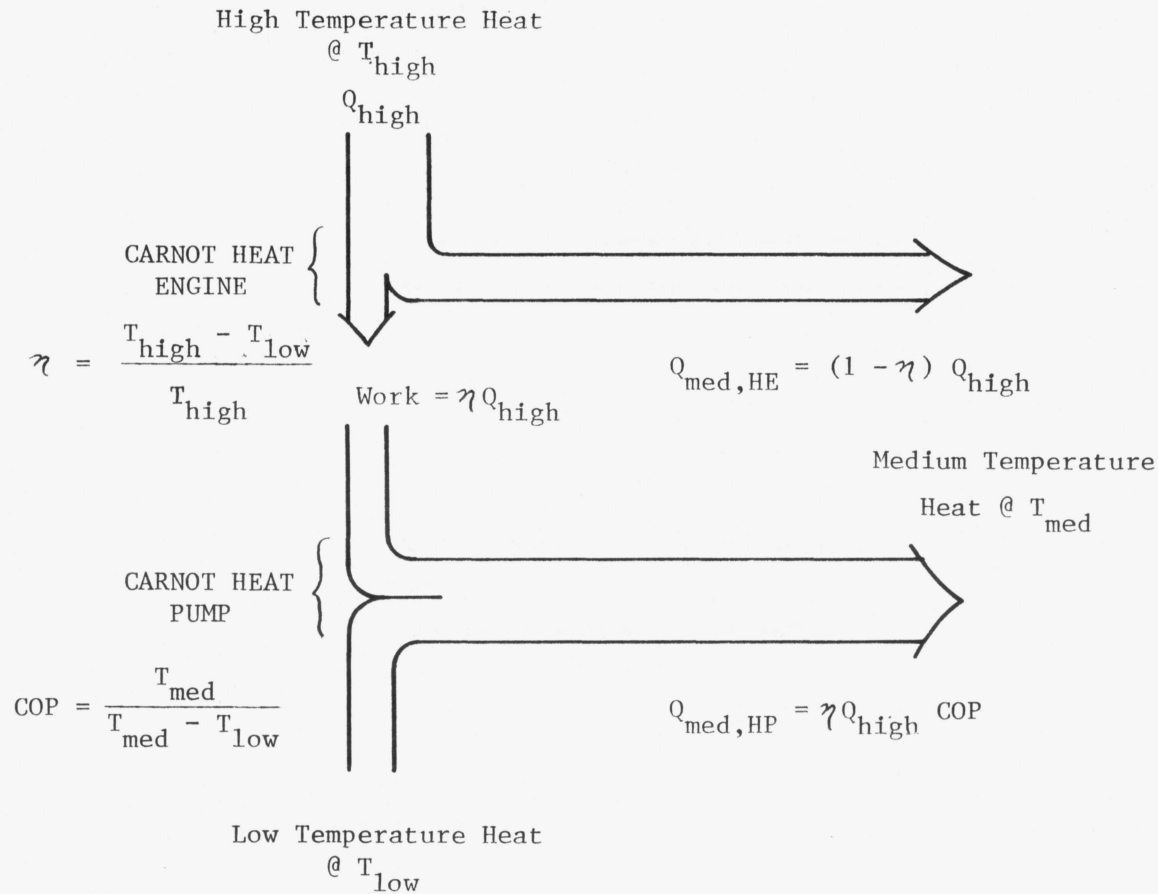


Figure 1-3 Carnot analysis of a heat-driven heat pump

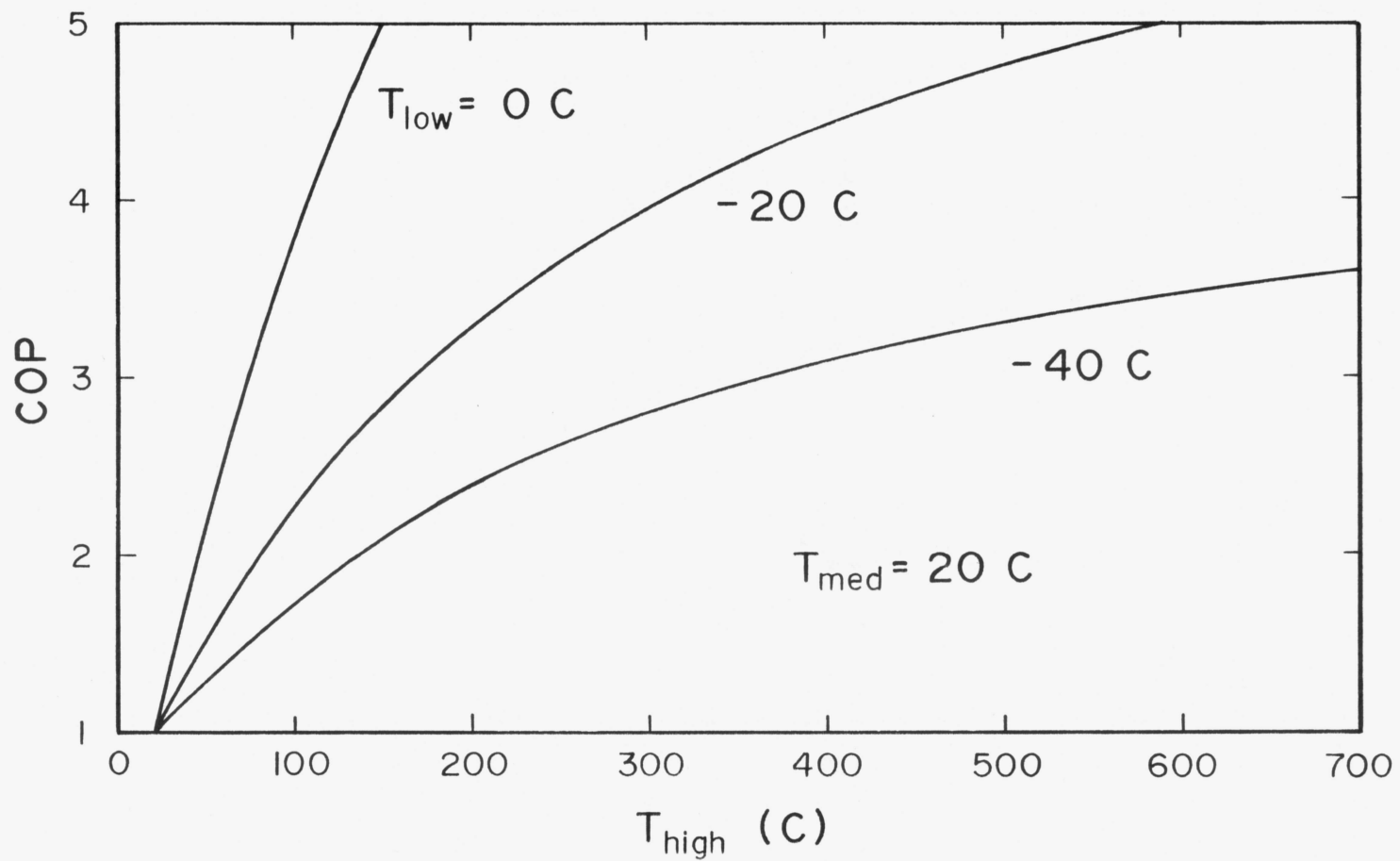


Figure 1-4 Carnot COPs for a heat-driven heat pump for a load temperature of 20 C

type of device was conceptually used in finding the maximum COP of heat-driven heat pumps. Although it qualifies as a heat-driven heat pump if considered as a single unit, it is actually composed of two distinct subunits (the heat engine and heat pump) with an exchange of mechanical work between them.

Such devices have been proposed. In one system, a linear free-piston Stirling engine fired by natural gas directly drives a reciprocating heat pump compressor (3). Both components are contained in a hermetically sealed unit with only refrigerant passing in and out. Although an elegantly simple concept, the first prototypes of this design have not been successful. Another design employs a Brayton cycle gas turbine magnetically coupled to a heat pump compressor (4).

This work, however, will deal with devices that do not involve mechanical work in their operation (except for possibly pumping liquids, etc.)--namely devices utilizing thermochemical processes.

### 1.3 Thermochemical Devices

A thermochemical process makes use of reversible chemical reactions and their accompanying heat effects. The general chemical reaction to be considered is:



where A and B are general chemical species. In the energy field, thermochemical processes can be used for energy transport and storage and heat pumping.

Energy storage or transport is achieved by inputting heat to the forward endothermic reaction (the charging process) while preventing the reverse reaction from occurring; the product is then stored until energy is needed (or transported to where energy is needed) at which time (or place) the reverse exothermic reaction (or discharging process) is allowed to occur. Since energy is stored in this scheme in the form of chemical reaction potential, the reaction products can be stored at ambient temperatures with no loss in energy storage capacity (except for the heat involved in cooling the products from the reaction temperature to ambient). This is in contrast to thermal energy storage devices (e.g., a hot water tank) which must be maintained at a high temperature.

One way to control when (or where) the reaction (Equation [1-5]) takes place is to choose substances which react only in the presence of a catalyst. This is done in the ADAM-EVA chemical heat pipe system (2). In this system, methane and water are reacted in the presence of a nickel catalyst to produce carbon monoxide and hydrogen; these gases are transported to the load where they are reacted (again in the presence of a nickel catalyst) to reform methane and water which are returned to the heat source to be recharged. A similar system using the reaction of  $\text{CO}_2$  and  $\text{CH}_4$  to form  $\text{CO}$  and  $\text{H}_2$  is used in the Solchem process (5,6).

A second method of controlling the reaction in a thermochemical process is possible if the product of the charging reaction is composed of two or more chemical species which can be separated until

heat from the discharging reaction is required. Separation is most easily accomplished if one species either precipitates or is evolved as a gas in the reaction. Most of the systems under current consideration use the latter method of separation (2).

When a gas is evolved in the charging reaction, it can either be stored, thus resulting in a closed system, or rejected to the atmosphere, yielding an open system. Because of cost and environmental considerations, any gas evolved in an open system would have to be a component of the atmosphere. Water vapor is usually used in open cycle devices. An example is a desiccant air conditioner (7,8) which utilizes the adsorption of water vapor onto a desiccant to dry out a process air stream; this stream is then sensibly and evaporatively cooled to meet a cooling load. The desiccant is recharged by heating.

In a closed cycle device, the gaseous species is condensed to avoid the need for large gas storage containers. The heat of condensation is released in this process and it can be utilized to meet part of the heating load. The condensate can be directly reacted in the discharging step, resulting in chemical energy storage system such as the sulfuric acid-water system proposed by Huxtable and Poole (9). The condensate can also be revaporized with heat from a low temperature (e.g., ambient) heat source before reaction in the discharging step to yield a heat pump.

## 1.4 Absorption Heat Pumps

Heat-driven heat pumps are most commonly based on reversible absorption processes. The absorption process involves an affinity between the absorbent and absorbate accompanied by a heat effect. Absorption takes place through the bulk of the absorbent, as contrasted with adsorption which is a surface process. The absorbent can be either a liquid solution or a solid. (A solid adsorbent could be employed in the same manner as a solid absorbent. For brevity, the term absorbent will be used.) An AHP can also be classified according to its mode of operation--either batch or continuous.

### 1.4.1 Cycle description and variations

The basic absorption heat pump cycle, shown in Figure 1-5, consists of four major components and operates in a continuous fashion. In the generator, high temperature heat (typically at 80 to 150 C) is applied to a mixture of refrigerant and absorbent to boil off refrigerant vapor, producing strong absorbent. (The term "strong absorbent" refers to a high affinity for absorbing refrigerant; the "weak absorbent" entering the generator has a low affinity for refrigerant.) The refrigerant vapor travels to the condenser where it releases the heat of condensation at an intermediate temperature (30 to 50 C).

The liquid refrigerant passes through a throttling device to the low pressure side of the system where it is vaporized by the addition of low temperature heat (at -20 to 10 C) in the evaporator. The refrigerant vapor is reabsorbed into the strong absorbent solution in

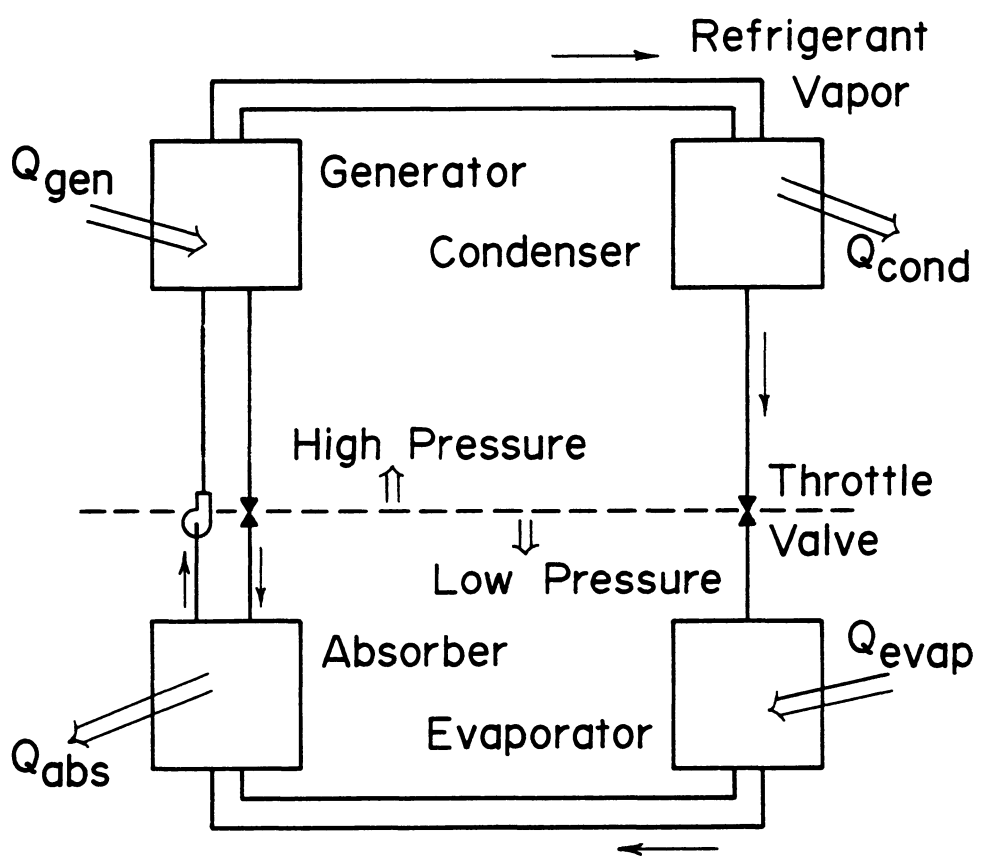


Figure 1-5 The basic absorption heat pump cycle

the absorber, releasing the heat of absorption at an intermediate temperature. The resulting weak absorbent is pumped to the high side pressure and returned to the generator, completing the cycle.

The actual heat pumping occurs between the evaporator and absorber. The process is driven by the reduction in the partial pressure of refrigerant which occurs over a mixture of refrigerant and absorbent. Thus, a given low side pressure will result in different temperatures in the evaporator and absorber.

Many variations on the basic cycle have been put forth (10). The cycle COP can be improved by adding a heat exchanger between the streams entering and leaving the evaporator and especially between the absorbent circulating between the generator and absorber. If the absorbent is volatile, the vapor produced in the generator will contain absorbent as well as refrigerant and must be purified; this is done in an analyzer and/or rectifier, which are basically a distillation column and partial condenser, respectively. A double-effect cycle is obtained by condensing the vapor from the first generator to supply heat to a second, lower pressure generator; the vapor produced in this generator is condensed in a condenser and combined with the condensate from the first effect before passing through the throttle valve. Johnston (11,12) has proposed and constructed modified absorption cycles involving complex heat exchanger geometries in an effort to reduce cycle irreversibilities. Streams of similar temperature are thermally contacted in heat exchangers formed of plates with milled fluid passages.

A simpler configuration for an absorption heat pump, operating in an intermittent or batch cycle, is also possible. The batch cycle consists of absorbent and refrigerant tanks connected by a vapor duct. These two tanks alternately serve as generator and condenser (in the charging mode) and then as absorber and evaporator (in the discharging mode). A disadvantage of the batch system is that in switching from charging to discharging and vice versa, the contents of the tanks must be brought to different temperatures; these sensible heat effects can result in a significant performance penalty (1). Batch systems are the most common way of employing solid absorbents, although it is possible to use a suspension of a solid absorbent and inert solvent in a continuous cycle (13,14).

It is possible to incorporate chemical energy storage into the absorption cycle; such systems have been termed chemical heat pumps. The nature of the batch cycle inherently includes storage. In a continuous system, storage is provided by inserting separate storage tanks (one each for the absorbent and refrigerant) into the cycle or by enlarging one or two of the components to serve a dual purpose (e.g., a combined condenser and refrigerant storage tank). Storage would be useful if the heat source were intermittent (such as solar energy or off-peak electricity) or to reduce the penalties of transient operation associated with an on-off control strategy. The addition of storage allows the charging and discharging portions of the cycle to operate independently; for example, to provide cooling, only the evaporator and absorber need operate. One example of a

continuous absorption heat pump with storage is shown in Figure 1-6. This configuration is the conventional absorption cycle with absorbent and refrigerant storage tanks added.

#### 1.4.2 Historical perspective

The use of the absorption process for heat pumping is not new. Bjurstrom and Raldow (15) have provided an historical survey of the absorption process, concentrating on the types of equipment developed to utilize this phenomena. They report that Sir John Leslie used a batch AHP (with sulfuric acid as the absorbent) to freeze water in 1810. The continuous absorption cycle was presented in a series of patents by Ferdinand Carré between 1859 and 1862. The first practical use of the absorption process was for refrigeration and in the early 1920's a number of periodic (batch) household units were developed by manufacturers in the United States and Germany. These met with limited success and were supplanted by the highly successful continuous units (notably the Servel refrigerator) in the 1930's. Bjurstrom and Raldow present a number of other applications and conclude their survey with a discussion of recent developments in chemical energy storage and chemical and absorption heat pumps.

The use of chemical reactions for energy storage was discussed by Goldstein at the 1961 UN conference (16). He discussed energy storage using aqueous solutions (e.g.,  $H_2SO_4$  and  $H_2O$ ) and solid absorbents (particularly solid hydrates) and computed energy storage densities for a number of chemical systems. While Goldstein points out many of the thermodynamic considerations applying to absorption heat pumps, he

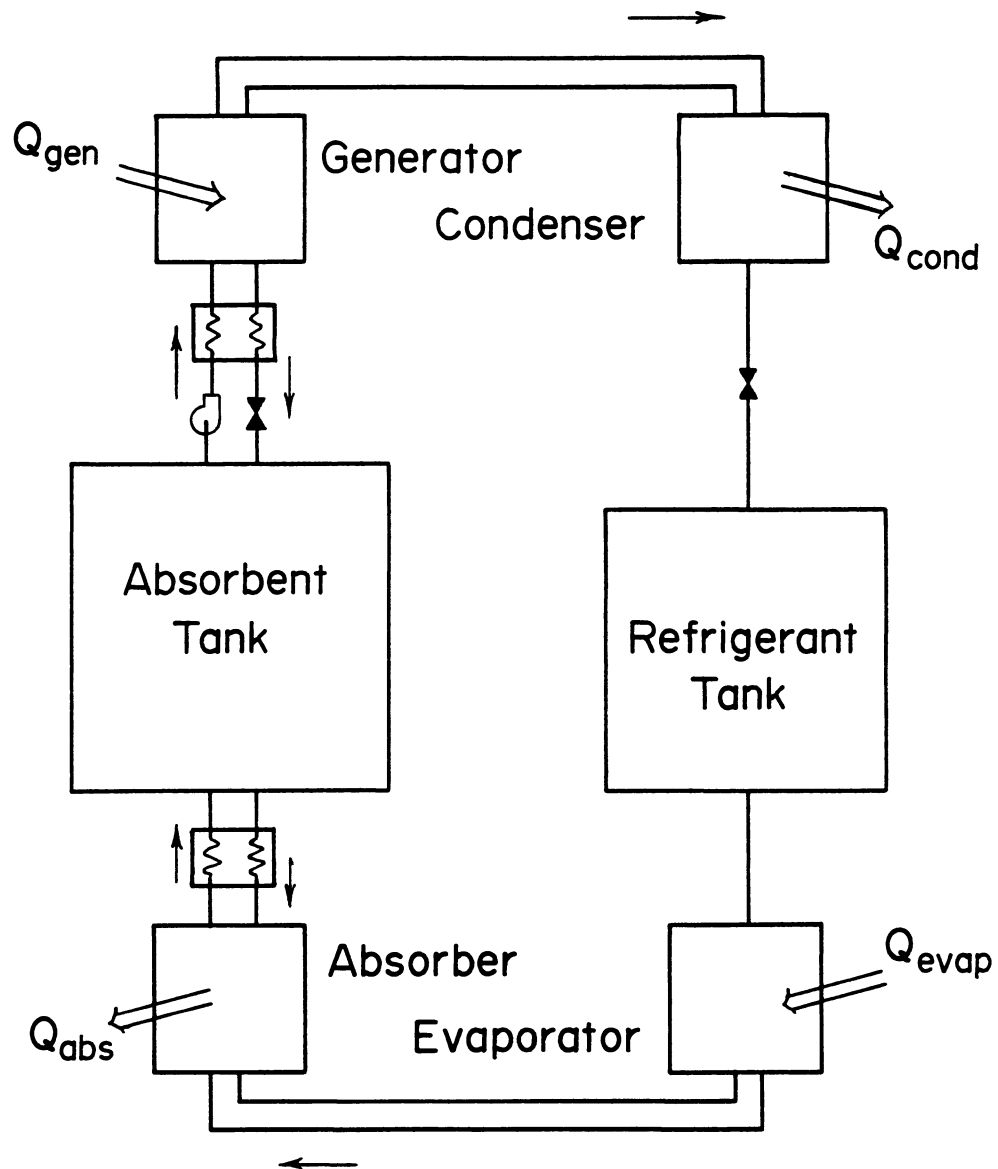


Figure 1-6 Continuous absorption heat pump cycle incorporating chemical energy storage

stops short of proposing these reactions as a means of heat pumping.

#### 1.4.3 Chemical systems for absorption heat pumps

The absorbent-refrigerant pair in an absorption heat pump must satisfy a number of requirements. Most importantly it must possess favorable thermodynamic characteristics, i.e., the ability to pump heat across a useful temperature difference with reasonable charging temperatures. The requirements for liquid absorbent systems have been discussed by Buffington (17). He sets out a number of criteria that should be met, including high solubility of refrigerant in the absorbent, rapid absorption kinetics and a nonvolatile absorbent. Solutions with a large negative deviation from Raoult's Law are required and Buffington reasons that small, polar molecules are the best choices for both absorbent and refrigerant. Gomez and Mansoori (18) have presented a technique for evaluating a given refrigerant-absorbent pair with limited thermodynamic data; the cycle COP is computed by fitting the chemical system to the Redlich-Kwong equation of state. Raldow and Wentworth (19) have investigated the thermodynamic requirements for an optimum solid absorbent chemical system for a given set of heat input and output temperatures.

Aside from purely thermodynamic requirements, a suitable chemical system must satisfy other, more practical considerations, as a number of authors have pointed out (17,20-22). The two most important features are suitable cost and safety factors; an otherwise suitable chemical would be unfeasible if it were too hazardous or costly.

Several authors, including Macriss (21) and Stephan and Scher (23), have surveyed a large number of chemical systems for use in absorption systems. The refrigerants considered include water, alcohols, ammonia, amines, halogenated hydrocarbons, and silanes; a wide variety of inorganic salts and organic compounds are candidates for the absorbent. Several systems which have received attention are sodium thiocyanate-ammonia (24,25); ethyltetrahydrofurfuraether (ETFE) and R123a (26); and tetraethyleneglycoldimethylether (E181) and R22 (difluoromonochloromethane) (27).

Ternary mixtures may offer advantages, particularly in reducing or avoiding the need for rectification of the refrigerant vapor. An example is a system utilizing ammonia or methylamine as the refrigerant and a mixture of lithium bromide and water as the absorbent (28).

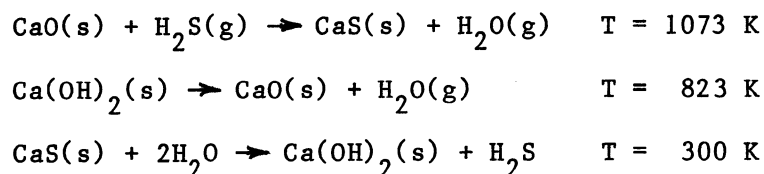
Most commercially produced machines utilize either the lithium bromide-water or ammonia-water systems. The use of water as a refrigerant has the advantage of a high heat of vaporization. Water is very inexpensive and very safe, but its low vapor pressure requires operation at very low pressures and its high freezing point precludes its use in refrigerating or low temperature heat pumping applications. Care must be taken to prevent the lithium bromide absorbent from crystalizing out of solution. The absorbent solution is also viscous and corrosive.

The use of ammonia as a refrigerant has the major advantage of a low freezing point (-78 C), but this is accompanied by high vapor

pressures (e.g., 2.0 MPa (20 atm) at 50 C) requiring heavy construction. Ammonia is toxic and a strong irritant. The safety hazard is aggravated by the high operating pressures: ammonia would leak out of a defective system. While water is an excellent absorbent for ammonia, it is volatile and rectification is necessary to separate it from the refrigerant vapor produced in the generator. Despite the disadvantages of these chemical systems, they have been made to work successfully in commercially produced machines.

The systems discussed thus far all condense the refrigerant to a liquid. The refrigerant vapor can also be absorbed into a second absorbent; an example is a system utilizing ammoniates of  $\text{FeCl}_2$  and  $\text{CaCl}_2$  (2).

A heat pump cycle can also be based on a set of three reversible reactions rather than the usual absorption cycle. Fujii, et. al. (29) propose a process to upgrade the temperature of an industrial waste heat stream, using an endothermic reaction at the temperature of the waste heat and exothermic reactions at low and high temperatures. An example of such a reaction scheme is:



This cycle could truly be called a chemical heat pump. Lauerhaus (30) has developed a technique to identify other such reaction cycles.

#### 1.4.4 Applications for absorption heat pumps

Presently, the primary application of absorption heat pumps is in air conditioning, particularly very large machines fired by low pressure steam in industrial and commercial applications. The most common application of AHPs in the past, domestic refrigeration, has now been almost entirely supplanted by vapor compression cycles. The potential of the absorption cycle is, however, much greater than its present limited use.

Space heating represents some 18 percent of the current energy use in the United States; approximately 87 percent of this is met by the direct combustion of fossil fuels (31). While recent furnace designs are achieving annual fuel utilization (first law) efficiencies over 90 percent, their second law efficiencies remains very low. Absorption heat pumps offer a way to achieve heating COPs greater than one, improving on the second law efficiency associated with meeting a heating load at 20 C with a heat source temperature of well over 1000 C. The same machine could also provide cooling at a primary energy efficiency comparable to an electrically-driven vapor compression heat pump (4).

The International Energy Agency (4) states that absorption heat pumps in heating applications will receive stiff market competition from high efficiency furnaces and vapor compression heat pumps, primarily in the area of initial cost. Nevertheless, the AHP remains under active development, with optimism high in Europe and Japan. In the United States, a residential AHP providing both heating and

cooling is under development by Phillips Engineering Company (27,32). Both the Trane Company and Carrier Corporation are developing "advanced concept" AHPs for commercial applications (33).

The absorption cycle is also one of the more feasible ways to obtain solar-powered cooling. Indeed, much of the recent absorption literature has been concerned with solar cooling. Machines which have been modified for solar operation are commercially available (34,35), (although the only U.S. manufacturer of residential scale absorption equipment has recently withdrawn from the market). But beyond inserting an essentially standard absorption chiller into a solar system with hot water or other thermal energy storage, an absorption heat pump combining heating, cooling, and chemical energy storage into a single unit has interesting possibilities.

### 1.5 Objectives

The primary objectives of this research are to develop the capability to model absorption heat pumps and to study them in space conditioning applications. Currently, absorption machines are designed more by a combination of art and cut-and-try methods than scientific analysis. While successful absorption machines have resulted from these traditional methods, their performance could almost certainly be improved by a detailed component and cycle analysis. This work develops simulation models for absorption heat pumps with the goal of enabling a more analytical approach to their study and design. Computer simulation is also useful for investigating a system existing only as a conceptual design and is

perhaps the only practical was to compare the effect of many design variables on the long term performance of systems with time-varying inputs.

The applications of a solar-driven system with chemical energy storage and a fuel-fired AHP without storage are investigated. These two applications require different modeling approaches. The system with storage is dominated by the state of charge of the storage tanks and this, combined with the highly variable nature of the solar and ambient temperature driving forces, dictates a long-term (annual) simulation with small (one hour or less) timesteps. For a system without storage, the response of the heat pump is typically much faster than changes in the building load and thus the heat pump would ideally operate at a quasi steady-state. While significant periods of transient operation may result from a control strategy, the steady-state performance must be characterized as a first step. A steady-state simulation permits a much more detailed study of the absorption cycle itself and the availability of experimental data makes this level of detail meaningful.

CHAPTER 2  
SIMULATION OF ABSORPTION HEAT PUMPS WITH CHEMICAL STORAGE  
IN SOLAR ENERGY SYSTEMS

Absorption heat pumps driven by solar energy in space heating and cooling applications are considered in this chapter. The possible advantages and disadvantages of AHPs in this application are discussed. A review of solar absorption heat pump work is presented, concentrating on systems with chemical storage and their modeling. Finally, the simulation model for an AHP system with chemical storage developed in this research is presented and its application in a solar energy system investigated.

### 2.1 Solar Energy Applications of AHPs With Chemical Storage

Because of its ability to combine heat pumping, heat-driven air conditioning and energy storage in a single device, the absorption heat pump has interesting possibilities for use in solar energy systems. The greater than one heating COP might allow the use of smaller solar collector areas; also, auxiliary energy might be input through the AHP, taking advantage of its COP in the backup heating mode. The highly variable nature of incident solar radiation and heating and cooling loads results in a need for energy storage; thus the low temperature, high density chemical energy storage in an absorption heat pump is very attractive.

But these advantages for solar operation do not come without penalties. The greater than one heating COP requires higher collector temperatures (and therefore lower collector efficiencies) as compared with a conventional solar heating system. The equipment that comprises an AHP with chemical storage is likely to be more complex than a conventional solar heating system, but perhaps comparable to a solar heating system combined with a solar-powered absorption air conditioner. Finally, chemical energy storage requires sizable quantities of chemicals which may be expensive or have safety hazards associated with them.

The continuous AHP is better suited for use in solar applications than the batch system in a number of ways. The temperatures of the two tanks in a batch system are significantly different in the charging and discharging cycles. Thus, if only a small quantity of solar heat were available during a charge cycle, the refrigerant tank would not be heated to a temperature useful for heating and no heat of condensation would be available to the load. For this same reason, it may not be feasible to input auxiliary energy through a batch AHP. Since backup heating would be required only when the AHP becomes fully discharged, an input of auxiliary heat would have to meet the heating load and heat the refrigerant tank to a usable temperature before operation with a COP greater than one is possible.

The batch AHP also has a serious limitation in air-conditioning operation. The peak cooling load (which requires operation in the discharge mode) is approximately coincident with the available solar

heat input (which implies operation in the charge mode). These drawbacks can be avoided, however, if two batch AHPs are used, with each being alternately charged and discharged (37). This arrangement would make the use of solid absorbents more feasible.

Taube and Furrer (13) point out that a significant amount of energy (for chemicals, storage tanks, etc.) is required to construct a chemical energy storage system. This storage capacity must be cycled many, many times (presumably saving fossil fuel in doing so, by storing solar energy for example) in order to repay the "borrowed" energy used in its construction. Based on this type of analysis, they conclude that long term (seasonal) chemical energy storage is not feasible, but that daily or weekly storage is.

## 2.2 Review of Solar Absorption Heat Pump Work

### 2.2.1 AHPs with thermal energy storage

An absorption heat pump without storage can be teamed with a separate thermal energy store. This type of system has received considerable attention in the literature and is the most common way of providing solar-powered cooling. A typical system which stores solar-heated water until needed by the chiller is shown in Figure 2-1. This same system could be used as a conventional liquid-based solar heating system by bypassing the absorption chiller.

Ward (38) has assessed the feasibility of solar-powered absorption cooling. He cites experimental studies that have confirmed that solar absorption cooling is technically feasible using

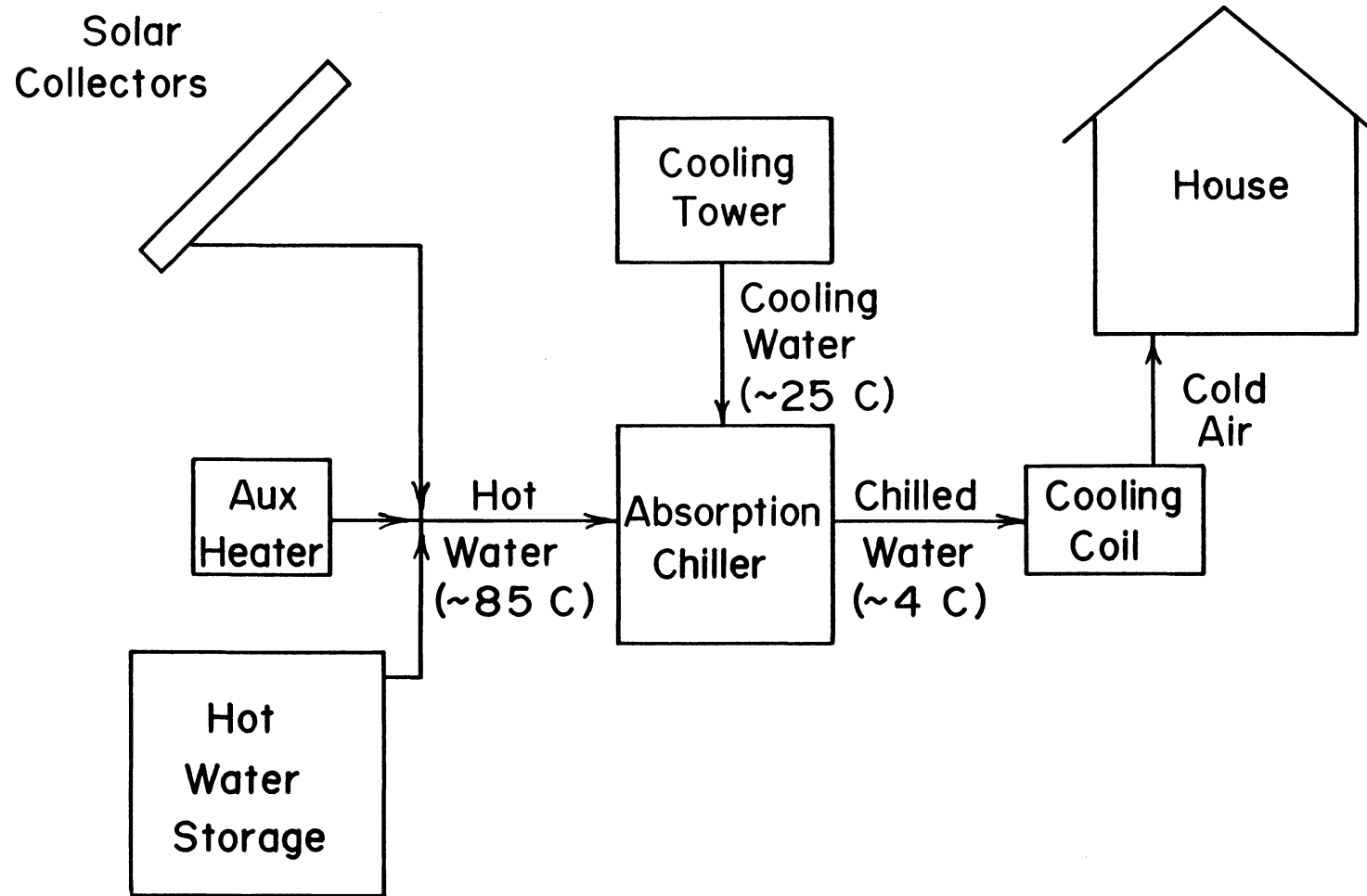


Figure 2-1 Solar-powered absorption chiller with hot-side thermal energy storage (temperatures shown are typical for a lithium bromide-water system)

flat plate solar collectors. Thermal losses from the hot water storage tank are a potential problem. If the storage is inside the building, losses will not only degrade the quality of the stored energy but will also increase the cooling load. Thus, Ward recommends outside hot water storage and also indoor chilled water storage.

Ward found the overall efficiency of absorption and vapor compression machines to be roughly equal in terms of primary energy (i.e., accounting for the conversion of heat into electrical energy). The solar-powered air conditioner was also compared to a conventional vapor compression machine on economic grounds. In this analysis, it was assumed that a solar heating system was already in place so that the cost of the collector, storage tank, etc. were not charged to the solar cooling system. The basic conclusion was that the economics of solar cooling are marginal and highly dependent on the economic parameters assumed in the analysis. Since a solar heating and cooling system with thermal storage is comparable in terms of system complexity to an AHP system with chemical storage, Ward's general conclusions might also apply to the AHP system.

Blinn (39) has modeled a lithium bromide-water chiller using a "black box" approach; equations for COP and capacity were fit to manufacturer's steady state performance data of the machine being studied (in this case the Arkla WF-36 water chiller). The steady-state performance was modified to account for start-up transients by assuming that all of the capacitance of the machine was lumped in the generator. This model was used to simulate the

performance of solar air conditioning in three locations with a range of collector areas. The presence of start-up transients was found to reduce COP and the cooling load met by solar by 5-8 percent compared to a machine which responded instantly. Blinn also compared various methods of providing back-up cooling and concluded that using a vapor compression air conditioner would be cheaper than firing the absorption chiller with auxiliary energy. (He did not, however, account for the capital cost of the separate vapor compression machine.)

A similar black box modeling technique, but not accounting for transient effects, was used by Butz, et al. (40) to simulate the performance of a solar heating and cooling system in the Albuquerque climate. The economic factors required for the solar system to be competitive with a conventional heating and cooling system were discussed. The model of Butz was extended by Oonk, et al. (41) and used in the design of a solar heating and cooling system in an experimental house at Colorado State University. A number of modeling studies of solar-powered absorption cooling have been presented in the literature. Most of these models are based on an analysis of the absorption cycle and will be discussed in Section 4.1.

Lazzarin (42) has tested an AHP used as a solar-assisted heat pump. In this system, low temperature (10 to 25 C) solar-heated water is supplied to the evaporator of a standard gas-fired lithium bromide-water absorption chiller. The performance of this system was simulated for several Italian locations and compared to a conventional

solar heating system and a system which could provide solar heat either to the heat pump or directly to the load. The dual-sink system resulted in the best performance of the three systems. The AHP system without direct solar heating met a higher fraction of the load with nonpurchased energy than the conventional solar system at low collector areas. At higher collector areas, the performance of the single-sink AHP system was limited by the requirement of supplying all of the heat through the heat pump and thus met a smaller fraction of the load.

#### 2.2.2 Solid absorbent AHP systems

A heat pump utilizing the solid absorbent calcium chloride has been extensively studied by Offenhartz and co-workers at EIC Corporation (43,44). Methanol was selected as the refrigerant since its polarity and small size promised a reactivity similar to that of water or ammonia without the problems of low freezing point or high vapor pressures, respectively. The flammability and toxicity of methanol were noted as potential problems. Calcium chloride was found to have the best properties among the salts screened. It is inexpensive and has a high reactivity with methanol (two moles  $\text{CH}_3\text{OH}$  per mole of  $\text{CaCl}_2$ ). An x-ray diffraction study revealed that the reaction of calcium chloride and methanol forms the distinct chemical species  $\text{CaCl}_2 \cdot \text{CH}_3\text{OH}$ . No side reactions were observed and the temperatures of methanolation and demethanolation are consistent with a solar-driven heat pumping application. Equilibrium and kinetic measurements were performed to characterize the pressure-temperature

relationship and the reactivity of calcium chloride and methanol.

Further work by Offenhartz, et. al. (43,44) dealt with the design, construction and testing of a bench scale  $\text{CaCl}_2\text{-CH}_3\text{OH}$  heat pump and a test unit of about one-fifth scale. Possibly the greatest disadvantage in the use of a solid absorbent is the difficulty of heat and mass transfer into a fixed absorbent bed. Mass transfer into the bed was aided by the use of flaked calcium chloride and by vapor flow channels between trays of absorbent. Heat transfer into the bed was accomplished by a network of externally finned tubes carrying the heat exchange fluid; the  $\text{CaCl}_2$  was packed into the space between the fins. The large heat exchanger area thus obtained compensated for the inherently low heat transfer coefficients of the packed bed. Offenhartz has also simulated the performance of AHPs and this work will be discussed in Section 2.2.5.

A system employing sodium sulfide as the absorbent and water as the refrigerant (termed the "Tepidus system") has been reported by Brunberg (45). A prototype system has been installed in a single family house in Sweden and is sized for seasonal storage of energy with 7000 kg of salt. A soil heat exchanger consisting of 900 m of plastic pipe provides the low temperature heat source. A novel application for the Tepidus system is to charge the salt tanks with industrial waste heat and then transport the tanks to the residence where they are discharged.

Tchernev (46) has proposed a system employing a zeolite to adsorb water vapor. The zeolite is contained within a solar collector where

incoming radiation drives off water vapor which is condensed (with the heat of condensation being used for heating or rejected) and stored. To provide cooling, water is evaporated and reabsorbed into the zeolite. This can occur only at night when the collector/zeolite store can lose heat to the surroundings; thus, some type of energy storage is needed to provide cooling during the day. Because of the high freezing point of water, this system is not used as a heat pump in winter; the heat of condensation is used to meet the heating load but the condensate merely drains back into the collector/zeolite store to complete the cycle. A similar system, used for refrigeration in the tropics, has been tested and modeled by Monnier and Dupont (47).

An energy storage system based on the decomposition of inorganic hydroxides (e.g.  $Mg(OH)_2$ ) to oxides (e.g.  $MgO$ ) has been proposed by Ervin (48) and Bauerle, et. al. (49). These reactions require very high charging temperatures (375 C for magnesium hydroxide) and thus their use would likely be limited to high temperature heat storage applications and not solar heat pumping.

### 2.2.3 Liquid absorbent systems

The sulfuric acid-water chemical heat pump has been extensively studied by Clark and co-workers at Rocket Research Company. The system originally proposed by Huxtable and Poole (9,50) was strictly an energy storage system. A dilute solution of acid was concentrated by the application of heat and stored; the water vapor driven off in this process was condensed and stored but the heat of condensation was rejected to ambient. Acid and liquid water were recombined to recover

stored energy. Sulfuric acid was chosen because of its low cost and high reactivity. This work included compiling materials compatibility and thermodynamic data for  $H_2SO_4-H_2O$  solutions.

The chemical energy storage system was then modified into a chemical heat pump. The construction and testing of a small scale heat pump operating in the batch mode is described by Clark, et al. (51-53). This test unit confirmed calculations of energy storage density and provided data on heat and mass transfer rates. (Modeling of this system is discussed in Section 2.2.5.)

The separation of the acid and water was accomplished by heating the entire acid tank. A similar approach (i.e., cooling the entire tank) did not work well for absorption, however. Water vapor was absorbed in the top layer of the acid, forming a water-rich region which diffused very slowly throughout the bulk of the acid. Agitating the acid improved the mass transfer performance, but at a high cost in pumping power. Absorption into an acid spray was acceptable at low acid concentrations but more concentrated solutions would not atomize. The most suitable technique found was absorption into a packed bed. This absorption column was located in the head space of the acid tank and also served as an entrainment separator during charging. Tests indicated that the charge and discharge rates were limited by heat transfer and not chemical reaction.

Further work by Clark, et al. (54) has been concerned with system optimization, economic analysis, and assessment of commercialization possibilities. A system similar to that shown in Figure 1-6 was

proposed for a solar heating and cooling application with seasonal storage for a commercial building. More recently, the sulfuric acid heat pump has been proposed for temperature boosting in industrial applications (55).

Jaeger and Hall (56,57) have investigated the ammonium nitrate-ammonia system. Ten compounds that react with ammonia to form liquids were identified from the literature and tested to determine their physical and thermodynamic characteristics. Of these ten,  $\text{NH}_4\text{Cl}$ ,  $\text{NH}_4\text{SCN}$  and  $\text{NH}_4\text{NO}_3$  were selected for further study. They were tested in a test reactor to determine heat transfer coefficients. Corrosion testing was also carried out. The  $\text{NH}_4\text{NO}_3$  system was chosen because of its lowest cost. (Daniels (58) has reported that  $\text{NH}_4\text{NO}_3$  is potentially explosive; he could not, however, find any mishaps in a refrigeration application.) A prototype residential system composed of two batch AHPs in parallel was designed; its cost was estimated to be about \$4,000.

#### 2.2.4 Absorbent suspended in an inert solvent

A solid absorbent can be suspended in an inert solvent, avoiding the difficulties of heat and mass transfer into a solid absorbent bed, but retaining the thermodynamic characteristics of a solid absorbent AHP. Taube and Furrer (13) have investigated an ammoniated salt suspension with kerosene as the solvent. They found that the use of liquid suspensions has a number of problems. The heat capacity of the solvent will lower the COP unless high effectiveness heat exchangers are employed. The storage and reactor volumes are increased (solid

content of the slurry is less than 25 percent) and there are potential problems with flammability of the solvent and carryover of the solvent vapor.

Suspensions of ammoniated salts have also been investigated by Wentworth (14). He found that a colloidal suspension of  $\text{CaCl}_2$  could be obtained with n-heptanol as the solvent ( $\text{NH}_3$  was the refrigerant). The vapor pressure-temperature relationship of this combination was confirmed to be independent of the concentration of refrigerant (i.e., characteristic of a solid absorbent). The reaction kinetics were found to be good; also, no side reactions were observed. Finally, methods of maintaining the suspension were investigated; bubbling ammonia through the slurry gave good reaction and required less solvent than stirring the suspension.

#### 2.2.5 Modeling of AHPs with chemical energy storage

Grassie and Sheridan (59) have extended the absorption air conditioner model of Duffie and Sheridan (60) to include absorbent and refrigerant storage. The performance during a single design day was simulated and described in some detail for a set of design parameters. From these simulations, it was concluded that chemical storage within the absorption cycle is feasible and offers advantages for solar operation.

Clark, et al. (51) describe a computer model of their sulfuric acid-water chemical heat pump. One part of the program calculates the required size of the storage tanks, heat exchangers and vapor duct for a given system size and required rate of charging and discharging.

The program was also used to simulate the performance of the system for a single charge and discharge cycle. Fairly detailed heat transfer relationships were taken into account. The pressure drop through the vapor duct was accounted for, but equilibrium of mass transfer processes was otherwise assumed. The model of Clark, et al. is quite detailed and gave good agreement with experimental results, but is specific to their particular system and is not suited to long-term performance simulations.

An extensive simulation study of solar AHPs has been carried out by Offenhartz, et al. This work began with a study of various energy storage options, including AHPs (2,61). The performance of a sulfuric acid-water chemical energy storage system was simulated (using the TRNSYS simulation program (36)) and found to be quite similar to a conventional hot water storage system except for a four-fold advantage in energy storage density. This system did not utilize the heat of condensation and thus had a maximum COP of unity; also, a low temperature heat source at a constant 5 C was assumed. The heating season performance of a calcium chloride-methanol heat pump with an ambient air heat source was also simulated. Its performance in the Madison climate was better than a solar system employing hot water storage if collectors with a low heat loss coefficient (e.g., evacuated tubular collectors) were used.

The performance of liquid and solid absorbent systems was again simulated by Offenhartz (62,63) using TRNSYS, extending and improving upon his earlier work. The liquid absorbent system studied had a

separate generator, condenser, evaporator, and absorber in addition to absorbent and refrigerant storage tanks (i.e., the system in Figure 1-6) and utilized either the  $\text{H}_2\text{SO}_4\text{-H}_2\text{O}$  or  $\text{NH}_4\text{NO}_3\text{-NH}_3$  chemical systems. The vessels were assumed to be fully mixed and equilibrium with respect to mass transfer processes was assumed. The heat and mass capacitance of the fluid in the small system components (e.g., generator) were accounted for; this necessitated the use of very small timesteps and thus resulted in large computing expenses.

The solid absorbent  $\text{CaCl}_2\text{-CH}_3\text{OH}$  chemical heat pump was also studied; it utilized two absorbent beds, which were alternately charged and discharged, along with a condenser, evaporator, and refrigerant storage tank. Pressure equilibrium was not assumed between the charging and discharging vessels; rather the ratio between the absolute temperatures of the two components exchanging methanol vapor (i.e., the charging bed and the condenser or the discharging bed and the evaporator) was assumed to be constant. This relationship was experimentally found to be "reasonably accurate." The heat capacity of the containers and heat exchange piping was also accounted for.

Heating and cooling simulations of the  $\text{CaCl}_2\text{-CH}_3\text{OH}$  and  $\text{H}_2\text{SO}_4\text{-H}_2\text{O}$  systems were carried out for AHPs located in the Washington, DC and Fort Worth, Texas, climates. These simulations were carried out for "typical" weeks in January and July for each of the two cities. The systems were sized to provide a high fraction (greater than 90 percent) of the cooling load. The reason for this requirement is that providing back up cooling with fossil fuel would be inefficient

because of the relatively low cooling COP and using a conventional vapor compression air conditioner would result in higher system costs and aggravate utility peak load problems. The requirement of 90 percent cooling provided by solar was satisfied by approximately 30 m<sup>2</sup> of evacuated tubular collectors in both locations for an average residence. The higher cooling load in Fort Worth was offset by greater solar insolation.

The sulfuric acid system had a cooling COP of 0.7 to 0.8 compared to 0.6 to 0.7 for the calcium chloride system. The collector temperatures in the liquid absorbent system varied widely, ranging from 70 C to about 200 C. This is in contrast to the solid absorbent system which had a much more constant collector temperature (in the range of 100-120 C). The H<sub>2</sub>SO<sub>4</sub>-H<sub>2</sub>O system also had a higher COP in the heating simulations. This was offset, however, by higher collector temperatures, so that both the solid and liquid absorbent systems provided nearly the same fraction of the load despite major differences in system configuration and performance details.

The ammonium nitrate-ammonia liquid absorbent system was compared to the sulfuric acid-water system. The performance of both systems was very similar, leading Offenhartz to suggest that the performance of liquid absorbent systems may be independent of the particular chemical system used.

#### 2.2.6 Previous work by author

A modeling study of absorption heat pumps in solar heating systems was carried out by the author in work leading to a masters

thesis (64). A summary of this work is presented by McLinden and Klein (65). A number of batch and continuous AHP configurations were presented and their possible advantages and disadvantages discussed. A simple equilibrium, steady-state analysis of the continuous AHP cycle was carried out for three chemical systems. The COPs at given generator, condenser, absorber and condenser temperatures for the sulfuric acid-water and lithium bromide-water systems were virtually identical and were higher than those for the sodium thiocyanate-ammonia system.

Models for use with the TRNSYS simulation program were developed for two configurations: the batch AHP and a continuous AHP with combined condenser/refrigerant storage tank and absorber/absorbent storage tank. Each of these models treated an entire AHP, including the control strategy, and considered heating operation only. These AHP systems were simulated with the sodium thiocyanate-ammonia chemical system and were compared to a conventional solar heating system for three locations. The continuous AHP provided a higher fraction of the load than the conventional system with low collector areas and/or low loss (high performance) collectors. With increasing collector area, the collector efficiency and heat pump COP decreased and the performance of the AHP and conventional systems approached each other. The batch system had a seasonal COP of approximately unity and gave a fraction non-purchased energy slightly lower than the conventional solar heating system over the entire range of collector areas.

The present work generalizes the earlier continuous AHP model and extends it to include cooling operation. A much more extensive simulation study is carried out with the new AHP model.

### 2.3 Transient Simulation and the TRNSYS Program

The nature of a solar-driven AHP with chemical storage necessitates a transient simulation over a heating or cooling season. In a transient simulation, the time period of interest is broken into timesteps and the external variables driving the system are supplied to the simulation at each timestep. The equations describing the simulated system are solved for each timestep with the end conditions of one timestep becoming the initial conditions for the next.

The equations describing the system of interest can be directly programmed and solved. A more general and flexible method is to decompose the system into a number of smaller sub-problems. These sub-problems would correspond to components in the physical system and would be easier to formulate than the entire system of equations. Furthermore, once a component model is formulated, it could be used in the simulation of many different systems.

The TRNSYS simulation program (36) developed at the University of Wisconsin uses this modular approach. The TRNSYS program was originally developed for the simulation of solar energy systems and more recently has been extended to include more general HVAC systems. It has a library of Fortran subroutines which model components typically found in solar energy and HVAC systems. The components present in a simulation and the manner in which they are connected are

specified by the user with a simple simulation language.

The differential and algebraic equations describing a physical system are solved numerically by TRNSYS. Variables which are present as time-derivatives in a component model are specified in the simulation deck and are solved by a modified Euler method. In this method the value of the integrated variable at the end of a timestep is a function of the value at the beginning of the timestep and the derivative evaluated at the midpoint of the timestep:

$$T_{\tau,i} = (T_{\tau-\Delta\tau} + f(\tau - \Delta t/2, T_{\tau-\Delta t/2,i-1}) \Delta t) \quad [2-1]$$

$$f(\tau, T) = dT/dt \quad [2-2]$$

where  $T$  is the integrated variable,  $\tau$  is time,  $\Delta t$  is the timestep and the subscripts refer to time and the iteration number. The value of the integrated variable at the midpoint of a timestep is given by:

$$T_{\tau-\Delta t/2,i-1} = 0.5 (T_{\tau,i-1} + T_{\tau-\Delta t}) \quad [2-3]$$

Algebraic equations are solved by successive substitution concurrently with the iteration for the differential equations. A component is called until its inputs between successive iterations have converged within a specified tolerance.

The absorption heat pump is just one component in the complete solar heating and cooling system. It is advantageous to model this system using a general simulation program in order to utilize its building load model, weather data processing routine, etc. The TRNSYS program is well-suited for the system of interest and was used.

#### 2.4 Description of Simulated System

The absorption heat pump modeled is a continuous, liquid absorbent system with a combined condenser/refrigerant storage tank and an absorber/absorbent storage tank as shown in Figure 2-2. This configuration is simpler than a system with separate generator, condenser, evaporator, and absorber and has a number of other potential advantages. By combining the condenser and absorber with the refrigerant and absorbent tanks, the heats of condensation and absorption can be stored by raising the temperature of the contents of the tanks. This feature would allow, for example, the heat of condensation generated during the charging process to be stored if it were not immediately needed to meet the heating load. In addition, the evaporator could operate during the daytime hours when ambient temperatures are higher, storing the heat of absorption for use at night. In an air conditioning application, the ability to store the heats of condensation and absorption would permit rejection of heat throughout the night. With this more constant heat rejection rate, cooling tower requirements would be reduced, possibly allowing the use of a "dry" rather than an evaporative cooling tower.

This configuration also has possible disadvantages. Storing the heat of condensation by raising the refrigerant tank temperature increases the temperature of the generator and that of the collector, thereby reducing collector efficiency. The required evaporator temperature in the discharging process is increased as storing the heat of absorption raises the absorbent tank temperature. Offenhartz

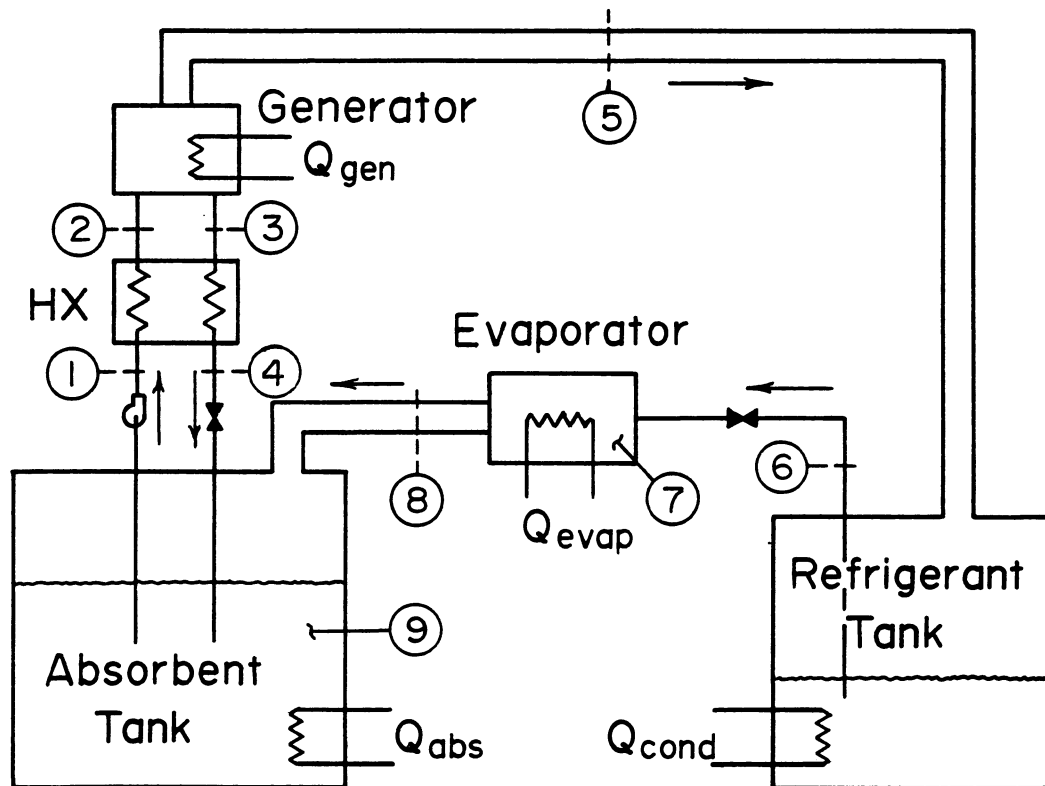


Figure 2-2 Absorption heat pump with combined condenser/refrigerant storage tank and absorber/absorbent storage tank

(66) has pointed out that thermodynamic availability may be lost by absorbing refrigerant directly in the absorbent tank rather than in a separate absorber where concentration can be controlled.

The chemical system chosen for use in this study employs ammonia as the refrigerant and a solution of sodium thiocyanate (NaSCN) and ammonia as the absorbent. This choice is based primarily on three considerations. First of all, the low freezing point of ammonia allows wintertime heat pumping. The NaSCN absorbent is non-volatile, avoiding the need for rectification. Finally, thermodynamic data is available for this pair (25,26). It is recognized that this chemical system may not be optimum from thermodynamic, safety and practical standpoints.

The effects of different chemical systems are considered by simulating an AHP using sulfuric acid and water. The data given in References (50) and (67) were used to generate the necessary property correlations. The vapor pressure of water was extrapolated below the freezing point to allow wintertime heat pumping. It is possible to use water below 0 C, as pointed out by Hiller and Clark (68), by adding an anti-freeze to the evaporator, although this would lower the vapor pressure and reduce the temperature difference across which heat could be pumped.

The complete heating and cooling system consists of the AHP, load, solar collector, ambient heat exchanger, etc. as shown in Figure 2-3. The AHP is connected to the load and ambient heat exchangers by heat exchange loops. These would be required to prevent any

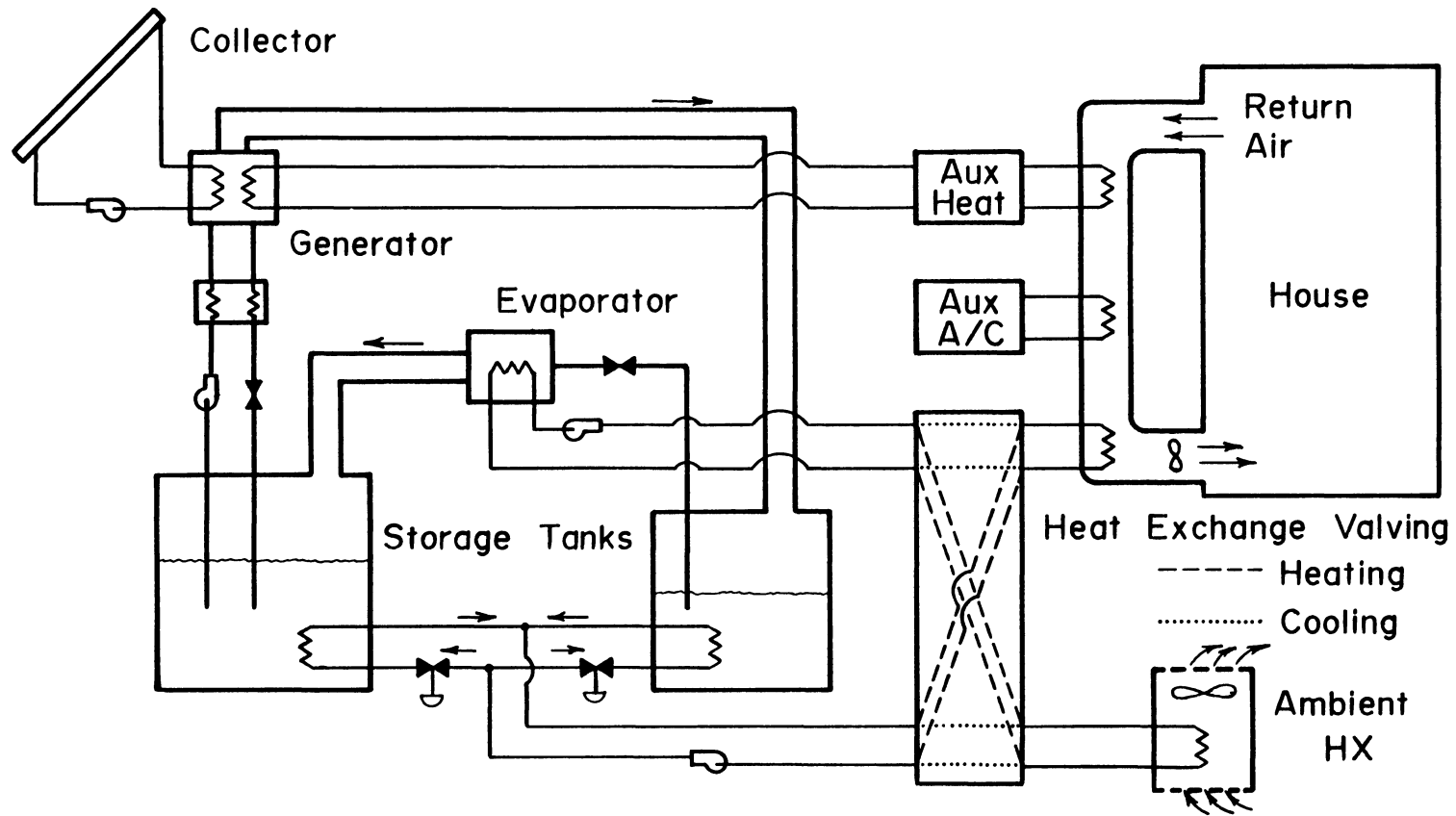


Figure 2-3 Absorption heat pump solar heating and cooling system

potentially hazardous chemicals in the AHP from leaking into the conditioned space. Heat exchange loops also permit switching from heating to cooling operation. Heat can be supplied to the generator by either the solar collectors or an auxiliary source. The auxiliary heat source and an auxiliary air conditioner directly supply the load when the solar AHP cannot.

## 2.5 Transient Simulation Model

### 2.5.1 Absorption heat pump component

The AHP model is based on mass and energy balances written around various parts of the cycle; it thus represents a thermodynamic approach rather than a "black box" approach using empirical performance curves. The property relations are supplied as Fortran function subroutines and are referenced directly by the component models, making the model itself independent of chemical system. The required subroutines are described in Appendix C.1 and are summarized in Table 2-1.

The major assumptions employed in the model are that:

1. the reaction rates are controlled by heat transfer resistances, i.e., mass transfer equilibrium is achieved
2. the thermal and mass capacitance of the generator and evaporator are negligible compared to those of the storage tanks
3. all vessels are fully mixed
4. the absorbent is completely non-volatile

Thus this model represents a limiting, best case analysis in several respects.

Table 2-1 Summary of property relations needed for the TRNSYS AHP model

Function name	Independent variables	Dependent variables	Description
HMIX	$T, x_{liq}$	$h_{liq}$	enthalpy of liquid mixture of absorbent and refrigerant
HVAP	$T, T_{sat}$	$h_{vap}$	enthalpy of refrigerant vapor
VPRES	$T, x_{liq}$	$P$	vapor pressure of liquid solution
TMIXH	$h_{liq}, x_{liq}$	$T_{sat}$	saturation temperature of liquid solution
TMIXVP	$P, x_{liq}$	$T_{sat}$	saturation temperature of liquid solution
TMIXUC	$U_{tot}, m_{ref}, m_{abs}, v_{tot}$ ( $mC_p$ ) container	$T_{sat}$	temperature of a two phase, two component mixture given total internal energy, volume and masses
RHOLQ	$T, x_{liq}$	$\rho_{liq}$	density of liquid mixture
RHOVP	$T, P$	$\rho_{vap}$	density of refrigerant vapor

Overall mass and energy balances are written for each tank and reaction vessel; absorbent mass balances are also written for the generator and absorbent tank. (In the following equations, numbered subscripts refer to points in Figure 2-2. The sign convention employed is that heat flows into the system are positive and mass flows are positive in the direction of the arrows in Figure 2-2.) For the generator plus heat exchanger, these balances yield:

$$0 = \dot{m}_1 - \dot{m}_4 - \dot{m}_5 \quad [2-4]$$

$$0 = x_1 \dot{m}_1 - x_4 \dot{m}_4 \quad [2-5]$$

$$0 = \dot{m}_1 h_1 - \dot{m}_4 h_4 - \dot{m}_5 h_5 + \dot{Q}_{\text{gen}} + \dot{Q}_{\text{aux}} + \dot{Q}_{\text{loss,g}} \quad [2-6]$$

For the refrigerant tank, the mass and energy balances give:

$$dm_c/dt = \dot{m}_5 - \dot{m}_6 \quad [2-7]$$

$$dU_c/dt = \dot{m}_5 h_5 - \dot{m}_6 h_6 + \dot{Q}_{\text{cond}} + \dot{Q}_{\text{loss,c}} \quad [2-8]$$

where  $m$  is mass flow rate,  $x$  is the mass fraction of absorbent,  $U$  is total internal energy and the  $\dot{Q}$  terms are heat flows described below.

The assumption of mass transfer equilibrium implies:

$$P_1 = P_2 = P_3 = P_4 = P_5 = P_6 \quad [2-9]$$

This high side pressure relates the temperature and concentration in the generator with the refrigerant tank temperature; by choosing two, the third is determined. This relationship is shown in Figure 2-4 where vapor pressure data for the NaSCN-NH<sub>3</sub> system are plotted as

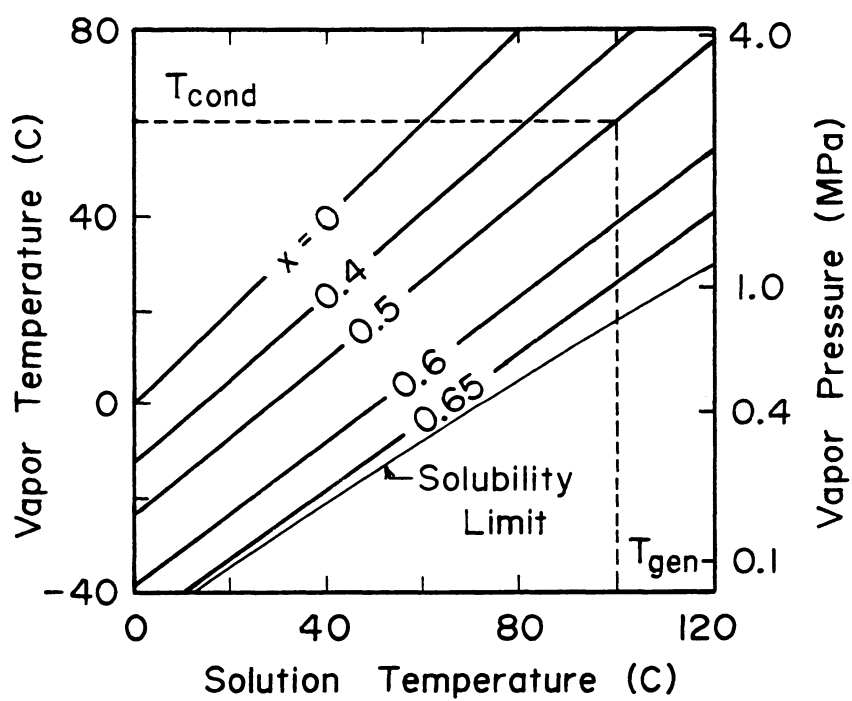


Figure 2-4 Relationship between condenser temperature and generator concentration and temperature for the NaSCN-NH<sub>3</sub> chemical system

vapor saturation (condenser) temperature versus liquid solution (generator) temperature. Note that the generator temperature is increased by an increase in concentration or condenser temperature.

Energy and mass balances on the counter-current heat exchanger yield:

$$\dot{m}_4 h_4 = \dot{m}_3 h_3 - \varepsilon_{g-a} (\dot{m}C)_{\min} (T_3 - T_1) \quad [2-10]$$

$$\dot{m}_3 = \dot{m}_4 \quad [2-11]$$

where  $\varepsilon_{g-a}$  is the effectiveness of the heat exchanger and  $(\dot{m}C)_{\min}$  is the minimum capacitance rate through the heat exchanger. (The heat exchanger effectiveness is that fraction of the maximum possible heat transfer which takes place (69).)

The  $Q_{aux}$  term in Equation [2-6] is the rate of auxiliary heat input to the generator. The remaining heat flows in [2-6] and [2-8] are given by simple heat transfer relations. Modeling the heat exchangers in the tanks as constant effectiveness devices yields:

$$\dot{Q}_{gen} = (\dot{m}C)_{hx,g} \varepsilon_g (T_{hx,g} - T_3) \quad [2-12]$$

$$\dot{Q}_{cond} = (\dot{m}C)_{hx,c} \varepsilon_c (T_{hx,c} - T_6) \quad [2-13]$$

where  $T_{hx,g}$  and  $T_{hx,c}$  are the temperatures of the heat exchange streams entering the generator and refrigerant tank. The tank losses (actually negative heat gains because of the sign convention) are:

$$\dot{Q}_{loss,g} = UA_g (T_{env} - T_3) \quad [2-14]$$

$$\dot{Q}_{\text{loss},c} = UA_c (T_{\text{env}} - T_6) \quad [2-15]$$

where  $T_{\text{env}}$  is the temperature of the tank environment.

A similar set of mass and energy balances can be written for the absorbent tank:

$$dm_a/dt = \dot{m}_4 + \dot{m}_8 - \dot{m}_1 \quad [2-16]$$

$$dm_{\text{abs},a}/dt = x_4 \dot{m}_4 - x_1 \dot{m}_1 \quad [2-17]$$

$$dU_a/dt = \dot{m}_4 h_4 + \dot{m}_8 h_8 - \dot{m}_1 h_1 + \dot{Q}_{\text{abs}} + \dot{Q}_{\text{loss},a} \quad [2-18]$$

and evaporator:

$$0 = \dot{m}_6 - \dot{m}_8 \quad [2-19]$$

$$0 = \dot{m}_6 h_6 - \dot{m}_8 h_8 - \dot{Q}_{\text{evap}} + \dot{Q}_{\text{loss},e} \quad [2-20]$$

The heat flows in [2-18] and [2-20] are described by expressions analogous to [2-12] to [2-15]. The assumption of mass transfer equilibrium implies:

$$P_7 = P_8 = P_9 \quad [2-21]$$

The above equations describing an AHP are implemented as two separate TRNSYS components--the generator and refrigerant storage tank and the evaporator and absorbent storage tank. (A pump component is also required.) This approach was felt to be the best compromise between the flexibility and generality of separate TRNSYS components for a generator, storage tank, etc. and the computational efficiency

of modeling the entire AHP including the control strategy as a single component.

For the solution of the generator and refrigerant tank, the mass and internal energy derivatives ([2-7] and [2-8]) are integrated by TRNSYS and supplied to the component. The refrigerant tank temperature and pressure are computed by the property relation TMIXU (described in Appendix C.1). An iterative loop is then entered for  $\dot{m}_5$ , the mass flow rate of vapor between the tanks; the initial guess for  $\dot{m}_5$  is that from the previous call to the component. With this value and the inputs of  $\dot{m}_1$ ,  $T_1$ ,  $x_1$  and  $\dot{m}_6$ , Equations [2-4], [2-5] and [2-9] to [2-15] can be solved. Equation [2-6] is used as a test for convergence; if this is not satisfied, a new  $\dot{m}_5$  is found by a secant method iteration. When the vapor flow rate has converged, the mass and energy derivatives ([2-7] and [2-8]) are calculated and returned to the TRNSYS integrator.

The calculations for the evaporator and absorbent storage tank are similar but do not involve an iterative loop. Again, the total internal energy of the storage tank is provided by a TRNSYS solution of the governing differential equation. The mass of absorbent is found by the difference between the total mass of refrigerant in the entire AHP (a constant) and the mass in the refrigerant tank:

$$m_{\text{ref,abs tank}} = m_{\text{ref,tot}} - m_{\text{ref,ref tank}} \quad [2-22]$$

The state of the absorbent tank contents determines the pressure and thus the temperature of the evaporator as well. With this

information, the remaining equations, including the derivative for internal energy, can be solved and the outputs of the component found.

### 2.5.2 Heating and cooling load model

The heating and cooling load modeled in this study represents a two-story house with 165 m<sup>2</sup> of floor and 22 m<sup>2</sup> of window area. It utilizes a transfer-function load model and temperature-level control as described in the TRNSYS manual (36). The infiltration rate is 0.5 air changes per hour and the walls and ceiling are insulated with 7.5 and 22.5 cm of fiberglass insulation, respectively. The overall loss coefficient is 167 W C<sup>-1</sup>. Internal heat generation averaged 656 W. Solar heat gains through windows are included but latent loads and domestic hot water loads are not.

### 2.5.3 Control strategy

An absorption heat pump system has a large number of control options which may have a significant effect on its performance. Several strategies have been investigated. The baseline control strategy is determined, in large part, by a multi-stage room thermostat with the heating/cooling mode determined by the time of year. The first stage heating mode is to use the heat of condensation to supply the load, provided that the refrigerant tank temperature is above some minimum useful temperature. When the room temperature falls below a second set point, heat from the absorbent tank is also used. (This order minimizes the generator, and thus collector,

temperature.) If the room temperature falls further, auxiliary heat is added to the generator and finally, below a fourth set point temperature, auxiliary heat is added directly to the load. All of these stages employ deadbands and can operate simultaneously except that auxiliary heat cannot be supplied both to the generator and directly to the load at the same time. The heating set points used in the simulations were 21, 20, 19 and 18 C with a 0.5 C deadband. Heat is extracted from ambient and added to the evaporator whenever the ambient temperature exceeds the evaporator temperature by a minimum value (2 C in the simulations).

Cooling is supplied by the AHP when the room temperature rises above the cooling set point and the evaporator temperature is below a maximum value. Auxiliary cooling is provided by a separate vapor compression device and is supplied directly to the load when the room temperature exceeds a second cooling set point. Cooling set points of 23 and 25 C were simulated. In the cooling season, heat is rejected to ambient whenever the refrigerant or absorbent tank temperature exceeds the ambient temperature by at least 2 C. The ambient heat exchanger is modeled as a "dry," constant effectiveness device and cooling water flows in parallel to the condenser and absorber.

The collector is controlled in the conventional manner with a differential on-off controller sensing the collector and generator temperatures. The collector and auxiliary input to the generator are not operated when the system is fully charged (to prevent crystallization of absorbent out of solution at high concentration).

In addition to the baseline control strategy, two other heating season control strategies were considered. In the first alternate strategy, the auxiliary energy input to the generator was disabled in order to study the interaction between solar and auxiliary energy supplied through the generator. Supplying auxiliary through the heat pump takes advantage of its greater than one COP but would result in a higher average state of charge of the system, leading to higher collector temperatures and reduced energy storage capacity for solar energy.

During times of marginal solar collection, the greater than one COP gained by supplying solar through the heat pump may be more than offset by low collection efficiency. During these times, the overall system performance might be improved if solar energy could "bypass" the generator and deliver heat at a lower temperature. In the second alternate control strategy, collected energy is delivered to the absorbent storage tank rather than to the generator when:

$$\frac{\eta_{\text{bypass}}}{\text{COP } \eta_{\text{gen}}} > 1 \quad [2-23]$$

where  $\eta_{\text{bypass}}$  and  $\eta_{\text{gen}}$  are the collection efficiencies when delivering heat to the absorbent tank and generator and the COP is an average value.

This option was implemented by computing each efficiency using the Hottel-Whillier (70) collector equation:

$$\eta_{\text{bypass}} = F_R(\tau\alpha) - F_R U_L \frac{(T_{\text{abs}} - T_{\text{amb}})}{G_T} \quad [2-24]$$

$$\eta_{\text{gen}} = F_R(\tau\alpha) - F_R U_L \frac{(T_{\text{gen}} - T_{\text{amb}})}{G_T} \quad [2-25]$$

where  $F_R$  is the collector heat removal factor,  $(\tau\alpha)$  is the transmittance-absorptance product,  $U_L$  is the collector loss coefficient,  $T_{\text{amb}}$  is the ambient temperature and  $G_T$  is the solar irradiance on the collector plane. If the generator is not operating, its temperature,  $T_{\text{gen}}$  is taken as the saturation temperature corresponding to the pressure over the refrigerant tank and the concentration in the absorbent storage tank. Although it would be difficult to physically implement, this control strategy serves to identify the performance implications of the greater than one heating COP of an absorption heat pump.

The baseline and alternative control options were included in a single controller component. This component returned control functions for the collector, solution pump, ambient and load heat exchangers, and auxiliary heating and cooling units.

#### 2.5.4 Conventional solar heating and cooling system

For comparison, a liquid-based solar heating system with sensible heat storage was simulated. It includes a solar-fired lithium bromide-water absorption chiller with an evaporative cooling tower. This system is modeled with standard TRNSYS components and was shown in Figure 2-1. Except for using the transfer function load model as

described above, it is very similar to the example solar heating and cooling system given in the TRNSYS manual (36).

## 2.6 System Simulations--Results and Discussion

Heating season and cooling season simulations were conducted with the absorption heat pump model to study AHPs in a solar application and to determine the effects of several design variables and control options. This investigation has been summarized by McLinden and Klein (70). The primary index of system performance is  $F_{NP}$ , the fraction of the total load met by non-purchased energy, defined as:

$$F_{NP} = 1 - Q_{aux}/Q_{load} \quad [2-26]$$

where  $Q_{aux}$  is the total auxiliary supplied and  $Q_{load}$  is the total energy used to meet the heating or cooling load. The important fixed parameters used in the simulation are as listed in Table 2-2 (except where noted in the text). The collector was modeled as a flat plate, but the values of  $F_{R U_L}$  and  $F_R(\tau\alpha)$  were chosen to represent an evacuated tubular collector. Such a collector was selected on the basis of earlier work by the author (64) and others (e.g., Offenhartz (62,63)). A collector with a higher loss coefficient is also investigated in relation to one of the control strategies.

### 2.6.1 Effects of collector area and storage mass

The AHP system was simulated using SOLMET TMY (typical meteorological year) (72) weather data for Columbia, Missouri, with three collector areas and two storage sizes (expressed as total mass

Table 2-2 Fixed parameters for the solar AHP simulation

## Collector

slope = latitude

$\dot{m}_{col}/A_{col}$	0.015 kg sec <sup>-1</sup> m <sup>-2</sup>
FR( $\tau\alpha$ )	0.55
$F_{R U_L}$	0.83 W m <sup>-2</sup> C <sup>-1</sup>

## Heat exchangers

$\epsilon_{g-a}$	0.75
$\epsilon$ (all other heat exchangers)	0.60
heat transfer fluid capacitance	3.5 kJ kg <sup>-1</sup> C <sup>-1</sup>

## Heat exchanger flow rates

$\dot{m}_{g-a}$	150 kg hr <sup>-1</sup>
$\dot{m}_{abs} + \dot{m}_{cond}$	1500 kg hr <sup>-1</sup>
$\dot{m}_{evap}$	1500 kg hr <sup>-1</sup>
$\dot{m}_{ambient}$ (air side)	2500 kg hr <sup>-1</sup>
$\dot{m}_{load}$ (air side)	2500 kg hr <sup>-1</sup>

## Storage tanks

height/diameter ratio	1.0
loss coefficient	0.437 W m <sup>-2</sup> C <sup>-1</sup>

of refrigerant and absorbent) to determine the effect of these variables on system performance and to identify appropriate base case values for subsequent comparisons. The timestep for most of the simulations was 0.2 hours.

The results of these simulations, presented in Figure 2-5, show that the AHP supplies a significant fraction of the heating load with non-purchased energy at zero collector area. This is because the auxiliary energy supplied through the heat pump can extract additional energy from ambient and deliver it to the load. In the cooling season, the  $F_{NP}$  curve starts at zero because here the useful energy flow is the low temperature heat extracted from the load. The cooling results for 1000 and 2000 kg of storage were virtually identical, indicating that a "plateau" may have been reached in the  $F_{NP}$  versus storage curve. For heating, the curves for the two storage sizes intersect; at low collector areas, increased tank losses offset any effect of greater storage capacity.

Monthly and seasonal average values of several quantities for the system with 1000 kg storage and 25 m<sup>2</sup> collector are shown in Table 2-3. The average collector operating temperature is quite high (137 C in January and 115 C in July). It is higher in January than July because of the higher condenser temperature and higher absorbent concentration. This is primarily because auxiliary energy input through the generator keeps the system at a moderately high state of charge during mid-winter. The high collector temperatures, combined with low ambient temperatures, result in a January collector

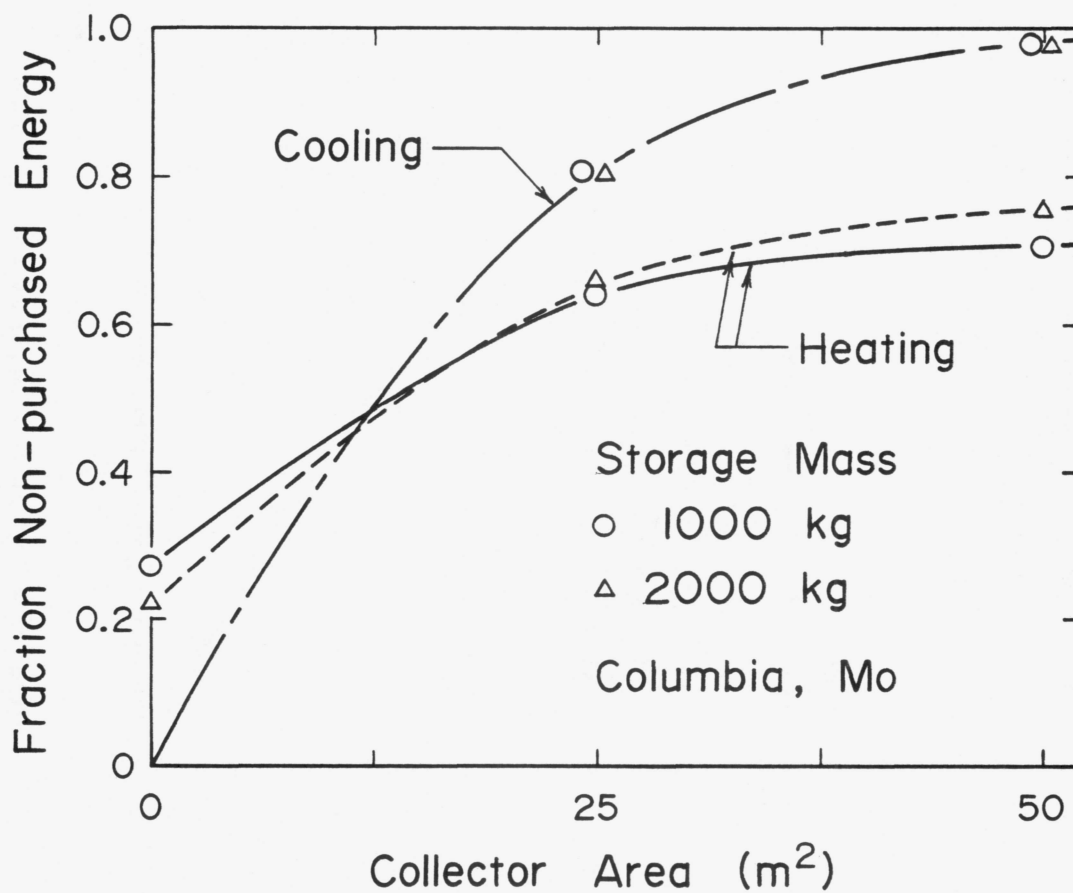


Figure 2-5 Effect of collector area and storage mass on seasonal  $F_{NP}$  for AHP system in Columbia

efficiency that is substantially lower than the July figure and roughly half of its maximum value (i.e.,  $F_R(\tau\alpha)$ ). The January heating COP is 1.40 and the July cooling COP is 0.55. The heating COP is penalized because of tank losses.

Table 2-3 Average collector and refrigerant tank temperature, absorbent tank concentration, collector efficiency, COP, tank losses and load for the base case simulation (Columbia, 1000 kg chemical storage, 25 m<sup>2</sup> collector)

	$F_{NP}$	$T_{col}$ (C)	$T_{cond}$ (C)	$x_{abs}$	$\eta_{col}$	COP	$Q_{loss}$ (GJ)	$Q_{load}$ (GJ)
January	0.54	137	39	0.59	0.28	1.40	0.4	8.5
Heating season (Oct-Apr)	0.64	151	49	0.61	0.20	1.33	4.2	36.5
July	0.71	115	33	0.52	0.42	0.55	0.3	6.1
Cooling season (May-Sept)	0.81	117	28	0.55	0.39	0.52	1.2	22.6

Simulations were also carried out in the Columbia climate with the conventional solar heating and cooling system. The results of these simulations are given in Figure 2-6. The conventional system, of course, provides no non-purchased energy with zero collector area. In the heating season the  $F_{NP}$  curve has a greater slope, especially at low collector areas, than the AHP system because of lower average collector temperatures. Thus, the performance of the two systems approach each other at high collector areas. In the cooling season, the performance of the two systems is qualitatively similar; the

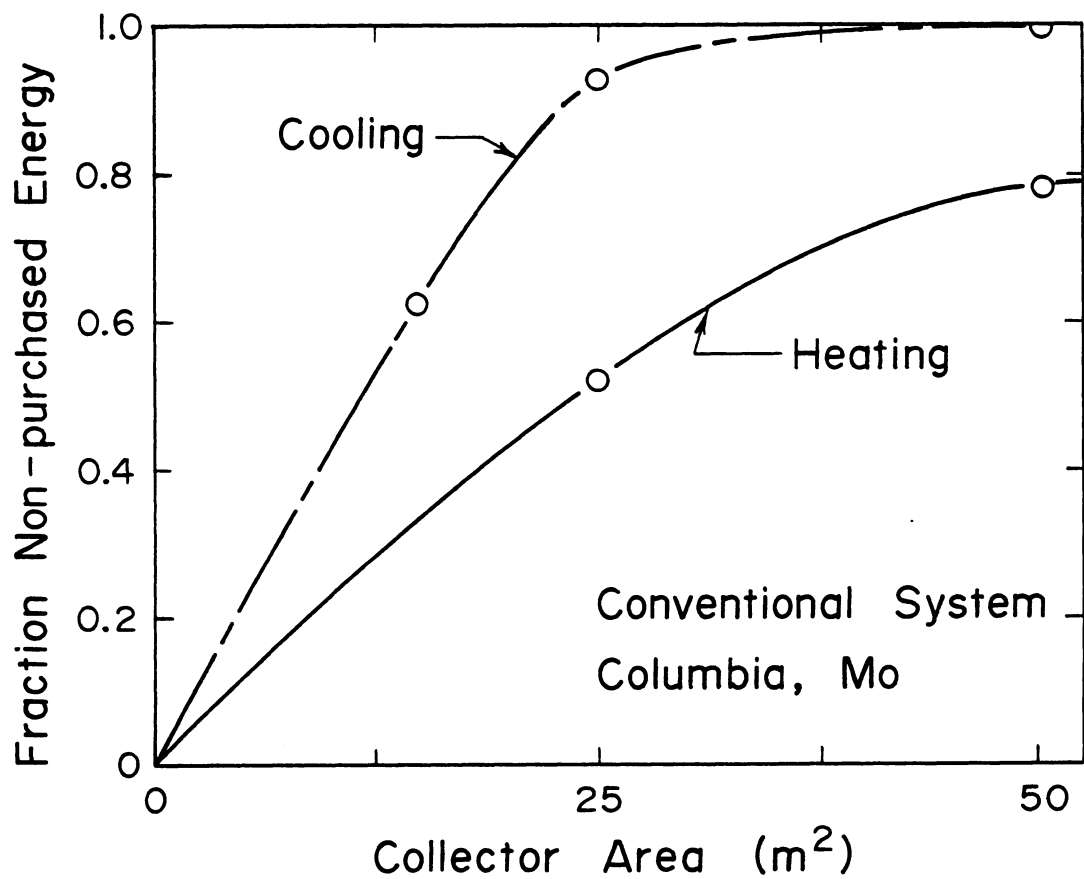


Figure 2-6 Effect of collector area on seasonal  $F_{NP}$  for conventional solar heating and cooling system in Columbia

LiBr-H<sub>2</sub>O absorption chiller provides a higher  $F_{NP}$  because of a combination of higher COP, lower collector temperatures, and the lower cooling water temperatures provided by the evaporative cooling tower.

#### 2.6.2 Effects of climate

The AHP system with 1000 kg of chemical storage was also simulated in the Madison, Wisconsin, and Fort Worth, Texas climates. The solar contribution to  $F_{NP}$  in the Madison heating season is relatively small as shown in Figure 2-7 due to a combination of lower ambient temperatures and radiation levels as compared with Columbia, leading to low collector efficiency. During the cooling season, however, 25 m<sup>2</sup> of collector meets 92 percent of the relatively small (12 GJ) load.

The opposite situation occurs in the Fort Worth climate. Here, 25 m<sup>2</sup> of collector can supply 84 percent of the 13 GJ heating load with non-purchased energy as shown in Figure 2-8. With 25 m<sup>2</sup> of collector, most of the auxiliary energy is required during a relatively few cold, cloudy days when the collector cannot operate; thus an additional 25 m<sup>2</sup> of collector results in only a small increase in  $F_{NP}$ . The large (34 GJ) cooling load in Fort Worth, however, leads to the lowest cooling  $F_{NP}$  of the three locations.

In order to evaluate the relative merits of the AHP system in the three locations, it is necessary to compare the magnitudes of the non-purchased energy provided by the system, rather than the fraction of the total load. These results are given in Table 2-4. (The loads vary with collector area because systems which meet a higher fraction

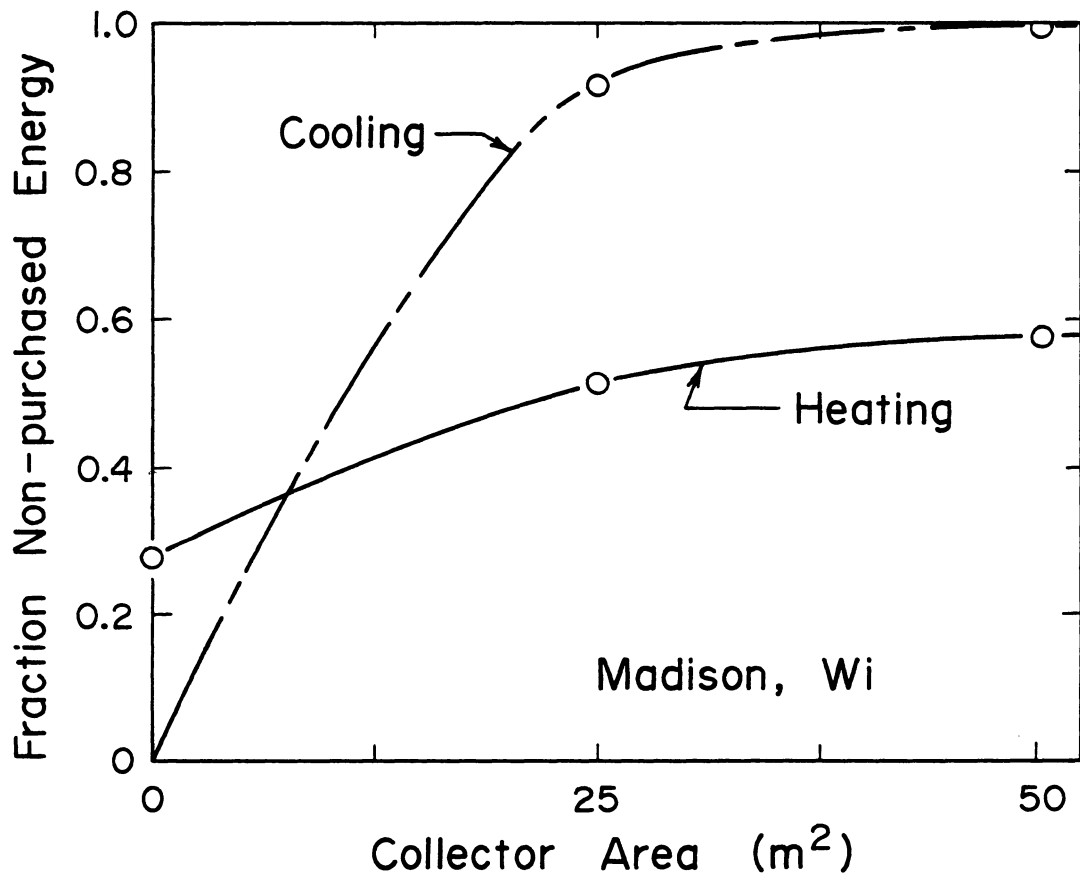


Figure 2-7 Effect of collector area on seasonal  $F_{NP}$  for AHP system in Madison

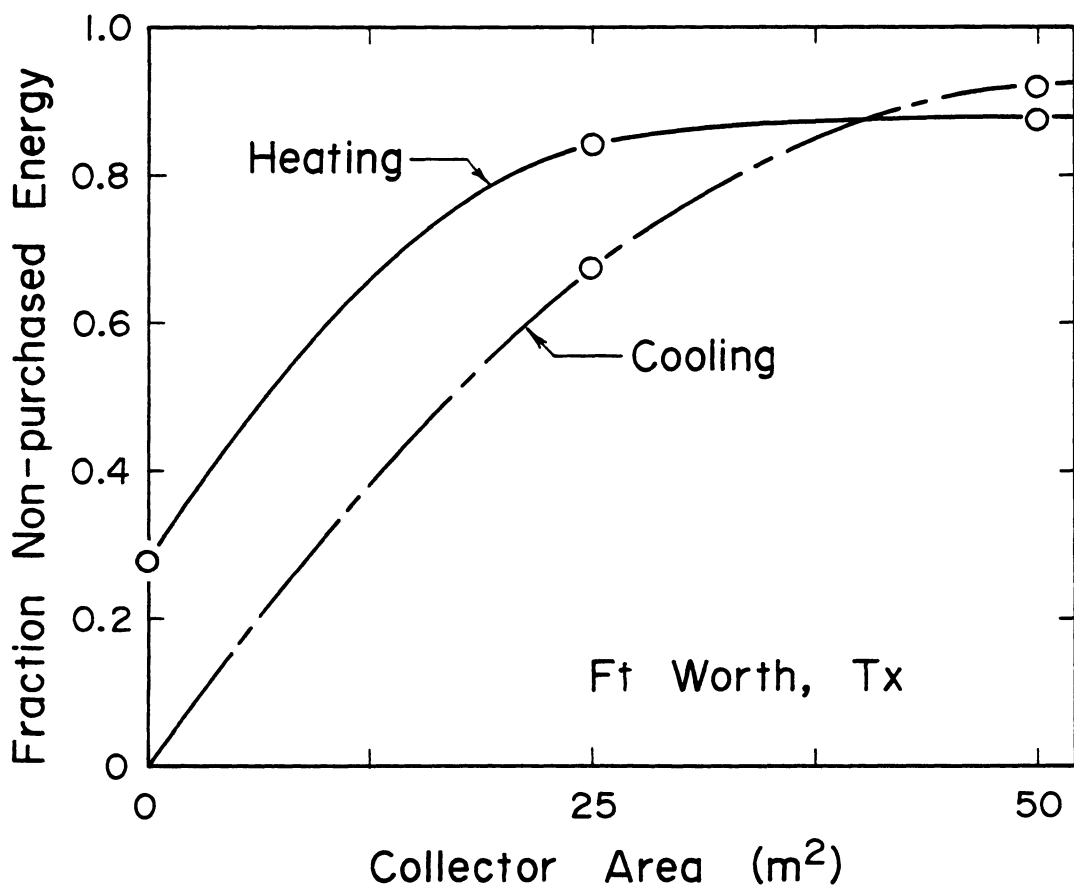


Figure 2-8 Effect of collector area on seasonal  $F_{NP}$  for AHP system in Fort Worth

Table 2-4 Effect of location and collector area on fraction non-purchased energy, load, and non-purchased energy delivered to the load for systems with 1000 kg chemical storage

Collector Area (m <sup>2</sup> )	Heating			Cooling			Annual
	F <sub>NP</sub>	Q <sub>load</sub> (GJ)	Q <sub>NP</sub> (GJ)	F <sub>NP</sub>	Q <sub>load</sub> (GJ)	Q <sub>NP</sub> (GJ)	Q <sub>NP</sub> (GJ)
Madison							
0	0.28	55.5	15.5	0	-	0	15.5
25	0.52	57.0	29.4	0.92	11.3	10.4	39.8
50	0.58	57.4	33.2	0.99	12.3	12.2	45.4
Columbia							
0	0.27	34.6	9.5	0	-	0	9.5
25	0.64	36.5	23.4	0.81	19.8	16.0	39.3
50	0.70	36.8	25.9	0.98	21.5	21.1	47.0
Fort Worth							
0	0.28	11.9	3.3	0	-	0	3.3
25	0.84	13.6	11.5	0.67	33.6	22.7	34.2
50	0.88	13.8	12.1	0.92	35.9	33.0	45.1

of the load keep the room temperature higher in the winter and lower in the summer.) The total amount of non-purchased energy provided over the entire year is quite similar between the three locations except for the zero collector area case. The incremental gain in total non-purchased energy in doubling the collector area from  $25 \text{ m}^2$  to  $50 \text{ m}^2$  is small.

### 2.6.3 Effects of storage mass and additional thermal capacitance

The absorption heat pump configuration studied has the ability to store chemical and thermal energy. The energy storage capacity of an absorption heat pump is the energy deliverable to the load as the system goes from fully charged to fully discharged. Using the  $\text{NaSCN-NH}_3$  chemical system, the maximum mass fraction of absorbent is about 0.65 due to the crystallization limit. The minimum useful mass fraction is about 0.50, corresponding to a heat pumping temperature difference of 30 C. Thus, if there are equal masses of absorbent and refrigerant in the cycle (to give  $x = 0.50$  when fully discharged), the amount of "active" refrigerant, (i.e., the amount that must be boiled off to yield a concentration of 0.65), is 46 percent of the refrigerant or 23 percent of the total system mass.

In a fully charged system, 77 percent of the system mass is in the absorbent tank with a concentration of 0.65. During discharging, the other 23 percent of the mass enters the absorbent tank as refrigerant vapor, yielding a final state with all of the mass in the absorbent tank. Assuming equal initial and final temperatures, the internal energy change in this process is 410 kJ per kg of total

system mass. For a system able to store thermal energy, the thermal storage capacity of the chemicals over say a 30 C temperature swing can be added to yield a total energy storage capacity for heating of roughly  $500 \text{ kJ kg}^{-1}$ . By comparison, a water tank with a 30 C temperature swing stores about  $125 \text{ kJ kg}^{-1}$ ; the maximum swing for unpressurized water storage in a heating application would be about 60 C (e.g., from 95 C to 35 C), yielding a capacity of  $250 \text{ kJ kg}^{-1}$ .

The cooling energy storage capacity would approximately be the fraction of "active" refrigerant multiplied by its heat of vaporization or  $290 \text{ kJ kg}^{-1}$ . Stored thermal energy is not directly usable during the cooling season but, as will be seen, may have other performance benefits. Unpressurized hot water storage for a conventional lithium bromide-water absorption chiller would have a useful temperature swing of about 20 C (95 to 75 C). Taking into account a COP of 0.7 for the chiller, the cooling storage capacity would be  $50 \text{ kJ kg}^{-1}$ . The energy storage capacities for the sulfuric acid-water chemical system are  $1150 \text{ kJ kg}^{-1}$  for heating and  $870 \text{ kJ kg}^{-1}$  for cooling.

It was argued above that the ability to store thermal energy has performance advantages. It is difficult, however, to separate the effects of the thermal storage from those associated with the chemical storage. By adding additional thermal storage to the system, the effects of the thermal storage are amplified and can be investigated. This thermal capacity is at an intermediate temperature and can be contrasted with the hot or cold side storage usually employed in solar

AHP systems without chemical storage. The additional capacitance was modeled as a separate water tank surrounding (and having the same temperature as) the refrigerant or absorbent tank.

The effects of thermal capacitance were simulated using August weather data for Columbia with systems having 100 or 500 kg of chemical storage and 5000 kJ C<sup>-1</sup> of thermal storage (corresponding to roughly 1200 kg of water) added either to the refrigerant tank or absorbent tank or split between the two. The results given in Table 2-5 show a moderate increase in the fraction of non-purchased energy supplied to the load with either increased chemical storage or thermal capacitance.

Table 2-5 Effect of chemical storage mass and additional thermal capacitance on  $F_{NP}$  for AHP system in Columbia (August results)

Added thermal capacitance (kJ C <sup>-1</sup> )		$F_{NP}$	
ref tank	abs tank	m = 100 kg	m = 500 kg
0	0	0.63	0.71
2500	2500	0.68	0.75
5000	0	0.69	0.76
0	5000	0.67	0.73

Figures 2-9 and 2-10 show the monthly average distribution of rejected heat (the sum of  $Q_{cond}$  and  $Q_{abs}$ ) over the day for the two storage masses and four cases of added thermal capacitance. The

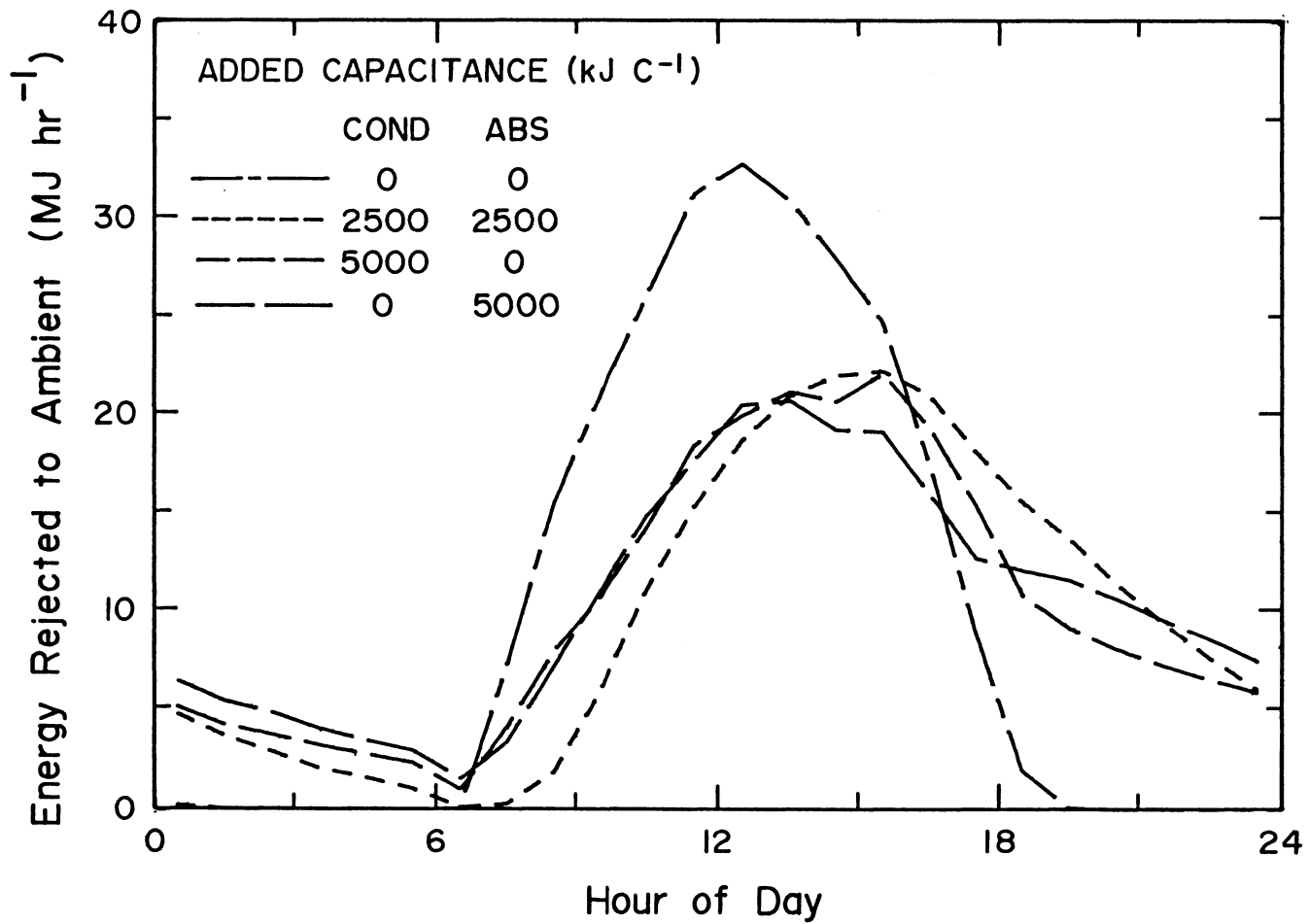


Figure 2-9 Monthly average diurnal distribution of heat rejected to ambient during August in Columbia for varying thermal capacitance added to storage tanks; chemical mass = 100 kg

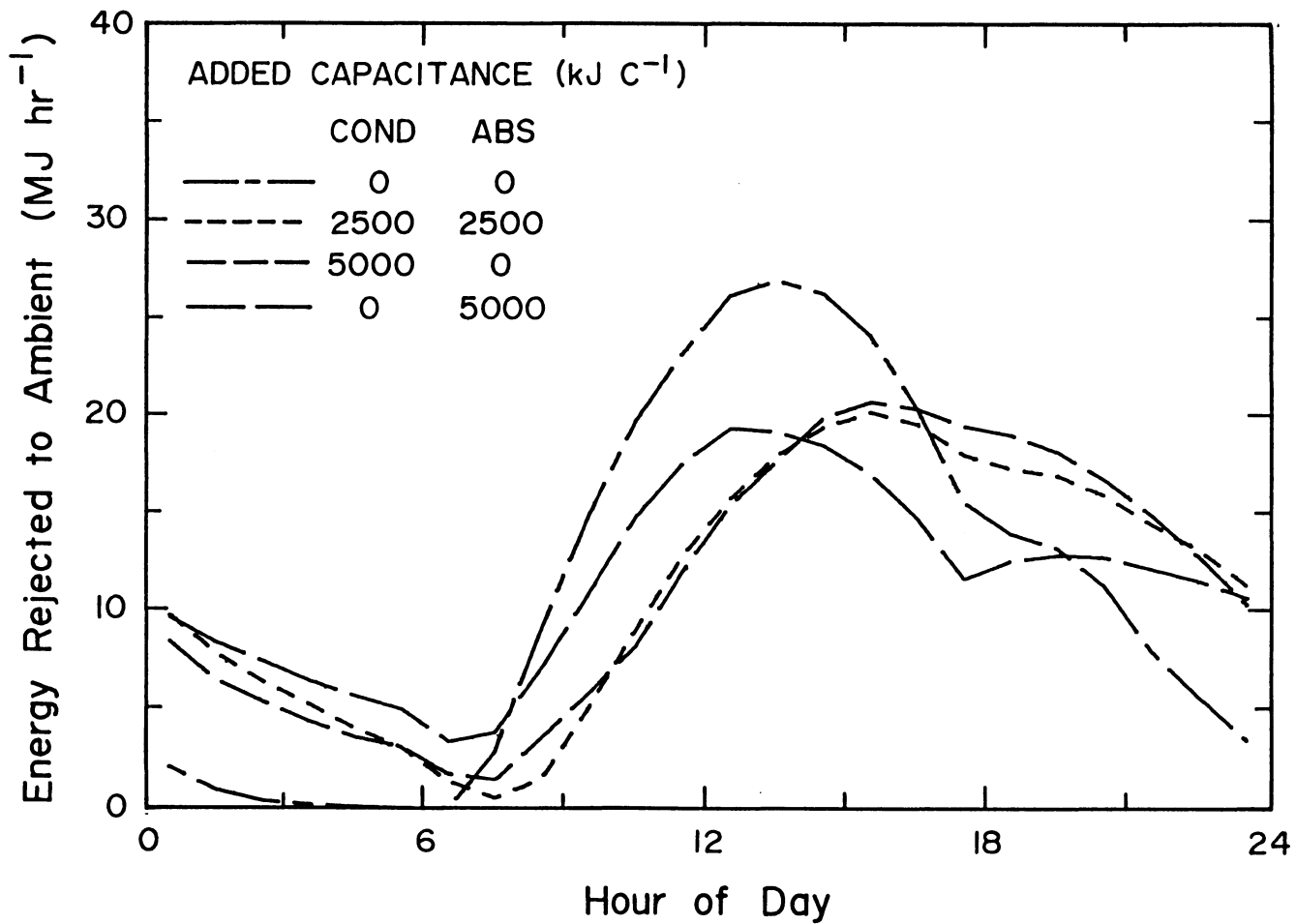


Figure 2-10 Monthly average diurnal distribution of heat rejected to ambient during August in Columbia for varying thermal capacitance added to storage tanks; chemical mass = 500 kg

system with 100 kg of chemical storage and no additional thermal capacitance is typically fully discharged at 8:00 pm and cannot operate again until solar is input the next morning. With additional chemical storage the system does not swing from fully discharged to fully charged back to discharged in the course of a day. Additional thermal capacitance and, to a lesser extent, greater chemical storage mass result in a more nearly even rejection of heat over the entire day. The combination of the larger storage mass and added thermal capacitance lowers the peak heat rejection rate from 33 to 19 MJ hr<sup>-1</sup> and shifts it to later in the day. This ability to level out the heat rejected to ambient might permit the use of a smaller ambient heat exchanger or a "dry" heat exchanger rather than an evaporative cooling tower. These results are not very sensitive to where the additional capacitance is placed; splitting it between the condenser and absorber appears to offer a compromise between highest  $F_{NP}$  and lowest peak heat rejection rate.

January results for a system with 500 kg of chemical storage and varying thermal storage are given in Table 2-6 and Figure 2-11. In heating operation, additional thermal capacitance in the absorbent tank lowers its temperature and results in greater heat extraction from ambient during daytime hours. The resulting lower daytime absorbent concentration leads to lower collector temperatures and a higher value of  $F_{NP}$ . There is less heat extracted from ambient during the night because of lower average absorbent concentrations as compared with the case of no added thermal capacitance. Adding

capacitance to the refrigerant tank has much less of an effect; there is little energy to store because the heat of condensation usually goes directly to the load. Increased tank losses (because of the larger tank surface area) decrease the value of  $F_{NP}$  for the case of 5000 kJ C<sup>-1</sup> added to the refrigerant tank.

Table 2-6 Effect of additional thermal capacitance on  $F_{NP}$ , absorbent tank concentration and collected energy for AHP system in Columbia (January results; chemical storage mass = 500 kg)

Added thermal capacitance (kJ C <sup>-1</sup> )		$F_{NP}$	$x_{abs}$	$Q_{col}$ (GJ)
ref tank	abs tank			
0	0	0.48	0.60	1.9
2500	2500	0.49	0.59	2.1
5000	0	0.46	0.60	1.8
0	5000	0.50	0.58	2.2

#### 2.6.4 Effects of chemical system

The effects of the refrigerant-absorbent pair on performance were investigated by simulating an AHP using the sulfuric acid-water chemical system, but otherwise having the base case parameters. The seasonal values of collector efficiency and COP for the sulfuric acid system (given in Table 2-7) are slightly higher than those for the NaSCN system (given in Table 2-3). The sulfuric acid system provides a significantly higher value of  $F_{NP}$ . Recall, however, that the

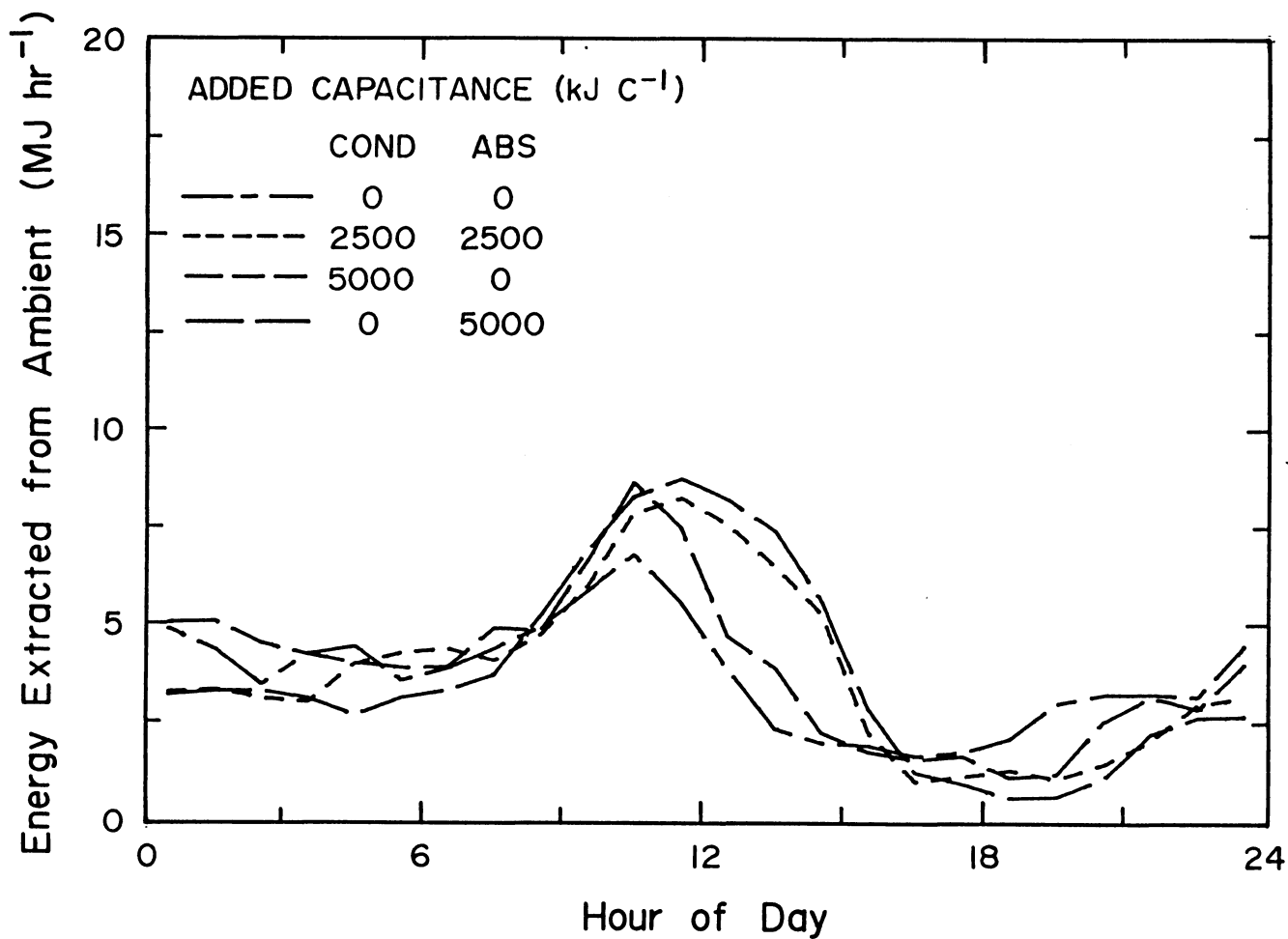


Figure 2-11 Monthly average diurnal distribution of heat extracted from ambient during January in Columbia for varying thermal capacitance added to storage tanks; chemical mass = 500 kg

sulfuric acid system was operated below the freezing point of water; thus the advantage of the  $\text{H}_2\text{SO}_4\text{-H}_2\text{O}$  system may not be practically realizable. This result is contrary to the speculation by Offenhartz (62) that the performance of all liquid absorbent chemical systems are similar; his conclusion was based on a limited comparison of the  $\text{H}_2\text{SO}_4\text{-H}_2\text{O}$  and  $\text{NH}_4\text{NO}_3\text{-NH}_3$  systems.

Table 2-7 Average collector temperature and efficiency, COP and fraction non-purchased energy for sulfuric acid-water AHP with 25 m<sup>2</sup> collector and 1000 kg chemical storage

	$T_{\text{col}}$ (C)	$\eta_{\text{col}}$	COP	$F_{\text{NP}}$
January	123	0.32	1.45	0.61
Heating season	163	0.24	1.37	0.73
July	100	0.42	0.66	0.81
Cooling season	111	0.40	0.59	0.89

The better performance of the sulfuric acid AHP is at least partially due to its higher equilibrium, steady-state COP (64). It also has a higher energy storage density and can pump heat across a slightly greater temperature difference than the  $\text{NaSCN-NH}_3$  system for a given charging temperature. (For example, a generator temperature of 80 C and a condenser temperature of 40 C would yield an equilibrium mass fraction in the generator of 0.52 for the  $\text{NaSCN}$  system and 0.63 for the  $\text{H}_2\text{SO}_4$  system; with these mass fractions in an absorber at 40 C, the equilibrium evaporator temperatures would be 6.8 C and 4.8 C for the  $\text{NaSCN}$  and  $\text{H}_2\text{SO}_4$  systems respectively.)

### 2.6.5 Effects of heat exchanger effectiveness

The sensitivity of performance to the effectiveness of the heat exchangers in the system was studied. The results are given in Table 2-8. The effectiveness of the counter-current heat exchanger between the generator and absorbent tank,  $\epsilon_{g-a}$ , was varied independently of all the others in the system,  $\epsilon$ . Heating season performance is not very sensitive to varying  $\epsilon_{g-a}$  but cooling season performance is quite markedly affected. With a lower  $\epsilon_{g-a}$  a greater fraction of the energy input to the generator is required merely to raise the temperature of the incoming stream to the generator temperature, leaving less energy to boil off refrigerant. (This effect is reflected in the ratio of  $Q_{cond}$  to  $Q_{abs}$ .) This is not a severe penalty in heating since this energy can be recovered in the absorbent tank, although at a COP of

Table 2-8 Effect of heat exchanger effectiveness on  $F_{NP}$  and the ratio of the heats of condensation and absorption for AHP system in Columbia (seasonal results)

$\epsilon$	$\epsilon_{g-a}$	$F_{NP}$		$Q_{cond}/Q_{abs}$	
		heat	cool	heat	cool
0.60*	0.75*	0.64	0.81	0.75	0.71
0.30	0.75	0.50	0.71	0.73	0.67
0.30	0.35	0.47	0.50	0.39	0.39

\*base case conditions

essentially unity. Cooling, however, can be produced only by the evaporation of refrigerant; thus anything which reduces the vapor production rate in the generator will affect performance.

#### 2.6.6 Effects of alternate control strategies

The effects of the two alternate heating season control options described earlier were investigated. The simulations were performed in the Columbia climate with  $25 \text{ m}^2$  of collector and 1000 kg of chemical storage and are compared to the base case results. Adding auxiliary energy through the heat pump takes advantage of its greater than one COP, but penalizes solar energy collection by raising the average absorbent concentration. This interaction is most pronounced when auxiliary input is high (i.e., mid-winter) and unimportant when solar is meeting a high fraction of the load as shown in Table 2-9. In April, solar supplies a high fraction of the load and the small quantity of auxiliary has little effect. In January, however, the alternate strategy of not supplying auxiliary through the generator significantly decreases the average absorbent concentration, resulting in lower collector temperatures, thus increasing the amount of solar energy collected. The overall performance (expressed by  $F_{NP}$ ), however, is reduced when auxiliary is not supplied through the generator. The gain in collector performance is more than offset by not taking advantage of the COP of the heat pump in the backup heating mode. This result applies to every month and the heating season as a whole.

Table 2-9 Effect of not supplying auxiliary energy through the heat pump on absorbent tank concentration, collector temperature, collected and auxiliary energy and  $F_{NP}$  for system in Columbia

A--Auxiliary through the heat pump (base case)

	$x_{abs}$	$T_{col}$ (C)	$Q_{col}$ (GJ)	$Q_{aux}$ (GJ)	$F_{NP}$
January	0.59	137	2.3	3.9	0.54
April	0.64	168	1.6	0.1	0.95
Heating season	0.61	151	14.7	12.9	0.64

B--No auxiliary input through the heat pump

January	0.56	121	2.8	4.5	0.45
April	0.64	169	1.7	0.1	0.94
Heating season	0.60	141	16.3	15.0	0.57

The benefit of a greater than one heating COP comes at the expense of higher collector temperatures and thus overall performance might be improved if solar energy could "bypass" the generator and supply energy to the lower temperature absorbent tank. This control option should be more important as the collector loss coefficient increases. A collector with a  $F_{R U_L}$  of  $3.3 \text{ W m}^{-2} \text{ C}^{-1}$  and a  $F_R(\tau\alpha)$  of 0.70 (representing a single-glazed, selective surface, flat plate collector) was simulated in addition to the base case (high performance) collector. Table 2-10 gives the results of these simulations.

For the high performance collector, the option of bypassing the generator resulted in a significantly larger total of collected energy as well as increased collector operating time. However, the value of  $F_{NP}$  is only slightly increased because much of the solar bypassing the generator is collected early and late in the heating season. During these times, the system is often fully charged and the collector is prevented from supplying energy to the generator. But it can (and does) supply energy to the absorbent tank where much of the additional collected energy is dissipated as increased tank losses. For this reason, the January results given in Table 2-10 are much more indicative of the actual merits of this strategy. These indicate that with high performance collectors there is a modest increase in  $F_{NP}$  as a result of this alternate control strategy.

The flat plate collector provided significantly less solar energy and gave a lower value of  $F_{NP}$  than the evacuated tubular collector.

Table 2-10 Effect of generator bypass control option and collector type on  $F_{NP}$ , collected energy, and collector operating time for system in Columbia

A--Evacuated tubular collector (seasonal results)

Bypass	$F_{NP}$	$Q_{col}$ (GJ)			col. on time (hrs)			
		gen	abs tank	total	gen	abs tank	total	
no*	0.64	14.7	0	14.7	698	0	698	
yes	0.67	10.7	11.3	22.0	480	654	1134	

B--Evacuated tubular collector (January results)

no*	0.54	2.3	0	2.3	112	0	112
yes	0.58	2.4	0.5	2.9	104	52	156

C--Flat plate collector (seasonal results)

no	0.47	7.6	0	7.6	400	0	400
yes	0.56	3.6	12.1	15.6	174	523	697

\*base case conditions

With the option of bypassing the generator, the collected energy and  $F_{NP}$  increased significantly (but were still lower than with the high performance collector). In this case, however, only 23 percent of the solar was input through the generator of the AHP. These results strongly suggest that a solar-driven absorption heat pump requires high performance collectors (such as evacuated tubes) for effective operation.

## 2.7 Summary and Conclusions for Solar AHP Systems

A model of an absorption heat pump which is based on mass and energy balances written around the components has been developed for use with TRNSYS. Simulations using this model have shown that a solar-driven AHP system can supply a significant fraction of a residential heating and cooling load with non-purchased energy. The annual non-purchased energy supplied to the load was similar for the three locations studied. In the Columbia climate, the AHP system gave a higher  $F_{NP}$  than a conventional solar heating system at small collector areas, while with larger areas, the  $F_{NP}$  of the two systems approached each other. In the cooling season, the AHP system gave a slightly lower  $F_{NP}$  than a solar-fired lithium bromide absorption chiller with hot water storage.

The collector temperatures are high and thus high performance collectors (such as evacuated tubes) are required for effective solar operation. The performance of the AHP is affected by the effectiveness of the heat exchangers in the system; the heat exchanger between the generator and absorbent tank has a large effect in cooling

operation. The refrigerant-absorbent pair has a significant effect on system performance, with the  $H_2SO_4$  system having better performance than the NaSCN- $NH_3$  pair.

The two alternative heating season control strategies investigated have little advantage in the Columbia climate compared to the baseline control strategy. Not supplying auxiliary energy through the heat pump increases solar energy collection at the expense of overall system performance. The option of "bypassing" the generator significantly improved performance only for the high loss collector studied.

Adding thermal capacitance and (to a lesser extent) additional chemical storage mass to the cycle had the effect of leveling out the daily profile of heat rejected to ambient during cooling operation. In the heating mode, additional thermal capacitance shifted the times of heat extraction from ambient more towards daytime hours. In most cases, additional thermal capacitance resulted in a higher value of  $F_{NP}$ . In cooling operation, the location of the additional capacitance had a small effect; in heating operation, however, adding thermal capacitance to the absorbent tank resulted in a larger gain in  $F_{NP}$  as compared to adding it to the refrigerant storage tank.

## CHAPTER 3

### EXPERIMENTAL INVESTIGATION OF AN ABSORPTION HEAT PUMP

An experimental investigation of an absorption heat pump was conducted during a five month period at the National Bureau of Standards in Gaithersburg, Maryland. The AHP was a prototype unit developed by Arkla Industries under contract to the U.S. Department of Energy and was sent to NBS for testing. This chapter describes the prototype heat pump and the experiments carried out at NBS. The results of this investigation are summarized by McLinden, Radermacher and Didion (73).

The testing of the heat pump was carried out in two phases. The overall steady-state and cyclic performance of the AHP as delivered by the manufacturer was first determined. A requirement of this phase of testing was to not make any modification to the machine which might affect its performance. With the first phase completed, a second series of tests designed to study the operation of the absorption cycle itself and to provide more detailed data for model verification were carried out. These tests required cutting into the cycle and varying the charge of the unit.

#### 3.1 Description of the AHP

In 1980, the U.S. Department of Energy contracted with Arkla Industries, Incorporated of Evansville, Indiana, to design an absorption heat pump and build a prototype. The design was to apply

the technology of existing absorption chillers to a heating application. The resulting unit was an air-to-water heat pump using ammonia and water as the refrigerant and absorbent. It is fired by natural gas and is designed for heating-only operation in a residential application. The complete absorption cycle, burner, controls, etc. are contained in a single package 1.22 by 0.52 by 0.99 m which would be located outside, only the load heat exchanger and load water circulating pump would be located inside.

The heat pump utilizes an ammonia-water absorption cycle (including an analyzer and rectifier) with the addition of a flue gas heat exchanger as shown in Figure 3-1. (This figure is adapted from a similar schematic provided by the manufacturer. The following description of the machine is drawn from conversations with Arkla engineers and inspection of the unit. This heat pump is also described by Kuhlenschmidt and Merrick (74).) The entire cycle is constructed of welded mild steel. A one percent sodium chromate solution acts as a corrosion inhibitor.

A single solution-filled vessel houses both the generator and analyzer. The generator comprises the lower segment of this vessel and is located within the burner box. The combustion products circulate around and transfer heat to the generator to boil off refrigerant vapor from the entering weak absorbent solution. The outlet for the resulting strong absorbent is located near the bottom of the generator.

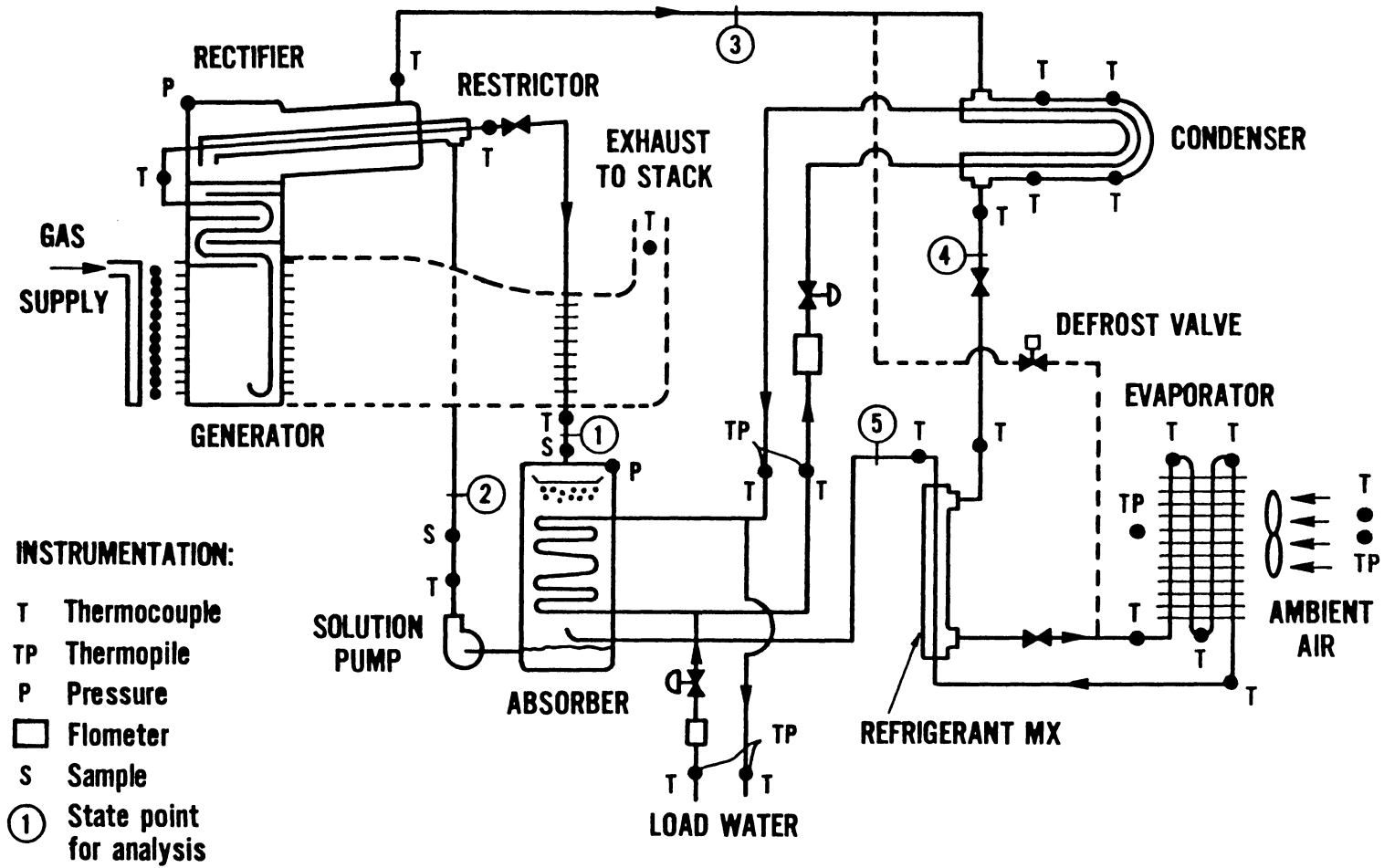


Figure 3-1 Schematic of the Arkla prototype absorption heat pump, including location of instrumentation

The analyzer countercurrently contacts the refrigerant vapor leaving and the weak absorbent entering the generator; the strong absorbent flows through the analyzer in a heat exchange coil. Baffle plates serve to increase the heat and mass exchange between the vapor and liquid. Mass transfer between the contacting streams removes water from the refrigerant vapor. The analyzer also acts as a heat exchanger, preheating the weak absorbent entering, and cooling the vapor and strong absorbent leaving the generator.

The rectifier further purifies the refrigerant vapor and heat exchanges the strong and weak absorbent streams. This component is a vessel extending horizontally from the vapor space at the top of the analyzer and contains a concentric tube heat exchanger. This "triple heat exchanger" preheats the weak absorbent flowing in the annulus by both cooling the strong absorbent flowing in the inner tube and partially condensing, and thus purifying, the refrigerant vapor on the outside of the heat exchanger. The condensate and weak absorbent mix as they flow into the analyzer.

The condenser is a concentric tube heat exchanger. Refrigerant vapor condenses in the annulus, transferring heat to the load heat exchange stream flowing countercurrently in the inner tube. To save space and reduce heat losses to ambient, the condenser is fabricated as a helical coil which fits around the absorber.

The refrigerant is vaporized by heat transfer with ambient air in the evaporator where it flows in series through three finned coils. A four-bladed fan blows ambient air across the coils. Defrosting of the

evaporator coil is accomplished by routing refrigerant vapor from the rectifier through the solenoid-operated defrost valve directly to the evaporator. During a defrost cycle, which lasts for approximately seven minutes, the burner, solution pump and fan are off and the residual heat in the cycle is utilized. A defrost is called for when the difference between the ambient and evaporator outlet temperatures exceeds a given value which depends on ambient temperature. In this prototype unit, these temperatures were monitored and the defrost cycle initiated manually.

The refrigerant streams entering and leaving the evaporator flow through the concentric tube refrigerant heat exchanger. For conditions where a high quality stream exits the evaporator, this heat exchanger increases the heat extracted from the ambient by reducing the quality of the evaporator inlet stream, thus increasing the amount of refrigerant that can be vaporized. The enthalpy of the absorber inlet is also increased. For conditions where a two phase stream enters the absorber, the refrigerant heat exchanger has little effect (and perhaps a detrimental effect by promoting a higher mass flow of refrigerant through the throttle.)

The Arkla AHP has two fixed-orifice throttling devices between the condenser and evaporator. The presence of a throttle ahead of the refrigerant heat exchanger would seem to be detrimental to the performance of that component. The pressure of the liquid refrigerant leaving the condenser is reduced to a value intermediate between the low and high side pressures. Because of flashing in the throttle, the

available temperature difference in the refrigerant heat exchanger is thus reduced.

Two throttle valves are used not to improve performance so much as to avoid the even worse performance that would result under certain conditions if only a single fixed orifice throttle were used (75). Under conditions where a two-phase mixture exits the evaporator, the heat transfer in the refrigerant heat exchanger is increased, resulting in increased sub-cooling of the refrigerant stream entering the throttle. As the quality of the throttle inlet stream decreases, the flow rate through the throttle for a given pressure drop increases. Thus, with a single throttle, a two-phase stream leaving the evaporator would result in a higher refrigerant flow rate which would further decrease the quality of the evaporator outlet. The throttle at the condenser outlet always provides some degree of flow control, although not eliminating this problem entirely. (This problem is associated with fixed throttles and would not be present with a controllable throttle. Fixed orifice throttles were used because of their lower first cost and greater reliability.)

In the falling-film type absorber, absorbent solution enters at the top and is distributed over heat exchange tubing wound into a helical coil. As the solution flows over the tubes and drips between rows, it absorbs refrigerant vapor. The resulting heat of absorption is transferred to the load heat exchange fluid flowing countercurrently within the tubes. The refrigerant inlet is near the bottom of the absorber. Any liquid entering with the refrigerant, along with the

weak absorbent dripping off the bottom row of heat exchange tubes, flows into a sump at the bottom of the absorber.

The inlet of the solution pump is coupled to the absorber and draws solution out of the sump. The positive displacement, diaphragm-type pump is hydraulically driven by a separate hydraulic pump.

The flue gas heat exchanger uses the exiting flue gases to heat the strong absorbent solution flowing to the absorber. This component extracts additional energy from the natural gas input and delivers it to the load heat exchange fluid in the top rows of the absorber. The higher strong absorbent temperature reduces the vapor capacity of the absorber, reducing to some extent the benefit of a higher combustion efficiency.

### 3.2 Test Facility

The test facility for absorption heat pumps at the National Bureau of Standards is centered around an environmental chamber. Much of the load water apparatus and instrumentation and data logging equipment were previously installed for investigations of an absorption chiller carried out by Lindsay and Didion (76) and Rademacher, Klein and Didion (77). This facility is shown schematically in Figure 3-2.

#### 3.2.1 Environmental chamber

The heat pump was tested in an environmental chamber with controlled dew point and dry bulb air temperatures. The desired dew

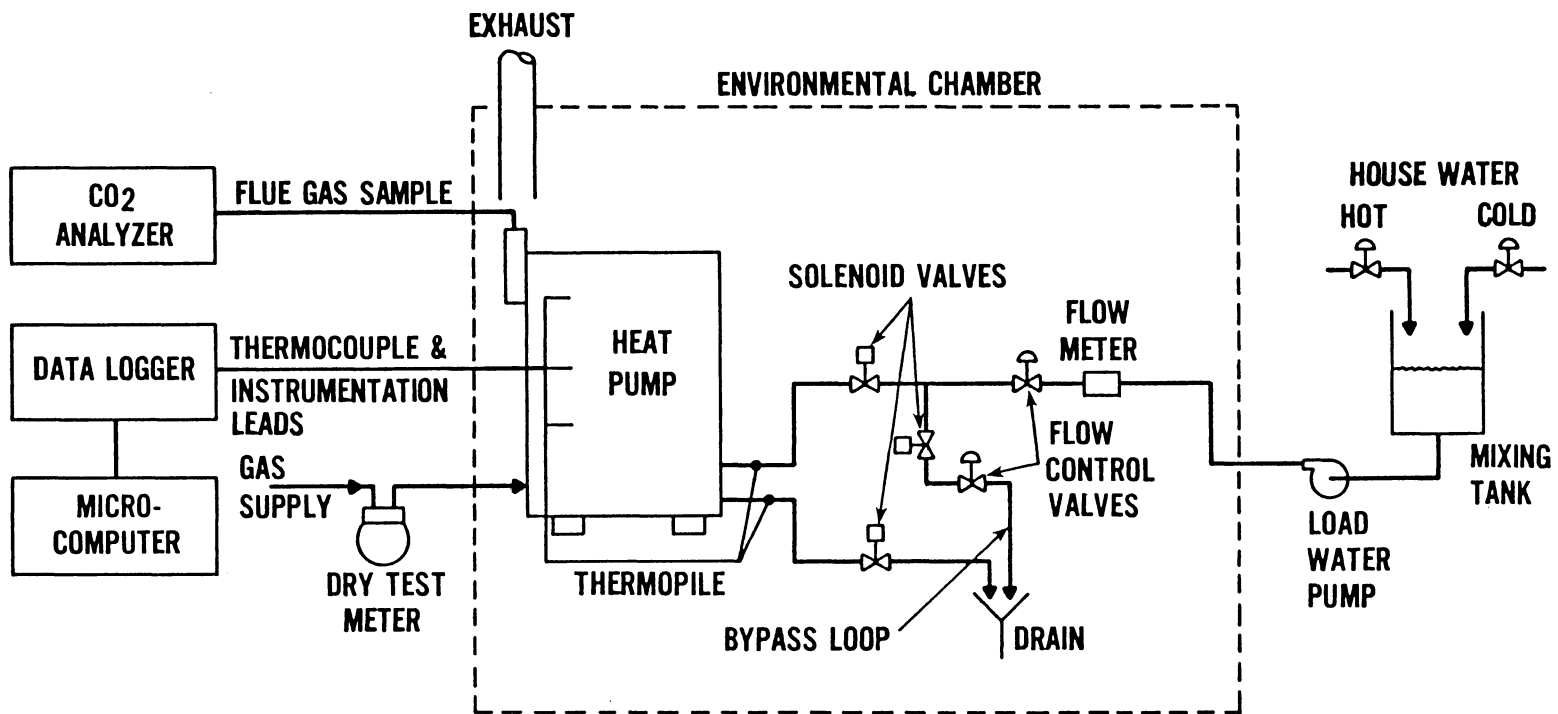


Figure 3-2 Heat pump test facility at the National Bureau of Standards

point temperature was obtained by passing the supply air through a cooling coil which was sprayed with water or an antifreeze solution to insure a saturated leaving air stream. This air stream was then brought to the desired dry bulb temperature by electric heating coils and delivered to the chamber through a plenum extending across the entire ceiling area. A uniform temperature was further insured by an additional circulating fan installed near the floor. The chamber air temperature was maintained within  $\pm 0.3$  C of a constant value during steady-state tests and within  $\pm 1$  C during cyclic tests. The flue gases were exhausted to the outside through a flexible duct installed near the heat pump stack.

### 3.2.2 Load water system

In normal operation, an antifreeze solution would circulate in a closed loop between the heat pump and the indoor heating coil. In the test facility, a once-through flow arrangement with tap water was employed. Hot and cold tap water were mixed in a supply tank and pumped into the environmental chamber. The flow rate was controlled by a pair of globe valves. Solenoid-operated valves either sent the flow to the heat pump or diverted it to the drain. This flow arrangement eliminated any transient effects of an indoor coil during cyclic operation and provided an constant ( $\pm 0.2$  C) water temperature to the heat pump.

Inside the heat pump, the load water split and flowed in parallel to the condenser and absorber. This flow split was preset by the manufacturer to provide approximately equal flows to the absorber and

condenser (78). After the first series of tests were completed, the internal piping of the heat pump was modified to independently control and measure these two flows.

### 3.2.3 Instrumentation

The mass flow rate of the load water was measured with a IIT-Barton turbine flow meter connected to a frequency counter. The temperature rise of the load water in flowing through the AHP was measured with a 16 junction copper-constantan thermopile installed in thermowells just outside of the machine. Thermocouples were also installed in the thermowells to determine the water temperature.

The ambient air temperature was measured with a 14 junction averaging thermocouple installed on the inlet louvers to the evaporator. To determine relative humidity, the wet bulb temperature was measured. For tests below freezing, the dew point temperature was either measured with a EG&G dew point hygrometer or taken to be the temperature of the cooling coil of the environmental chamber.

The natural gas input to the burner was measured with a Sprague dry volume flow test meter. The gas temperature and pressure were measured at the meter inlet with a thermocouple and manometer, respectively. The volume of gas used by the heat pump over a given time period was corrected to standard conditions and multiplied by the higher heating value of the gas, which was determined by a calorimeter on the NBS site, to obtain the energy supplied. The heat lost through the exhaust stack was determined by a combustion analysis. A sample of the flue gases was drawn continuously and passed through a

desiccant column. The CO<sub>2</sub> content of the flue gas was measured with an MSA Lira infrared analyzer which was calibrated using standard CO<sub>2</sub> samples. A Lynn oxygen analyzer was also used. The resulting values of excess combustion air were averaged and combined with the temperature of the flue gases (measured with a six junction averaging chromel-alumel thermocouple) to compute the burner efficiency.

In addition to these data, the temperatures at various point in the cycle (as indicated in Figure 3-1) were measured with copper-constantan thermocouples attached to the outside of the tubes. The thermocouple sites were heavily insulated. The pressure in the rectifier and absorber vapor spaces were measured with Transducers, Inc. pressure transducers. Bourdon tube pressure gauges were also installed on the same pressure taps. The electrical energy needed to power the solution pump, fan, and controls was measured with a General Electric watt-hour meter connected to a Landis and Gry pulse counter.

The output signals of the thermocouples, thermopiles, and pressure transducers were scanned by a Fluke data logger and transferred to a Cromenco or Hewlett-Packard microcomputer for storage and later analysis. The remaining instrumentation readings were recorded manually. The output of the load water thermopile was also sent to an Esterline-Angus strip chart recorder; this provided a trace of the heating capacity of the heat pump and was the primary indicator of whether steady-state operation had been reached.

After the first series of tests were completed, additional instrumentation was installed. A Foxboro turbine flow meter and

control valve were installed in the load water line to the condenser. A 10 junction copper-constantan thermopile was installed between the inlet water thermowell and a thermowell at the condenser outlet. These measurements allowed the heat of condensation to be calculated.

A thermopile was installed to measure the temperature drop of the air flowing across the evaporator. The air velocity was measured by a 35 point traverse of an Envit vane anemometer across the face of the evaporator coil. The temperature difference was multiplied by a measured correction factor to account for the non-uniform temperature distribution and combined with the average air velocity to calculate the ambient heat supplied to the evaporator.

Sample taps for the strong and weak absorbent were provided by the manufacturer at the absorber inlet and solution pump outlet, respectively. Small diameter tubing was run from these taps to the outside of the heat pump cabinet and terminated in needle valves. Solution samples were taken and analyzed by titration as described in Section 3.3.2. Finally, a Flow Technology turbine flowmeter was installed in the strong absorbent line near the absorber inlet.

### 3.3 Test Procedure

#### 3.3.1 Steady-state tests

The steady-state tests followed, where applicable, the procedures outlined by Parken, et al. (79) for the testing of vapor compression heat pumps. The heat pump, environmental chamber, and load water supply were operated until steady conditions were obtained (typically

90 minutes). A steady-state test lasting for 30 minutes was then started. The data logger recorded thermocouple, thermopile, and pressure transducer readings every two minutes; the gas, electric and turbine meters were recorded at the beginning and end of the test. The combustion analysis was done midway through the test. Average values for all measurements were then used for analysis.

The primary indices used for the performance of the AHP were COP and capacity. The heating capacity of the unit was determined by the flow rate and temperature rise of the load water:

$$\dot{Q}_{\text{load}} = \dot{m}_{\text{load}} C_p \Delta T_{\text{load}} \quad [3-1]$$

with the literature value of the heat capacity of water being used. The coefficient of performance is defined as:

$$\text{COP} = \frac{\dot{Q}_{\text{load}}}{\dot{Q}_{\text{gas}} + \dot{E}_{\text{elec}}} \quad [3-2]$$

where  $\dot{Q}_{\text{gas}}$  and  $\dot{E}_{\text{elec}}$  are the gas and electric energy inputs to the heat pump.

### 3.3.2 Absorbent solution sampling

Sampling of the strong and weak absorbent solution was done immediately after the conclusion of a steady-state test with the heat pump still operating. The strong and weak absorbent streams are sub-cooled liquids at the operating pressure of the AHP but flash to a two-phase mixture at atmospheric pressure. In order to prevent the loss of ammonia, samples were taken into a solution of sulfuric acid.

The sample lines were purged into flasks containing 125 ml of 5 N (for the strong absorbent sample) or 1 N sulfuric acid for the weak absorbent sample until a methyl red indicator changed color. (This quantity of acid corresponded to the flow of solution necessary to purge the sample line volume.)

A sample was taken into a preweighed 125 ml flask containing 50.0 ml of sulfuric acid of known normality (approximately 1.00 N) and methyl red indicator. The solution was allowed to flow from the sample line through a short length of flexible tubing, into glass tubing extending into the acid at the bottom of the flask until the indicator changed color. The tubing was then stoppered. A duplicate sample was taken and the procedure repeated for the other sample tap. The flasks were reweighed (using a Mettler analytical balance) to determine the quantity of sample taken and titrated back to the endpoint with sulfuric acid to determine the amount of ammonia in the sample. The ammonia concentration of the absorbent solution could then be calculated.

### 3.3.3 Cyclic tests

In the cyclic tests, which also followed the procedures of (79), part load operation was simulated by manually cycling the heat pump on and off. The chamber and water supply were allowed to reach the desired conditions and then the heat pump was turned on and operated until the capacity just reached its steady-state value as indicated by the strip chart recorder. The unit was then turned off for the predetermined time and cycled on and off for two or three complete

cycles until a reproducible capacity behavior was observed. The next cycle was then used for the determination of cyclic performance. During the "off" portion of the cycle, load water did not flow through the heat pump but the load water system continued to operate with the water being diverted past the heat pump to insure a constant temperature.

The total heat provided by the AHP during a cycle is given by:

$$Q_{\text{load,cyc}} = \dot{m}_{\text{load}} C_p \int_{t_0}^{t_2} \Delta T dt \quad [3-3]$$

where the temperature rise of the water flowing through the unit,  $\Delta T$ , is integrated between  $t_0$ , the time at which the unit is turned on and  $t_2$ , when the machine shuts off. This was determined by integrating with a planimeter the output of the load water thermopile recorded on the strip chart recorder. The energy input to the machine during a cycle is the sum of the gas input from  $t_0$  to  $t_1$ , the time that the burner was operating, and the electrical input for the entire cycle length,  $\tau$ . (The heat pump continues to operate for a 3.5 to 4 minute "spindown" period after the burner shuts off to recover residual heating capacity.) The cyclic coefficient of performance is:

$$\text{COP}_{\text{cyc}} = \frac{Q_{\text{load}}}{\int_{t_0}^{t_1} \dot{Q}_{\text{gas}} dt + \int_0^{\tau} \dot{E}_{\text{elec}} dt} \quad [3-4]$$

Here the integration is done by the gas and electric meters.

The cyclic performance can also be expressed as a fraction of the steady-state performance. The heating load factor,  $\Gamma_h$ , represents the fractional capacity in cyclic operation:

$$\Gamma_h = \frac{Q_{\text{load,cyc}}}{\tau} \frac{1}{\dot{Q}_{\text{load,ss}}} \quad [3-5]$$

where  $Q_{\text{load,ss}}$  is the steady-state capacity at the same ambient temperature. The COP penalty in cyclic operation is given by the part load factor:

$$\text{PLF} = \frac{\text{COP}_{\text{cyc}}}{\text{COP}_{\text{ss}}} \quad [3-6]$$

where  $\text{COP}_{\text{ss}}$  is the steady-state coefficient of performance.

### 3.4 Steady-State Test Results

#### 3.4.1 Overall performance tests

In the first series of tests, the performance of the heat pump in steady-state operation was tested over a range of ambient and inlet load water conditions. The coefficient of performance and capacity for a range of ambient temperatures are shown in Figure 3-3 for a load water temperature of 41 C and flow rate of 0.38 l sec<sup>-1</sup> (which are the manufacturer's design conditions). The COP and capacity curves have similar shapes because of the nearly constant energy inputs. The gas input varied from 13.4 to 14.3 kW and the electric input from 0.55 to 0.65 kW; both inputs were higher at lower temperatures.

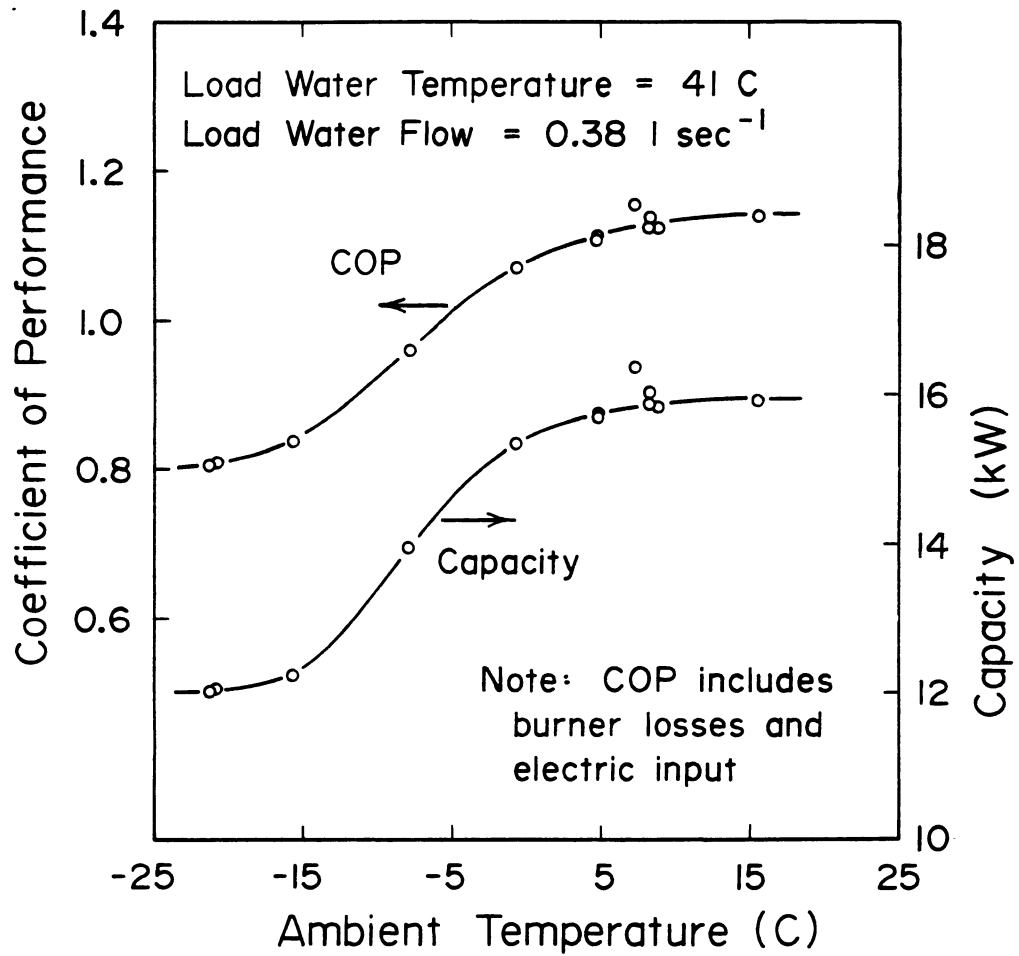


Figure 3-3 Coefficient of performance and heating capacity for the Arkla AHP as a function of ambient temperature

The performance levels off at both high and low ambient temperatures. Below about 0 C, a two-phase mixture of liquid and vapor refrigerant exits the evaporator; this was indicated by a constant temperature profile through the evaporator. At the extreme case of -21 C, the COP of 0.81 is slightly lower than the combustion efficiency of 0.84; thus, any heat extracted from ambient is offset by heat losses from the unit. Above about 5 C, the performance is relatively insensitive to ambient temperature, indicating that the evaporator (i.e., the only component having significant heat exchange with the ambient) is not the limiting component in the cycle under these conditions.

Most of these tests were carried out at an ambient relative humidity of approximately 80 percent as directed by (79). Although frost might be expected to form on the evaporator coil at this humidity, very little actually did because of the small temperature drop of the ambient air flowing across the evaporator.

The effect of varying inlet load water temperature on COP is shown in Figure 3-4. At ambient temperatures of -21 C and -9 C, the COP decreases as inlet water temperature increases. At an ambient temperature of 8 C, performance does not depend on water temperature over the range investigated.

The load water flow rate was varied 6 percent above and 16 percent below the nominal value of  $0.38 \text{ l sec}^{-1}$  at 8 C and -8 C ambients with only minor effects on COP and capacity as indicated in Table 3-1. A wider variation in flow rate, especially lower flows,

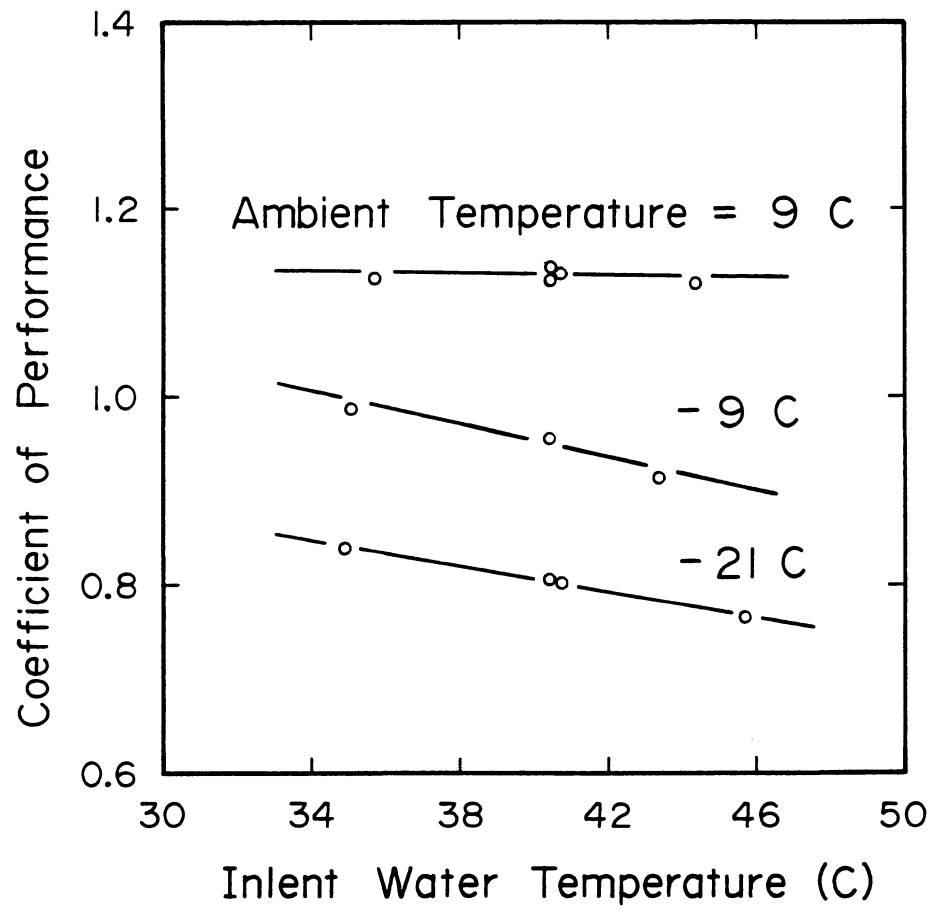


Figure 3-4 Effect on COP of varying inlet load water temperature for three ambient temperatures

would be expected to result in a greater variation in performance. The range of flow rates was constrained. The load water pump was not capable of flows over  $0.4 \text{ l sec}^{-1}$ . At flows below about  $0.3 \text{ l sec}^{-1}$ , a high temperature limit switch on the load water outlet shut off the burner. (This safety device is designed to sense a low flow of load water and prevent the resulting high pressure in the condenser.)

Table 3-1 Effect of varying load water flow on the COP and heating capacity of the Arkla AHP for two ambient temperatures

Load flow ( $\text{l sec}^{-1}$ )	Ambient Temperature (C)	COP	Capacity (kW)
0.32	-9.0	0.98	14.2
0.37	-8.0	0.96	13.9
0.40	-8.9	0.98	14.3
0.32	8.4	1.13	15.9
0.37	8.2	1.13	15.8

#### 3.4.2 Cycle investigation tests

Upon completion of the first set of tests, the additional instrumentation described in Section 3.2.3 was installed. A second set of steady-state tests was carried out to more closely examine the individual components of the absorption cycle and to investigate the design variables of load water split and refrigerant charge. These tests were carried out with dew point temperatures sufficiently low to ensure no frost or condensation on the evaporator coil.

The split of load water between the condenser and absorber was investigated at -8 C and 8 C ambients. The most pronounced effect is in the pressures as indicated in Table 3-2. With a higher flow through the condenser, the high side (generator and condenser) pressure is decreased and the low side (absorber and evaporator) pressure is increased. A small, but interesting, effect is seen in the solution concentrations. At higher condenser flows, the ammonia concentration in the strong absorbent is lower, presumably because more ammonia is contained in the condenser as a liquid. This would decrease the ammonia fraction in the generator and is also consistent with the lower generator pressure. The effect on COP is small, indicating that, at least for the total flows investigated, the cooling water split is not a critical parameter. (For all subsequent tests, the condenser and absorber flows were equal.)

Table 3-2 Effects of varying condenser and absorber flows on system pressures, concentrations, and COP

Total flow (l/sec)	Fraction of total to cond	Ambient Temp (C)	Pressure (MPa)		NH <sub>3</sub> conc		COP
			gen	abs	strong	weak	
0.34	0.33	-8.9	2.25	0.24	0.137	0.322	0.97
0.34	0.50	-8.7	2.10	0.25	0.134	0.320	0.97
0.35	0.35	8.3	2.25	0.35	0.179	0.367	1.18
0.33	0.51	8.6	2.20	0.38	0.173	0.369	1.16
0.28	0.67	8.3	2.17	0.42	0.162	0.361	1.16

The performance of this absorption heat pump is sensitive to the total amount of refrigerant in the cycle. This is a result of the interaction between the absorber and the rest of the cycle. As the ambient temperature decreases, the evaporator temperature and thus evaporator and absorber pressure also decrease. Because the absorber operates at a relatively constant temperature (determined largely by the load water temperature), a lower pressure dictates a lower (i.e., stronger) concentration for the absorbent. The majority of the absorbent in the cycle is contained in the generator, analyzer and absorber; since the absorption cycle is closed, the total amount of absorbent is constant and a lower absorbent concentration can be achieved only by displacing refrigerant contained in these components to elsewhere in the cycle.

This excess refrigerant will accumulate in the evaporator, condenser, and refrigerant heat exchanger. But not all of the excess refrigerant can be displaced out of the generator, analyzer, and absorber, leading to a higher than optimum absorbent concentration. The result is a higher than optimum low side pressure, reducing the temperature difference for heat pumping in the evaporator and resulting in a two-phase mixture exiting the evaporator at low ambient temperatures. Conversely at high ambient temperatures there is insufficient refrigerant in the system, resulting in an excessively low evaporator pressure and temperature.

To study these effects, the refrigerant charge of the heat pump was varied above and below the original charge of the unit. (The

total amount of water in the cycle was not varied except to periodically replace the small amount lost in sampling.) The effects of refrigerant charge on evaporator pressure and temperature are given in Table 3-3. At the lower ambient temperature, higher refrigerant charges result in a two-phase mixture leaving the evaporator, as indicated by the low values of  $Q_{\text{evap}}$  (the rate of heat extraction from ambient) and the identical evaporator inlet and outlet temperatures. As the charge was reduced, the evaporator pressure decreased and the temperature difference between the ambient and evaporator increased, thus increasing  $Q_{\text{evap}}$ . At the lowest charge, the small temperature rise for the refrigerant leaving the evaporator indicates nearly complete vaporization. (Because of the small quantity of water in the refrigerant, this temperature rise indicated a high quality, rather than superheated, stream.)

At the higher ambient temperature (8 C), the lower ammonia charges also resulted in lower evaporator pressures and temperatures. But since the exiting refrigerant was nearly completely vaporized for all cases at this temperature, the effect on  $Q_{\text{evap}}$  was much smaller.

The dependence of solution concentrations on the refrigerant charge and ambient temperature are also given in Table 3-3. The absorbent concentrations were lower at the lower ambient temperature. They were also lower with reduced refrigerant charges; this is consistent with the lower absorber pressures observed. It is interesting to note the nearly constant difference of 0.19 between the strong and weak absorbent concentrations.

Table 3-3 System pressures and concentrations, and evaporator conditions for varying refrigerant charges and ambient temperatures

Relative NH <sub>3</sub> charge (kg)	Ambient Temp (C)	Pressure (MPa)		NH <sub>3</sub> conc		Evap Temp (C)		$\dot{Q}_{\text{evap}}$ (kW)
		gen	abs	strong	weak	inlet	outlet	
+1.0	-9.1	2.15	0.27	0.169	0.363	-10.8	-10.9	0.9
+0.6	-8.4	2.14	0.26	0.149	0.342	-11.2	-11.3	2.2
0	-8.7	2.10	0.25	0.134	0.320	-12.1	-12.1	2.8
-0.5	-8.9	2.10	0.21	0.096	0.280	-13.7	-12.5	5.5
+1.0	8.8	2.22	0.44	0.200	0.393	2.4	3.4	6.5
+0.6	8.0	2.22	0.41	0.186	0.381	0.8	8.0	7.0
0	8.6	2.20	0.38	0.173	0.369	-0.4	8.8	6.6
-0.5	7.5	2.15	0.27	0.129	0.316	-7.5	6.8	7.1

Ammonia charge is relative to original charge of heat pump

The overall effect of a decreased refrigerant charge is to give a more nearly constant COP over a range of ambient temperatures as shown in Figure 3-5. An increased charge improves the performance at high ambient temperatures but decreases it at low temperatures; a reduced charge results in a more nearly constant COP over a range of ambient temperatures.

According to the manufacturer(78), the optimum refrigerant charge would result in a temperature difference between the ambient and evaporator sufficient to result in a small (2 C) temperature rise for the refrigerant flowing through the evaporator. A higher temperature rise would require a lower absorber pressure; no temperature rise would indicate incomplete vaporization in the evaporator. The charge of the unit as received from the manufacturer was optimized for operation at an ambient temperature of approximately 2 C. The highest and lowest charges investigated were optimized for 8 C and -8 C ambients, respectively.

#### 3.4.3 Component analysis

A turbine flowmeter was installed in the cycle to measure the flow rate of the strong absorbent (absorber inlet) stream. This flow information, along with pressure, composition and temperature measurements taken at various points in the cycle allowed the computation of the heat flows for the various components in the cycle. These calculated heat flows can then be compared to measured quantities, providing a check on the consistency of the measurements.

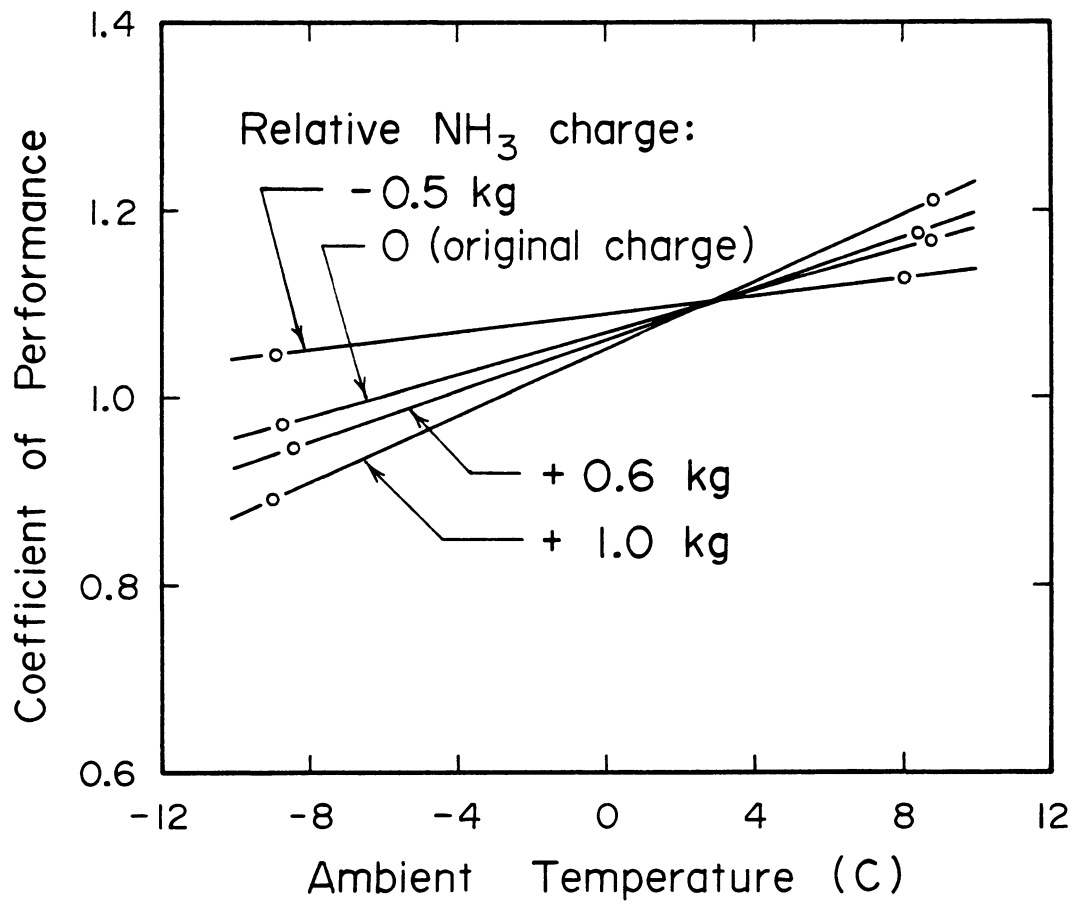


Figure 3-5 COP of the Arkla AHP as a function of ambient temperature and relative refrigerant charge

Overall and ammonia mass balances can be written for the absorber to yield the weak absorbent and refrigerant flowrates in terms of the (measured) strong absorbent flowrate,  $\dot{m}_1$ , and concentrations:

$$\dot{m}_5 = \dot{m}_1 \frac{x_2 - x_1}{x_5 - x_2} \quad [3-7]$$

$$\dot{m}_2 = \dot{m}_1 + \dot{m}_5 \quad [3-8]$$

where the subscripts refer to state points indicated in Figure 3-1. The refrigerant composition,  $x_5$ , was found by assuming the vapor leaving the rectifier to be saturated at the measured temperature and pressure. The heat flows for the generator, condenser and evaporator can be found by energy balances (for this analysis, the generator, analyzer, rectifier, and flue gas heat exchanger are treated as a single unit as are the evaporator and refrigerant heat exchanger):

$$\dot{Q}_{\text{gen}} = \dot{m}_1 h_1 + \dot{m}_3 h_3 - \dot{m}_2 h_2 \quad [3-9]$$

$$\dot{Q}_{\text{cond}} = \dot{m}_4 h_4 - \dot{m}_3 h_3 \quad [3-10]$$

$$\dot{Q}_{\text{evap}} = \dot{m}_5 h_5 - \dot{m}_4 h_4 \quad [3-11]$$

The solution pump is considered along with the absorber to yield:

$$\dot{Q}_{\text{abs}} = \dot{m}_2 h_2 - \dot{m}_1 h_1 - \dot{m}_5 h_5 - \dot{E}_{\text{pump}} \quad [3-12]$$

Note that  $\dot{Q}_{\text{abs}}$  includes not only the heat evolved in the absorption of ammonia vapor but also the sensible cooling of the hot inlet stream exiting the flue gas heat exchanger. The pump work plus losses

imparted to the fluid were estimated to be 120 W.

The conditions existing in the various streams for a test at 8 C and standard flow conditions are given in Table 3-4. The ammonia-water properties given by the Institute of Gas Technology (80) were used. The results of the energy balance calculations, along with the measured heat quantities are given in Table 3-5. The agreement between the calculated and measured heats of condensation is very good and confirms the usual practice of calculating the flow rates based on that heat measurement. The fact that the measured  $\dot{Q}_{\text{cond}}$  is high is consistent with the condenser being a concentric tube heat exchanger which is physically wrapped around, and in thermal contact with, the warmer absorber. A portion of the difference in  $\dot{Q}_{\text{abs}}$  would also be accounted for by a heat loss to the condenser. The discrepancy in the heats of evaporation is within the error tolerances of the air velocity and temperature measurements. The error in the overall energy balance is consistent with a small heat loss from the warm components of the heat pump to ambient.

### 3.5 Cyclic Performance of the Absorption Heat Pump

#### 3.5.1 Cyclic test results

In normal operation, a heat pump will cycle on and off to meet varying loads, thus the cyclic performance is of interest. Part load operation was simulated by cycling the heat pump on and off in a predetermined pattern. Cycling rates of 1.5 and 3 cycles per hour at 50 percent burner on time were tested; at 20 percent on time, the

Table 3-4 Conditions of streams in the absorption cycle for an ambient temperature of 8.6 C, standard load water conditions, and original refrigerant charge

Stream	flow rate (kg sec <sup>-1</sup> )	Temp (C)	Pressure (MPa)	NH <sub>3</sub> conc	Enthalpy (kJ kg <sup>-1</sup> )
1	0.0164	76.1	0.38	0.173	216
2	0.0215	47.6	2.20	0.369	-26
3	0.0051	73.8	2.20	0.994	1375
4	0.0051	45.7	2.20	0.994	216
5	0.0051	34.5	0.38	0.994	1344

Table 3-5 Measured and calculated heat flows for the components of the Arkla AHP

Component	Heat flows (kW)		
	measured	calculated	difference
generator	11.5	11.2	0.31
condenser	-6.1	-6.0	-0.16
absorber	-10.3	-11.1	0.85
evaporator	6.6	5.8	0.80
error in energy balance*	1.7	0	

\*energy balance:  $\dot{Q}_{\text{gen}} + \dot{Q}_{\text{evap}} + \dot{Q}_{\text{cond}} + \dot{Q}_{\text{abs}}$

rates were decreased to 1 and 2 cycles per hour following the parabolic behavior of thermostats as discussed in (81). The slower cycling rate is sometimes used for absorption chillers. The tests were performed at the design load water conditions and an ambient temperature of 8 C, except for a single test at a -8 C ambient.

The results of these tests, expressed in terms of the part load and heating load factors, are presented in Figure 3-6. These tests indicate that there is a substantial performance penalty associated with cyclic operation for this heat pump. At a heating load equal to 20 percent of the steady-state capacity, for example, the COP is reduced by 30 to 34 percent from the steady-state value. The slower cycling rate results in somewhat better performance. It is not clear, however, whether it would provide adequate comfort in a heating application because of the longer off periods.

The part load factor for the single test at an ambient temperature of -8 C was 0.04 lower than the corresponding test at 8 C. This indicates that at least a portion of the performance degradation upon cycling is due to heat losses to ambient while the heat pump is off.

The capacity of the heat pump as a function of time for a cyclic test with 10 minutes on, 10 minutes off is shown in Figure 3-7. This response is typical. The capacity rose very quickly when the machine turned on as the warm load water which was sitting in the unit flowed out across the exit thermopile. The capacity then dropped and began to rise towards steady-state after about 3 minutes. (The cause of the

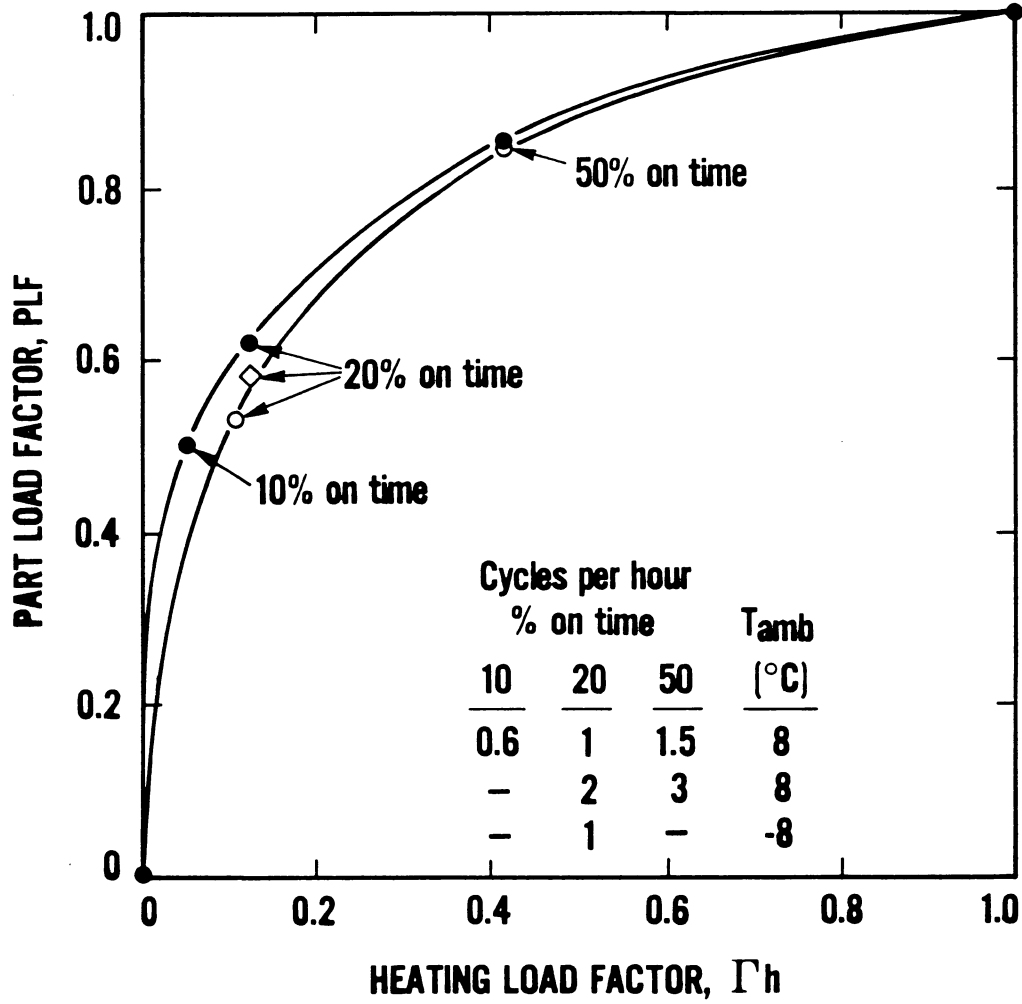


Figure 3-6 Cyclic performance of the Arkla AHP in terms of part load and heating load factors for two cycling rates

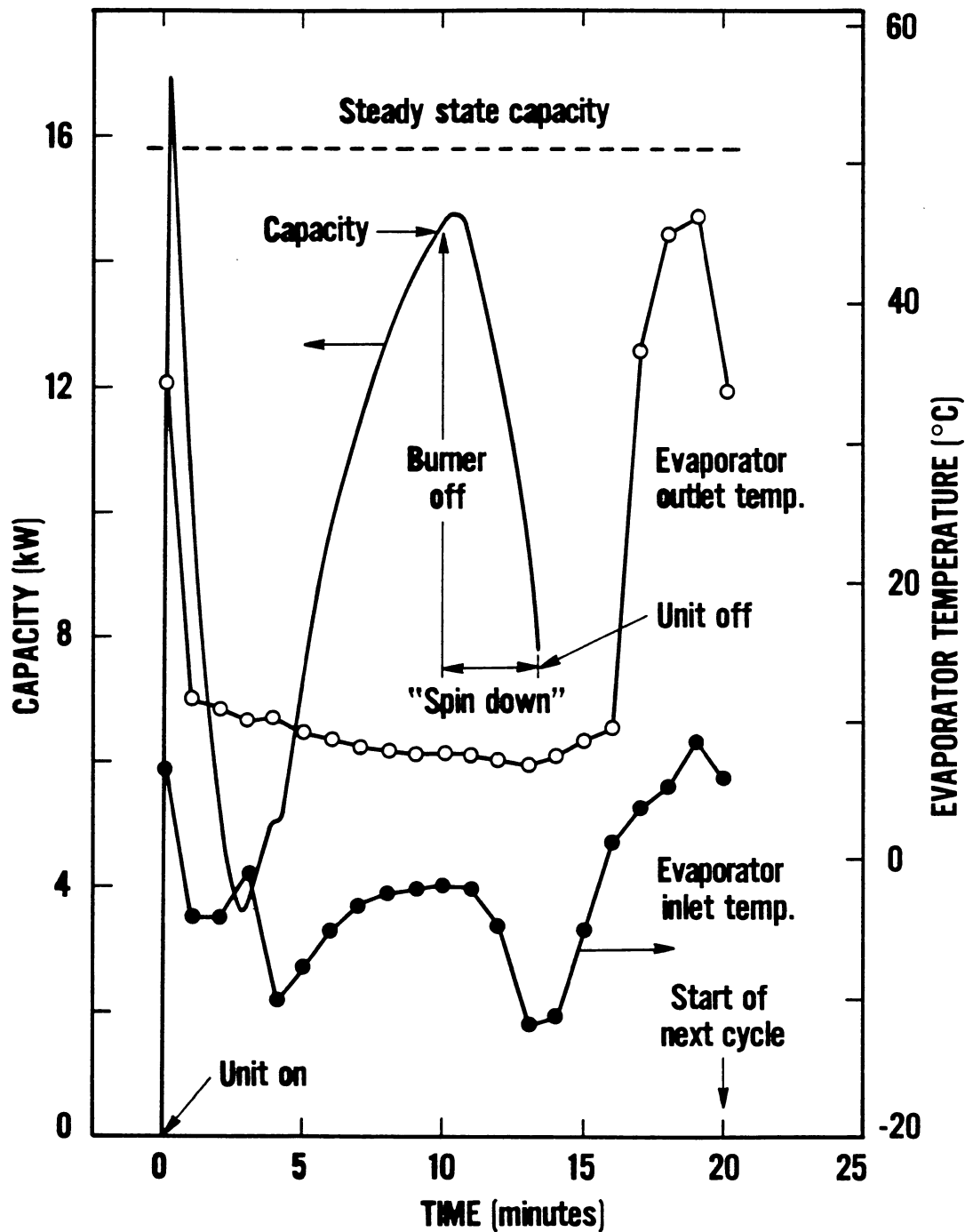


Figure 3-7 Heating capacity and evaporator inlet and outlet temperatures as a function of time for a cyclic test with a 50 percent burner on time

small "bump" in the curve at 4 minutes was not determined but was very reproducible and appeared in varying degrees in all the tests.) The unit had not reached steady-state when the burner shut off, the capacity continued to rise briefly and then fell off sharply during the spindown cycle.

While the machine was off, the difference in the high and low side pressures caused solution to migrate from the generator to the absorber, from there it backed up into the evaporator. (This was deduced from the evaporator temperatures, which are also plotted in Figure 3-7.) This migration of solution into the evaporator resulted in a significant heat loss to ambient. (In several instances, small quantities of frost which had accumulated on the evaporator coil were observed to melt and steam off after the spindown cycle.) Because of the solution migration, when the heat pump cycled back on, the absorber was partially filled with (and the generator depleted of) solution. Solution migration would interfere with the normal operation of these components until the solution pump could return the solution to the generator.

Another heat loss to ambient occurred from the generator. Although the burner was shut off during spindown, the burner blower continued to operate. Ambient air was thus drawn past the hot generator for 3.5 to 4 minutes. The other components of the heat pump were heavily insulated and lost heat much more slowly.

### 3.5.2 Cyclic performance considering the effects of load

The effects of cyclic operation discussed in the previous section can be combined with the steady-state performance presented in Section 3.4 to yield a more realistic assessment of the Arkla AHP operating in an actual application. If a heating load as a function of ambient temperature is assumed, the part load factor from Figure 3-6 can be combined with the steady-state COP to yield a cyclic COP as a function of ambient temperature. A heating load varying linearly between 12 kW at -20 C and a balance temperature of 16 C was assumed, representing a well-insulated house in a moderately cold climate. The part load behavior at the higher cycling rate tested and 8 C ambient was assumed to apply for all conditions. This analysis somewhat overestimates the cyclic COP because the effects of frosting of the evaporator coil and of lower ambient temperatures on the part load factor were not considered.

The results of this simple analysis are presented in Figure 3-8. At the lower ambient temperatures, the cyclic COP is only slightly lower than the steady-state values. As the temperature increases, the heat pump would operate a smaller fraction of the time and as a result, the cyclic COP peaks at about -3 C and then falls off very rapidly. The cyclic COP of the AHP does not exceed unity and for most of the temperature range would be comparable to a well designed furnace.

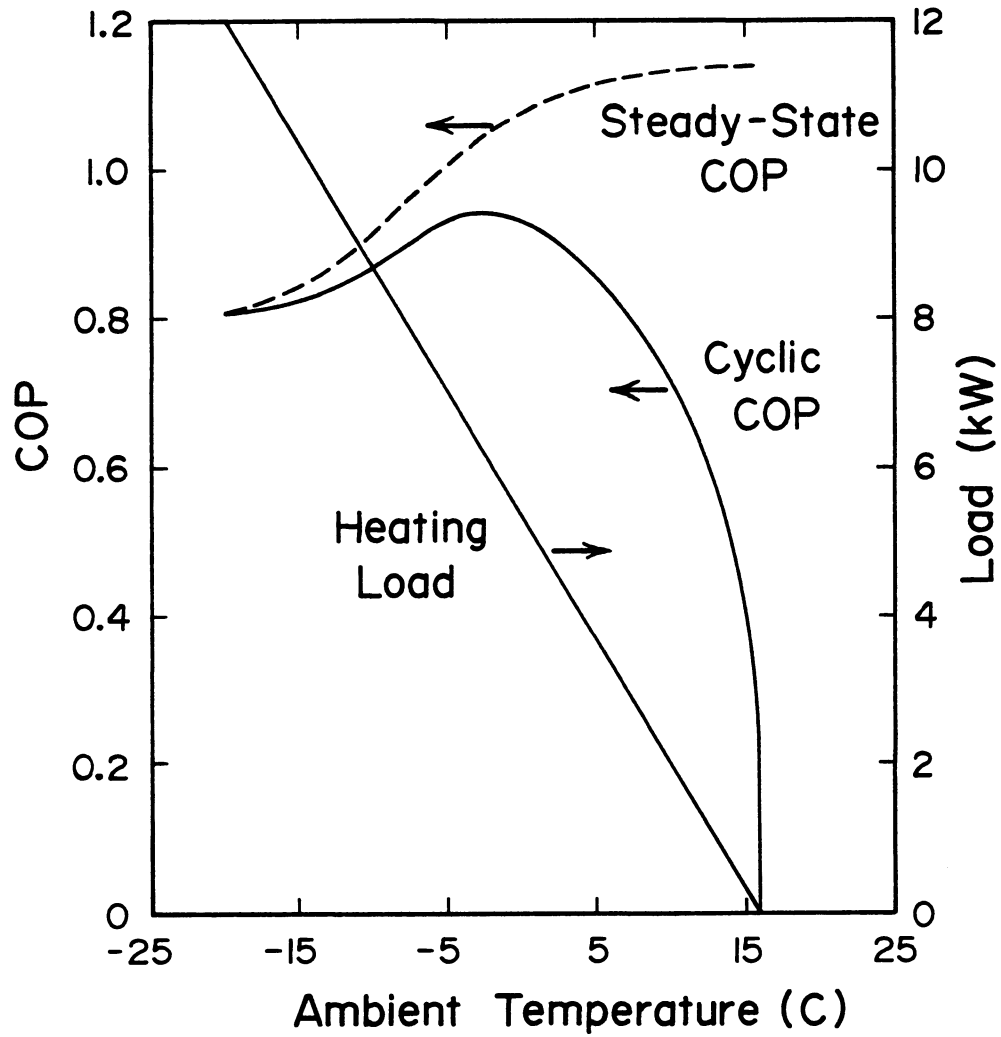


Figure 3-8 Assumed heating load and calculated cyclic COP for the Arkla AHP as a function of ambient temperature

### 3.5.3 Frost accumulation test

The effects of frost accumulation on the evaporator coil were investigated according to the procedures outlined in (79). The heat pump was brought to steady-state operation at a 1.5 C ambient with -1 C dew point (corresponding to a relative humidity of 80 percent). A defrost cycle was manually initiated and upon its completion, the frost accumulation test was begun. The evaporator accumulated frost very slowly and operated for 8.4 hours before requiring defrosting. The average COP and capacity over the test were 0.96 of steady-state, dry coil values at the same ambient conditions.

### 3.6 Summary and Conclusions for the Experimental Investigation

A prototype absorption heat pump developed by Arkla Industries was tested in an environmental chamber under steady-state and cyclic operating conditions. The steady-state COP (including burner losses) and capacity depended most strongly on ambient temperature and ranged from 0.81 and 12.0 kW at -21 C to 1.14 and 15.9 kW at 16 C. Lower inlet load water temperatures resulted in slightly higher COPs, especially at lower ambient temperatures. Varying the load water flow rate and distribution between condenser and absorber had minor effects on COP for the relatively narrow ranges tested.

The performance of the heat pump was sensitive to refrigerant charge. There is no single optimum charge; rather the optimum varies with ambient temperature. A higher refrigerant charge results in higher COPs at high ambient temperatures but a lower COP at low temperatures; a lower charge results in a more nearly constant COP.

The measured heat flows agreed well with those calculated using measured absorbent concentrations, strong absorbent flow rate, and system temperatures.

The prototype AHP tested showed a significant performance degradation in cyclic operation. Although the steady-state COP was greater than unity for ambient temperatures above -5 C, the cyclic COP calculated for a representative residential application has a maximum of 0.94 at -3 C. These results would suggest modifications to the heat pump design to improve cyclic operation or possibly some type of storage system designed to reduce the need for cycling.

## CHAPTER 4

### STEADY-STATE MODELING OF ABSORPTION HEAT PUMPS

This chapter first reviews the absorption heat pump models which have appeared to date in the literature; several of these models are sufficiently detailed and similar to the model presented here to warrant detailed discussion. A number of other models are also discussed briefly. The general nature of the problem is considered, including a discussion of several general purpose simulation programs and the need for, and goals of, the present model. The steady-state simulation program developed is then presented, including the treatment of individual components. Finally a comparison with experimental data is presented along with a sensitivity study of the Arkla prototype AHP.

#### 4.1 Review of Existing Absorption Heat Pump Models

##### 4.1.1 Koenig, et al.

In perhaps the earliest serious detailed modeling effort of the absorption cycle, Koenig, et al. (82) at Carrier Corporation carried out an analysis of a gas-fired ammonia-water absorption chiller. The machine was a residential-sized unit; the condenser and absorber were air-cooled and a water loop connected the evaporator and load heat exchangers. The analysis was carried out by writing mass and energy balances and heat transfer relationships (using constant heat transfer

coefficients) for each component in the cycle. Equilibrium was assumed between contacting liquid and vapor using the polynomial fits of ammonia-water properties developed by Jain and Gable (83).

Several of the components were divided into nodes and required iterative loops to converge on the outlet conditions of counterflow streams. The refrigerant leaving the condenser was assumed to be subcooled by a constant amount and the high side pressure was varied to meet this condition. The low side pressure was varied iteratively to obtain a constant subcooling in the solution leaving the absorber. For each iteration of the low side pressure, the performance of the evaporator and refrigerant heat exchanger was calculated. The convergence of the entire cycle was based on the temperature of the weak absorbent entering the solution pump. The weak absorbent concentration was input to the simulation and was varied in an outermost iteration loop to obtain the maximum cooling capacity. This iteration corresponded to adjusting ("trimming") the refrigerant and/or absorbent charge on an actual machine.

Although the use of this program in the design and development of absorption heat pumps is mentioned, no simulation results or comparisons with experimental data were presented. While this model requires a number of assumptions regarding system states, it represents a significant accomplishment. Unfortunately, this work was presented only at a conference and has received very limited circulation; it is not publically available.

#### 4.1.2 A.D. Little Company

A steady-state AHP simulation model has been developed by the A.D. Little Company (84) as part of a larger program sponsored by Allied Chemical Company and the U.S. Department of Energy to develop an absorption heat pump using organic working fluids. The refrigerant is R133a and the absorbent is ethyltetrahydrofurfural ether (ETFE). The machine modeled is currently under development by Phillips Engineering Company (27,32). It is a residential-sized gas-fired unit which both heats and cools by the switching of heat exchange loops to the load and ambient. The model was based on mass and energy balances and heat transfer relations for the components in the cycle. The equations are solved by a set of nested successive substitution loops which are built into the program code.

An approach to equilibrium (similar to that defined by Duffie and Sheridan (60)) was assumed for mass transfer in the generator and absorber. The treatment of these two components was similar; each was broken into several sections with balance and transfer equations written for each section. The heat exchange processes were treated with constant heat transfer coefficients except for the evaporator and precooler which were treated as constant effectiveness devices. The values of overall heat transfer coefficient were estimated from correlations and experimental experience and were supplied to the model as parameters. Pressure drops (except across throttle valves) were not accounted for.

Because equations were not written for the throttle valves and refrigerant and absorbent inventory, the A.D. Little model requires as inputs the high and low side pressures and the concentration of the generator feed stream. The weak absorbent mass flow rate is also required; this is equivalent to assuming a constant mass flow rate pump.

The results predicted by the model were in good agreement with experimental results. The average error in stream temperatures was 1.2 C, the simulated heat flows were within 10 percent and the COPs agreed within 10 to 15 percent.

#### 4.1.3 Anand, et al.

Anand and co-workers at the University of Maryland at College Park have carried out a range of investigations of lithium bromide-water absorption chillers. In an early work, Allen, et al. (85) developed a steady-state model with the performance of the various components expressed in terms of overall heat transfer conductances. The primary use of the model was to investigate, for varying UA values, the range of inlet firing and cooling water temperatures over which useful cooling could be produced.

In another work Anand, et al. (86) estimated the seasonal performance of a solar-powered absorption air conditioner using stochastic weather models. But here the emphasis was on characterizing ambient weather conditions (and thus operating conditions for the chiller) in terms of a joint probability matrix of solar radiation and temperature. The absorption machine was merely an

example system and was modeled with empirical curve fits to performance data.

Finally, Anand, et al. (87) have carried out a transient analysis of a residential-sized lithium bromide-water chiller. The main feature of this work is that the transient response of the hydrodynamic processes in an absorption cycle are considered. For example, the refrigerant vapor entering the condenser is modeled as condensing on the heat exchange tubes, building up a film which becomes unstable and drips off; the condensate must then fill up a connecting tube before finally entering the evaporator. The other components were treated in a similar fashion.

The transient response of isolated components to step changes in inlet conditions representative of chiller start-up were investigated. The predicted time constants ranged from a few seconds for strong absorbent circulating through the absorber to as much as 16 minutes for the evaporator. In an analysis of the complete cycle, the absorber and the condensate film growth portion of the condenser model were replaced with quasi-steady-state models. The predicted response of the model was in good agreement with start-up responses measured by Auh (88).

#### 4.1.4 Vliet, et al.

Vliet and co-workers at the University of Texas at Austin have modeled a double-effect lithium bromide-water absorption chiller (89,90). Although no particular machine was modeled, the design details of double-effect units manufactured by the Trane Company were

used as a general guide. The model is based on heat transfer relationships and mass and energy balances for the various components in the cycle. The equations are solved iteratively using a combination of the Wegstein convergence algorithm (discussed in section 4.5.8) for recyclic information loops and transient mass and energy balances for the generators, condenser, and absorber. The transient equations are solved by a simple Euler integration and account for the inventory of refrigerant and absorbent in the system.

The component models assume mass transfer equilibrium and employ overall heat transfer coefficients. The film coefficients for pure species (including two-phase mixtures) are estimated from generalized correlations. Coefficients for lithium bromide-water solutions are based on correlations specific to that mixture; a constant coefficient typical of commercial machines is assumed in the absorber. Assumed values of the heat transfer coefficients at the "nominal condition" were used for the two sensible heat exchangers in the cycle; these values were then scaled for varying flow rates. Constant mass flow rate and centrifugal solution pumps were modeled. The throttle on the second generator refrigerant line was modeled both as a fixed orifice and as an ideal "float valve" which passes only saturated liquid. The other throttles were implied via assumptions of saturated liquid or vapor leaving the generator and evaporator, respectively.

This model was used in a parametric study of external and design variables. The parameters were varied one at a time with all others being held at a nominal condition (chosen to represent typical

operating conditions). A conclusion of this study was that double-effect systems can be operated with lower firing water temperatures (as low as 100 C) than generally accepted. The cooling COP of 1.15 at 100 C was slightly lower than for higher firing water temperatures but the cooling capacity was markedly reduced. The temperatures of the heat exchange streams had a strong effect on performance but flow rates did not. The float valve type throttle and constant mass flow rate solution pump gave better performance over a broader range of conditions as compared to a fixed orifice restrictor and centrifugal pump. Finally, any pressure drop between the evaporator and absorber was found to cause a significant loss in performance.

This model suffers from a lack of generality and flexibility. Much of the equation solving logic as well as many of the mass and energy balances and even component parameters and initial guesses for stream conditions are included in single main program. Although refrigerant properties are contained primarily in function subroutines, the properties of the lithium bromide-water system are directly incorporated into the code of the main program in several instances. Although transient balances are written for several components, no discussion of transient behavior is presented. An inspection of the program listing (given in Reference (89)) reveals no way to input transient forcing functions. Apparently the transient equations are used as an aid in solving the overall system of equations (improving the stability of iterative loops) and to account for the inventory of refrigerant and absorbent.

In a related project, Andberg and Vliet (91) have presented a theoretical analysis of an absorber. A falling-film type absorber is represented as a laminar absorbent film flowing down a vertical isothermal plate in the presence of refrigerant vapor. This system is solved for the lithium bromide-water system by finite difference methods. Results are presented in terms of "absorption percentage" (which is the same as the "approach to equilibrium" of Duffie and Sheridan (60)), and "percent absorption length,"  $L_{Ap}$ , which is the plate length necessary to achieve a given absorption percentage.

The  $L_{Ap}$  was found to be proportional to the 1.33 power of mass flow rate per unit plate width. Varying the solution inlet concentration and temperature, vapor pressure and wall temperature over relatively narrow ranges were found to affect the  $L_{Ap}$  by less than six percent. The results are presented for the lithium bromide-water system rather than in terms of general fluid properties. A calculation sequence for the design of absorbers was also given.

#### 4.1.5 Grossman, et al.

Grossman and co-workers have carried out a number of studies concerning the absorption cycle. Reference (92) discusses three modifications to a lithium bromide-water chiller used in solar cooling applications: a solution preheater, a generator with two separate heat exchangers and a cycle with two separate generators. These modifications are designed to allow the input of auxiliary heat to the generator while still making use of solar-heated water at marginal temperatures.

The performance of the modified cycles was investigated with a computer model briefly described by Lando, et. al. (93). Energy and mass balances were written for the main components of the cycle; heat transfer was treated with constant UA values and mass transfer equilibrium was assumed. The model solves the complete set of equations describing the system using an iterative technique.

Grossman, Blanco and Childs (94,95) have simulated an absorption heat pump operating in a reverse or temperature-boosting cycle. A lithium bromide-water cycle is used to boost the temperature of a waste heat stream (at approximately 60 C) by 20 to 40 C, rejecting heat to a sink at approximately 15 C. The simulation model is an extension of that by Lando, et. al. (93). The analysis showed that the temperature boosting capacity was increased by an increase in the waste heat supply temperature or a decrease in the sink temperature. The COP of the cycle was relatively constant at about 0.5 for a wide range of waste heat and cooling water temperatures. Adiabatic gas-liquid contacting sections at the top of the absorber and desorber were found to increase the COP and temperature boost. The effects of varying solution mass flow rate and a constant temperature deviation from the assumption of equilibrium in the adiabatic absorption and desorption sections were also studied.

In a more detailed, theoretical analysis, Grossman (96,97) has investigated the process occurring in an idealized absorber. This analysis deals with the simultaneous heat and mass transfer occurring as refrigerant vapor is absorbed into a laminar liquid film flowing

down a plate. The cases of adiabatic and constant temperature plates are treated. The system was defined by differential heat and mass diffusion equations with boundary conditions given at the entrance, wall and vapor-liquid interface. These balances were written in terms of Sherwood, Nusselt and Reynolds numbers and dimensionless temperature and concentration profiles. The liquid flow was assumed to enter the system at a uniform concentration and temperature (equal to the wall temperature for the constant wall temperature case) and be hydrodynamically fully developed for the entire length of the plate. Equilibrium was assumed and natural convection and shear forces neglected at the vapor-liquid interface. The physical properties of the liquid film were assumed to be constant with the vapor-liquid equilibrium behavior linearized about the inlet conditions.

The temperature and concentration profiles both across the film and down the length of the plate were solved by finite difference methods and by an analytical solution using Fourier series. These solutions involve very lengthy calculations and would not be suitable for use in an absorber model in a heat pump simulation.

An integral solution was also used to solve for the bulk average concentration and temperature down the length of the plate. This solution divides the plate into the regions of developing concentration and temperature profiles, developed temperature but developing concentration profile, and fully developed flow. A numerical integration is used to solve for the boundary between the later two regions. The integral solution is better suited for use in

an absorber model where detailed information on the temperature and concentration profiles is not required. Grossman's integral solution is similar to an analysis by Nakoryakov and Grigor'eva (98) which will be discussed in Section 4.5.4.

#### 4.1.6 Other absorption heat pump models

A number of other investigators have developed absorption heat pump models. These models are often used as one unit in a system study and in general make a large number of assumptions regarding system states. While the assumptions may be reasonable for a machine operating under normal conditions and are therefore acceptable for system studies, they are questionable for a detailed investigation of the absorption cycle itself or for machine design purposes.

Kaushik and Sheridan (99) have presented an analysis of an ammonia-water AHP driven by solar energy. Sufficient assumptions are made, and state points supplied, to permit a non-iterative calculation of the cycle. The effects of generator, absorber, condenser and evaporator temperature, refrigerant concentration and heat exchanger effectiveness on cycle COP are determined for three variations of the absorption cycle.

Trommelmans, et al. (28) have developed a model for an AHP using R22 (difluoromonochloromethane) and E181 (tetraethyleneglycol-dimethylether) as working fluids. The E181 absorbent is non-volatile and thus a rectifier is not needed, making the system similar to some lithium bromide-water machines. The primary assumptions were a constant generator temperature and constant superheat and subcooling

in the evaporator and condenser respectively. The effects of absorber area, solution circulation rate and solution heat exchanger UA were investigated.

Elsayed, et al. (100) simulate a lithium bromide-water chiller connected to a solar collector and hot water storage tank. Mass and energy balances (including one differential equation for the temperature of the storage tank) were written around each of the components and combined with simple linearizations of property data to yield a set of equations describing the system. These equations were then solved using nested iteration loops to predict the performance of the system over the course of a day.

A residential-sized ammonia-water chiller manufactured by Arkla Industries has been modeled by Klein (101). The heat exchange processes assume constant UA values and the program requires the solution pump mass flow rate and the high and low side pressures as inputs. The model is modular in nature but the components present and the iteration between them are part of the program itself and cannot be changed by the user. The model parameters were empirically adjusted to agree with test results at one ambient temperature. Using these values, a sensitivity study was performed by singly varying each of the input parameters five percent above and below its base value to determine the change in machine capacity. The capacity was found to be most sensitive to the inlet chilled water temperature and evaporator pressure. The capacity was relatively insensitive to changes in heat transfer area.

#### 4.1.7 Synopsis of existing AHP models

As discussed above, a number of absorption heat pump models have been presented in the literature. But to varying degrees, they all fall short of the goal of a flexible model which would allow the simulation of a variety of system configurations and refrigerant-absorbent pairs. To simulate a machine which has not been built and to be fully useful in design studies, a model should require only design data as program inputs. System states (e.g. high side pressure or weak absorbent concentration) which can be obtained only by testing or by experience with other, similar machines should not be required as inputs. Most of the existing models require system states as program inputs; although an assumption such as a constant subcooling in the condenser may be applicable for a given machine under normal operating conditions, it cannot be true for all possible operating conditions or component parameters. Although a major use of simulation is to study machines or configurations which have not been built, a simulation model should be validated against experimental data.

#### 4.2 Characterization of System

The solution of a system as complex as an absorption heat pump cycle involves a large number of equations. While it is clear that it must be possible to write a sufficient set of equations to completely describe any real physical system, it is instructive to actually carry out this exercise.

The system to be considered is shown in Figure 4-1. This is somewhat simplified from the configuration of the Arkla heat pump but contains all of the essential components of the cycle. There are also two additions to the cycle at the absorber: a liquid-vapor stream splitter component which allows only vapor to flow to the absorber and a stream mixer which recombines the weak absorbent out of the absorber with any liquid refrigerant or unabsorbed vapor. This analysis is based on the implicit assumption that by specifying the conditions of the input streams to a particular component (along with design parameters), the conditions of the outlet stream(s) are uniquely specified. These outlet streams are, in turn, inputs for other components. A second assumption is that a stream is completely specified by its stream type (i.e. heat exchange fluid versus absorbent-refrigerant mixture), mass flow rate and the three thermodynamic variables of pressure, composition and enthalpy. This implies that any two phase streams passing between components are in thermodynamic equilibrium.

For the 20 total streams in the system, the stream type is known a priori, leaving four variables per stream; including the generator heat input, there are thus 81 variables, requiring 81 relations to specify the system. The external operating variables must be input to the cycle; these consist of the heat exchange streams and the generator heat input:

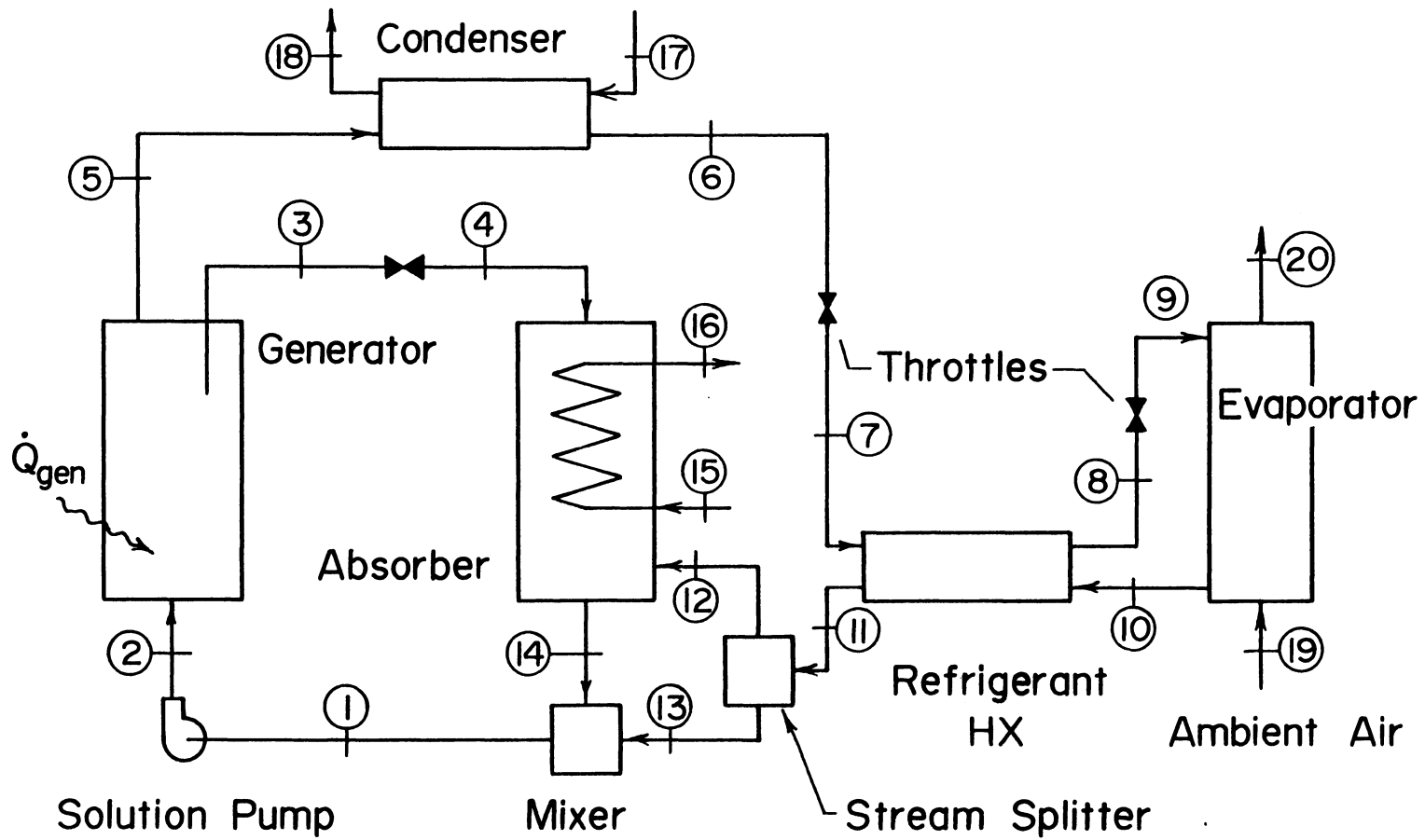


Figure 4-1 Schematic for the characterization of the absorption heat pump cycle

$$\dot{m}_{15}, P_{15}, x_{15}, h_{15}$$

$$\dot{m}_{17}, P_{17}, x_{17}, h_{17}$$

$$\dot{m}_{19}, P_{19}, x_{19}, h_{19}$$

$$\dot{Q}_{\text{gen}}$$

The assumptions of no leakage or reaction and negligible pressure drop for the heat exchange streams yield:

$$\dot{m}_{16} = \dot{m}_{15} \quad \dot{m}_{18} = \dot{m}_{17} \quad \dot{m}_{20} = \dot{m}_{19} \quad [4-1]$$

$$x_{16} = x_{15} \quad x_{18} = x_{17} \quad x_{20} = x_{19} \quad [4-2]$$

$$P_{16} = P_{15} \quad P_{18} = P_{17} \quad P_{20} = P_{19} \quad [4-3]$$

Overall energy, mass and refrigerant balances for the generator yield:

$$\dot{m}_2 h_2 + \dot{Q}_{\text{gen}} - \dot{m}_3 h_3 - \dot{m}_5 h_5 = 0 \quad [4-4]$$

$$\dot{m}_2 - \dot{m}_3 - \dot{m}_5 = 0 \quad [4-5]$$

$$\dot{m}_2 x_2 - \dot{m}_3 x_3 - \dot{m}_5 x_5 = 0 \quad [4-6]$$

Similar energy balances can be written around each of the other ten components in the cycle. Independent mass and refrigerant balances can be written for only nine other components (but there are two equations for each of the two streams entering the refrigerant heat exchanger). This would yield a total of 33 relations.

The assumption of negligible pressure drop across all components (except the solution pump and throttle valves) yields 11 relations:

$$P_2 = P_3 = P_5 = P_6 \quad [4-7]$$

$$P_7 = P_8 \quad [4-8]$$

$$P_9 = P_{10} = P_{11} = P_{12} = P_{13} = P_{14} = P_1 = P_4 \quad [4-9]$$

The assumption of negligible pressure drop could be replaced by relationships for the pressure drop across each component; for example:

$$P_8 - P_7 = f(\dot{m}_7, x_7, h_7, \dots) \quad [4-10]$$

where  $f$  is some function relating pressure drop to the conditions in a particular component.

Heat transfer rate equations can be written for each of the four heat exchangers in the cycle. For the absorber this would give:

$$\dot{m}_{19}(h_{19} - h_{20}) = \dot{Q}_{abs} = (UA)_{abs} \Delta T_{lm} \quad [4-11]$$

where  $\dot{Q}_{abs}$  is the rate of energy removed by the heat exchange stream,  $(UA)_{abs}$  is an overall heat transfer coefficient-area product and  $\Delta T_{lm}$  is a log mean average temperature difference. (The temperature of a stream is a unique (and known) function of its pressure, composition and enthalpy, so that no additional unknowns have been introduced.)

The particular absorber configuration considered can absorb only vapor. Any liquid entering with the refrigerant is combined with the

weak absorbent stream in the stream mix component.) Thus if stream 11 is a two phase mixture the liquid-vapor separator component must compute the composition and enthalpy of the vapor portion:

$$h_{12} = f(P_{11}, x_{11}, h_{11}) \quad [4-12]$$

$$x_{12} = f(P_{11}, x_{11}, h_{11}) \quad [4-13]$$

If stream 11 is superheated vapor, then streams 11 and 12 are identical:

$$h_{12} = h_{11} \quad [4-14]$$

$$x_{12} = x_{11} \quad [4-15]$$

The rate of vapor absorption is given by a mass transfer relationship:

$$\dot{m}_{12} = f(\text{streams } 4, 12, 15) \quad [4-16]$$

If the generator is treated as a fully mixed tank, the enthalpies of the leaving streams are related such that their temperatures are equal:

$$T_3 = T_5 \quad [4-17]$$

Furthermore, if the geometry is such that only saturated vapor can leave in stream 5:

$$x_5 = f(P_5, T_5) \quad [4-18]$$

The characteristics of the solution pump must be specified. Depending on the design of the pump and the geometry of the inlet, it might be approximated as a constant mass or volumetric flow rate device. Alternately, given the pump design parameters, it may be possible to calculate the mass flow rate as function of the pressure rise and inlet conditions:

$$\dot{m}_2 = f(P_1, P_2, x_1, h_1) \quad [4-19]$$

Functions relating the flow rate through the three throttle valves to the pressure drop and stream conditions can be written; for example:

$$\dot{m}_7 = f(P_6, P_7, x_6, h_6) \quad [4-10]$$

The geometry of the generator plus absorber throttle may be such that only saturated liquid can leave the generator. In this case the relationship for that throttle can be replaced by:

$$x_3 = f(P_3, T_3) \quad [4-21]$$

It is also possible to control a throttle such that, for example, the refrigerant stream undergoes a constant temperature rise in the evaporator. Physically, the relationship between mass flow rate and pressure drop must always be satisfied, but here an additional variable would be the opening of the valve. This valve opening would in turn be set by the controller mechanism so that together an expression of the control set point:

$$T_{10} - T_9 = \Delta T_{\text{set}} \quad [4-22]$$

would replace the throttle valve relationship.

Thus far, 79 relationships have been presented. The remaining two relationships needed to fully describe the system are contained in an inventory balance. The absorption cycle (exclusive of the external heat exchange streams) is a closed system and, thus the total amount of absorbent and refrigerant in the system must be a constant:

$$m_{a,\text{tot}} = \sum_{i=1,N} m_{a,i} \quad [4-23]$$

$$m_{r,\text{tot}} = \sum_{i=1,N} m_{r,i} \quad [4-24]$$

where  $m_{a,\text{tot}}$  and  $m_{r,\text{tot}}$  are the total mass of absorbent and refrigerant in the system, respectively and  $m_{a,i}$  is the mass of absorbent contained within the  $i^{\text{th}}$  component. The total masses in the system are design variables. The masses within each component are related to the conditions and design variables (including volume) for that component.

While this analysis was carried out for a system slightly different from the one to be modeled, the same general results would be obtained. Adding additional components would result in more unknowns but additional equations would be available to describe the system. For a closed system, the inventory relationships are required. Models which do not employ an inventory analysis must make assumptions regarding system states.

### 4.3 Steady-State Modeling Techniques

There are three basic approaches for the solution of large sets of simultaneous equations such as that presented in the preceding section (102,103). In the equation-based (or simultaneous) approach, the entire system of equations is solved simultaneously. This method is often computationally efficient but generally requires extensive effort to set up the simulation. Equation-based methods are under development but have not seen widespread use except in specialized applications.

Large sparse systems of equations can be decomposed into sub-problems. In this modular approach, the subproblems can correspond to components in the physical system. The solution iterates between components with the outputs from one component being the inputs to another. Initial guesses for a minimum set of "tear streams" are needed to start the iteration.

The final approach combines elements of the first two. In the simultaneous-modular method, the response of the components is linearized by perturbing the inputs about a set of initial guesses. This yields a system of linear equations which are solved simultaneously using matrix techniques to arrive at a new set of estimates for the stream variables. The process is repeated until convergence is obtained. This approach has the promise of combining the computational efficiency of the equation-based approach with the flexibility of the modular approach and is currently under development.

A number of general process simulation programs utilize the modular approach (103), including the FLOWTRAN (104) and ASPEN (105,106) programs for steady-state simulation of chemical processes and the TRNSYS simulation program (36) for the transient simulation of solar energy, HVAC, and other transient systems. In all of these programs, there are a collection of subroutines representing different pieces of equipment; an input language to specify the components present, their parameters and how they are connected; and a main program which calls the subroutines in the proper order to carry out the simulation.

An absorption heat pump cycle is essentially a small scale chemical plant and would be a possible candidate for simulation by the FLOWTRAN or ASPEN programs. The ASPEN program is in the public domain and would be the most economical and logical choice. The components available in ASPEN are similar to those needed to model an AHP. There are enough differences, however, to necessitate either extensive revision of existing models or the writing of new components. Substantial effort would be required to learn the ASPEN simulation language and the format required of new components. Also, extensive computer time would be needed to repeatedly link together the numerous subroutines comprising the ASPEN program during component debugging.

Because of these difficulties associated with using an existing, general-purpose simulation program a separate, simpler simulation program was written for the modeling of absorption heat pumps. The intent is to use ideas from the more general simulation programs for

guidance in program structure and numerical techniques. While perhaps less "user friendly," a separate AHP simulation program should be better suited to the task at hand.

#### 4.4 Steady-State Absorption Heat Pump Model

The goal of this research is to develop an absorption heat pump model that is as general and flexible as possible and to validate this model this model with experimental data from the Arkla prototype AHP. The model developed is steady-state, modular and stream-based. Components in the simulation are separate subroutines which correspond, in most cases, to physical components in the real cycle. Although the need to model the Arkla AHP has lead to assumptions of configuration for various components, the structure of the program allows modification of components or the addition of new components to model other systems. Property relations are referenced directly in the component routines and are supplied as separate Fortran subroutines.

Inputs and outputs for each component are specified by stream numbers. Each stream represents a one-dimensional array containing the stream type (e.g. refrigerant-absorbent mixture), mass flow rate, pressure, composition, enthalpy, temperature and equilibrium quality. This manner of passing information between components is more convenient than specifying each input variable as an output of some other component (as the TRNSYS program does) and makes it easier to relate simulation results to a system diagram or experimental results. There are also "data streams" which can be used to pass other types of information (e.g. a heat flow or control function).

The overall structure of the program is shown in Figure 4-2. The first step is to read the input deck which specifies information on the simulation as a whole (such as the total number of streams and components, convergence tolerances and the order in which components are to be called); the inputs, outputs and parameters for each component; the state of input streams and data; and initial guesses for the pressures and tear streams. The components are called in the order specified in the input deck, except that this sequence can be altered by a convergence component in order to iterate on a tear stream. (The details of tear stream convergence will be discussed in Section 4.5.8.)

When the entire cycle has been converged for a given set of pressures, the inventory of absorbent and refrigerant computed by each component are summed and compared to the total (input) inventory. New guesses for pressures are then found by a two-variable secant method (described in Section 4.5.8) and the cycle iteration begins again.

The pairing of the inventory relations to pressure is only one possible choice. The inventory relations represent two equations which are dependent on the conditions in the various components; thus they could have been used, in principle, to set any two variables which affect the inventory. The present choice was based on a number of considerations. First of all, the high and low side pressures represent two variables that convey much information--most of the streams are at one of these two pressures. The formulation of several of the component models is simplified if pressures are input rather

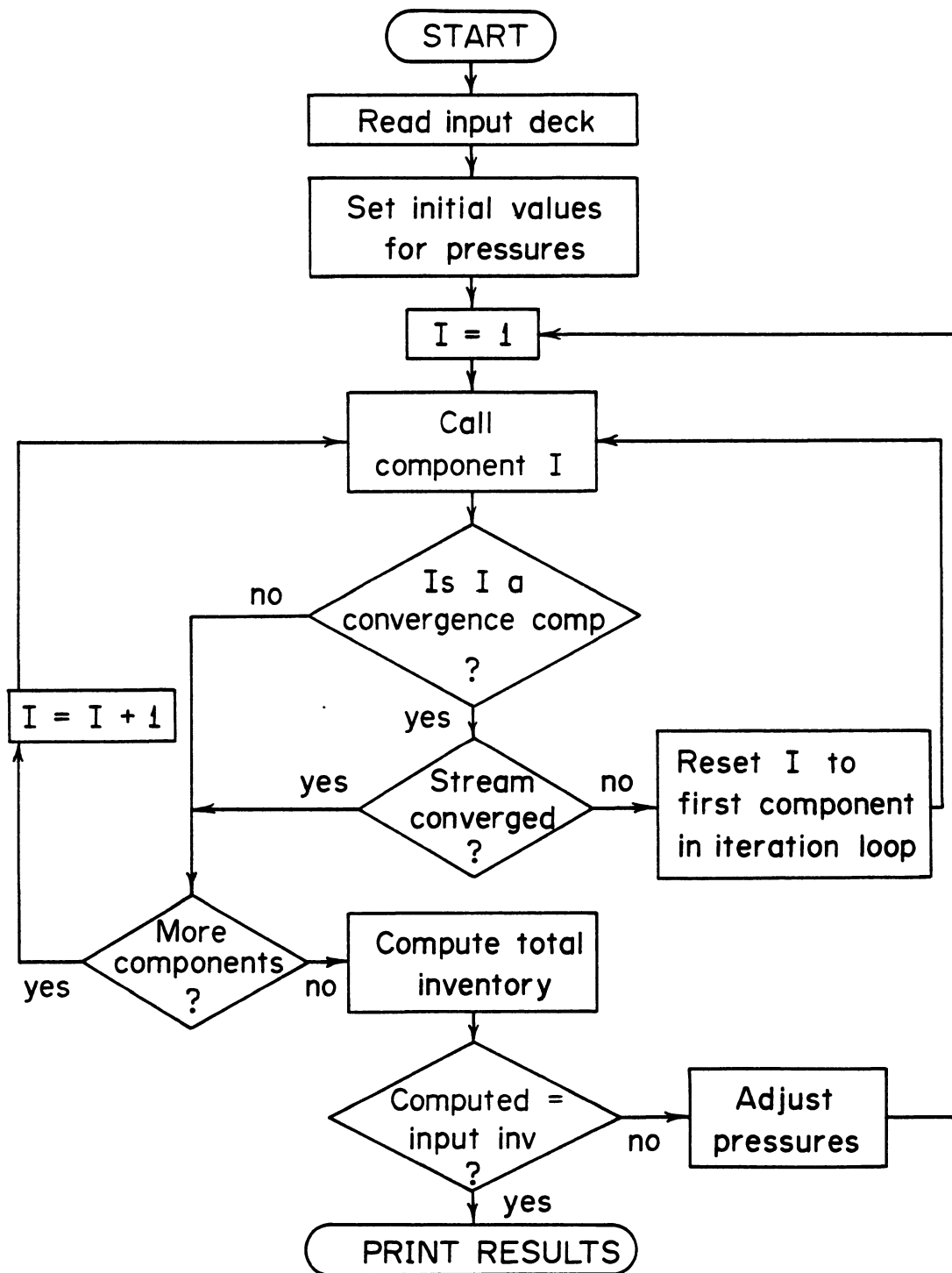


Figure 4-2 Overall structure of the steady-state simulation program

than calculated. It was experimentally observed that changing the inventory of refrigerant had a significant effect on the low side pressure. Finally, since these pressures were measured in all of the tests, good initial guesses are available. In the current model, pressure drops are neglected, thus the pressures computed by the inventory relations are the high and low side pressures which exist throughout several components. If pressure drops were considered, the pressures set by the inventory analysis would be those existing at specific points in the cycle.

#### 4.5 Component Descriptions

The mathematical formulation and implementation of the various components needed to model an absorption heat pump cycle are described in this section. The exact specification of inputs, parameters, etc. can be found in Appendix B. In developing the component models, pressure drops and heat losses to the surroundings are neglected. The property relations used with this simulation program are described in Appendix C.2 and are summarized in Table 4-1.

##### 4.5.1 Generator

The generator is a vessel in which weak absorbent is heated to boil off a refrigerant-rich vapor; producing strong absorbent. The generator is treated as a fully mixed tank with known heat input. The input stream is the incoming weak absorbent, with outputs of strong absorbent and refrigerant vapor. This component is treated in two parts: a heating section and separator section as shown in Figure

Table 4-1 Summary of property relations referenced by the steady-state simulation model

Function name	Independent variables	Dependent variables	Description
TSAT	$P, x_{liq}$	$T_{liq}$	saturation temperature of liquid solution
XLQ	$T, P$	$x_{liq}$	saturation composition of liquid solution
XLQV	$P, x_{vap}$	$x_{liq}$	composition of liquid in equilibrium with vapor
XVP	$P, x_{liq}$	$x_{vap}$	composition of vapor in equilibrium with liquid
PSAT	$T, x_{liq}$	$P$	saturation vapor pressure
HLQ	$T, x_{liq}, P$	$h_{liq}$	enthalpy of liquid
HVP	$T, x_{vap}, P$	$h_{vap}$	enthalpy of vapor
CP	$T, x, P$	$C_p$	heat capacity of liquid or vapor
YT	$P, x, h$	$Y, T$ $x_{liq}, x_{vap}$ $h_{liq}, h_{vap}$	saturation temperature and quality of a stream (including two phase)
VLQ	$T, x_{liq}, P$	$v_{liq}$	specific volume of liquid
VVP	$T, x_{vap}, P$	$v_{vap}$	specific volume of vapor

4-3. Energy, mass and refrigerant balances on the heating section yield:

$$\dot{m}_1 h_1 + \dot{Q}_{\text{gen}} - \dot{m}_2 h_2 = 0 \quad [4-25]$$

$$\dot{m}_2 = \dot{m}_1 \quad [4-26]$$

$$x_2 = x_1 \quad [4-27]$$

For the separator section,  $h_2$  and  $x_2$ , along with the pressure are input to the property relation YT which calculates the enthalpy, composition and temperature of the resulting liquid and vapor fractions. The mass flow rates of the outlet streams are related to the equilibrium quality at point 2:

$$\dot{m}_3 = \text{MAX}(0, 1 - y_2) \dot{m}_2 \quad [4-28]$$

$$\dot{m}_4 = \dot{m}_2 - \dot{m}_3 \quad [4-29]$$

where MAX is the maximum function and  $y$  is quality defined as:

$$y = \frac{h - h_{\text{liq}}}{h_{\text{vap}} - h_{\text{liq}}} \quad [4-30]$$

The total volume of the generator is separated into liquid and vapor portions. The vapor portion could be either an actual vapor space or it could represent the void fraction of the boiling absorbent solution. The inventory in each portion is treated as having a specific volume equal to that of the corresponding leaving stream. The specific volume,  $v$ , of each stream can be computed using the

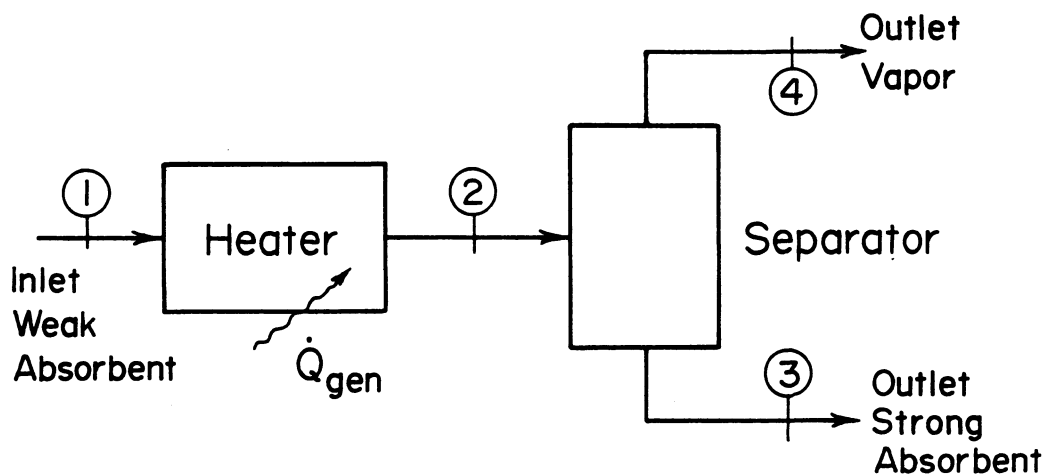


Figure 4-3 Schematic representation of the generator model

property relations:

$$v_3 = VLQ(T_3, x_3, P) \quad [4-31]$$

$$v_4 = VVP(T_4, x_4, P) \quad [4-32]$$

The inventory of refrigerant and absorbent is then found:

$$m_{r,gen} = x_3 \frac{V_{liq}}{v_3} + x_4 \frac{V_{vap}}{v_4} \quad [4-33]$$

$$m_{a,gen} = (1 - x_3) \frac{V_{liq}}{v_3} + (1 - x_4) \frac{V_{vap}}{v_4} \quad [4-34]$$

where  $V_{liq}$  and  $V_{vap}$  are the volumes of the liquid and vapor portions of the generator.

#### 4.5.2 Analyzer

The analyzer contacts the weak absorbent entering, and the refrigerant vapor leaving the generator to preheat the absorbent stream and purify the refrigerant; the strong absorbent exiting the generator flows up through the analyzer in a heat exchanger coil, thus also serving to preheat the weak absorbent. It is basically a distillation column with the addition of a heat exchanger extending the entire length of the column. The analyzer is modeled as a series of equilibrium stages. Each stage, like the component as a whole, has three input and three output streams as shown in Figure 4-4.

For stage  $i$  of an  $N$  stage column, overall mass, refrigerant and energy balances can be written. (The subscripts refer to the stream numbers in Figure 4-4; a stream is identified as being liquid, vapor or heat exchange and is assigned the number of the stage it is leaving.)

$$\dot{m}_{\text{liq},i+1} + \dot{m}_{\text{vap},i-1} = \dot{m}_{\text{liq},i} + \dot{m}_{\text{vap},i} \quad [4-35]$$

$$\begin{aligned} x_{\text{liq},i+1} \dot{m}_{\text{liq},i+1} + x_{\text{vap},i-1} \dot{m}_{\text{vap},i-1} = \\ x_{\text{liq},i} \dot{m}_{\text{liq},i} + x_{\text{vap},i} \dot{m}_{\text{vap},i} \end{aligned} \quad [4-36]$$

$$\dot{m}_{\text{hx},i-1} = \dot{m}_{\text{hx},i} \quad [4-37]$$

$$x_{\text{hx},i-1} = x_{\text{hx},i} \quad [4-38]$$

$$\begin{aligned} \dot{m}_{\text{liq},i+1} h_{\text{liq},i+1} + \dot{m}_{\text{vap},i-1} h_{\text{vap},i-1} + \dot{m}_{\text{hx},i-1} h_{\text{hx},i-1} = \\ \dot{m}_{\text{liq},i} h_{\text{liq},i} + \dot{m}_{\text{vap},i} h_{\text{vap},i} + \dot{m}_{\text{hx},i} h_{\text{hx},i} \end{aligned} \quad [4-39]$$

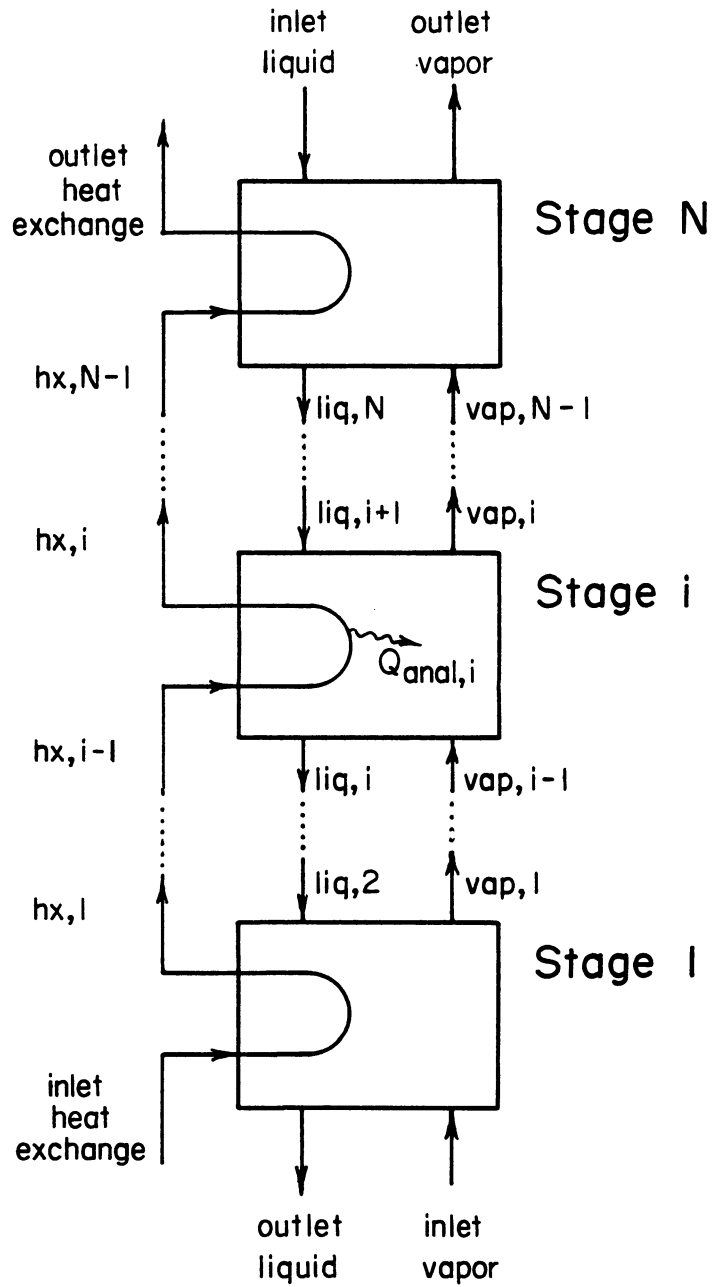


Figure 4-4 Modeling of the analyzer with equilibrium stages

The assumption of an equilibrium stage implies that the leaving vapor and liquid streams are in thermodynamic equilibrium:

$$T_{\text{vap},i} = T_{\text{liq},i} = \text{TSAT}(P_i, x_{\text{liq},i}) \quad [4-40]$$

$$h_{\text{liq},i} = \text{HLQ}(T_{\text{liq},i}, x_{\text{liq},i}, P_i) \quad [4-41]$$

$$x_{\text{vap},i} = \text{XVP}(P_i, x_{\text{liq},i}) \quad [4-42]$$

$$h_{\text{vap},i} = \text{HVP}(T_{\text{vap},i}, x_{\text{vap},i}, P_i) \quad [4-43]$$

The functions TSAT, HLQ, XVP and HVP are property routines described in Appendix C.2. Furthermore (except for the top stage), the incoming liquid stream is an output of an equilibrium stage and thus a saturated liquid:

$$T_{\text{liq},i+1} = \text{TSAT}(P_{i+1}, x_{\text{liq},i+1}) \quad [4-44]$$

$$h_{\text{liq},i+1} = \text{HLQ}(T_{\text{liq},i+1}, x_{\text{liq},i+1}, P_{i+1}) \quad [4-45]$$

For the top stage, the state of the input liquid stream replaces equation [4-45].

Finally, the heat flow across the heat exchanger is given by:

$$\dot{Q}_{\text{anal}} = \dot{m}_{\text{hx},i} (h_{\text{hx},i-1} - h_{\text{hx},i}) \quad [4-46]$$

$$\dot{Q}_{\text{anal},i} = (UA)_i \frac{T_{\text{hx},i-1} - T_{\text{hx},i}}{\ln\left(\frac{T_{\text{hx},i-1} - T_{\text{liq},i}}{T_{\text{hx},i} - T_{\text{liq},i}}\right)} \quad [4-47]$$

where  $(UA)_i$  is the overall heat transfer coefficient-area product for

stage  $i$ ; it is set to the UA for the entire analyzer divided by the number of stages.

The system of equations [4-35] through [4-47] cannot be solved explicitly and the implementation of these equations into the analyzer component requires two concentric iteration loops. In the outer loop, a guess is made for the mass flow rate and composition of the liquid leaving the bottom stage. Equations [4-40] to [4-43] are evaluated for stage 1. It is then necessary to make a guess for  $x_{liq,2}$ ; with this value, Equations [4-35] to [4-38] can be solved. The overall energy balance [4-39] is used to check the guess for  $x_{liq,2}$  and generate a new value by the secant method. The computed values for  $\dot{m}_{liq,2}$  and  $x_{liq,2}$  then become the guess values for the second stage and the process is repeated up the column to stage  $N - 1$ . The inputs to the top stage are all known and thus the calculation procedure is slightly different. An iteration for  $T_{hx,N}$  is required, with [4-46] and [4-47] equated to provide a check on the assumed value.

If the guessed values for the flow rate and composition of the liquid stream leaving the bottom stage are correct, the values of  $\dot{m}_{liq,N}$  and  $x_{liq,N}$  computed by stages  $N$  and  $N - 1$  will be identical. If they are not equal (within a convergence tolerance) a new set of guesses for  $\dot{m}_{liq,1}$  and  $x_{liq,1}$  are generated by a two-variable secant method (described in Section 4.5.8) and the calculation returns to the bottom of the column. If the analyzer has only a single stage, the calculation order for the top stage is used and the iteration for  $\dot{m}_{liq,1}$  and  $x_{liq,1}$  is not needed.

The volume and resulting mass inventory in the analyzer are divided into three separate parts--the internal volume of the heat exchanger, and the liquid and vapor volumes of the contacting streams. The vapor volume corresponds to a vapor void fraction for the two contacting streams. The inventory is calculated on a stage-by-stage basis, with the specific volumes of the streams evaluated at the exit conditions of the stage.

#### 4.5.3 General N-stream heat exchanger

The condenser, evaporator, rectifier, and refrigerant and flue gas heat exchangers in the Arkla AHP are all heat exchangers with no mass transfer between streams. While these components are different in configuration, the basic balances necessary to model them are the same and thus a single subroutine, written in a general manner, can model all of these components. The rectifier has the most complex geometry and necessitates a model capable of handling at least three streams, including one which is counterflow to the others. Most of the heat exchangers have at least one stream that is two phase; in some cases (e.g., the refrigerant heat exchanger) both streams are two phase.

For configurations which involve co- or counter-current flow the situation to be modeled is shown in Figure 4-5. An energy balance on a differential element,  $dz$ , in the heat exchanger yields:

$$\pm \dot{m}_i dh_i / dz = \sum_{j=i+1, N} \dot{Q}_{ji} - \sum_{j=1, i-1} \dot{Q}_{ij} \quad [4-48]$$

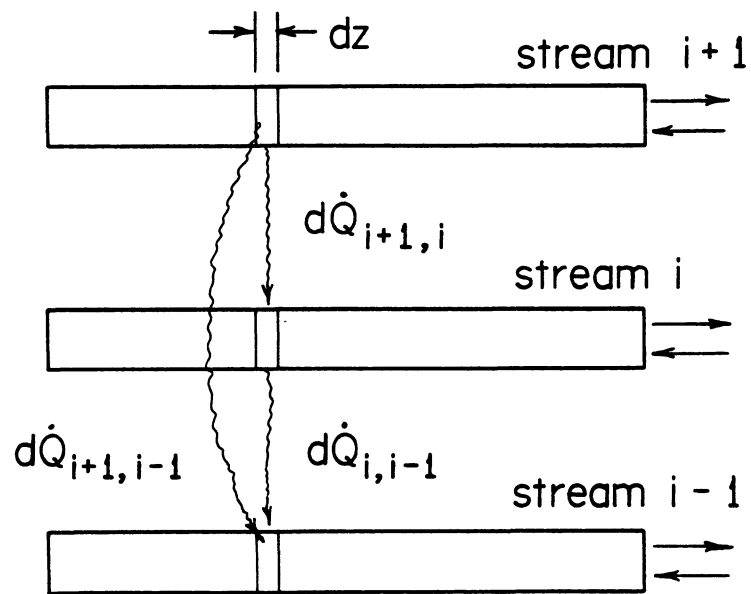


Figure 4-5 General N-stream heat exchanger component schematic

where  $z$  is a nondimensional position and the sign of the left hand term depends on the flow direction of stream  $i$ . The  $\dot{Q}_{ij}$  terms represent a flow of heat from stream  $i$  to stream  $j$ . To prevent counting a given heat flow twice, the summation includes only flows from lower to higher numbered streams. The heat flow is given by:

$$\dot{Q}_{ij} = (UA)_{ij}(T_i - T_j) \quad [4-49]$$

The overall heat transfer coefficient-area product between streams  $i$  and  $j$  at a given location is given by:

$$(UA)_{ij} = \frac{1}{\frac{1/hc_{ij} + R_{f,ij}}{A_{ij} + e_{fin}A_{fin,ij}} + \frac{R_{w,ij}}{A_{w,ij}} + \frac{1/hc_{ji} + R_{f,ji}}{A_{ji} + e_{fin,ji}A_{fin,ji}}} \quad [4-50]$$

where:  $A_{ij}$  = area of stream  $i$  in thermal contact with stream  $j$

$R_{f,ij}$  = fouling resistance for  $A_{ij}$

$A_{fin,ij}$  = extended surface (fin) area for  $A_{ij}$

$e_{fin,ij}$  = fin efficiency for surface  $A_{fin,ij}$

$R_{w,ij}$  = resistance for wall between streams  $i$  and  $j$

$A_{w,ij}$  = log mean average area of wall between streams  $i$  and  $j$

The  $hc_{ij}$  terms are heat transfer coefficients which in general are functions of the conditions of stream  $i$ . (In the model, the conditions of stream  $i$  are supplied to a separate subroutine which returns a value for the heat transfer coefficient.)

The heat transfer with crossflow streams is treated with the concept of heat exchanger effectiveness (69). The effectiveness for a

fully-mixed cross flow stream is given by:

$$\epsilon = \frac{(\dot{m}C)_{\text{cross}}}{(\dot{m}C)_{\text{min}}} \left[ 1 - \exp \left( - \frac{\gamma(\dot{m}C)_i}{(\dot{m}C)_{\text{cross}}} \right) \right] \quad [4-51]$$

where the subscripts cross and i refer to the crossflow and co- or countercurrent streams respectively,  $(\dot{m}C)_{\text{min}}$  is the minimum capacitance rate of the two streams and the dimensionless parameter  $\gamma$  is given by

$$\gamma = 1 - \exp \left( -UA/(\dot{m}C)_i \right) \quad [4-52]$$

The UA value is calculated by Equation [4-50] as before. If one of the streams is two-phase its heat capacity is treated as infinite and Equation [4-51] reduces to:

$$\epsilon = 1 - \exp \left( -UA/(\dot{m}C)_{\text{min}} \right) \quad [4-53]$$

The heat flow for crossflow is given by:

$$Q_{ij} = \epsilon(\dot{m}C)_{\text{min}}(T_i - T_j) \quad [4-54]$$

Equation [4-48] can be integrated down the length of the heat exchanger to give the outlet conditions of the streams:

$$h_{i,\text{out}} = h_{i,\text{in}} + \frac{1}{\dot{m}_i} \int_{z=0}^{z=1} \left( \sum_{j=i, l+N} \dot{Q}_{ji} - \sum_{j=1, i-1} \dot{Q}_{ij} \right) dz \quad [4-55]$$

This equation cannot be solved analytically unless a large number of simplifying assumptions are made; thus a numerical solution is necessary.

The heat exchanger component in the AHP simulation employs a standard fourth-order Runge-Kutta solution (107) to Equation [4-48]. This solution starts at one end of the heat exchanger and proceeds down its length; the outlet state of any counterflow stream must be initially guessed. The heat exchanger is divided into nodes. At the beginning of the first node, the temperature and quality of the streams are found, the heat transfer coefficients are evaluated and the  $(UA)_{ij}$  and  $\dot{Q}_{ij}$  terms computed by [4-50] and [4-49] or [4-54]. The first estimate of  $dh_i/dz$  are then obtained by [4-48]; these slopes are then extrapolated to find the enthalpies at the midpoint of the node. The process of evaluating temperatures, heat transfer coefficients, and the  $(UA)_{ij}$  and  $\dot{Q}_{ij}$  terms is repeated to give a total of four estimates of  $dh_i/dz$ . In each case the slopes are based on conditions obtained by an extrapolation of the previous set of slopes. The second and third set of  $dh_i/dz$  are based on conditions at the midpoint of the node and the final  $dh_i/dz$  are based on conditions at the end of the node. An average set of slopes is given by:

$$\left. \frac{dh_i}{dz} \right|_{\text{avg}} = \frac{1}{6} \left( \left. \frac{dh_i}{dz} \right|_1 + 2 \left. \frac{dh_i}{dz} \right|_2 + 2 \left. \frac{dh_i}{dz} \right|_3 + \left. \frac{dh_i}{dz} \right|_4 \right) \quad [4-56]$$

The conditions at the end of the node are then obtained.

If a stream has gone from single to two-phase (or vice versa) within a given node, it is likely that the heat transfer coefficients and temperature differences between streams have changed significantly. When this occurs, the node is subdivided at the point

of the phase transition. This point is given by:

$$z_s = z_{in} + (z_{out} - z_{in}) \frac{h_{i,in} - h_{sat}}{h_{i,out} - h_{i,in}} \quad [4-57]$$

where  $z_{in}$  and  $z_{out}$  are the starting and ending points of the original node,  $z_s$  is the location of the phase transition and  $h_{sat}$  is the enthalpy of saturated liquid or vapor. If multiple phase transitions occur, the node is subdivided at the minimum value of  $z_s$ .

It was found to be necessary to carry out a similar checking for phase transitions at each extrapolation in the Runge-Kutta method. Figure 4-6 depicts the enthalpy and temperature profiles that would exist in a heat exchanger with an evaporating stream nearing the saturated vapor state. For simplicity, this figure is drawn for a pure component evaporating, an isothermal heat exchange stream and constant heat transfer coefficients. The actual behavior of the evaporating stream enthalpy is shown by dotted lines: the enthalpy increases steadily at first and then flattens out as the stream reaches saturation and its temperature approaches that of the heat exchange stream. The behavior of the unmodified Runge-Kutta solution is shown by the solid lines and arrows. The first estimate of  $dh_i/dz$  (indicated by "slope 1" in the figure) is in the correct direction, but is extrapolated past the phase transition point. Because temperature changes rapidly with enthalpy for a superheated vapor, the temperature predicted at the midpoint of the node is higher than that of the heat exchange stream. Since the temperature difference has

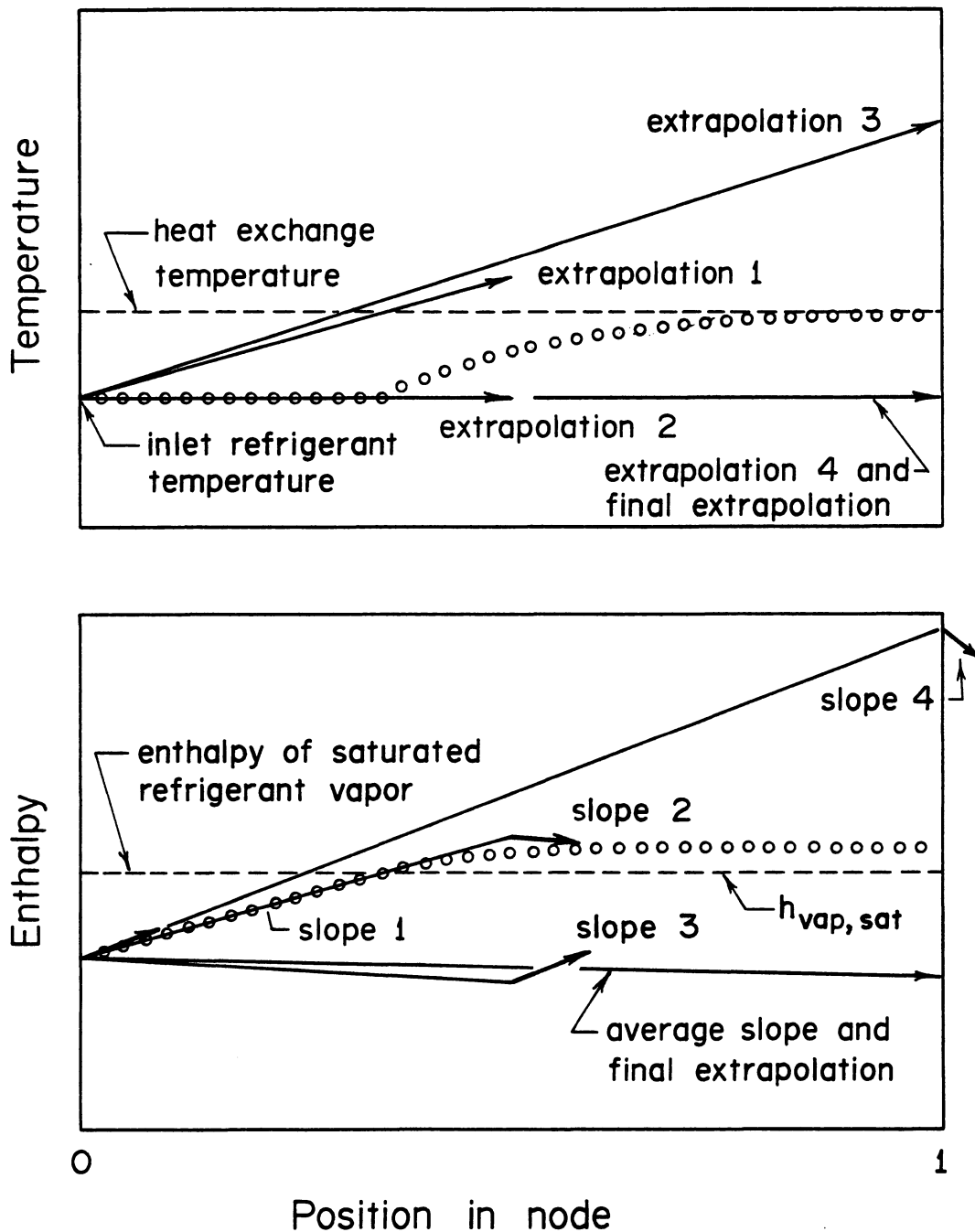


Figure 4-6 Behavior of the unmodified fourth-order Runge-Kutta integration for the solution of an evaporator node nearing saturation (behavior of physical system shown as dotted line)

reversed sign, the second estimate of  $dh_i/dz$  is also of the reverse sign. This yields an estimated enthalpy at the midpoint which is lower than the starting value, which is physically impossible. The third extrapolation again results in a temperature reversal. The average slope is negative and the final extrapolation yields an outlet enthalpy for the evaporating stream lower than its inlet value. The same problems could be repeated in the next node, with the result that with the unmodified Runge-Kutta method the evaporating stream would never reach saturation.

To avoid this problem (which was actually encountered when using the heat exchange component to model an evaporator) each extrapolation in the Runge-Kutta solution is checked for phase transitions, these points are calculated with [4-57]. The second and third sets of slopes are calculated using conditions existing halfway to any phase transition point and the fourth slope is calculated at the phase transition point.

The outlet states of the current node are reset to the inlet states of the next node and the above calculations are repeated until the end of the heat exchanger is reached. (The exception is that for crossflow streams, the inlet state to all nodes is identical and the final outlet state is the weighted average of the outlet states from each node.) If a counterflow stream is present, the enthalpy of that stream at the end of the heat exchanger is compared to the inlet enthalpy. If they do not agree within a convergence tolerance, a new guess is generated for the outlet enthalpy and the calculations are

repeated for the entire heat exchanger. The improved guess is generated by Mueller's method (107); in this method the three previous guesses and resulting enthalpy differences at the end of the heat exchanger are used to construct a parabola to find the next guess. The second and third guesses (needed before Mueller's method can be used) are generated by successive substitution and the secant method respectively.

A number of numerical integration schemes were investigated for the heat exchanger component. The fourth order Runge-Kutta method was initially selected and worked well, but required substantial amounts of computer time. In tests of the entire absorption cycle, this component accounted for approximately 80 percent of the total CPU time used. While this figure is not unreasonable considering that five components in the cycle were modeled, it did present the opportunity to significantly improve the computational efficiency of the entire simulation by modifying a single component. A simple Euler integration and second and fourth order Runge-Kutta integrations were tested. (The second order Runge-Kutta method is equivalent to a modified Euler method without iteration.)

The system tested represents a condenser; a single-phase heat exchange streams flows countercurrently to a refrigerant stream which enters as a saturated vapor and exits as a low quality two phase mixture. The values of the total heat flow for various numbers of nodes are presented in Table 4-2. The simple Euler integration required more than 40 nodes for the heat flow to be within one percent

of the actual value (obtained by running the fourth order Runge-Kutta integration with 100 nodes). The second and fourth order Runge-Kutta methods require only about 20 and five nodes respectively to achieve the same accuracy. While the simple Euler integration involves only one evaluation of heat flow per node compared to two and four for the second and fourth order Runge-Kutta solutions, it required the most CPU time for a given accuracy. The Euler method required more than ten seconds to obtain one percent accuracy, compared to six seconds for the second order Runge-Kutta and three seconds for the fourth order Runge-Kutta integrations.

Table 4-2 Comparison of heat flows for a condenser simulated with Euler and second and fourth order Runge-Kutta integrations for varying numbers of nodes

No. nodes	Heat flow (kW)			Percent difference*		
	Euler	2 <sup>nd</sup> R-K	4 <sup>th</sup> R-K	Euler	2 <sup>nd</sup> R-K	4 <sup>th</sup> R-K
3	-	-	5.51	-	-	-3.4
5	4.42	5.02	5.65	-22.4	-11.7	-0.7
10	5.10	5.49	5.69	-10.4	-3.6	-0.1
20	5.43	5.62	5.68	-4.6	-1.2	-0.2
40	5.60	5.67	5.69	-1.7	-0.5	+0.01

\* Percent difference relative to value obtained using 100 nodes with fourth order Runge-Kutta method

The mass inventory of each stream in the heat exchanger is computed node-by-node in parallel with the integration of heat flow. The volume of each stream is divided equally between the nodes and a

weighted average of the specific volumes at the beginning, midpoint and end of the node is used in calculating the mass in a node. The inventory calculations are bypassed for any stream with a zero volume, thereby providing a means to exclude an external heat exchange stream from the inventory analysis.

#### 4.5.4 Falling-film absorber

In a falling-film absorber, absorbent solution flows over a heat exchange surface in the presence of refrigerant vapor, transferring the heat of absorption to a heat exchange fluid. A common configuration for the heat exchanger and the one treated here is a bank or coil of tubes with the absorbent solution dripping from one row to the next. An absorber has three inputs (strong absorbent, refrigerant and heat exchange streams) and two outputs (weak absorbent and heat exchange streams) as shown in Figure 4-7.

The bank of tubes is separated into rows and the heat and mass transfer processes occurring in the absorber are dealt with on a row-by-row basis. Each row of tubes is approximated as an isothermal plate. Since there are typically many rows of tubes in an absorber, the heat exchange stream undergoes only a small temperature rise in flowing through a single row. The absorbent solution is assumed to mix fully as it drips from one row of tubes to the next.

The analysis of Grigor'eva and Nakoryakov (98,108) for absorption into a laminar film flowing over an isothermal plate is used to treat the heat and mass transfer for each row of the absorber. (Their analysis was chosen over a similar one presented by Grossman (96,97)

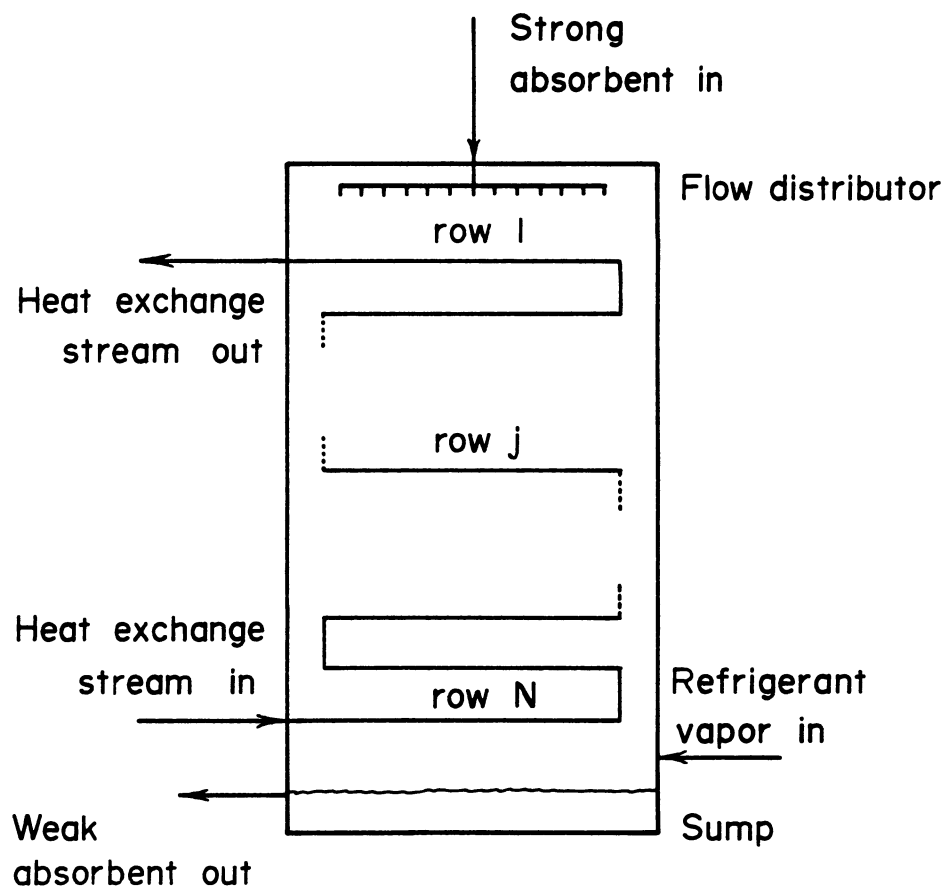


Figure 4-7 Falling film absorber component schematic

because it was simpler to implement and would therefore require less computation time.) The analysis begins with differential continuity and energy equations. The boundary conditions assume that the absorbent enters the top of the plate at a uniform composition and temperature (equal to the plate temperature) and flows down the plate with a uniform velocity profile and constant thickness. Equilibrium is assumed to exist at the vapor-liquid interface and all heat of absorption at the interface is conducted into the film. The vapor phase is assumed to be pure refrigerant. In order to allow a closed form solution, the relationship between saturation liquid composition and temperature at a given vapor pressure is linearized about the inlet condition; all other properties are taken to be constant.

The solution of the system is carried out by assuming that a linear temperature profile exists through the film and that no absorbed vapor diffuses to the wall before the end of the plate. These assumptions limit the solution to the region of developed temperature profile but developing concentration profile, and would be applicable for an absorbent with a small Lewis number. (The Lewis number used here is the ratio of the mass to thermal diffusivities and is the inverse of that used by Grigor'eva and Nakoryakov.)

The surface (or interfacial) temperature resulting from this analysis is given by:

$$T_s = \frac{\left(\frac{\pi \alpha z}{Le u \delta^2}\right)^{0.5} T_w + Ka \frac{b}{d} - Ka \frac{x_o}{d}}{\left(\frac{\pi \alpha z}{Le u \delta^2}\right)^{0.5} - Ka} \quad [4-58]$$

where  $T_w$  is the wall temperature,  $z$  is the distance from the plate entrance,  $x_o$  is the inlet concentration,  $Le$  and  $\alpha$  are the Lewis number and thermal diffusivity for the absorbent and  $u$  is the film velocity. The constants  $b$  and  $d$  are defined by the linearization of the vapor-liquid equilibrium behavior:

$$x = b + dT \quad [4-59]$$

$Ka$  is analogous to a phase transition criteria and is given by:

$$Ka = d r_\alpha / C_p \quad [4-60]$$

where  $r_\alpha$  is the heat of absorption, including the phase transition and heat of solution, and  $C_p$  is the heat capacity of the absorbent.

With the assumption of a linear temperature profile, the heat flux at the wall is given by:

$$\dot{q}_{wall} = \frac{k(T_s - T_w)}{\delta} \quad [4-61]$$

The mass flux at the surface,  $\dot{q}_m$ , is related to the heat transfer by:

$$\dot{q}_m = \dot{q}_{wall} \frac{x_{eq} - x_o}{r_\alpha x_o} \quad [4-62]$$

where  $x_{eq}$  is the equilibrium composition of absorbent at the wall temperature and vapor pressure.

In applying the above results of Grigor'eva and Nakoryakov to the case of flow over a cylinder, additional analysis is required. To approximate a cylinder as a flat plate it is necessary to find some appropriate average velocity and resulting film thickness. The velocity of a liquid film flowing down a plate with slope  $\beta$  is given by Bird, et al. (109):

$$u = \frac{\rho g \delta^2 \sin \beta}{3\mu} \quad [4-63]$$

where  $\rho$  and  $\mu$  are the fluid density and viscosity and  $g$  is the acceleration of gravity. The mass flow rate of liquid per unit plate width is given by:

$$\Gamma = u \rho \delta \quad [4-64]$$

Combining [4-63] and [4-64] yields:

$$u = \frac{g \Gamma^2 \sin \beta}{3 \rho \mu} \quad [4-65]$$

The average velocity over a horizontal cylinder is obtained by integrating Equation [4-65] from  $\beta = 0$  to  $\beta = \pi$ :

$$v_{avg} = \frac{1}{\pi} \left( \frac{g \Gamma^2}{3 \rho \mu} \right)^{1/3} \int_0^{\pi} \sin^{1/3} \beta \, d\beta \quad [4-66]$$

The integral was evaluated numerically using Simpson's rule to yield:

$$v_{\text{avg}} = \frac{1.794}{\pi} \left( \frac{g \Gamma^2}{\rho \mu} \right)^{1/3} \quad [4-67]$$

The corresponding film thickness is:

$$\delta = \frac{\pi}{1.794} \left( \frac{\Gamma \mu}{\rho^2 g} \right)^{1/3} \quad [4-68]$$

The average heat and mass fluxes down the length of the plate can be found by integrating Equation [4-61]:

$$\dot{q}_{\text{avg}} = 1/z \int_0^z \dot{q} dz \quad [4-69]$$

This yields:

$$\dot{q}_{\text{avg}} = 2 \left[ \frac{z^{0.5}}{\theta} + \frac{Ka}{\theta^2} \ln \left( 1 - \frac{\theta}{Ka} z^{0.5} \right) \right] \quad [4-70]$$

where  $\theta$  is a collection of terms:

$$\theta = \left( \frac{\pi \alpha}{Le u \delta^2} \right)^{0.5} \quad [4-71]$$

Combining [4-70] and [4-62] yields the average mass flux:

$$\dot{q}_{\text{m,avg}} = \frac{2 (x_{\text{eq}} - x_o)}{r_\alpha x_o} \left[ \frac{z^{0.5}}{\theta} + \frac{Ka}{\theta^2} \ln \left( 1 - \frac{\theta}{Ka} z^{0.5} \right) \right] \quad [4-72]$$

The first step in the implementation of the above relations is to evaluate the fluid dependent parameters  $b$ ,  $d$ ,  $r_\alpha$  and  $Ka$  at the strong

absorbent inlet conditions. An initial guess is then made for the outlet enthalpy of the countercurrent heat exchange stream. (For the second and subsequent call to the absorber component, the converged values from the previous call is used.)

The row-by-row calculations begin at the top. The heat from the film for row  $j$  is given by:

$$\dot{Q}_{\text{abs},j} = \dot{q}_{\text{avg},j} A_{t,o} \quad [4-73]$$

The heat transfer to the bulk of the heat transfer fluid is given by:

$$\dot{Q}_{\text{abs},j} = UA_j (T_{s,j} - T_{\text{hx},j}) \quad [4-74]$$

where the transfer coefficient is given by:

$$UA_j = \frac{1}{\frac{1/hc_{\text{ins}}}{A_{t,\text{ins}}} + \frac{R_w}{A_{t,\text{lm}}}} \quad [4-75]$$

where  $hc_{\text{ins}}$  is the convective heat transfer coefficient for the inside of the tube and  $R_w$  is the thermal resistance of the tube wall. The values of  $\dot{Q}_{\text{abs}}$  given by Equations [4-73] and [4-74] must be equal; the value of  $T_s$  required to satisfy this equality is found iteratively using the secant method.

The amount of vapor absorbed in row  $j$  is then computed :

$$\dot{m}_{\text{vap},j} = qm_j A_{t,o} \quad [4-76]$$

The conditions of the absorbent solution leaving the row (which are

set to those entering the next row) are given by:

$$\dot{m}_{a,j+1} = \dot{m}_{a,j} + \dot{m}_{vap,j} \quad [4-77]$$

$$x_{a,j+1} = \frac{\dot{m}_{a,j} x_{a,j} + \dot{m}_{vap,j} x_{vap,j}}{\dot{m}_{a,j+1}} \quad [4-78]$$

$$h_{a,j+1} = \frac{\dot{m}_{a,j} h_{a,j} + \dot{m}_{vap,j} h_{vap,j} - \dot{Q}_{abs,j}}{\dot{m}_{a,j+1}} \quad [4-79]$$

The enthalpy of the heat exchange stream in the next lower row is given by:

$$h_{hx,j+1} = h_{hx,j} - \frac{\dot{Q}_{abs,j}}{\dot{m}_{hx}} \quad [4-80]$$

where the negative sign on the  $\dot{Q}_{abs}$  term is a result of the countercurrent flow of the heat exchange stream.

At the bottom of the absorber, the computed enthalpy of the heat exchange stream is compared to the value at the absorber inlet. If necessary, a new guess for the outlet enthalpy is made by the secant method and the calculation returns to the top row. Finally any unabsorbed vapor is combined with the outlet weak absorbent stream.

In implementing this analysis, problems were encountered which required two modifications to the procedure outlined above. The heat flux given by [4-70] is proportional to the vapor absorption flux. This behavior is correct if the assumption of equal inlet absorbent solution and tube wall temperatures is met. In many cases, however,

the temperature of the inlet absorbent solution is considerably higher than that of the tube wall. In these cases it is possible that the heat flux calculated using a constant coefficient for the falling film (i.e., not accounting for the effects of mass transfer) is higher than that predicted by [4-70]. The absorption of vapor can only increase the heat flux over that existing for a simple falling film. To avoid this underprediction of heat flow, the heat flux is calculated both by [4-70] and by assuming a constant film coefficient with the maximum value being used.

The rate of mass transfer given by Equation [4-72] is independent of the inlet vapor mass flow rate. In the second modification to the absorber, the cumulative amount of vapor absorbed is summed; if this value exceeds the inlet vapor flow rate, no further mass transfer occurs. Subsequent tubes serve only to heat exchange the absorbent solution with the coolant stream. The heat transfer is calculated using a constant heat transfer coefficient for the falling film.

The mass inventory of absorbent solution resides as a film on each row of tubes and in a sump at the bottom. The mass on the tubes is found using the film thickness calculated by Equation [4-68]:

$$m_j = A_{t,o} \delta_j / v_j \quad [4-81]$$

The mass of refrigerant and absorbent is then calculated using the concentration for that row. The mass contained in the sump is :

$$m_{\text{sump}} = V_{\text{sump}} / v_{\text{weak abs}} \quad [4-82]$$

where the specific volume is evaluated at the conditions leaving the absorber. The mass of vapor associated with the fixed vapor volume is based on the specific volume of the vapor portion of the inlet refrigerant stream. The mass of the heat exchange fluid in each row can be included in the inventory analysis by specifying a positive volume for the heat exchanger. This option would be needed for a machine employing a solution-cooled absorber.

#### 4.5.5 Throttle valves

A throttle valve reduces the pressure and regulates the flow of a stream. The mass balance for a throttle is trivial; the throttling process is essentially isenthalpic, making the energy balance very simple as well:

$$\dot{m}_{\text{out}} = \dot{m}_{\text{in}} \quad [4-83]$$

$$x_{\text{out}} = x_{\text{in}} \quad [4-84]$$

$$h_{\text{out}} = h_{\text{in}} \quad [4-85]$$

The relationship between mass flow rate, pressure drop and stream conditions is much more complex and depends on the geometry of the particular throttle. The throttle valves in the Arkla heat pump are fixed orifice devices. The mass flow rate across a sharp-edged orifice for single phase flow is given by Bird, et al. (109):

$$\dot{m} = C_d A_o \left( \frac{2 \Delta P}{v_o (1 - A_o/A)} \right)^{0.5} \quad [4-86]$$

where  $C_d$  is a discharge coefficient,  $A_o$  and  $A$  are the throat and pipe areas respectively, and  $\Delta P$  is the pressure drop across the orifice.

For flows which are two-phase (either upon entering the throttle or because of flashing within the throttle), [4-86] is applicable if homogeneous flow is assumed, with  $v$  being a weighted average of the liquid and vapor specific volumes. Although Collier (110) states that this assumption underestimates the flow rate, it does suggest that the flow rate will be a function of the quality in the throttle:

$$\dot{m} = C_d A_o \left( \frac{2 \Delta P}{(y v_{\text{vap}} + (1 - y)v_{\text{liq}})(1 - A_o/A)} \right)^{0.5} \quad [4-87]$$

James (111) has suggested an empirical correction to [4-87] replacing the quality by the quality raised to the 1.5 power. If this is done, [4-87] can be rearranged to give:

$$\frac{\Delta P}{\dot{m}^2} = \frac{(1 - A_o/A)}{2C_d^2 A_o^2} \left( v_{\text{liq}} + (v_{\text{vap}} - v_{\text{liq}}) y^{1.5} \right) \quad [4-88]$$

At a sufficiently high Reynolds number, the discharge coefficient is nearly constant and for a throttle in a given application, the liquid and vapor specific volumes will also be approximately constant. Thus, Equation, [4-88] can be reduced to a linear form:

$$\Delta P/\dot{m}^2 = C_1 + C_2 y^{1.5} \quad [4-89]$$

where  $C_1$  and  $C_2$  are groupings of approximately constant terms in [4-88]. This result is also valid for single phase flows if  $y$  is

replaced by zero or unity for subcooled liquid or superheated vapor flows, respectively.

The data for the 16 cycle investigation tests were fit to Equation [4-89] by the method of least squares using the Minitab program (112). For the condenser throttle, values for the parameters  $C_1$  and  $C_2$  were  $23300 \text{ MPa sec}^2 \text{ kg}^{-2}$  and  $678000 \text{ MPa sec}^2 \text{ kg}^{-2}$  with an  $r^2$  factor of 0.98. The experimental data and least squares line are shown in Figure 4-8. (Uncertainty regarding the quality for the throttle at the evaporator inlet did not permit a similar empirical fit. Both the pressure drop and mass flow rate were supplied to this throttle in the simulation.)

The throttle model computes the mass flow rate for a given pressure drop. The computed flow rate will, in general, not be equal to the flow rate input to the throttle, thus resulting in a discontinuity in mass flow rate. The throttles are used to adjust the flow rate in the various portions of the cycle and while it may be disconcerting to have a temporary violation of a mass balance, they are indeed satisfied when the cycle has converged.

#### 4.5.6 Solution pump

The solution pump in the Arkla AHP is a diaphragm-type positive displacement pump. Such a device delivers an approximately constant volumetric flow rate (based on inlet conditions). The mass flow rate is related to the volumetric flow rate,  $\dot{v}_{\text{pump}}$ , by:

$$\dot{m} = \dot{v}_{\text{pump}} / v_{\text{in}} \quad [4-90]$$

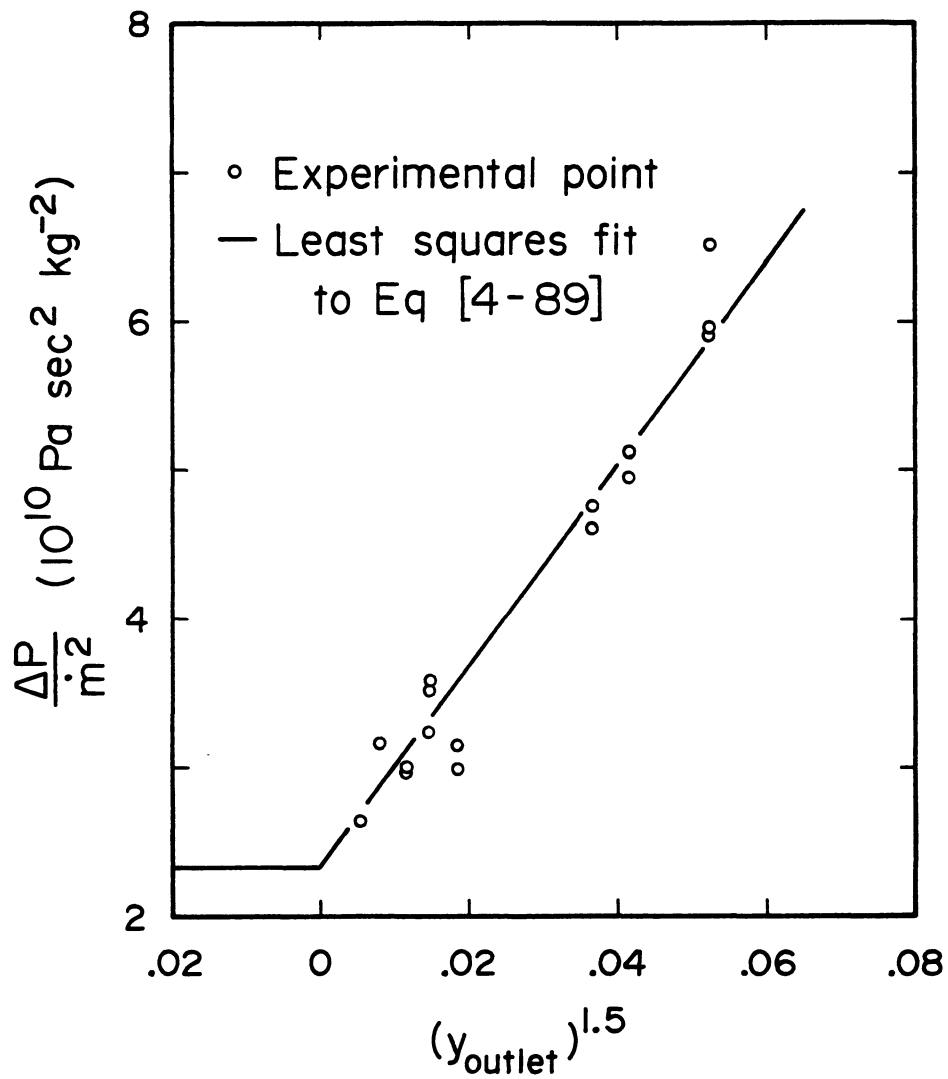


Figure 4-8 Flowrate-pressure drop behavior as a function of outlet quality for the condenser throttle

where  $v_{in}$  is the specific volume of the inlet stream. The inlet to the solution pump in the Arkla heat pump is situated in a sump at the bottom of the absorber and thus will pump only liquid under normal operating conditions. For this situation, the inlet specific volume is relatively constant and a constant volumetric flow will result in an approximately constant mass flow rate.

The pump model implements both constant volumetric and mass flow rate options. In both cases, the outlet pressure is supplied to the pump component. The mass inventory in the solution pump is assumed to be negligible.

#### 4.5.7 Stream mixer/vapor-liquid separator

It is necessary to have a component that will mix a number of inlet streams (e.g., the weak absorbent and rectifier reflux streams entering the analyzer). The option of separating the resulting stream into liquid and vapor fractions was also implemented. This component was modeled as separate mixing and separating sections as shown in Figure 4-9. Mass, refrigerant and energy balances for the mixing section yield:

$$\dot{m}_{mix} = \sum_{i=1,N} \dot{m}_i \quad [4-92]$$

$$x_{mix} = 1/\dot{m}_{mix} \sum_{i=1,N} x_i \dot{m}_i \quad [4-93]$$

$$h_{mix} = 1/\dot{m}_{mix} \sum_{i=1,N} \dot{m}_i h_i \quad [4-94]$$

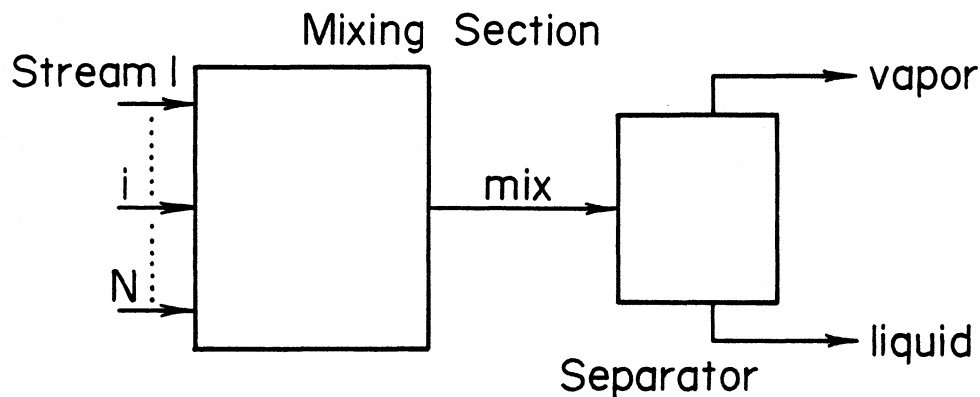


Figure 4-9 Schematic representation of the stream mixer/vapor-liquid separator model

where the subscript *mix* refers to the stream leaving the mixing section and the summations are carried out over all *N* entering streams. The pressure of the outlet is taken to be that of inlet stream 1. The temperature and quality of the mixed stream is found using the property routine *YT* (described in Appendix C.2); this routine also calculates the enthalpy and composition of the liquid and vapor fractions. The mass flow rates of the separated streams are given by:

$$\dot{m}_{\text{liq}} = \text{MAX}(0, 1 - y_{\text{mix}}) \dot{m}_{\text{mix}} \quad [4-95]$$

$$\dot{m}_{\text{vap}} = \dot{m}_{\text{mix}} - \dot{m}_{\text{liq}} \quad [4-96]$$

where *MAX* is the maximum function.

The stream mixer/separator component is a straightforward implementation of Equations [4-92] to [4-96]. Up to five streams can

be input to the component and one combined or two single-phase streams are output depending on the value of a parameter. The mass inventory for this component is assumed to be negligible.

#### 4.5.8 Convergence component

A modular simulation usually involves the iteration of a number of recyclic information loops such as that depicted in Figure 4-10. In this figure, the solution of component A requires the output from B and vice versa. The solution of this system requires iteration on a tear stream. (Rudd and Watson (113) discuss tear streams in detail and the selection of the minimum number of tear streams required for a given system.) The variable  $x$  for stream 3 is guessed, the calculations in components A and B are then carried out yielding a revised value for stream 3,  $f(x)$ . The correct value of  $x$  is that which results in an identical value of  $f(x)$ .

The convergence of tear streams and recycle loops in the simulation is carried out by a separate convergence component which must be explicitly specified in the simulation deck. It is called as the final component in a recycle loop. The current property values of the tear stream are compared with those on the previous call to determine convergence. If the stream has not converged, the stream values are modified and a pointer variable is reset to call the first component in the recycle loop. When a tear stream has converged within a specified tolerance, the next component in the simulation is called. The convergence component implements both a Wegstein and two-variable secant method iteration. The secant iteration was

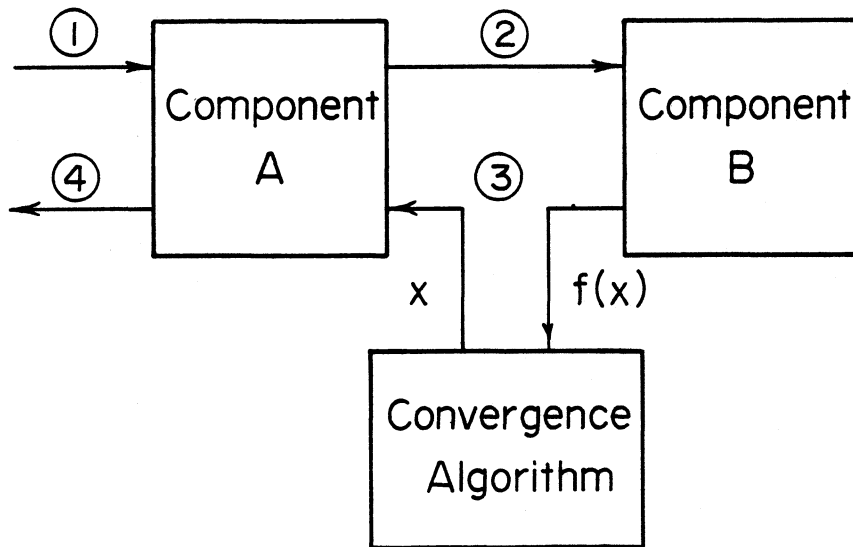


Figure 4-10 Recyclic information loops and the location of the convergence component in a simulation

programmed in an attempt to improve on the convergence of the Wegstein method; however, the Wegstein iteration resulted in faster convergence except for a few cases having strong interactions between variables.

The Wegstein iteration method (104) (also termed Aitken's method) defines a new guess for  $x$  in terms of the previous  $x$  and  $f(x)$  values:

$$x_{n+1} = q_n x_n + (1 - q_n) f(x_n) \quad [4-97]$$

The factor  $q_n$  is termed the acceleration parameter. If  $q_n$  is zero, the Wegstein method reduces to successive substitution; positive values of  $q_n$  correspond to a damped iteration compared to successive substitution while negative values correspond to an accelerated solution. (A "bounded Wegstein" method is obtained if bounds are placed on the allowable values of  $q_n$ .) The acceleration parameter is

defined in terms of a slope,  $s$ :

$$q_n = s/(s - 1) \quad [4-98]$$

$$s = \frac{f(x_n) - f(x_{n-1})}{x_n - x_{n-1}} \quad [4-99]$$

This slope and the Wegstein iteration have a simple geometric interpretation as shown in Figure 4-11. The line drawn through the points  $(x_n, f(x_n))$  and  $(x_{n-1}, f(x_{n-1}))$  has a slope  $s$ . The intersection of this line with the line  $x = f(x)$  gives the next guess for  $x$ . The path taken by successive substitution is also shown. In the convergence component, the bounded Wegstein method is applied independently to each variable of the tear stream.

The familiar Newton's method for finding the root of an equation and the related secant method can be extended to higher dimensions to solve systems of equations (107). In two dimensions the system to be solved is:

$$g_1(x_i, y_i) = x_i - f(x_i) = 0 \quad [4-100]$$

$$g_2(x_i, y_i) = y_i - f(y_i) = 0 \quad [4-101]$$

where  $x$  and  $y$  are the two iteration variables and the subscript refers to the  $i^{\text{th}}$  iteration. Newton's method expands [4-100] and [4-101] in a Taylor series about the guess  $(x_i, y_i)$ ; the series is truncated after the first derivative terms and solved for an improved set of guesses:

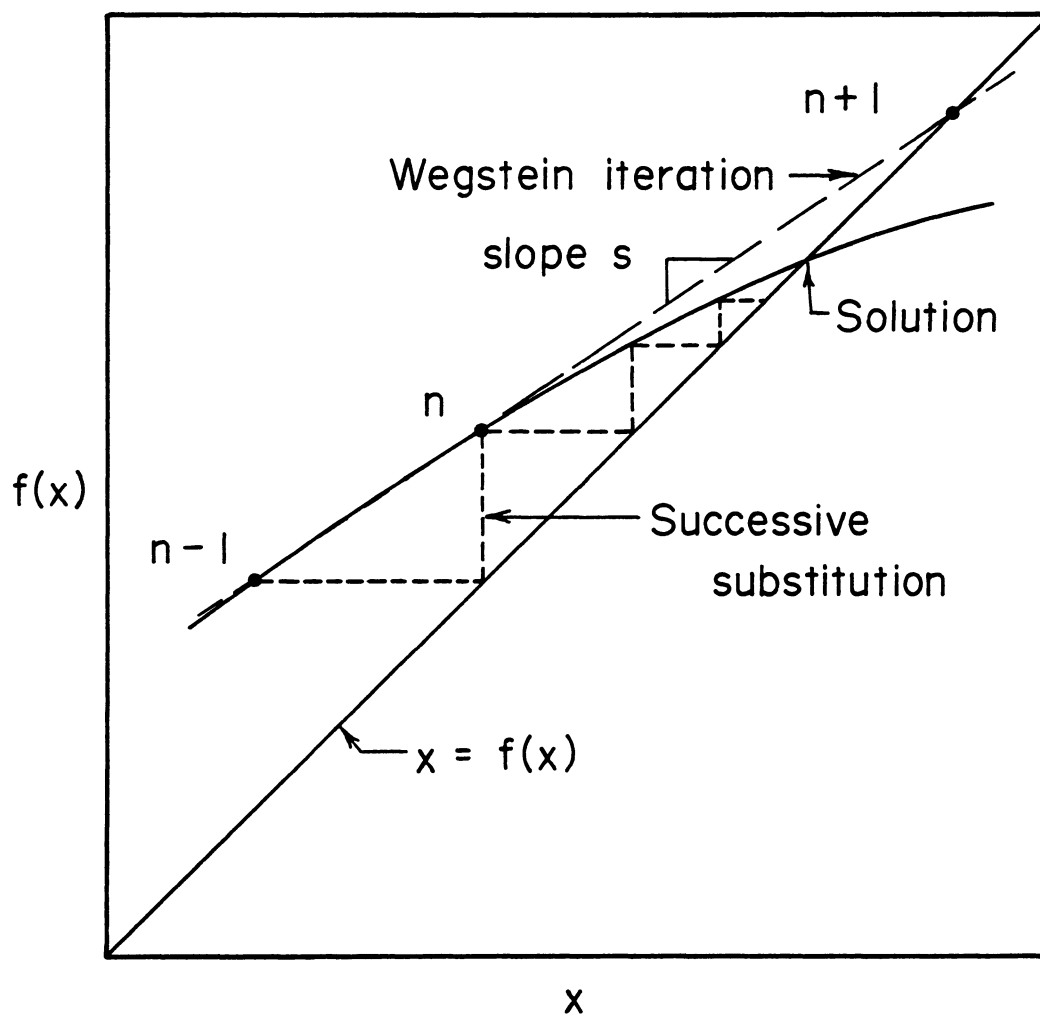


Figure 4-11 Geometric interpretation of the Wegstein and successive substitution iteration methods

$$x_{i+1} = x_i + \frac{\begin{vmatrix} -g_1 & \partial g_1 / \partial y \\ -g_2 & \partial g_2 / \partial y \end{vmatrix}}{\det} \quad [4-102]$$

$$y_{i+1} = y_i + \frac{\begin{vmatrix} \partial g_1 / \partial x & -g_1 \\ \partial g_2 / \partial x & -g_2 \end{vmatrix}}{\det} \quad [4-103]$$

where the denominator in both cases is a determinate of partial derivatives:

$$\det = \begin{vmatrix} \partial g_1 / \partial x & \partial g_1 / \partial y \\ \partial g_2 / \partial x & \partial g_2 / \partial y \end{vmatrix} \quad [4-104]$$

If the partial derivatives cannot be found analytically (as is generally the case in a simulation problem), they must be numerically approximated. Starting with an initial guess  $(x_0, y_0)$ , successive substitution can be used to generate an improved guess  $(x_1, y_1)$ . The functions  $g_1$  and  $g_2$  are then evaluated at  $(x_1, y_0)$  and  $(x_1, y_1)$  to allow computation of the partial derivatives by a difference relation:

$$\frac{\partial g_1}{\partial x} = \frac{g_1(x_1, y_0) - g_1(x_0, y_0)}{x_1 - x_0} \quad [4-105]$$

$$\frac{\partial g_1}{\partial y} = \frac{g_1(x_1, y_1) - g_1(x_1, y_0)}{y_1 - y_0} \quad [4-106]$$

An improved guess  $(x_2, y_2)$  is obtained by [4-102] through [4-106]; the

functions  $g_1$  and  $g_2$  are each evaluated at  $(x_2, y_1)$  and  $(x_2, y_2)$  and used with  $(x_1, y_1)$  to continue the iteration.

This method of generating partial derivatives requires one less set of function evaluations per iteration than the method suggested by Gerald (107) but is applicable only if the functions  $g_1$  and  $g_2$  are sufficiently linear. In the implementation of this method in the convergence component, the two variables involved in the iteration are specified in the parameter list; successive substitution is used for the remaining stream variables. This iteration method is also used in the iteration for concentration and flow rate in the analyzer component.

A similar two variable secant method was used for the iteration of system pressures to match the input and calculated refrigerant and absorbent inventory. In this case, however, the inventory functions were not linear in pressure and the method of calculating partial derivatives given by [4-105] and [4-106] was not suitable. A second starting value for pressures  $(x_1, y_1)$  was required in addition to  $(x_0, y_0)$ . The inventory functions were also evaluated at the points  $(x_1, y_0)$  and  $(x_0, y_1)$  to generate the partial derivatives. The next guess for the pressures,  $(x_2, y_2)$ , was obtained by [4-102] to [4-104]. Each subsequent iteration for system pressures required function evaluations at the points  $(x_1, y_2)$ ,  $(x_2, y_1)$  and  $(x_2, y_2)$ .

## 4.6 Simulation of the Prototype AHP

### 4.6.1 Cycle representation

The representation of the Arkla absorption heat pump cycle with the components of the steady-state simulation model is depicted in Figure 4-12. For the most part, there is a direct correspondence between physical components in the AHP with simulation components. The generator, analyzer and rectifier, which are integrated in the physical cycle, are treated as three separate components in the simulation; a stream mix component is also required to combine the weak absorbent and reflux streams leaving the rectifier. The triple heat exchanger configuration of the rectifier is treated by specifying a three-stream heat exchanger with a zero heat transfer area between the strong absorbent and vapor streams. The heat input to the generator is taken to be a known value.

The condenser, evaporator, and refrigerant and flue gas heat exchangers are simulated with the heat exchanger component. The flue gas heat exchanger is modeled as a cross flow device; the condenser and refrigerant heat exchangers have a counterflow geometry. The evaporator of the Arkla AHP has a combination counter/cross flow arrangement. Ambient air flows over an evaporator coil in a cross flow fashion; the air and refrigerant streams flow countercurrently to each other between the three banks of coils. This flow arrangement was approximated as a strictly countercurrent flow in the simulation to avoid the need for additional iteration loops and convergence components.

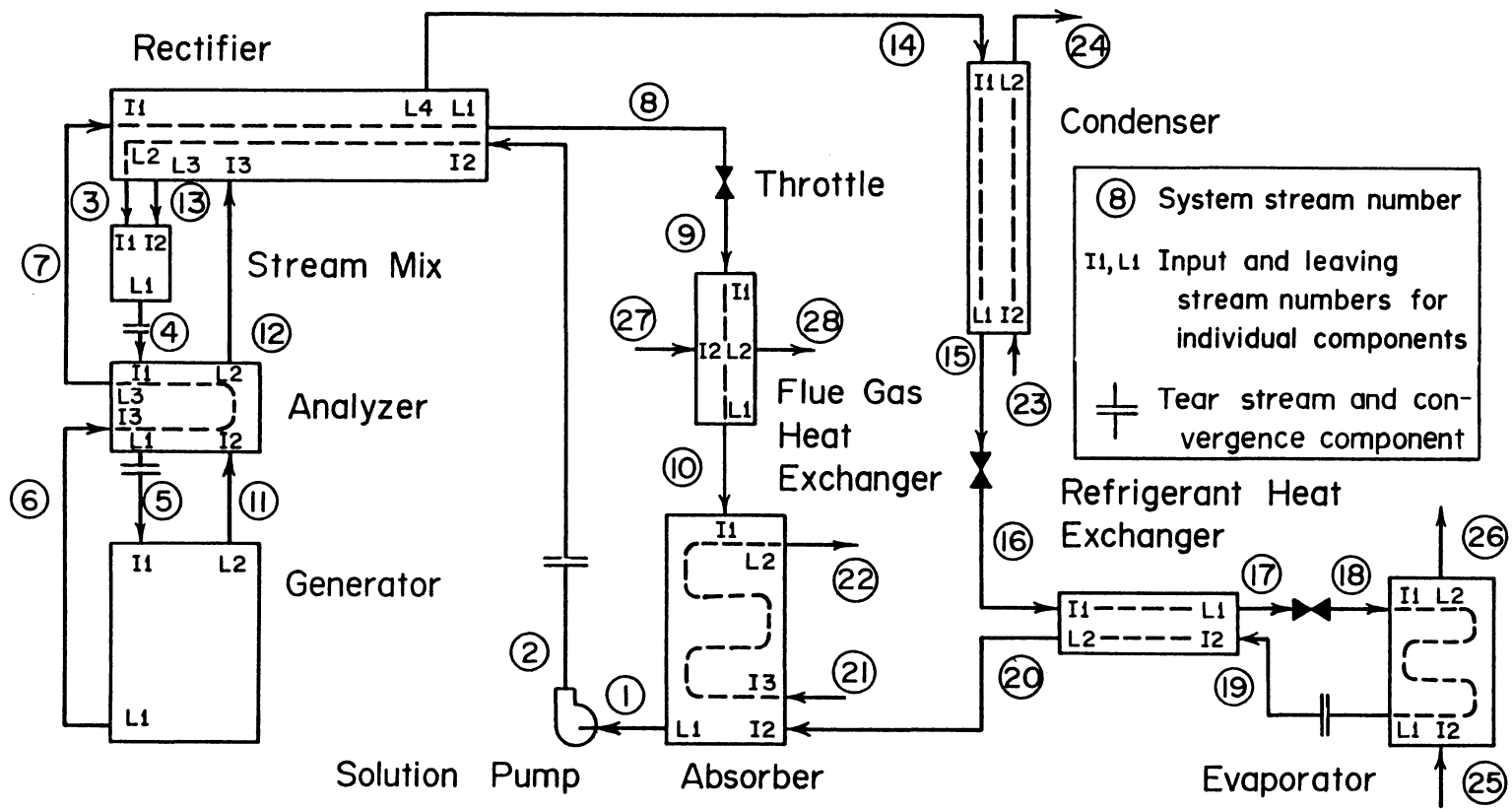


Figure 4-12 Simulation schematic for the Arkla prototype absorption heat pump

The absorber is simulated using the falling-film absorber model. An assumption made in this model is that the entering absorbent solution is at the temperature of the wall of the heat exchange tube; because of the flue gas heat exchanger, the entering solution will be substantially warmer than the exiting heat exchange fluid. This will result in a high predicted vapor absorption rate for the first few rows of heat exchange tubes.

The solution pump is treated as a constant mass flow rate device. The throttle at the condenser outlet is modeled as described in Section 4.5.5; a fit to experimental data was used for the throttle parameters. The absorber and evaporator throttles serve to reduce their respective streams to the low side pressure at a specified flow rate.

#### 4.6.2 Iteration sequence

The tear streams necessary for the iteration of the absorption cycle are the solution pump outlet, weak absorbent inlet and outlet streams of the analyzer, and the evaporator refrigerant outlet (streams 2, 4, 5 and 19 in Figure 4-12). These streams are converged by separate convergence components. The iteration sequence for the entire cycle is depicted in Figure 4-13. (This sequence is specified in the simulation deck and is thus flexible.) The analyzer inlet and outlet streams are converged simultaneously by two sequential convergence components. This arrangement was found to require fewer total component calls than separate convergence loops (i.e., converging the generator and analyzer before proceeding to the

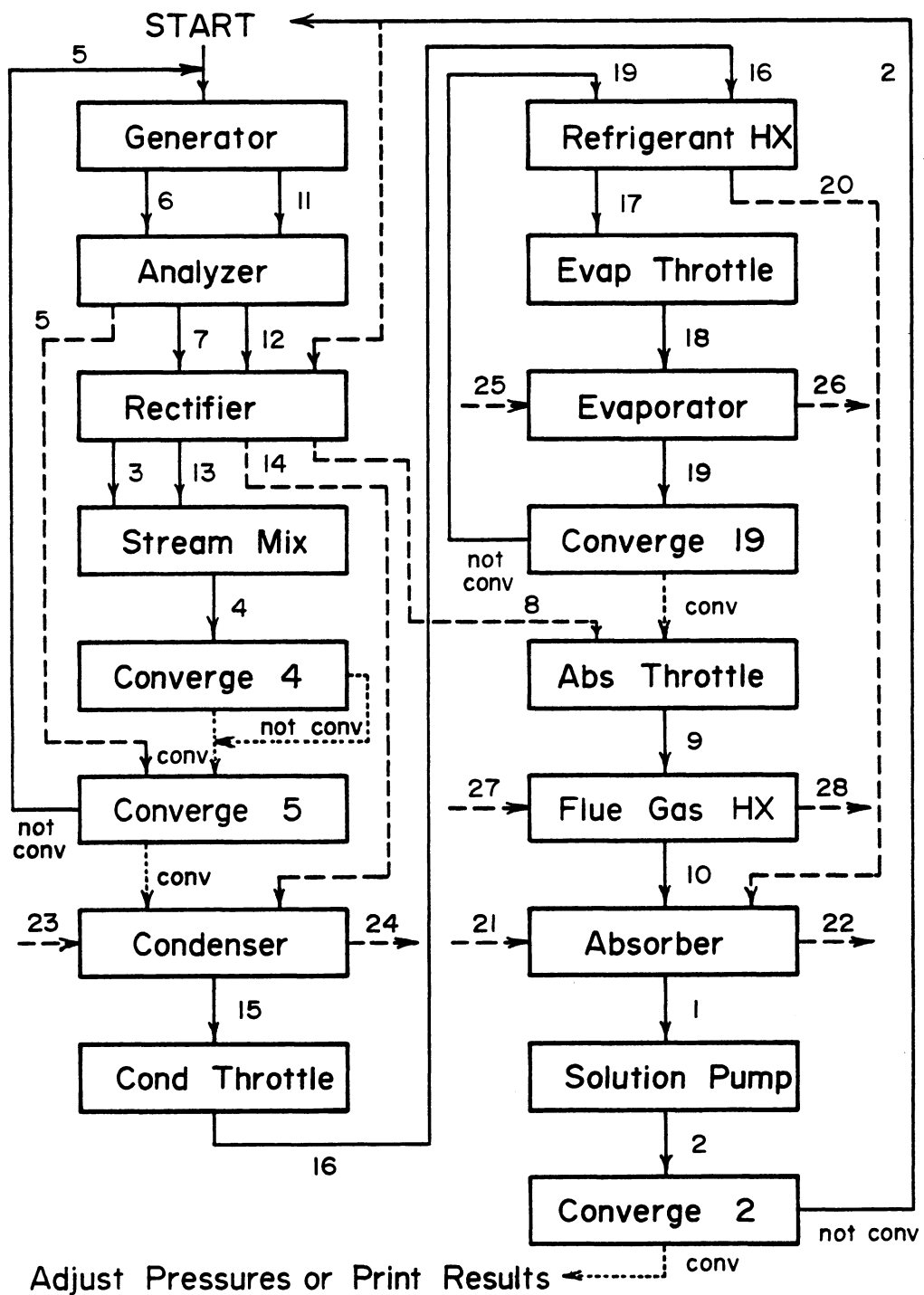


Figure 4-13 Iteration sequence for the simulation of the Arkla AHP

rectifier). All of the convergence components used a bounded Wegstein iteration.

#### 4.6.3 Estimation of heat pump parameters

The parameters necessary to specify the heat pump components fall into the general categories of the specification of simulation options (e.g. whether or not to print intermediate component iterations or whether a heat exchanger is counter, cross, or co-current flow), parameters related to physical dimensions (such as heat exchanger areas and component volumes), heat and mass transfer parameters, and the flow characteristics for the pump and throttles. The major parameters in the simulation are given in Table 4-3. Detailed specifications for the Arkla heat pump were not available and thus it was necessary to estimate many of the parameters. Where possible, these were based on direct measurements of the unit. In some cases it was necessary to adjust parameters to give reasonable agreement with a limited number (3 to 5) of experimental tests; the parameters were then checked with an independent set of three to five experimental tests.

The volumes and heat exchange areas for the condenser, evaporator, and refrigerant heat exchanger were directly calculated from measured dimensions. The number of nodes in the various heat exchangers were selected to give heat transfer rates within one percent of the values obtained with a large number of nodes. The number of rows of heat exchange tubes in the absorber was estimated from the overall height of the absorber (allowing space for a flow

Table 4-3 Primary component parameters for the simulation of the Arkla absorption heat pump

Generator:	
heat input (varies with ambient temperature)	10.2 - 10.6 kW
liquid volume	0.0052 m <sup>3</sup>
vapor volume	0.0013 m <sup>3</sup>
Analyzer:	
number of equilibrium stages	1
overall UA for heat exchanger	0.1 kW C <sup>-1</sup>
liquid volume	0.0075 m <sup>3</sup>
vapor volume	0.0030 m <sup>3</sup>
volume in heat exchanger	0.0020 m <sup>3</sup>
Rectifier:	
area: weak absorbent to vapor	0.32 m <sup>2</sup>
area: weak absorbent to strong absorbent	0.25 m <sup>2</sup>
heat transfer coefficients:	
vapor	2.0 kW m <sup>-2</sup> C <sup>-1</sup>
strong absorbent	1.8 kW m <sup>-2</sup> C <sup>-1</sup>
weak absorbent	2.5 kW m <sup>-2</sup> C <sup>-1</sup>
weak absorbent volume	0.0004 m <sup>3</sup>
strong absorbent volume	0.0007 m <sup>3</sup>
vapor volume	0.007 m <sup>3</sup>
Condenser:	
heat exchange area	0.25 m <sup>2</sup>
refrigerant volume	0.0024 m <sup>3</sup>
load water volume	0

Table 4-3 (continued)

Refrigerant heat exchanger:	
heat exchanger area	0.16 m <sup>2</sup>
annulus volume	0.0013 m <sup>3</sup>
inner tube volume	0.0004 m <sup>3</sup>
Flue gas heat exchanger:	
overall UA	0.06 kW C <sup>-1</sup>
Absorber:	
heat exchanger area	1.2 m <sup>2</sup>
number of heat exchange rows	30
effective plate length	0.02 m
viscosity of absorbent solution	0.0007 Pa s
diffusion coefficient for solution	2.0 x 10 <sup>-9</sup> m <sup>2</sup> s <sup>-1</sup>
thermal diffusivity for solution	1.1 x 10 <sup>-7</sup> m <sup>2</sup> s <sup>-1</sup>
vapor volume	0.011 m <sup>3</sup>
sump volume	0.0009 m <sup>3</sup>
load water volume	0
Solution pump:	
mass flow rate	0.0227 kg s <sup>-1</sup>
Heat transfer coefficients:	
load water	7.2 kW m <sup>-2</sup> C <sup>-1</sup>
condensing ammonia (condenser and ref HX annulus):	
subcooled liquid	0.4 kW m <sup>-2</sup> C <sup>-1</sup>
two phase	8.0 kW m <sup>-2</sup> C <sup>-1</sup>
superheated vapor	0.1 kW m <sup>-2</sup> C <sup>-1</sup>
evaporating ammonia (evaporator and inner tube of ref HX):	
subcooled liquid	0.16 kW m <sup>-2</sup> C <sup>-1</sup>
two phase	3.0 kW m <sup>-2</sup> C <sup>-1</sup>
superheated vapor	0.1 kW m <sup>-2</sup> C <sup>-1</sup>

distributor and sump) and an assumed tube spacing equal to the tube diameter. The heat exchanger in the absorber consists of three spirals of tubes in parallel; the total area was based on the number of rows, the outside diameter of the absorber, and an assumed spacing between the three spirals. The heat flow in the flue gas heat exchanger was determined from the measured temperature rise of the strong absorbent; the temperature and flow rate of the inlet flue gases were calculated from the combustion analysis. These values then allowed estimation of the overall UA of the flue gas heat exchanger.

The internal dimensions of the analyzer and rectifier could not be measured and because of the integrated nature of these components, data were not available to allow the calculation of the various heat flows. The generator, analyzer, rectifier and stream mixer (along with two convergence components) were simulated to arrive at parameters for this portion of the cycle. The values obtained were confirmed to be within physically reasonable limits, but otherwise are subject to considerable uncertainty.

Heat transfer coefficients for boiling and condensing ammonia were estimated according to the recommendations of ASHRAE (114) and Threlkeld (115). At vapor qualities above 90 percent and below 10 percent, the heat transfer coefficient was varied linearly from the two-phase values and the appropriate single phase value. Coefficients for the load water flow were estimated from the Dittus-Boelter equation.

The parameters for the condenser throttle were empirically determined as described in Section 4.5.5. The solution pump mass flow rate was an average value of the flow rate for the weak absorbent stream calculated for the cycle investigation tests. (These flowrates were based on the measured heat of condensation and absorbent concentrations.)

#### 4.7 Comparison with Steady-State Experimental Data

The performance of the Arkla prototype AHP was simulated using the parameters outlined in Table 4-3. These simulations were carried out at ambient and load water conditions measured for several of the experimental tests, allowing a direct comparison. The measured low and high side pressures were supplied to the simulation. (The use of the inventory analysis to iterate for pressures will be discussed separately in Section 4.9.) For these comparisons, the COP of the absorption cycle itself will be used; this COP does not include burner losses or electric power input and is defined as the sum of the heat flows delivered to the load divided by the heat input to the generator plus flue gas heat exchanger:

$$\text{COP}_{\text{cycle}} = \frac{\dot{Q}_{\text{cond}} + \dot{Q}_{\text{abs}}}{\dot{Q}_{\text{gen}} + \dot{Q}_{\text{flue hx}}} \quad [4-107]$$

Simulations were carried out over a range of ambient temperatures with the standard load water conditions of  $0.38 \text{ l sec}^{-1}$  and  $41 \text{ C}$ . The simulated and measured COPs are shown in Figure 4-14. The qualitative behavior of the two sets of results is similar. The simulated COPs

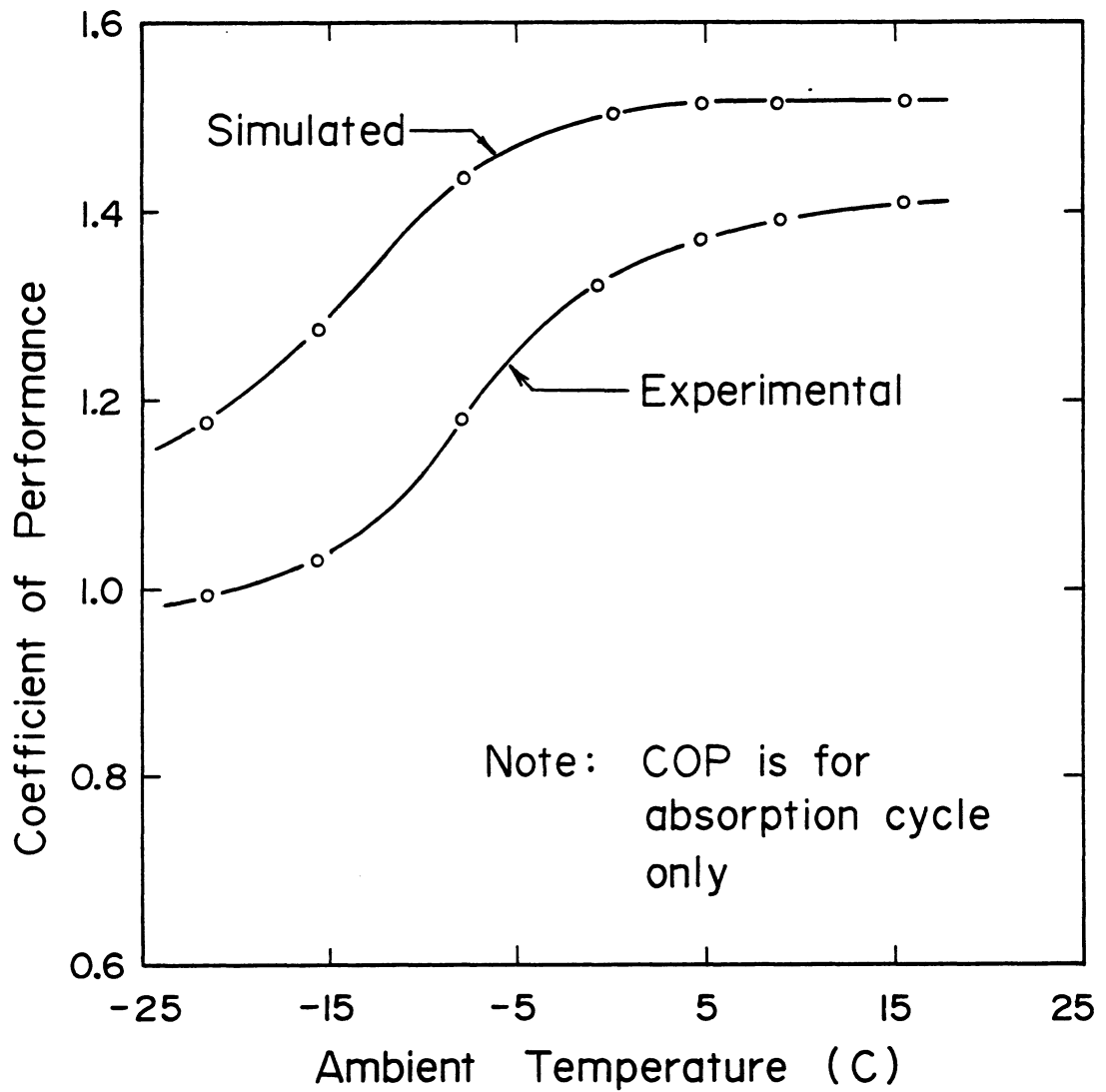


Figure 4-14 Measured and simulated cycle COPs for the Arkla AHP as a function of ambient temperature

are consistently high (by 0.11 at 15 C to 0.18 at -21 C). The magnitudes of these differences are larger than the experimental error. As will be discussed in the next section, uncertainties in the simulation parameters can result in an error in COP of 0.13. Apart from experimental and simulation uncertainties, one explanation for the discrepancy is that the model does not account for heat losses to the surroundings; inclusion of such losses would lower the COP, especially at the lower ambient temperatures. Recall that the error in the experimental energy balance was consistent with a heat loss to ambient as discussed in Section 3.4.3.

The simulated COP levels out more at high ambient temperatures as compared to the experimental results. Conversely, at low ambient temperatures, the COP does not level out as much as experimentally observed. It is likely that the reason for this behavior is related to conditions in the evaporator. The simulated evaporator inlet temperature (i.e., the approximate temperature of the bulk of the vaporization process) is lower than the measured temperatures by 2 to 3 C as indicated in Table 4-4. This temperature difference is unlikely to be the result of a faulty thermocouple since several thermocouples down the length of the evaporator gave consistent readings. An erroneous measurement of the low side pressure would result in an error in the calculated saturation temperature; however the pressure transducers were calibrated immediately before installation. The most likely explanation for the discrepancy in evaporator temperature is that there is a significant pressure drop

Table 4-4 System pressures and measured and simulated COPs and stream temperatures for varying ambient temperatures

T <sub>amb</sub> (C)	Pressure (MPa)		COP		Stream Temperatures (numbers refer to Figure 4-12)											
					2		8		10		14		18		19	
	low	high	test	sim	pump out test sim	abs thrt test sim	abs in test sim	cond in test sim	evap in test sim	evap out test sim						
-21.4	0.158	2.02	0.99	1.17	38	52	57	83	73	79	76	75	-23	-24	-23	-24
-15.7	0.192	2.00	1.03	1.27	40	52	56	83	72	82	73	75	-18	-20	-18	-20
-8.0	0.243	2.01	1.18	1.43	42	56	57	86	73	86	73	78	-12	-14	-12	-14
-0.9	0.299	2.06	1.32	1.50	45	55	58	83	74	84	73	75	-7	-9	-6	-1
4.7	0.336	2.08	1.37	1.52	46	54	58	80	74	83	71	73	-3	-6	5	5
8.8	0.352	2.10	1.39	1.52	46	54	58	80	74	85	71	72	-2	-5	9	9
15.5	0.360	2.13	1.41	1.52	46	53	59	80	74	85	72	72	-1	-4	16	16

between the evaporator and the absorber (where the pressure was measured). Since the pressure drop through the evaporator and refrigerant heat exchanger was not accounted for in the model, the simulated evaporator pressure will be low for a given absorber pressure.

The low evaporator pressure in the simulation resulted in a greater temperature difference between the ambient and evaporator, resulting in higher heat flows. The evaporator outlet stream is essentially completely vaporized at an ambient temperature of  $-0.9\text{ C}$  in the simulation (as indicated by the temperature rise through the evaporator given in Table 4-4 and the outlet quality given in Table 4-5). In the experiments, a similar temperature rise occurs only above about  $4\text{ C}$ . Once the evaporator outlet stream is completely vaporized, an increase in ambient temperature has little effect (as indicated by the values of the evaporator heat flow in Table 4-5) and thus the COP is relatively constant. At the low ambient temperatures, the lower simulated evaporator temperature resulted in an increased heat flow from ambient, yielding higher COPs. Similar effects resulting from a pressure drop between the evaporator and absorber were noted by Vliet, et al. (89,90).

Measured and simulated temperatures for several streams are given in Table 4-4. In general, there is reasonable agreement between the values. The simulated temperature of the absorbent leaving the rectifier was consistently high (with an RMS error of  $25\text{ C}$ ), indicating that the heat exchange area and/or heat transfer

coefficients between the strong and weak absorbent in the rectifier were underestimated. The temperature of the strong absorbent leaving the flue gas heat exchanger is also high but by a smaller margin (10 C); the temperature of this stream tended to be self-correcting since the flue gas temperature was input to the simulation. The simulated solution pump outlet (weak absorbent) temperature was high by an average of 11 C. This difference may be a result of an underestimation of the absorber area or the high strong absorbent temperature and high refrigerant vapor quality inlet to the absorber.

Simulated stream compositions and heat flows are given in Table 4-5 for the range of ambient temperatures. The concentrations of the strong and weak absorbent generally decreased with decreasing ambient temperature. At lower ambient temperatures, the low side pressure decreases, requiring a lower concentration in the absorber for a given absorber temperature. A minimum in the solution concentrations occurred between -8 and -15 C, resulting in even poorer performance for the test at an ambient temperature of -21 C. The absorber heat transfer and the refrigerant qualities leaving the evaporator and entering the absorber followed the same trend as the evaporator heat. The heat flow in the refrigerant heat exchanger was small for evaporator outlet qualities close to a saturated vapor; only when a two phase stream exited the evaporator did a significant amount of heat transfer occur in the refrigerant heat exchanger. The heat flow in the condenser is nearly constant over the range of ambient temperatures because the refrigerant flow (which is also nearly

Table 4-5 Simulated stream qualities and concentrations, refrigerant mass flow rate, and heat flows for varying ambient temperatures

	Ambient temperature (C)						
	-21.4	-15.7	-8.0	-0.9	4.7	8.8	15.5
Qualities:							
evap outlet	0.32	0.49	0.75	0.98	0.99	0.99	0.99
abs vapor in	0.57	0.72	0.96	0.995	1.00	1.00	1.01
Compositions (mass fraction ammonia):							
strong abs	.089	.088	.086	.099	.110	.116	.117
weak abs	.275	.274	.275	.290	.301	.307	.307
refrigerant	.995	.995	.994	.995	.996	.997	.997
generator vap	.631	.628	.619	.666	.702	.718	.721
analyzer vap	.875	.874	.867	.891	.906	.912	.913
Refrigerant flow rate (kg/sec)							
	.0047	.0046	.0047	.0049	.0049	.0049	.0049
Heat flows (kW):							
condenser	5.3	5.3	5.4	5.5	5.5	5.6	5.5
refrigerant HX	1.6	1.5	1.4	0.4	0.4	0.3	0.2
evaporator	2.0	3.0	4.6	5.3	5.4	5.5	5.5
absorber	7.1	8.1	9.6	10.2	10.4	10.6	10.6
analyzer	2.0	2.0	2.0	2.0	2.0	2.0	2.0
rectifier:							
s.a. to w.a.	5.3	5.3	5.4	5.0	5.0	4.9	5.0
vapor to w.a.	4.3	4.2	4.3	3.8	3.6	3.4	3.4
flue gas HX	-0.1	-0.1	0.0	0.1	0.2	0.4	0.4
generator	10.6	10.6	10.5	10.4	10.3	10.2	10.2

constant) is completely condensed and slightly subcooled for all cases. The vapor produced by the generator has a lower water content as the strong absorbent concentration increases with increasing ambient temperature. As a result, the vapor from the analyzer has a higher ammonia content and less rectification is required as reflected in the heat transfer from the vapor to the weak absorbent in the rectifier.

A comparison of simulation results with measured absorbent compositions and heat flows is presented in Table 4-6 for two ambient temperatures. (The results are for different tests than those presented above and thus do not correspond to the values presented in Tables 4-4 and 4-5.) The simulated strong and weak absorbent compositions were both low by 0.04. The simulated difference between the strong and weak absorbent compositions was only 0.005 greater than the experimentally observed value of 0.19. The simulated condenser heat flow was low by 0.2 to 0.4 kW, corresponding to slightly low values of the refrigerant mass flow rate. The heat transfer in the evaporator was low at the high ambient temperature because of the low simulated refrigerant flow rate and high at the low temperature because of a low evaporator temperature (as discussed above). The simulated heat flow for the absorber is slightly high for both tests; the discrepancy at the low ambient temperature can be explained by the higher evaporator heat.

The Arkla AHP was also simulated with varying inlet load water temperature at three ambient temperatures, mirroring the experiments

Table 4-6 Comparison of measured and simulated compositions, heat flows, and refrigerant mass flow rate for tests at two ambient temperatures

	Ambient Temperature (C)			
	-8.7		8.6	
	test	sim	test	sim
Compositions:				
strong absorbent	0.133	0.099	0.173	0.122
weak absorbent	0.319	0.292	0.368	0.319
Heat flows (kW):				
condenser	5.8	5.6	6.1	5.7
evaporator	2.8	3.9	6.6	5.6
absorber	8.4	8.8	10.3	10.6
Refrigerant flow				
rate (kg/sec)	0.0051	0.0049	0.0054	0.0051

discussed in Section 3.4.1. These results are presented in Table 4-7. The simulated COPs are consistently above the measured values for the reasons discussed above. However the variation in COP for a change in water temperature from the design conditions ( $\Delta$ COP) showed good agreement with experimental results for the two higher ambient temperatures but was high at an ambient temperature of -21 C.

A lower load water temperature in the absorber results in lower absorber and evaporator pressures. At the two lowest ambient temperatures, this lower evaporator pressure (and thus temperature) resulted in a larger heat flow from ambient, increasing the COP. At the highest ambient temperature, the refrigerant leaving the evaporator is nearly completely vaporized for all three water temperatures and thus variations in the low side pressure had much less effect. The effect of varying load water temperatures on the solution concentrations reversed between the extremes of ambient temperature because of competing effects. The lower absorber temperature resulting from a lower load water temperature would permit a higher (less strong) absorbent concentration, but the lower pressure resulting from such a change would require a stronger (lower concentration) absorbent for the same absorber capacity.

#### 4.8 Sensitivity Study of an Absorption Heat Pump

The sensitivity of the Arkla AHP to changes in design parameters was studied by means of a factorial design in order to determine the most critical parameters affecting the heat pump performance. This analysis also serves to estimate the uncertainty in simulated COP

Table 4-7 System pressures, COP, change in COP from standard load water conditions, and simulated solution compositions and heat of evaporation for varying inlet load water temperature at three ambient temperatures

Temperatures (C)		Pressures (MPa)		Simulated COP	$\Delta$ COP		Compositions		$\dot{Q}_{\text{evap}}$ (kW)
ambient	load water	low	high		test	sim	s.a.	w.a.	
-21.4	34.9	0.148	1.77	1.28	+0.04	+0.11	0.086	0.271	3.0
	40.7	0.158	2.02	1.17	-	-	0.089	0.275	2.0
	45.6	0.164	2.26	1.11	-0.04	-0.06	0.090	0.282	1.4
-8.0	35.1	0.223	1.81	1.50	+0.03	+0.07	0.091	0.280	5.3
	40.4	0.243	2.01	1.43	-	-	0.086	0.275	4.6
	43.3	0.245	2.16	1.36	-0.06	-0.07	0.089	0.282	3.9
8.8	35.7	0.309	1.92	1.51	-0.01	-0.01	0.121	0.309	5.6
	40.5	0.352	2.10	1.52	-	-	0.116	0.307	5.5
	44.3	0.384	2.29	1.53	+0.01	+0.01	0.112	0.309	5.5

arising from uncertainties in simulation parameters. In this study, twelve design variables were varied above and below the base values described in Section 4.6.3; the ambient temperature and low and high side pressures were also varied.

A factorial design is useful for investigating the effects of a number of variables with a minimum number of experimental (or in the present case, simulation) data points. (A thorough discussion of factorial designs may be found in Box, Hunter and Hunter (116)). The most common design, and the one employed here, is a factorial design where the design factors are varied between two levels. The analysis assumes that the response to changes in these factors is linear over the range studied.

The results of the analysis are "main effects" for each factor and "interactions" between factors. A main effect is the response of a dependent variable (e.g., COP) to a change from the low to high level of a factor (e.g., ambient temperature). The main advantage of a factorial design over investigating the various factors individually is that the factorial design provides a measure of the interactions between sets of variables. A "two-factor interaction" between, for example, ambient temperature and evaporator area would be the effect on COP resulting from both variables simultaneously changing from their low to high levels; this interaction effect is in addition to the effects of varying each factor independently. There are also three- and four-factor interactions, up to a k-factor interaction (where k is the number of variables investigated).

To fully investigate  $k$  factors at two levels would require  $2^k$  tests. For sufficiently large values of  $k$ , however, the higher-order interactions are usually negligible and a fractional factorial design requiring fewer runs is sufficient. Such a design reduces the number of runs at the expense of confounding certain effects and interactions. Means are available, however, to ensure that main effects and low-level interactions (which are likely to be significant) are confounded only with high order interactions (which are likely to be negligible).

In the study of the Arkla AHP, 15 variables were investigated with 32 simulations. This yields a factorial design of resolution IV, meaning that main effects are confounded only with three-factor and higher interactions but that two-factor interactions are confounded with each other. The heat exchange areas for the condenser, evaporator, absorber, rectifier and refrigerant heat exchanger and the UA value for the analyzer were varied 20 percent above and below the base values given in Section 4.6.3. The flow parameters for the solution pump and throttle were varied plus and minus five percent; the number of rows of heat exchange tubes in the absorber was varied between 25 and 35. One and two equilibrium stages in the analyzer were investigated. The low and high side pressures and generator heat input were varied five percent above and below their base values. These ranges approximately correspond to the uncertainty in the variables. (The uncertainties in heat transfer coefficients were lumped with those of the heat exchanger areas.) Ambient temperatures

of -8 and -1 C were chosen for the low and high levels of that factor, representing a range in which ambient temperature has a significant effect on COP.

The results of this analysis, in terms of effects on COP, are given in Table 4-8. The average value of COP and the main effect of ambient temperature agree with the results presented in the previous section. The ambient temperature effect of 0.071 indicates that, averaged over all the other variables, the COP increases by this value as the ambient temperature is increased from the low (-8 C) to high (-1 C) level. The low and high side pressures have a significant effect on COP. An increased low side pressure decreases the temperature difference for heat transfer in the evaporator; this is reflected in the negative value for this effect. An increased high side pressure increases the temperature in the condenser, increasing the condenser heat flow and thus COP. The effect of generator heat input is negative, suggesting that the condenser and evaporator are not capable of handling the increased refrigerant flow rate resulting from a higher generator heat input.

Among the various heat exchanger area factors, the condenser and evaporator areas had the largest effects. The effect of evaporator area is consistent with an evaporator that is not fully vaporizing the refrigerant stream flowing through it as discussed in Section 4.7. In the condenser, the exiting refrigerant stream is a low quality two phase mixture under certain conditions and thus the performance is improved by an increase in condenser area.

Table 4-8 Main effects for the factorial analysis of the Arkla AHP

Factor	low level	high level	Effect
Average			1.426
Ambient temperature (C)	-8	-1	+0.071
Pressures (MPa)			
low (absorber) @T <sub>amb</sub> = -8	0.231	0.255	-0.072
@T <sub>amb</sub> = -1	0.284	0.314	
high (rectifier) @T <sub>amb</sub> = -8	1.91	2.11	+0.063
@T <sub>amb</sub> = -1	1.95	2.16	
Generator heat input (kW)	9.93	10.97	-0.035
Heat exchanger areas (m <sup>2</sup> )			
condenser	0.20	0.30	+0.056
refrigerant HX	0.13	0.19	-0.002
evaporator	2.86	4.29	+0.055
absorber	0.95	1.42	-0.008
rectifier (s.a. to w.a.)	0.20	0.30	+0.004
rectifier (vap to w.a.)	0.26	0.38	0.000
Analyzer UA (kW m <sup>-2</sup> C <sup>-1</sup> )	0.08	0.12	+0.003
Analyzer stages	1	2	+0.001
Absorber heat exchange rows	25	35	+0.004
Solution pump flow (kg s <sup>-1</sup> )	0.0216	0.0238	-0.004
Throttle parameter C <sub>1</sub> (MPa s <sup>2</sup> kg <sup>-2</sup> )	22100	24500	+0.006

The remaining factors had effects smaller than 0.01. (These effects are significant in the statistical sense because a numerical simulation is subject to only small uncertainties arising from machine precision and convergence tolerances for iteration loops, not the larger random errors associated with experimental results.) The relative insensitivity of performance to the analyzer, rectifier and refrigerant heat exchanger areas, and area and number of heat exchange tubes in the absorber suggests that these components are oversized, so that a relatively large (20 percent) change in area results in only a small performance change. The negative effects for the absorber and refrigerant heat exchanger areas might indicate that an optimum value has been exceeded or that the three-factor interactions these main effects are confounded with are significant. The effects associated with the solution pump and throttle valve flow rates are also small; it is more likely that the sizing of these components was optimized in the design of the Arkla AHP.

The ranges for the variables investigated in the factorial design were chosen to correspond to the uncertainties in the corresponding simulation parameters. Thus the main effects can also be interpreted as errors in the simulated COP arising from uncertainties in the parameters supplied to the model. The total error resulting from errors due to individual uncertainties is given by (116):

$$\omega_{\text{tot}} = \left( \sum_{i=1, N} (\omega_i)^2 \right)^{0.5} \quad [4-108]$$

where  $\omega_i$  is the error (main effect) associated with factor  $i$ .

The total error in COP given by [4-108] (excluding the effect of ambient temperature) is 0.13. Although this value is specific to the design investigated here, its magnitude indicates that parameter values must be known to a high precision to obtain accurate results for COP. In AHP design studies, it would be necessary to "calibrate" the model parameters with experimental data. Even in the absence of experimental measurements, however, the model is useful for investigating the changes in performance resulting from changes in a design parameter.

In addition to the average COP and 15 main effects, the factorial analysis yielded 16 interaction effects. Of these, six had absolute values greater than 0.01. However, these interaction terms are highly confounded among the 105 two-factor interactions present for 15 variables. In order to resolve some of these interactions, an additional factorial design was carried out for five variables having significant effects on COP. The selection of these variables was based on the assumption that factors having small main effects are also likely to have small interactions with other factors. The low and high side pressures, generator heat input, and condenser and evaporator areas were varied between the low and high levels presented above; all other variables were held at their low levels. A half-fraction of 16 runs yielded a resolution V design with main effects confounded only with four-factor interactions; two-factor interactions are confounded only with three-factor interactions and not each other.

The results of this second factorial design are given in Table 4-9. The average and main effects are slightly different from the values in Table 4-8, indicating that there is an interaction with ambient temperature. A number of substantial interaction effects exist among the five variables investigated in this design. Some of these are readily understood. For example, the main effects of condenser area and high side pressure are both positive since increasing either factor increased the heat flow in the condenser. The interaction between these two factors, however, is negative, indicating that the effect of increasing both factors simultaneously has an effect less than the sum of the individual factors. A similar interaction is seen between the low side pressure and evaporator area.

Other interactions are not so easily explained, such as the interaction between the low side pressure and condenser area. These interactions are a result of the complex nature of the absorption cycle and demonstrate the difficulty of designing an AHP. It is not possible to optimize components individually; rather the cycle as a whole must be considered, illustrating the advantage of a simulation design tool.

#### 4.9 Inventory Analysis and Pressure Iteration

In Section 4.2 it was shown that an analysis of the refrigerant and absorbent inventory was necessary to fully specify the state of an AHP. The simulation model pairs the inventory relationships with the low and high side pressures in the heat pump. This pairing can work

Table 4-9 Main effects and interactions for the second factorial analysis of the Arkla AHP

Factor	low level	high level	Effect
Average			1.387
Pressures (MPa)			
low (absorber)	0.231	0.255	-0.085
high (rectifier)	1.91	2.11	+0.032
Generator heat input (kW)	9.93	10.97	-0.046
Heat exchanger areas (m <sup>2</sup> )			
condenser	0.20	0.30	+0.033
evaporator	2.86	4.29	+0.068

Interaction	(confounded with)	Value
$P_{low} \times P_{high}$	$(\dot{Q}_{gen} \times A_{cond} \times A_{evap})$	-0.027
$P_{low} \times \dot{Q}_{gen}$	$(P_{high} \times A_{cond} \times A_{evap})$	+0.004
$P_{low} \times A_{cond}$	$(P_{high} \times \dot{Q}_{gen} \times A_{evap})$	-0.025
$P_{low} \times A_{evap}$	$(P_{high} \times \dot{Q}_{gen} \times A_{cond})$	+0.020
$P_{high} \times \dot{Q}_{gen}$	$(P_{low} \times A_{cond} \times A_{evap})$	-0.011
$P_{high} \times A_{cond}$	$(P_{low} \times \dot{Q}_{gen} \times A_{evap})$	-0.017
$P_{high} \times A_{evap}$	$(P_{low} \times \dot{Q}_{gen} \times A_{cond})$	+0.021
$\dot{Q}_{gen} \times A_{cond}$	$(P_{low} \times P_{high} \times A_{evap})$	-0.015
$\dot{Q}_{gen} \times A_{evap}$	$(P_{low} \times P_{high} \times A_{cond})$	+0.003
$A_{cond} \times A_{evap}$	$(P_{low} \times P_{high} \times \dot{Q}_{gen})$	+0.021

in two ways--a known inventory can be used to iterate for pressures or known pressures can be supplied to the simulation and the resulting inventory calculated. The latter method was employed in the simulations presented in the previous two sections.

The ammonia and water inventories were calculated for the series of tests at varying ambient temperatures. In the corresponding set of experimental tests (from which the simulation pressures were obtained), the charge of the heat pump was not varied and thus the calculated inventories should also be constant. The calculated inventories presented in Table 4-10 show small variations between tests. The calculated amount of mass in the system, however, is substantially different than the estimated initial charge of seven liters of ammonia and water (i.e., 4.3 kg ammonia and 7 kg water) reported by the manufacturer (78).

The distribution of the inventory among the various components in the cycle is given in Table 4-11 for an ambient temperature of -8 C. The generator and analyzer contain 56 percent of the ammonia and 89 percent of the water in the cycle and thus any errors in these components will markedly affect the inventory of the entire cycle. The liquid and vapor volumes of these two components were assumed to be constant with a composition of the corresponding leaving stream. Although the total volume of these components is essentially constant, the relative fractions occupied by liquid and vapor can change. There is also a continuous change in composition between the top and bottom of the generator and analyzer. Sufficient information to allow a more

Table 4-10 Refrigerant and absorbent inventories for varying ambient temperatures calculated using measured system pressures in the simulation

Temperature	Inventory (kg)	
	Ammonia	Water
-21	3.55	12.83
-16	3.48	12.86
-8	3.48	12.90
-1	3.05	12.61
5	3.39	12.38
9	3.53	12.26
16	3.58	12.23
average	3.44	12.58
std deviation	0.18	0.29

Table 4-11 Distribution of refrigerant and absorbent inventory within the absorption cycle calculated for an ambient temperature of -8 C

Component	Inventory (kg)	
	Ammonia	Water
Generator	0.39	4.08
Analyzer	1.57	7.36
Rectifier	0.25	0.70
Condenser	0.21	0.00
Refrigerant heat exc	0.75	0.00
Evaporator	0.07	0.00
Absorber	0.25	0.76
All other components	0.00	0.00

complete inventory modeling of these components was not available. Errors in the calculated system inventories also arise from neglecting the mass contained in the connecting piping and components such as the solution pump.

The use of the inventory relationships to iterate for the low and high side pressure was tested by supplying to the simulation the total ammonia and water masses calculated at experimentally measured pressures. The iterations for pressure, starting from initial values five percent above and below the measured values, and the resulting inventories are given in Table 4-12 for a test at an ambient temperature of -9 C. The pressures and inventories converged to within 0.3 percent of their correct values with ten iterations of the absorption cycle.

This convergence to the correct pressures demonstrates, in principle, the use of the inventory analysis to calculate a pair of system variables which would otherwise have to be supplied to the simulation or inferred via assumptions of system states. In practice, however, if the system pressures were known a priori within the five percent limits used for the starting values of the above example, there would be no need for the inventory iteration. Unfortunately however, the iteration does not reliably converge for starting guesses far removed from the correct values.

The reason for the failure of the inventory iteration to converge for more realistic initial guesses can be understood by examining the behavior of the inventory functions. Contours of constant refrigerant

Table 4-12 Iterations in pressure and resulting refrigerant and absorbent inventories for an ambient temperature of -9 C; input inventories calculated for system pressures of 0.246 and 2.101 MPa

Iteration	Pressure (MPa)		Inventory (kg)	
	low	high	ammonia	water
0	0.234	2.00	3.21	13.03
1	0.258	2.00	3.66	12.66
2	0.234	2.21	3.90	12.62
3	0.258	2.21	4.35	12.10
4	0.255	2.21	4.29	12.18
5	0.258	2.06	3.90	12.41
6	0.255	2.06	3.83	12.49
7	0.2463	2.06	3.67	12.67
8	0.255	2.096	3.94	12.44
9	0.2463	2.096	3.79	12.60
Input inventories			3.80	12.59

and absorbent inventory are shown in Figure 4-15 as functions of the low and high side pressure. The surfaces have substantial curvature and thus a linear iteration algorithm such as the two-variable secant method has difficulty converging. Furthermore, the inventory surfaces have similar shapes so that at the intersection of given ammonia and water contours defines a line in the pressure plane rather than a sharply defined point.

The inventory contour plot also indicates that the ammonia and water inventories cannot be varied independently of each other. For example, an inventory of 4.0 kg of ammonia intersects with only a narrow range of water inventories (of approximately 12.4 kg). Such a narrow range of allowable charges would not be experienced in an actual machine. A low water charge, for example, would merely result in a lower liquid level in the analyzer. The modeling of the generator and analyzer inventory did not, however, allow for changing liquid and vapor volumes. Thus, the simplified inventory modeling of these components is at least partially responsible for the failure of the inventory iteration.

The general relationship between the ammonia inventory and system pressures shown in Figure 4-15 does correspond with the experimentally observed behavior. The calculated ammonia inventory increased with increasing low and high side pressures. Similarly, increasing the ammonia charge of the Arkla AHP was experimentally observed to increase the system pressures (as discussed in Section 3.4.2).

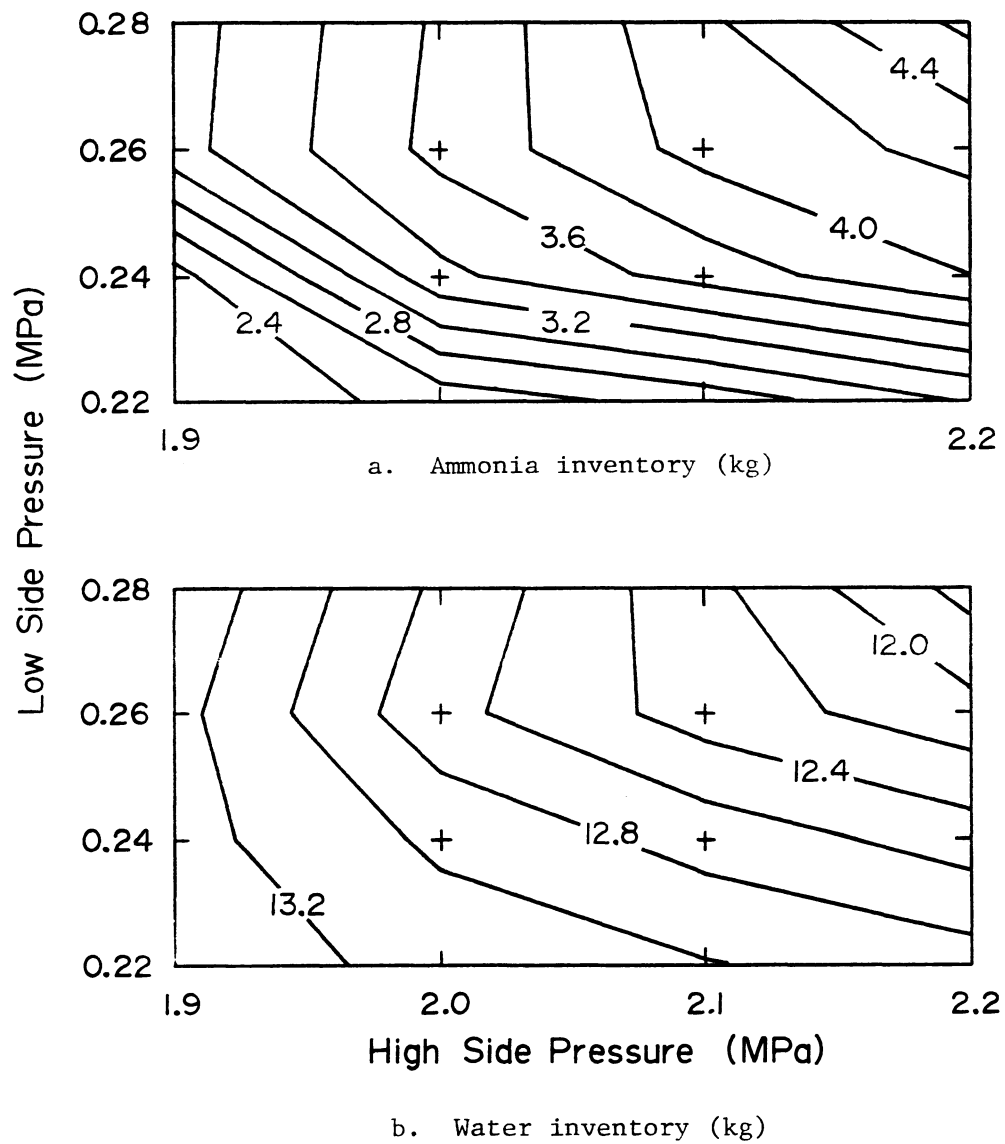


Figure 4-15 Contours of constant inventory as functions of low and high side system pressures for the Arkla AHP at an ambient temperature of  $-9^{\circ}\text{C}$ ; (inventory functions evaluated at intersections of grid ticks)

#### 4.10 Summary and Conclusions for the Steady-State Modeling of Absorption Heat Pumps

A modular steady-state simulation program for absorption heat pumps has been developed. It is written to be independent of any particular refrigerant-absorbent system and pairs an analysis of the mass inventory in the components to the system pressures. The need for the inventory analysis was demonstrated by an examination of the variables necessary to fully specify the state of an absorption cycle and the relationships available to solve for them. The generality, flexibility and level of detail of the model represent an advance over other models presented in the literature.

The models formulated for the various components in the cycle neglected pressure drops and heat losses to the surroundings. A known heat input was assumed for the generator; the analyzer was modeled as a series of equilibrium stages and an analysis of simultaneous heat and mass transfer was applied to each row of heat exchange tubes in the falling-film absorber. A general N-stream heat exchanger component employing a finite difference formulation was used for the rectifier, condenser, evaporator and refrigerant and flue gas heat exchangers. Also developed were an empirical model for an orifice type throttle valve, a constant flow rate solution pump component and a component for the convergence of tear streams in the simulation.

The model was compared with experimental data for the Arkla prototype AHP. Simulations were carried out at ambient and load water conditions and system pressures measured for experimental tests, permitting a direct comparison. The qualitative behavior of the

simulated and measured COPs were in agreement. The simulated COPs were high by 0.11 to 0.18 for varying ambient temperatures; this difference is likely caused by not considering pressure drops and heat losses to the surroundings in the model. Simulations for varying inlet cooling water temperatures correctly predicted the trends in COP resulting from a change in this external variable. These results, although pointing out needed refinements to the model, demonstrate its validity and usefulness in the study of AHPs.

A factorial design investigating the effects of 15 design and operating variables on the heating COP was carried out to study the design of the Arkla AHP, provide a further test of the simulation, and provide an estimate of the variation in COP arising from uncertainties in the simulation parameters. The factors of ambient temperature, low and high side pressure, generator heat input, and condenser and evaporator area had effects on COP ranging in magnitude from 0.035 to 0.072 (for a change of 7 C in temperature and variations of  $\pm 5$  percent in pressures and heat input and  $\pm 20$  percent in heat exchanger areas). Similar changes in the absorber, analyzer, rectifier and refrigerant heat exchanger areas, the number of analyzer stages and absorber heat exchanger rows, and solution pump and throttle flow parameters had effects of less than 0.01. A second factorial design revealed substantial interactions between the variables of low and high side pressure, generator heat input, and condenser and evaporator areas. The estimated error bound on COP arising from uncertainties in the simulation parameters was 0.13.

With measured pressures supplied to the simulation, the refrigerant and absorbent inventories calculated for a range of ambient temperatures were within five percent of constant values. However the use of the inventory relations to iterate for the system pressures was not successful due to the non-linear character of the inventory functions and oversimplifications made in the modeling of the inventory in components with changing liquid and vapor volumes. The general trends between system pressures and the calculated ammonia inventory did correspond with the experimentally observed behavior.

## CHAPTER 5

### CONCLUSIONS AND RECOMMENDATIONS

This work has dealt with absorption heat pumps in three areas: the simulation of a solar-fired system with chemical energy storage, the experimental investigation of a prototype gas-fired AHP, and the development of a steady-state absorption heat pump simulation program. A summary of the major results of this research may be found as the concluding section of the three previous chapters. This chapter presents more general conclusions about absorption heat pumps and recommends areas for further study.

A transient simulation model of an absorption heat pump with chemical energy storage has been developed for use with the TRNSYS program. The level of detail in this model, which represents a limiting case approach in several respects, was appropriate for the long-term simulation of a system which had not been physically built. Simulations have shown that the solar-fired AHP system with chemical storage can provide a significant fraction of a residential heating load with non-purchased energy. However, the performance is substantially higher than a conventional solar heating system only at low collector areas and then because of the auxiliary heat supplied through the AHP. In cooling operation, the performance of the AHP system was slightly lower than a solar-fired lithium bromide-water chiller with thermal energy storage.

These performance comparisons, combined with the equipment complexity and safety and environmental hazards associated with significant quantities of chemical storage make it unlikely that solar-driven AHPs with chemical energy storage will be practical in residential or commercial applications. Thus, it is recommended that further modeling efforts be directed at more promising applications of absorption heat pumps.

A prototype gas-fired AHP developed by Arkla Industries was successfully tested, providing experimental data for comparison to the steady-state simulation model. The performance, especially the cyclic performance, of this heat pump was disappointing. The steady-state COP (including burner losses and electric input) was less than unity for ambient temperatures below  $-5^{\circ}\text{C}$  and the cyclic COP calculated for a representative residential application never exceeded unity. Compared to a high efficiency furnace this machine would, at best, have an equal seasonal performance but at an almost certainly higher cost.

This rather gloomy appraisal does not, however, apply to fuel-fired AHPs in general. The absorption heat pump has the potential to significantly improve on the efficiency of current space heating systems. But to be cost effective, innovative cycle designs (such as those proposed by Johnston (11,12)) need to be pursued to improve efficiency and reduce materials requirements. Multiple effect units and the use of ternary mixtures are also promising. The cyclic performance could be improved by restricting solution migration during

off periods or by reducing the total solution and heat exchanger mass which must be brought to a steady-state condition upon start-up. The need for cycling could be reduced by some means of energy storage.

A modular steady-state simulation program for absorption heat pumps has been developed and applied to the Arkla prototype AHP. A comparison of simulations and experiments showed generally good agreement but also revealed areas where further refinement of the model is needed. The assumptions of negligible pressure drops through components (particularly between the evaporator and absorber) and heat losses to the surroundings were identified as sources of discrepancy with experimental results.

The pairing of the absorbent and refrigerant inventory analysis to the system pressures was not entirely successful. The need for the inventory analysis in order to fully specify the state of the absorption cycle was demonstrated but its use to iterate for system pressures was not successful. The inventory iteration did not reliably converge due to oversimplifications in the modeling of the inventory in components with changing liquid volumes and the inability of the two-variable secant method to converge for the non-linear inventory functions. Improved inventory models should be developed. The convergence might also be improved by a more sophisticated iteration technique.

In addition to improving the inventory analysis and removing the assumptions of negligible heat losses and pressure drops, the model should be modified to allow the use of ternary refrigerant-absorbent

mixtures. Effort should be directed at reducing the required computation time of the model, particularly for the evaluation of thermodynamic properties. The eventual extension of the model to include transient behavior should be considered.

The level of complexity in the current model is suitable for detailed investigations of the absorption cycle or, if validated against a similar machine, for the design of AHPs. The general nature of the model will allow its use in the study of a wide variety of designs. The further development of this model and its use in the identification and design of promising AHP cycles (ideally in conjunction with experiments) is recommended.

## APPENDIX A

### USER DOCUMENTATION FOR TRNSYS COMPONENTS

This appendix contains specifications for the TRNSYS components developed in this research. The absorption heat pump with chemical energy storage was modeled with two separate TRNSYS components; the controller and heat exchange switching components are also described. Listings of these routines are given in Appendix E.1. The TRNSYS manual (36) should be consulted for the requirements of the entire simulation deck.

#### A.1 Absorption Heat Pump Subsystem

A continuous AHP with chemical energy storage is modeled by a combination of a TYPE32 and TYPE33 component. Each of these components represent two interconnected tanks as shown in Figure A-1. These components are described in terms of "hot-side" and "cold-side" tanks. The TYPE32 component models a generator (the hot side) with negligible thermal and mass capacitance and a condenser/refrigerant storage tank (the cold side). TYPE33 models a zero capacitance evaporator and an absorber/absorbent storage tank. A solar collector model delivering heat to the hot-side tank is also built into the model. The overall AHP system thus modeled was shown in Figure 2-2. The inputs, parameters, derivatives and outputs of the two AHP components are similar and will be described together. System state points are defined by Figure A-1.

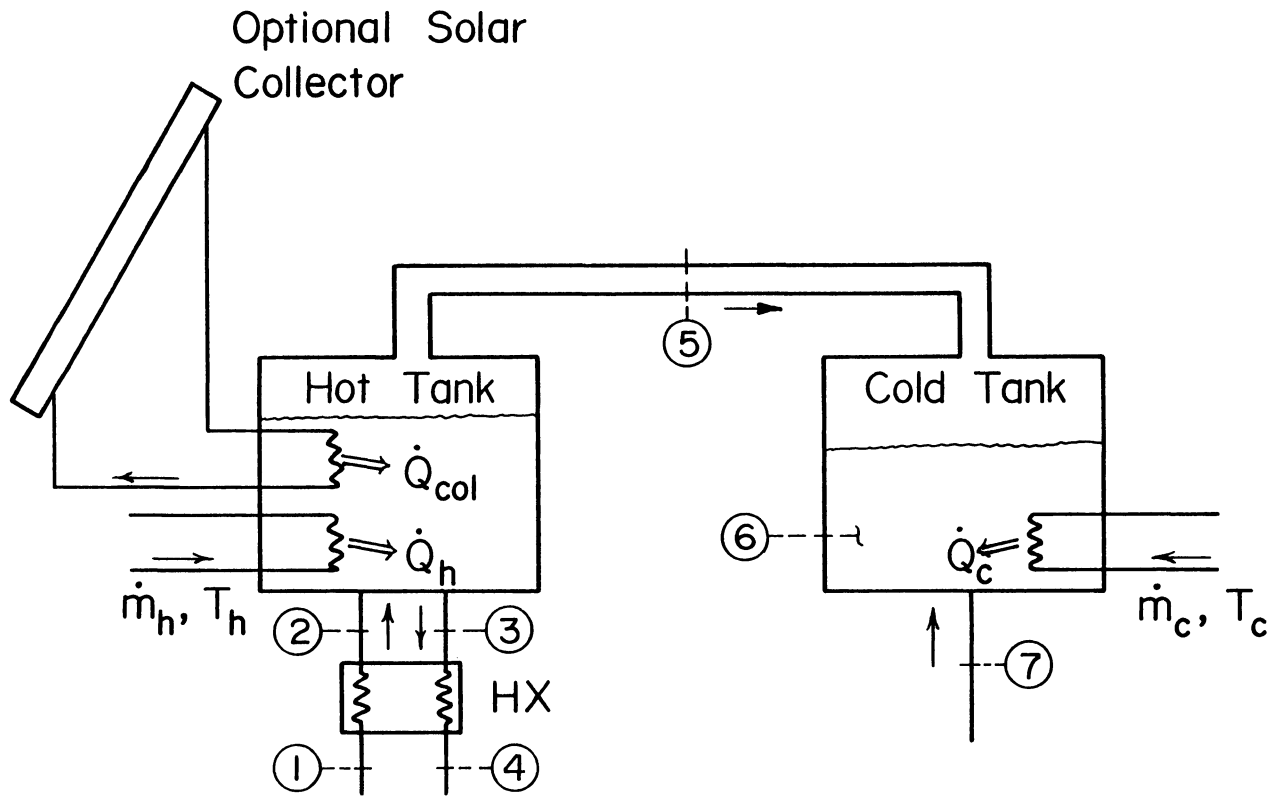


Figure A-1 Schematic representation of the TRNSYS absorption heat pump subsystem component

Parameters: 11 to 16

Note: \* indicates input or parameter that is ignored for TYPE32

+ indicates input or parameter that is ignored for TYPE33

\*+1 - (not used)

\*2 -  $V_h$ , volume of hot tank

3 -  $UA_h$ , loss coefficient for hot tank

\*4 -  $(mC_p)_h$ , capacitance of hot tank (excluding contents)

+5 -  $V_c$ , volume of cold tank

6 -  $UA_c$ , loss coefficient of cold tank

+7 -  $(mC_p)_c$ , capacitance of cold tank (excluding contents)

8 -  $C_{p,h}$ , heat capacity of hot-side heat exchange fluid

9 -  $C_{p,c}$ , heat capacity of cold-side heat exchange fluid

\*10 -  $m_{a,tot}$ , total mass of absorbent in system

\*11 -  $m_{r,tot}$ , total mass of refrigerant in system

The following parameters are required only if the internal solar collector model is used:

12 -  $A_{col}$ , solar collector area

13 -  $F_{R,L}$ , collector heat exchange factor, loss coefficient product

14 -  $F_R(\tau\alpha)$ , collector heat exchange factor, transmittance-absorptance product

15 -  $\dot{m}_{col}$ , collector mass flow rate

16 -  $C_{p,col}$ , heat capacity of collector heat exchange fluid

Inputs: 16 to 19

- 1 -  $\dot{m}_1$ , mass flow rate of stream 1
- 2 -  $T_1$ , temperature of stream 1
- 3 -  $x_1$ , absorbent mass concentration of stream 1
- \*4 -  $\dot{m}_4$ , mass flow rate of stream 4
- +5 -  $\dot{m}_7$ , mass flow rate of stream 7
- 6 -  $T_7$ , temperature of stream 7
- 7 -  $\dot{m}_h$ , mass flow rate of hot-side heat exchange stream
- 8 -  $T_h$ , temperature of hot-side heat exchange stream
- 9 -  $\epsilon_h$ , effectiveness of hot-side heat exchanger
- 10 -  $\dot{m}_c$ , mass flow rate of cold-side heat exchange stream
- 11 -  $T_c$ , temperature of cold-side heat exchange stream
- 12 -  $\epsilon_c$ , effectiveness of cold-side heat exchanger
- 13 -  $\epsilon_{hx}$ , effectiveness of countercurrent heat exchanger
- 14 -  $T_{env}$ , temperature of tank environment
- 15 -  $\dot{Q}_{aux}$ , specified heat flow into hot tank
- \*16 -  $m_{r,cond}$ , mass of refrigerant in the condenser

The following inputs are required only if the internal solar collector model is used:

- 17 -  $H_T$ , solar radiation incident on collector plane
- 18 -  $T_{amb}$ , ambient temperature
- 19 -  $\gamma_{col}$ , control function (0 or 1) for solar collector

Derivatives: 1 or 2

- 1 -  $U_{tot}$ , total internal energy of tank
- +2 -  $m_r$ , mass of refrigerant in condenser (TYPE32 only)

Output s: 19

- 1 -  $T_3$ , temperature of hot tank
- 2 -  $\dot{m}_4$ , mass flow rate out of hot tank
- 3 -  $T_4$ , temperature of stream 4
- 4 -  $x_4$ , concentration of hot tank
- 5 -  $\dot{m}_5$ , mass flow rate of vapor between tanks
- 6 -  $T_6$ , temperature of cold tank
- 7 -  $-\dot{m}_7$ , negative of mass flow rate of stream 7
- 8 -  $T_7$ , temperature of stream 7
- 9 -  $\dot{Q}_h$ , heat transfer across hot-side heat exchanger
- 10 -  $T_{h,r}$ , return temperature of heat exchange stream from hot side heat exchanger
- 11 -  $\dot{Q}_c$ , heat transfer across cold-side heat exchanger
- 12 -  $T_{c,r}$ , return temperature of heat exchange stream from cold side heat exchanger
- \*13 -  $m_{tot,h}$ , total mass in hot tank
- +14 -  $m_{tot,c}$ , total mass in cold tank
- \*15 -  $dU_h/dt$ , rate of change of internal energy of hot tank
- +16 -  $dU_c/dt$ , rate of change of internal energy of cold tank
- 17 -  $\dot{Q}_{loss}$ , tank heat losses
- 18 -  $\dot{Q}_{col}$ , collected solar energy
- 19 -  $T_{col}$ , outlet temperature of solar collector

## A.2 AHP Controller Component

A separate TRNSYS component was developed to model the baseline and alternate control strategies described in Section 2.5.3. The alternate strategies are disabled by setting the appropriate parameters to a very high or low value as described below.

Parameters: 24

- 1 -  $T_{\text{set,h1}}$ , first stage heating set point (heat from refrigerant tank)
- 2 -  $T_{\text{set,h2}}$ , second stage heating set point (heat from both storage tanks)
- 3 -  $T_{\text{set,h3}}$ , third stage heating set point (auxiliary heat input to generator)
- 4 -  $T_{\text{set,h4}}$ , fourth stage heating set point (auxiliary heat supplied to load)
- 5 -  $T_{\text{set,c1}}$ , first stage cooling set point (cooling supplied by AHP)
- 6 -  $T_{\text{set,c2}}$ , second stage cooling set point (cooling supplied by auxiliary)
- 7 -  $\dot{m}_{\text{pump}}$ , mass flow rate of solution pump
- 8 -  $\dot{m}_{\text{col}}$ , mass flow rate through solar collector
- 9 -  $m_{\text{cond,min}}$ , minimum mass in refrigerant storage tank to operate evaporator
- 10 -  $x_{\text{max}}$ , maximum absorbent concentration in storage tank to avoid crystallization
- 11 -  $x_{\text{dead}}$ , deadband associated with  $x_{\text{max}}$

- 12 -  $T_{\min}$ , minimum useful temperature for extracting heat from storage tanks
- 13 -  $T_{\max}$ , maximum temperature for storage tanks; above this temperature, heat is rejected to ambient during heating operation
- 14 -  $\dot{Q}_{\text{aux}}$ , rate of energy supply by auxiliary heat source
- 15 -  $T_{\text{dead},1}$ , temperature deadband for heating and cooling set points
- 16 -  $T_{\text{dead},2}$ , temperature deadband for ambient heat exchanger
- 17 -  $\Delta T_{\text{col,on}}$ , temperature differential to turn collector on
- 18 -  $\Delta T_{\text{col,off}}$ , temperature differential to turn collector off
- 19 -  $F_{R U_L}$ , loss parameter for solar collector
- 20 -  $F_R(\tau\alpha)$ , transmittance parameter for solar collector
- 21 -  $T_{A/C,\text{on}}$ , maximum evaporator temperature for cooling to be supplied by AHP
- 22 -  $T_{A/C,\text{off}}$ , maximum evaporator temperature for AHP to continue to supply cooling
- 23 - BPR, bypass ratio; ratio of collection efficiencies at which solar is bypassed into absorbent tank, approximately equal to COP for the "generator bypass" control option; set to large value (e.g., 10000) to disable this option; (see discussion of control strategies in Section 2.5.3)
- 24 -  $N_{\text{stk}}$ , stickiness of controller; (see discussion of controller sticking in (36))

Inputs: 11

- 1 -  $\gamma_{\text{seas}}$ , time of year:
  - 1 - heating
  - 2 - cooling
- 2 -  $T_{\text{load}}$ , heating/cooling load (room) temperature
- 3 -  $T_{\text{sink}}$ , temperature of heat source/sink (e.g., ambient)
- 4 -  $T_{\text{cond}}$ , temperature of condenser/refrigerant storage tank
- 5 -  $T_{\text{abs}}$ , temperature of absorber/absorbent storage tank
- 6 -  $x_{\text{abs}}$ , absorbent concentration in absorbent storage tank
- 7 -  $m_{\text{cond}}$ , mass in refrigerant storage tank
- 8 -  $T_{\text{amb}}$ , ambient temperature
- 9 -  $H_{\text{T}}$ , solar radiation incident on collector plane
- 10 -  $T_{\text{col,g}}$ , collector temperature for heat delivered to generator
- 11 -  $T_{\text{col,a}}$ , collector temperature for heat delivered to absorbent tank

Derivatives: 0

Outputs: 16

- 1 -  $\gamma_{\text{mode}}$ , heating/cooling mode:
  - 1 heating
  - 1.5 heating mode with rejection of condenser heat to ambient
  - 2 cooling
- 2 -  $\gamma_{\text{gen}}$ , control function (0 or 1) for operation of solution pump
- 3 -  $\gamma_{\text{cond}}$ , control function for operation of condenser heat exchanger

- 4 -  $\gamma_{\text{evap}}$ , control function for operation of evaporator heat exchanger
- 5 -  $\gamma_{\text{abs}}$ , control function for operation of absorber heat exc.
- 6 -  $\gamma_{\text{aux,g}}$ , control function for supplying auxiliary heat to generator
- 7 -  $\gamma_{\text{aux,l}}$ , control function for supplying auxiliary heat to load
- 8 -  $\gamma_{\text{aux,cool}}$ , control function for supplying auxiliary cooling to load
- 9 -  $\gamma_{\text{col,g}}$ , control function for delivering collected energy to generator
- 10 -  $\gamma_{\text{col,a}}$ , control function for delivering collected energy to absorbent storage tank
- 11 -  $\gamma_{\text{rej}}$ , control function for rejecting heat from condenser to ambient
- 12 -  $\dot{m}_{\text{pump}}$ , solution pump mass flow rate
- 13 -  $\dot{Q}_{\text{aux,g}}$ , auxiliary energy input to generator
- 14 -  $\dot{Q}_{\text{aux,l}}$ , auxiliary energy supplied to load
- 15 -  $\dot{m}_{\text{col,g}}$ , collector mass flow rate for heat to generator
- 16 -  $\dot{m}_{\text{col,a}}$ , collector mass flow rate for heat to absorbent tank

### A.3 Heat Exchange Switching Component

This component models the ambient and load heat exchangers as constant effectiveness devices and connects them to the evaporator or condenser and absorber heat exchangers depending on the heating/cooling mode. The condenser and absorber heat exchangers are assumed to be connected in parallel. The sum of the flow rates through these two exchangers is constant and thus the flow through each will depend on whether one or both are operating. The option of specifying different heat transfer effectivenesses for these two flow conditions is provided. The effectiveness of the load and ambient heat exchangers is separately specified for heating and cooling operation, allowing for the different conditions that may exist for these different modes.

Parameters: 14

- 1 -  $\epsilon_{load,h}$ , effectiveness of load heat exchanger for heating
- 2 -  $\epsilon_{load,c}$ , effectiveness of load heat exchanger for cooling
- 3 -  $\epsilon_{amb,h}$ , effectiveness of ambient heat exchanger in heating
- 4 -  $\epsilon_{amb,c}$ , effectiveness of ambient heat exchanger in cooling
- 5 -  $\epsilon_{cond}$ , effectiveness of condenser heat exchanger for full flow through condenser
- 6 -  $\epsilon_{cond,s}$ , effectiveness of condenser heat exchanger for flow split between condenser and absorber
- 7 -  $\epsilon_{abs}$ , effectiveness of absorber heat exchanger for full flow through absorber

- 8 -  $\epsilon_{abs,s}$ , effectiveness of absorber heat exchanger for flow split between condenser and absorber
- 9 -  $\dot{m}_{load}$ , mass flow rate across air side of load heat exchanger
- 10 -  $\dot{m}_{amb}$ , mass flow rate across air side of ambient heat exchanger
- 11 -  $\dot{m}_{c+a}$ , mass flow rate through condenser plus absorber heat exchangers
- 12 -  $\dot{m}_{evap}$ , mass flow rate through evaporator heat exchanger
- 13 -  $C_{p,hx}$ , heat capacity of heat exchanger fluid
- 14 -  $C_{p,sink}$ , heat capacity of heat source/sink fluid (e.g., ambient air)

Inputs: 9

- 1 - heating cooling mode:
  - 1 heating
  - 1.5 heating with condenser heat rejected to ambient
  - 2 cooling
- 2 -  $T_{hx,cond}$ , temperature of condenser heat exchange stream
- 3 -  $\gamma_{cond}$ , control function for condenser heat exchanger
- 4 -  $T_{hx,abs}$ , temperature of absorber heat exchange stream
- 5 -  $\gamma_{abs}$ , control function for absorber heat exchanger
- 6 -  $T_{hx,evap}$ , temperature of evaporator heat exchange stream
- 7 -  $\gamma_{evap}$ , control function for evaporator
- 8 -  $T_{hx,load}$ , temperature of load heat exchange stream
- 9 -  $T_{sink}$ , temperature of heat source/sink (e.g., ambient)

Derivatives: 0

Outputs: 13

- 1 -  $\dot{m}_{\text{cond}}$ , mass flow rate through condenser heat exchanger
- 2 -  $\dot{m}_{\text{abs}}$ , mass flow rate through absorber heat exchanger
- 3 -  $T_{\text{hx,c+a,r}}$ , return temperature for condenser/absorber heat exchange stream
- 4 -  $\dot{m}_{\text{evap}}$ , mass flow rate through evaporator heat exchanger
- 5 -  $T_{\text{hx,evap,r}}$ , return temperature for evaporator heat exchange stream
- 6 -  $\dot{m}_{\text{load}}$ , air side mass flow rate for load heat exchanger
- 7 -  $T_{\text{hx,load,r}}$ , return temperature for load heat exchange stream
- 8 -  $\dot{Q}_{\text{load}}$ , heat transfer rate to load
- 9 -  $\dot{m}_{\text{sink}}$ , air side mass flow rate for ambient heat exchanger
- 10 -  $T_{\text{hx,sink,r}}$ , return temperature for ambient heat exchange stream
- 11 -  $\dot{Q}_{\text{sink}}$ , energy transfer rate from heat source/sink
- 12 -  $\epsilon_{\text{cond}}$ , effectiveness of condenser heat exchanger
- 13 -  $\epsilon_{\text{abs}}$ , effectiveness of ambient heat exchanger

## APPENDIX B

### USER DOCUMENTATION FOR STEADY-STATE AHP SIMULATION PROGRAM

This appendix gives specifications for the simulation deck and component parameters necessary to run the steady-state absorption heat pump simulation program. A complete listing of the program along with a sample simulation deck is given in Appendix E.

#### B.1 Simulation Deck

The simulation deck specifies general parameters for the simulation as a whole; inputs, outputs and parameters for each of the components in the simulation; values for input (e.g., heat exchange) stream variables; and initial guesses for tear streams. The simulation deck must be arranged in the specified order. The deck is read as free format (except that variables starting with I, K, L and N are integers and must not contain a decimal point). The deck is as follows:

LUR, LUP

--logical unit from which the remainder of the deck is to be read  
(this first card is read with the default logical unit for the  
system (i.e., READ (\*,\*))

--logical unit to which output is written

NUNIT, NSTR, NSTYPE, NSTRIC, NDAT, NDATIC, NPRES, NINV, IPRT

--total number of components in simulation

- total number of streams
- number of stream types (e.g., air versus a refrigerant-  
absorbent mixture)
- number of streams with initial conditions, including both  
external heat exchange streams and tear streams
- number of data "streams" (used to pass information such as  
heat flows to or from a component)
- number of data streams with initial valued specified
- number of system pressures
- number of inventory relationships available (program is  
currently limited to 2)
- level of printing detail:
  - 0 - print only final results
  - 1 - also list iterations for system pressures
  - 2 - also list inputs and outputs to convergence components
  - 3 - also list inputs and outputs for each component

Each stream type requires a single data image specifying:

ISTYPE, NPROP, NPCONV

- index for stream type
- total number of properties for stream (program currently has  
seven: stream type, mass flow rate, pressure, refrigerant  
mass concentration, specific enthalpy, temperature, and  
equilibrium vapor quality)

--number of properties to be checked for convergence (e.g., if  
 NPCONV = 5, the temperature and quality (which are related to  
 P, x, h) are not checked by the convergence components)

(KPINV(I), I = 1, NINV)

--specification for the elements of the pressure array that are  
 to be set by the inventory analysis

NITMAX, NPITMX, NFITMX, STRTOL, CHGTOL

--maximum number of iterations for internal loops in components

--maximum number of iterations for pressure (inventory)

--maximum number of iterations for internal loops in property  
 routines

--relative convergence tolerance for the convergence components

--relative convergence tolerance for the inventory iteration

(KCALL(I), I = 1, NUNIT)

--order in which components are to be called

(CDATA(I), I = 1, NDAT)

--labels for data streams; these can be up to 8 characters long  
 and must appear in a 5A8 format

Each component in the simulation is specified by the following  
 set of data images. If the specified number for a particular item is  
 zero, the corresponding card in the simulation deck must be omitted  
 (e.g., if the value specified for NIDAT is zero, the card specifying  
 the IDAT(I) must not be present). The specifications for the various  
 components are given in Section B.2.

IUNIT, ITYPE, ILABEL, NIFLO, NIDAT, NLFLO, NLDAT, NPAR

--unit number

--type number of unit

--flag for label, if ILABEL > 0 a component label must be present

--number of input flow streams to component

--number of input data streams to component

--number of flow streams leaving component

--number of data streams leaving component

--number of component parameters

LABEL

--up to 40 characters, used to identify units in output

(IFLO(I), I = 1, NIFLO)

--the system stream numbers that are input to the component

(IDAT(I), I = 1, NIDAT)

--the system data stream numbers that are input to the component

(LFLO(I), I = 1, NLFLO)

--the system stream numbers leaving the component

(LDAT(I), I = 1, NLDAT)

--the system data stream numbers leaving the component

(PAR(I), I = 1, NPAR)

--parameters needed to specify component

Following the specification of the components, the total inventory of refrigerant and absorbent present in the system and the initial values for pressures must be set:

(PINV(I), I = 1, NINV)

--total inventory of the NINV chemical species; if the PINV(I)  
are less than zero, the inventory iterations will be bypassed

(P(I), I = 1, NPRES)

--values or initial guesses for the system pressures

(PMIN(I), PMAX(I), I = 1, NPRES)

--bounds on system pressures, the inventory iteration will not  
vary the pressures outside of these limits

For each of the NSTRIC input or tear streams, the following two  
images are required to specify the stream values or initial guesses.  
(If the specification for the enthalpy, quality or temperature is  
replaced by -9999.9, an initialization routine will calculate that  
quantity in terms of the other stream variables.)

ISTR

--stream number

(STREAM(ISTR,J), J = 1, NPROP)

--the stream variables are

1 - stream type: 1 - absorbent-refrigerant mixture

2 - ambient air

2 - mass flow rate

3 - pressure

4 - refrigerant mass concentration (0 for air)

5 - specific enthalpy

6 - temperature

7 - vapor quality

The value of each data stream input to the simulation must be supplied:

IDAT, DAT(IDAT)

--number of data stream

--value of data stream

Finally, the existence of any data for the heat transfer coefficient routine, HSUB, must be specified:

IHSUB, LURHS

--if IHSUB > 0, data is to be supplied to the HSUB routine

--logical unit from which data is to be read

The current version of HSUB requires fixed values of single and two phase heat transfer coefficients for each negative specification of a component heat transfer coefficient parameter (e.g., parameter 8 in the absorber):

HLIQ, H2P, HVAP

--subcooled liquid heat transfer coefficient

--two phase coefficient

--superheated vapor coefficient

These heat transfer values are read directly by the HSUB subroutine independently of the main simulation deck. The HSUB routine could thus be modified to accommodate more detailed heat transfer data.

## B.2 Component Specifications

Each component in the simulation is identified by a unit number (which is unique) and a type number (which, for example, identifies it as an absorber). The streams input to and output from individual components must be related to the system stream numbers. This section details the input and output streams and parameters for each of the component models. Heat transfer coefficients may be specified as a constant value, or if the parameter is negative, a film coefficient will be calculated by the HSUB routine. The inventory analysis, or portions of it, can be bypassed by specifying a zero value for the corresponding volume parameter. Several components have an option to print results of internal calculations or iterations; this printout would be useful in the debugging of a system.

### B.2.1 Type 1 generator

Input flow streams: 1

1 - weak absorbent

Input data streams: 1

1 -  $\dot{Q}_{\text{gen}}$ , heat input to generator

Output flow streams: 1 or 2

if 1 output stream:

1 - heated stream

if 2 output streams:

1 - saturated strong absorbent

2 - saturated refrigerant vapor

Output data streams: 0

Parameters: 3

1 -  $N_{\text{str}}$ , number of output streams

2 -  $V_{\text{liq}}$ , volume of liquid portion of generator

3 -  $V_{\text{vap}}$ , volume of vapor portion

### B.2.2 Type 2 falling-film absorber

Input flow streams: 3

- 1 - strong absorbent
- 2 - refrigerant vapor
- 3 - heat exchange stream

Input data streams: 0

Output flow streams: 2

- 1 - weak absorbent
- 2 - heat exchange stream

Output data streams: 1

- 1 -  $\dot{Q}_{abs}$ , heat transfer from heat exchange stream

Parameters: 15

- 1 -  $N_{row}$ , number of rows of heat exchange tubes
- 2 -  $V_{vap}$ , volume of vapor space
- 3 -  $V_{sump}$ , volume of liquid sump
- 4 -  $V_{hx}$ , internal volume of heat exchange tubing
- 5 - IFTY, specification of heat exchange stream flow, currently only IFTY = 3 (countercurrent flow) is implemented
- 6 -  $A_{tube,o}$ , outside area of heat exchange tubes
- 7 -  $A_{tube,ins}$ , inside area of heat exchange tubes
- 8 -  $hc_{ins}$ , inside film coefficient
- 9 -  $R_w$ , heat exchange tube wall resistance
- 10 -  $h_{film}$ , heat transfer coefficient for absorbent film flowing over heat exchange tubes
- 11 -  $z_{tube}$ , effective plate length for heat exchange tube

- 12 -  $\mu_{\text{abs}}$ , viscosity of absorbent solution
- 13 -  $D_{\text{AB}}$ , mass diffusion coefficient for refrigerant in absorbent solution
- 14 -  $\alpha_{\text{abs}}$ , thermal diffusivity of absorbent solution
- 15 - IPRT, level of printing within absorber component:
  - 0 - no printing
  - 1 - summary of enthalpy (heat exchange stream) iteration
  - 2 - tube by tube results
  - 3 - iterations for tube wall temperature

### B.2.3 Type 3 pump

Input flow streams: 1

1 - inlet solution

Input data streams: 0

Output flow streams: 1

1 - outlet solution

Output data streams: 0

Parameters: 3

1 - mode:

1 - constant outlet mass flow rate

2 - constant outlet volumetric flow rate (specific volume  
based on inlet conditions)

2 -  $\dot{m}_{\text{pump}}$  or  $\dot{v}_{\text{pump}}$ , flow rate

3 - index for outlet pressure (i.e., index for KPINV(I) array)

#### B.2.4 Type 4 throttle valve

Input flow streams: 1

1 - inlet solution

Input data streams: 0

Output flow streams: 1

1 - outlet solution

Parameters: 2 to 6

1 - mode:

1 - outlet flow rate equal to inlet flow rate

2 - outlet flow rate given by Equation [4-89]

2 - index for outlet pressure (i.e., index for KPINV(I) array)

if mode = 2 also specify:

3 -  $C_1$ , constant in Equation [4-89]

4 -  $C_2$ , constant in [4-89]

5 -  $\dot{m}_{o,\min}$ , lower bound on outlet flow rate

6 -  $\dot{m}_{o,\max}$ , upper bound on outlet flow rate

### B.2.5 Type 5 general N-stream heat exchanger

Input flow streams: 2 to 3

Input data streams: 0

Output flow streams: 2 to 6

Output flow streams correspond to inlet streams except that if an outlet stream is separated into liquid and vapor streams, the vapor fraction is assigned the next higher leaving stream number. For example, if input stream 2 is separated, the leaving liquid and vapor streams are 2 and 3 respectively and input stream 3 corresponds to leaving stream 4.

Output data streams: 1 or 3

for two flow streams:

1 -  $\dot{Q}_{12}$ , heat flow from stream 1 to 2

for three flow streams:

1 -  $\dot{Q}_{12}$

2 -  $\dot{Q}_{13}$

3 -  $\dot{Q}_{23}$

Parameters: 13 to 47

1 - N, number of flow streams (current limit is 3)

2 -  $N_{\text{node}}$ , number of nodes to use in Runge-Kutta solution

3 - IPRT, level of printing:

0 - no printing from heat exchanger component

1 - summary of enthalpy iteration and nodal temperatures, qualities, etc. for last iteration

2 - nodal temperatures, etc. for each iteration of enthalpy

- 4 - enthalpy iteration with which to start parabolic interpolation (in place of secant method)
- 5 - not used
- 6 to 5+N -  $V_i$ , volume of stream i (specify zero value if stream is not to be included in inventory analysis)
- 6+N to 5+2N - IFTY(I), flow direction for stream i (A maximum of one countercurrent and one cross flow stream may be specified. If 0.01 is added to these values, the stream will be split into liquid and vapor fractions at the outlet of the heat exchanger.)
- 1 - co-current flow
- 2 - cross flow
- 3 - countercurrent flow
- 6+2N to 5+2N+N! -  $A_{ij}$ , area of flow stream i in thermal contact with flow stream j; specify in order:  $A_{12}$ ,  $A_{13}$ ,  $A_{21}$ ,  $A_{23}$ ,  $A_{31}$ ,  $A_{32}$
- 6+2N+N! to 5+2N+2(N!) -  $hc_{ij}$ , heat transfer coefficient of flow stream i for surface in thermal contact with flow stream j; if  $hc_{ij} < 0$ , the coefficient is calculated by routine HSUB

The following parameters are optional (values of zero are assumed if not specified):

- 6+2N+2(N!) to 5+2N+3(N!) -  $A_{fin,ij}$ , extended surface (fin) area of flow stream i in thermal contact with flow stream j
- 6+2N+3(N!) to 5+2N+4(N!) -  $e_{fin,ij}$ , fin efficiency for fin area  $A_{fin,ij}$

6+2N+4(N!) to 5+2N+5(N!) -  $R_{\text{wall},ij}$ , wall resistance between  
streams i and j ( $R_{\text{wall},ij}$  and  $R_{\text{wall},ji}$  should be equal)  
6+2N+5(N!) to 5+2N+6(N!) -  $R_{\text{foul},ij}$ , fouling resistance  
associated with area  $A_{ij}$

### B.2.6 Type 6 analyzer

Input flow streams: 3

- 1 - weak absorbent
- 2 - refrigerant vapor
- 3 - heat exchange stream (i.e., strong absorbent)

Input data streams: 0

Output flow streams: 3

- 1 - weak absorbent
- 2 - refrigerant vapor
- 3 - heat exchange stream

Output data streams: 1

- 1 -  $\dot{Q}_{anal}$ , heat transfer rate to heat exchange stream

Parameters: 6

- 1 -  $N_{stage}$ , number of equilibrium stages
- 2 -  $UA_{anal}$ , overall heat transfer coefficient-area product for entire analyzer
- 3 - IPRT, level of printing:
  - 0 - no printing from analyzer component
  - 1 - print summary of m and x iterations
  - 2 - print summary of stage-by-stage calculations
- 4 -  $V_{liq}$ , liquid volume of contacting streams
- 5 -  $V_{vap}$ , vapor volume of contacting streams
- 6 -  $V_{hx}$ , internal flow volume of heat exchanger

### B.2.7 Type 7 flow mixer/stream splitter

Input flow streams: 1 to 5

Input data streams: 0

Output flow streams: 1 or 2

1 - mixed stream or liquid fraction

2 - vapor fraction

Output data streams: 0

Parameters: 2

1 -  $N_{\text{input}}$ , number of input streams

2 -  $N_{\text{output}}$ , number of output streams:

1 - mixed outlet stream

2 - outlet stream split into liquid and vapor portions

### B.2.8 Types 8 and 9

Types 8 and 9 are currently not assigned. Referencing these types will result in an error message but the simulation will not terminate. The TYPE8 and TYPE9 subroutine entry points are referenced in the simulation program and are thus available for the insertion of additional components.

### B.2.9 Type 10 convergence component

Input flow streams: 1

Input data streams: 0

Output flow streams: 1

(The the input and output stream numbers are equal.)

Output data streams: 0

Parameters: 5 or 9

1 - mode (If 0.1 is added to this value, the simulation will continue if the maximum number of iterations is exceeded, otherwise the simulation terminates.)

1 - bounded Wegstein iteration

2 - two-variable secant method iteration

2 - unit number for first component in current iteration loop

3 -  $IT_{max}$ , maximum number of iterations

for mode = 1 (Wegstein iteration):

4 -  $q_{min}$ , lower bound on acceleration parameter (-2.0 suggested)

5 -  $q_{max}$ , upper bound on acceleration parameter (0.5 suggested)

for mode = 2 (secant iteration):

4 -  $IV_1$ , property number for first variable in iteration

(e.g., x = 4, h = 5)

5 -  $IV_2$ , property number for secant variable in secant iteration

6 -  $V_{1,min}$ , lower iteration bound for variable  $IV_1$

7 -  $V_{1,max}$ , upper iteration bound for variable  $IV_1$

8 -  $V_{2,min}$ , lower iteration bound for variable  $IV_2$

9 -  $V_{2,max}$ , upper iteration bound for variable  $IV_2$

### B.3 Example Simulation Deck and Program Output

The following simulation deck and program output is for a test at an ambient temperature of -8 C and the nominal component parameters. The first card specifies that the simulation deck is to be read from logical unit 12 with output sent to logical unit 3. For convenience in starting multiple runs at different conditions, the deck is separated into three files containing the specification of the simulation parameters, the conditions of external and tear streams, and parameters for the HSUB routine.

12 3  
 17 28 2 8 10 1 3 2 1  
 1 7 5  
 2 7 5  
 1 2 2 2 2  
 1 3  
 12 0 15 0.0001 1.00  
 1 2 3 4 5 6 7 8 9 10 11 12 13 14 15 16 17  
 QGEN QANAL QR-SA-WAQR-00-00QR-WA-VP  
 QCOND QREFHX QEVAP QFLUEHX QABS  
 1 1 1 1 1 2 0 3  
 GENERATOR  
 5  
 1  
 6 11  
 2 0.0052 0.0013  
 2 6 1 3 0 3 1 6  
 ANALYZER  
 4 11 6  
 5 12 7  
 2  
 1.0 0.1 0.0075 0.0030 0.0020 1  
 3 5 1 3 0 4 3 23  
 RECTIFIER  
 7 2 12  
 8 3 13 14  
 3 4 5  
 3 5 0 99 99 0.0004 0.0007 0.0069 1 3 1.01  
 0.25 0.00 0.25 0.32 0.00 0.32  
 2.50 0.00 1.80 1.80 0.00 2.00  
 4 7 1 2 0 1 0 2  
 RECTIFIER STREAM MIX  
 3 13  
 4  
 2 1  
 5 10 1 1 0 1 0 5  
 CONVERGE ANALYZER INLET  
 4  
 4  
 1.1 6 9 -2.0 0.5  
 6 10 1 1 0 1 0 5  
 CONVERGE ANALYZER OUTLET  
 5  
 5  
 1.1 1 9 -2.0 0.5  
 7 5 1 2 0 2 1 13  
 CONDENSER  
 14 23  
 15 24  
 6  
 2 5 0 99 4 0.0024 0.0 1 3 0.25 0.25 -1.0 7.21  
 8 4 1 1 0 1 0 6  
 CONDENSER THROTTLE  
 15  
 16  
 2 2 23300. 678000. 0.0030 0.0100  
 9 5 1 2 0 2 1 13  
 REFRIGERANT HEAT EXCHANGER  
 16 19  
 17 20  
 7  
 2 4 0 99 99 0.0013 0.0004 1 3 0.160 0.160 -3 -2  
 10 4 1 1 0 1 0 2  
 EVAPORATOR THROTTLE  
 17

```

18
1.0 1
11 5 1 2 0 2 1 17
EVAPORATOR
18 25
19 26
8
2 6 0 99 99 0.0049 0.00 1 3 3.20 3.98 -2 0.020 0.0 57.8 0.0 0.88
12 10 1 1 0 1 0 5
CONVERGE EVAPORATOR OUTLET
19
19
1.1 9 6 -2.0 0.5
13 4 1 1 0 1 0 2
ABSORBER THROTTLE
8
9
1 1
14 5 1 2 0 2 1 13
FLUE GAS HEAT EXCHANGER
9 27
10 28
9
2 1 0 99 99 0.0 0.0 1 2 0.120 0.120 1.0 1.0
15 2 1 3 0 2 1 15
ABSORBER
10 20 21
1 22
10
30 0.0111 0.0009 0.00 3. 1.27 1.10 7.2 0.0 3.0 0.02 0.7E-3
2.0E-9 1.1E-7 0
16 3 1 1 0 1 0 3
SOLUTION PUMP
1
2
1 0.0227 3
17 10 1 1 0 1 0 5
CONVERGE PUMP OUTLET
2
2
1.1 1 12 -2.0 0.5

0.0 0.0
0.246 0.768 2.101
0.20 0.30 1.8 2.4
2
1.0 0.0227 2.101 0.299 -9999.9 48.0 -9999.0
4
1.0 0.0234 2.101 0.323 -9999.9 115.0 -9999.9
5
1.0 0.0224 2.101 0.230 -9999.9 130.0 -9999.9
19
1.0 0.0048 0.246 0.997 750.0 -9999.9 -9999.9
21
1.0 0.1671 0.100 0.000 -9999.9 40.7 -9999.9
23
1.0 0.1703 0.100 0.000 -9999.9 40.7 -9999.9
25
2.0 1.663 0.100 0.000 -9999.9 -8.7 -9999.9
27
2.0 0.108 0.100 0.000 -9999.9 85.0 -9999.9
1 10.49

1 12
0.40 8.0 0.11
0.16 3.0 0.10
0.40 8.0 0.11

```

STREAM	TYPE	MF (KG/SEC)	P (MPA)	X	H (KJ/KG)	T (C)	Y
1	1	0.022700	0.2460	0.2921	48.83	45.33	0.0286
2	1	0.022700	2.1010	0.2921	48.83	54.85	-0.2587
3	1	0.022700	2.1010	0.2921	445.20	122.96	0.0440
4	1	0.024378	2.1010	0.3125	424.70	118.94	0.0472
5	1	0.022255	2.1010	0.2123	466.70	135.02	0.0000
6	1	0.017809	2.1010	0.0990	675.79	170.08	0.0000
7	1	0.017809	2.1010	0.0990	561.01	145.48	-0.0874
8	1	0.017809	2.1010	0.0990	275.19	82.99	-0.3052
9	1	0.017809	0.2460	0.0990	275.19	83.33	-0.0133
10	1	0.017809	0.2460	0.0990	278.48	84.06	-0.0111
11	1	0.004446	2.1010	0.6659	1988.56	170.08	1.0000
12	1	0.006569	2.1010	0.8915	1652.10	135.02	1.0000
13	1	0.001678	2.1010	0.5886	147.29	75.48	0.0000
14	1	0.004891	2.1010	0.9954	1369.44	75.48	1.0000
15	1	0.004891	2.1010	0.9954	232.70	49.25	-0.0163
16	1	0.004891	0.7680	0.9954	232.70	17.10	0.1318
17	1	0.004891	0.7680	0.9954	-56.30	-10.36	-0.1079
18	1	0.004891	0.2460	0.9954	-56.30	-13.97	0.0130
19	1	0.004891	0.2460	0.9954	731.84	-13.96	0.6098
20	1	0.004891	0.2460	0.9954	1020.84	-13.88	0.8285
21	1	0.167100	0.1000	0.0000	173.49	40.70	-0.1096
22	1	0.167100	0.1000	0.0000	226.41	53.45	-0.0861
23	1	0.170300	0.1000	0.0000	173.49	40.70	-0.1096
24	1	0.170300	0.1000	0.0000	206.14	48.57	-0.0951
25	2	1.663000	0.1000	0.0000	-8.73	-8.70	1.8610
26	2	1.663000	0.1000	0.0000	-11.04	-11.01	1.8502
27	2	0.108000	0.1000	0.0000	85.52	85.00	2.3027
28	2	0.108000	0.1000	0.0000	84.98	84.46	2.3002

## DATA

QGEN	10.4900	QANAL	2.0441	QR-SA-WA	5.0903	QR-00-00	0.0000
QR-WA-VP	-3.9073	QCOND	5.5595	QREFHX	1.4134	QEVAP	-3.8545
QFLUEHX	-0.0585	QABS	-8.8436				

NPITER = 0

PRESSURES:

0.2460 0.7680 2.1010

UNIT	TYPE	KCALL	NCALL	INVENTORY		
1	1	1	46	0.45	4.00	GENERATOR
2	6	2	46	1.74	7.16	ANALYZER
3	5	3	46	0.27	0.69	RECTIFIER
4	7	4	46	0.00	0.00	RECTIFIER STREAM MIX
5	10	5	46	0.00	0.00	CONVERGE ANALYZER INLET
6	10	6	46	0.00	0.00	CONVERGE ANALYZER OUTLET
7	5	7	8	0.24	0.00	CONDENSER
8	4	8	8	0.00	0.00	CONDENSER THROTTLE
9	5	9	18	0.76	0.00	REFRIGERANT HEAT EXCHANGER
10	4	10	18	0.00	0.00	EVAPORATOR THROTTLE
11	5	11	18	0.08	0.00	EVAPORATOR
12	10	12	18	0.00	0.00	CONVERGE EVAPORATOR OUTLET
13	4	13	8	0.00	0.00	ABSORBER THROTTLE
14	5	14	8	0.00	0.00	FLUE GAS HEAT EXCHANGER
15	2	15	8	0.27	0.74	ABSORBER
16	3	16	8	0.00	0.00	SOLUTION PUMP
17	10	17	8	0.00	0.00	CONVERGE PUMP OUTLET

TOTAL

3.80 12.59

APPENDIX C  
PROPERTY RELATIONS

C.1 Sodium Thiocyanate-Ammonia System

Correlations of thermodynamic properties for the NaSCN-NH<sub>3</sub> chemical system were developed from published data. It is assumed that the NaSCN absorbent is non-volatile and thus the vapor phase is pure ammonia. Fortran routines for the TRNSYS AHP components employing these correlations are given in Appendix E.1.

C.1.1 Empirical property relations

The data of Sargent and Beckman (25) for the enthalpy of NaSCN-NH<sub>3</sub> solutions was fit to an equation of the form:

$$\begin{aligned}
 h \text{ (kJ kg}^{-1}\text{)} = & a_{11} + a_{12}x + a_{13}x^2 + a_{14}x^3 + a_{15}x^4 \\
 & + (a_{21} + a_{22}x + a_{23}x^2 + a_{24}x^3 + a_{25}x^4) T \\
 & + (a_{31} + a_{32}x + a_{33}x^2 + a_{34}x^3 + a_{35}x^4) T^2 \\
 & + (a_{41} + a_{42}x + a_{43}x^2 + a_{44}x^3 + a_{45}x^4) T^3 \quad [C-1]
 \end{aligned}$$

where the  $a_{ij}$  coefficients are given in Table C-1.

The enthalpy of ammonia vapor given by VanWylen and Sonntag (117) was fit to an equation of the form:

$$\begin{aligned}
 h \text{ (kJ kg}^{-1}\text{)} = & b_{11} + b_{12}T_{\text{sat}} + b_{13}T_{\text{sat}}^2 + b_{14}T_{\text{sat}}^3 \\
 & + (b_{21} + b_{22}T_{\text{sat}} + b_{23}T_{\text{sat}}^2 + b_{24}T_{\text{sat}}^3) T \\
 & + (b_{31} + b_{32}T_{\text{sat}} + b_{33}T_{\text{sat}}^2 + b_{34}T_{\text{sat}}^3) T^2 \quad [C-2]
 \end{aligned}$$

Table C-1 Correlation coefficients for the polynomial fits of liquid and vapor enthalpy for the NaSCN-NH<sub>3</sub> chemical system

Liquid solution		Ammonia vapor	
a <sub>11</sub>	182.79	b <sub>11</sub>	1446.1
a <sub>12</sub>	162.62	b <sub>12</sub>	-1.4779
a <sub>13</sub>	85.158	b <sub>13</sub>	-0.02532
a <sub>14</sub>	1030.09	b <sub>14</sub>	1.865 x 10 <sup>-4</sup>
a <sub>15</sub>	535.55	b <sub>21</sub>	2.5045
a <sub>21</sub>	4.3411	b <sub>22</sub>	0.0183
a <sub>22</sub>	2.7739	b <sub>23</sub>	2.769 x 10 <sup>-4</sup>
a <sub>23</sub>	-2.6074	b <sub>24</sub>	4.661 x 10 <sup>-7</sup>
a <sub>24</sub>	4.7551	b <sub>31</sub>	-0.00119
a <sub>25</sub>	-2.7135	b <sub>32</sub>	-8.265 x 10 <sup>-5</sup>
a <sub>31</sub>	6.420 x 10 <sup>-4</sup>	b <sub>33</sub>	-9.536 x 10 <sup>-7</sup>
a <sub>32</sub>	-0.02617	b <sub>34</sub>	7.704 x 10 <sup>-9</sup>
a <sub>33</sub>	0.09395		
a <sub>34</sub>	-0.07371		
a <sub>35</sub>	0.005144		
a <sub>41</sub>	7.481 x 10 <sup>-5</sup>		
a <sub>42</sub>	1.111 x 10 <sup>-4</sup>		
a <sub>43</sub>	-5.428 x 10 <sup>-4</sup>		
a <sub>44</sub>	0.001086		
a <sub>45</sub>	-5.058 x 10 <sup>-4</sup>		

where the  $b_{ij}$  are given in Table C-1 and  $T_{sat}$  is the saturation temperature of the vapor at the temperature  $T$  given by:

$$T_{sat} = -245.0 - \frac{2245.7}{\ln P - 15.23} \quad [C-3]$$

The density of ammonia vapor was approximated by use of the Pitzer accentric factor method as described by Smith and VanNess (118):

$$\rho_{vap} \text{ (kg m}^{-3}\text{)} = \frac{17.03 P}{Z R (T + 273.15)} \quad [C-6]$$

where  $R$  is the gas constant and  $Z$  is the compressibility factor:

$$Z = 1 + (B_0 + \omega B_1) P_r / T_r \quad [C-7]$$

The accentric factor  $\omega$  is 0.250 for ammonia;  $P_r$  and  $T_r$  are the reduced pressure and temperature and the coefficients  $B_0$  and  $B_1$  are given by:

$$B_0 = 0.083 - 0.422 T_r^{-1.6} \quad [C-8]$$

$$B_1 = 0.139 - 0.172 T_r^{-4.2} \quad [C-9]$$

Finally, the density of NaSCN-NH<sub>3</sub> solutions was fit to a simple polynomial form using the data of Blytas and Daniels (24):

$$\rho_{liq} \text{ (kg m}^{-3}\text{)} = 653.9 + 392.9x + 442.6x^2 + (-1.419 + 0.858x + 0.791x^2) T \quad [C-10]$$

### C.1.2 Subroutine TMIXU

The subroutine TMIXU computes the temperature of a two phase, two component mixture (one component is assumed to be non-volatile) in a tank as a function of the total mass of each of the components, the total internal energy of the mixture and the volume of the tank. This subroutine finds the temperature and liquid phase composition that satisfy the equations:

$$U_{\text{tot}}/m_{\text{tot}} = f u_{\text{liq}}(T, x) + (1 - f) u_{\text{vap}}(T, P) + (mC_p)_{\text{tank}}/m_{\text{tot}} (T - T_{\text{reference}}) \quad [\text{C-11}]$$

$$V_{\text{tot}}/m_{\text{tot}} = f v_{\text{liq}}(T, x) + (1 - f) v_{\text{vap}}(T, P) \quad [\text{C-12}]$$

where  $U_{\text{tot}}$  and  $V_{\text{tot}}$  are the total internal energy and volume of the tank and the subscripts tot, liq, and vap refer to the total contents of the tank and the liquid and vapor phases respectively. The parameter  $f$  is the mass fraction of the tank contents in the liquid phase and  $(mC_p)_{\text{tank}}$  represents the thermal capacitance of the tank, excluding the refrigerant and absorbent it contains. The concentration in the liquid phase is given by:

$$x_{\text{liq}} = \frac{m_{\text{abs}}}{(m_{\text{ref}} + m_{\text{abs}}) f} \quad [\text{C-13}]$$

where  $m_{\text{ref}}$  and  $m_{\text{abs}}$  are the total masses of refrigerant and absorbent in the tank. The pressure  $P$  is a function of  $T$  and  $x$ ; thus, [C-11] and [C-12] are functions only of  $T$  and  $f$  and can be solved iteratively.

## C.2 Ammonia-Water Chemical System

Thermodynamic properties for the ammonia-water system were derived from an equation of state presented by Schultz (119). Equations are supplied for the molar Gibbs free energy of pure liquid and gaseous ammonia and water and their liquid and vapor mixtures. These are given in terms of the following reduced variables:

$$\begin{aligned} \text{temperature:} & \quad \theta = T / T_s \\ \text{pressure:} & \quad \pi = P / P_s \\ \text{free energy:} & \quad G_R = G_m / (RT_s) \end{aligned}$$

where the subscript m indicates a molar quantity and the reference values for the reduced properties are:

$$\begin{aligned} T_s &= 100 \text{ K} \\ P_s &= 1 \text{ MPa} \end{aligned}$$

For the pure components, the reduced free energy of the vapor is given by:

$$\begin{aligned} G_{R,\text{vap}} &= h_{0,\text{vap}} - \theta s_{0,\text{vap}} - B_1 \theta \ln(\theta/\theta_0) + (B_1 - B_2 \theta)(\theta - \theta_0) \\ &+ (B_2/2 - B_3 \theta/2)(\theta^2 - \theta_0^2) + (B_3/3 - B_4 \theta/3)(\theta^3 - \theta_0^3) \\ &+ B_4/4 (\theta^4 - \theta_0^4) + \theta \ln(\pi/\pi_0) + (A_1 \theta + A_2)(\pi - \pi_0) \\ &+ A_3 (\theta/\pi + \theta \pi_0/\theta_0^2 - 2\pi_0/\theta_0) \end{aligned} \quad [\text{C-14}]$$

where  $h_{0,\text{vap}}$ ,  $s_{0,\text{vap}}$ ,  $\theta_0$ ,  $\pi_0$ , and the  $A_i$  and  $B_i$  terms are separate sets of constants for ammonia and water and are given in Table C-2. The reduced free energy of the pure liquid is:

$$\begin{aligned}
G_{R,liq} = & h_{0,liq} - \theta s_{0,liq} - D_1 \theta \ln(\theta/\theta_0) + (D_1 - D_2 \theta)(\theta - \theta_0) \\
& + D_2/2 (\theta^2 - \theta_0^2) + (C_1 + C_3 \theta)(\pi - \pi_0) \\
& + C_2/2 (\pi^2 - \pi_0^2) + C_4 \theta^2 (\pi - \pi_0)
\end{aligned} \tag{C-15}$$

Again, the constants are given in Table C-2.

For gaseous mixtures, an ideal solution is assumed:

$$\begin{aligned}
G_{R,vap}^{mix} = & x_m G_{R,vap}^a + (1 - x_m) G_{R,vap}^w \\
& + \theta x_m \ln(x_m) + \theta (1 - x_m) \ln(1 - x_m)
\end{aligned} \tag{C-16}$$

where the superscript indicates either the pure components or an ammonia-water mixture. The expression for the free energy of a liquid mixture is:

$$\begin{aligned}
G_{R,liq}^{mix} = & x_m G_{R,liq}^a + (1 - x_m) G_{R,liq}^w \\
& + \theta [x_m \ln(x_m) + (1 - x_m) \ln(1 - x_m)] \\
& + \{F_1 + F_2 \pi + (F_3 + F_4 \pi)/\theta + (F_5 + F_6 \pi)/\theta^2 \\
& + [(F_7 + F_8 \pi + (F_9 + F_{10} \pi)/\theta)(2x_m - 1)]\} x_m (1 - x_m)
\end{aligned} \tag{C-17}$$

where the constants  $F_1$  to  $F_{10}$  are given in Table C-2. The term within the braces in [C-17] is the excess Gibbs free energy and is represented by a three-suffix Margules equation with the binary parameters A, B being a function of temperature and pressure:

$$A = F_1 + F_2 \pi + (F_3 + F_4 \pi)/\theta + (F_5 + F_6 \pi)/\theta^2 \tag{C-18}$$

$$B = F_7 + F_8 \pi + (F_9 + F_{10} \pi)/\theta \tag{C-19}$$

Table C-2 Dimensionless coefficients for the Schultz equation of state for ammonia-water mixtures

Pure Components			Mixture	
	Ammonia	Water		
A <sub>1</sub>	-0.159379	-0.049731	F <sub>1</sub>	18.1901
A <sub>2</sub>	1.63843	1.04617	F <sub>2</sub>	-0.121603
A <sub>3</sub>	-4.50079	-5.20084	F <sub>3</sub>	-99.5037
B <sub>1</sub>	4.32139	4.14441	F <sub>4</sub>	0.672809
B <sub>2</sub>	-0.462406	-0.140368	F <sub>5</sub>	84.4263
B <sub>3</sub>	0.194902	0.040182	F <sub>6</sub>	-1.02601
B <sub>4</sub>	-0.014597	-0.001673	F <sub>7</sub>	2.43329
C <sub>1</sub>	0.0386536	0.0242044	F <sub>8</sub>	0.026458
C <sub>2</sub>	-0.00011033	-4.58 x 10 <sup>-6</sup>	F <sub>9</sub>	-1.28324
C <sub>3</sub>	-0.0125573	-0.00263238	F <sub>10</sub>	-0.106125
C <sub>4</sub>	0.00371324	0.00059429		
D <sub>1</sub>	6.18881	7.72211		
D <sub>2</sub>	1.26706	0.393864		
θ <sub>0</sub>	3.2515	5.0699		
π <sub>0</sub>	2.1410	3.0000		
h <sub>0,vap</sub>	26.476	60.744		
h <sub>0,liq</sub>	5.1289	21.849		
s <sub>0,vap</sub>	8.2657	13.403		
s <sub>0,liq</sub>	1.7003	5.7314		

### C.2.1 Pressure-temperature-composition behavior

Schultz presents the equation of state only in terms of Gibbs free energy and thus it is necessary to derive the needed thermodynamic relationships from  $G_R$ . The vapor and liquid compositions and saturation pressure,  $P$ , are related by:

$$x_{m,vap} P = \gamma^i x_{m,liq} P^i \quad [C-20]$$

where  $\gamma^i$  is an activity coefficient, the superscripts refer to the component, and  $P^i$  is the vapor pressure of pure  $i$  at the same temperature. Equation [C-20] assumes an ideal solution in the vapor phase; an assumption that was also made in the equation of state. The Antoine equation was used for the vapor pressure of the pure components with coefficients given by Reid, et al. (120). Combining the [C-20] equations for the two components with the relationship between the water and ammonia mole fractions yields expressions for the saturation pressure and mole fraction of ammonia in the vapor:

$$P = \gamma^a x_{m,liq} P^a + \gamma^w (1 - x_{m,liq}) P^w \quad [C-21]$$

$$x_{vap} = \frac{\gamma^a x_{m,liq} P^a}{\gamma^a x_{m,liq} P^a + \gamma^w (1 - x_{m,liq}) P^w} \quad [C-22]$$

The activity coefficients are related to the total excess Gibbs free energy,  $G^E$ :

$$RT \ln(\gamma^i) = \left( \frac{\partial G^E}{\partial n^i} \right)_{T, P, n_j} \quad [C-23]$$

where the derivative is with respect to the mole number of component  $i$  with the temperature, pressure, and mole number of the other component being held constant. For a three-suffix Margules expression for the excess Gibbs free energy, the activity coefficients are given by Reid, et al. (120):

$$\begin{aligned} \ln(\gamma^a) = & A/\theta (1 - 2x_m + x_m^2) \\ & + B/\theta (-1 + 6x_m - 9x_m^2 + 4x_m^3) \end{aligned} \quad [C-24]$$

$$\ln(\gamma^w) = (A/\theta - 3B/\theta) x_m^2 + 4B/\theta x_m^3 \quad [C-25]$$

The above equations provide a means of calculating the saturation temperature, pressure, or liquid or vapor composition as a function of any two of the remaining variables. To implement these relationships in the property routines, however, requires iterative calculations. For the calculation of saturation temperature as a function of pressure and liquid composition, a secant method iteration in  $1/T_{\text{sat}}$  is used. The initial guess for  $T_{\text{sat}}$  is given by:

$$T_{\text{sat}} = T_{\text{sat}} + (2x_m - x_m^2) (T_{\text{sat}} - T_{\text{sat}}) \quad [C-13]$$

where  $T_{\text{sat}}$  and  $T_{\text{sat}}$  are the saturation temperature of pure ammonia and water at the given pressure. The factor  $(2x_m - x_m^2)$  was found to give a better first guess than a simple weighted average of the two pure component temperatures. For a given guess of  $T_{\text{sat}}$ , the vapor pressures of the pure components can be calculated, followed by the activity coefficients. The convergence is checked with [C-21]. The equilibrium vapor composition is found by the same calculation

procedure except that [C-22] is employed when the iteration for  $1/T_{\text{sat}}$  has converged.

For the computation of the liquid composition given temperature and pressure, the pure component saturation temperatures and pressures and the binary parameters A and B can be found. An iteration for the liquid composition is carried out with the initial guess is generated by rearranging [C-21]. The activity coefficients are then calculated. The second iterative valued for composition is obtained by solving [C-21] for  $x_m$  and thereafter the secant method is used until [C-21] is satisfied.

The calculation of saturation pressure as a function of temperature and liquid composition uses as a first guess:

$$P_{\text{sat}} = x_m^2 P^a + (1 - x_m)^2 P^w \quad [\text{C-27}]$$

The activity coefficients are then calculated and Equation [C-21] is used as a check for convergence. A second guess for  $P_{\text{sat}}$  is generated by rearranging [C-21] and the iteration proceeds by the secant method. (This iteration converges very rapidly since the activity coefficients are weak functions of P.)

To find the vapor composition at a specified temperature and pressure, the equilibrium liquid composition is first found. Then the vapor composition is found as a function of pressure and liquid composition as described above. The calculation of the equilibrium liquid composition at a given pressure and vapor composition involves a secant method iteration for the liquid composition. The iteration

continues until the value of vapor composition calculated with the guessed liquid composition and input pressure agrees with the input vapor composition.

### C.2.2 Enthalpy

The molar specific enthalpy is related to the Gibbs free energy by:

$$h_m = -T^2 \frac{\partial}{\partial T} \left( \frac{G_m}{T} \right)_P \quad [C-28]$$

In terms of the reduced variables this becomes:

$$h_m = -RT_s \theta^2 \frac{\partial}{\partial \theta} \left( \frac{G_R}{\theta} \right)_\pi \quad [C-29]$$

For the pure gaseous and liquid components this yields:

$$\begin{aligned} h_{m,\text{vap}} = RT_s \left[ h_0 + B_1(\theta - \theta_0) + B_2/2 (\theta^2 - \theta_0^2) \right. \\ \left. + B_3/3 (\theta^3 - \theta_0^3) + B_4/4 (\theta^4 - \theta_0^4) \right. \\ \left. + A_2 (\pi - \pi_0) + 2A_3 (\pi/\theta - \pi_0/\theta_0) \right] \quad [C-30] \end{aligned}$$

$$\begin{aligned} h_{m,\text{liq}} = RT_s \left[ h_0 + D_1(\theta - \theta_0) + D_2/2 (\theta^2 - \theta_0^2) \right. \\ \left. + C_1(\pi - \pi_0) + C_2/2 (\pi^2 - \pi_0^2) - C_4\theta^2(\pi - \pi_0) \right] \quad [C-31] \end{aligned}$$

For gaseous mixtures, the mixing terms in the expression for Gibbs free energy drop out of the derivative to yield the ideal solution assumption:

$$h_{m,\text{liq}}^{\text{mix}} = x_m h_{m,\text{liq}}^a + (1 - x_m) h_{m,\text{vap}}^w \quad [C-32]$$

An ideal solution is not assumed for liquid mixtures and thus the expression for the liquid mixture enthalpy is more complicated:

$$\begin{aligned}
 h_{m,\text{liq}}^{\text{mix}} &= x h_{m,\text{liq}}^{\text{a}} + (1 - x) h_{m,\text{liq}}^{\text{w}} \\
 &+ RT_s x_m (1 - x_m) \left\{ F_1 + F_2 \pi \right. \\
 &+ 2(F_3 + F_4 \pi)/\theta + 3(F_5 + F_6 \pi)/\theta^2 \\
 &\left. + [F_7 + F_8 \pi + 2(F_9 + F_{10} \pi)/\theta] (2x_m - 1) \right\} \quad [\text{C-33}]
 \end{aligned}$$

The implementation of the enthalpy relationships into the property routines is a straightforward application of [C-30] to [C-33]. No iterative calculations are required.

### C.2.3 Specific volume

The specific volume is given simply by the partial derivative of free energy with respect to pressure:

$$v_m = \left( \frac{\partial G_m}{\partial P} \right)_{x_m, T} \quad [\text{C-34}]$$

Or in terms of the reduced variables:

$$v_m = \frac{RT_s}{P_s} \left( \frac{\partial G_R}{\partial \pi} \right)_{x_m, \theta} \quad [\text{C-35}]$$

The specific volumes of the gaseous and liquid phases of the pure components are given by:

$$v_{m,\text{vap}} = RT_s/P_s (\theta/\pi + A_1 \theta + A_2 + A_3/\theta) \quad [\text{C-36}]$$

$$v_{m,\text{liq}} = RT_s/P_s (C_1 + C_2 \pi + C_3 \theta + C_4 \theta^2) \quad [\text{C-37}]$$

The specific volume of a gaseous mixture is again given by a weighted average of the volumes of the two components:

$$v_{m,vap}^{mix} = x_m v_{m,vap}^a + (1 - x_m) v_{m,vap}^w \quad [C-38]$$

The corresponding expression for liquid mixtures is:

$$\begin{aligned} v_{m,liq}^{mix} = & x_m v_{m,liq}^a + (1 - x_m) v_{m,liq}^w \\ & + \frac{RT_s}{P_s} x_m (1 - x_m) \left\{ F_2 + F_4/\theta + F_6/\theta^2 + \right. \\ & \left. + (F_8 + F_{10}/\theta) (2x_m - 1) \right\} \end{aligned} \quad [C-39]$$

#### C.2.4 Subroutine YT

The thermodynamic state of the streams in the simulation are specified in terms of pressure, composition and enthalpy. However, temperature and quality are more easily comprehended and are needed in some of the component models (e.g., for the calculation of heat flows). Thus, a subroutine calculating the temperature and quality of a stream (and also the composition and enthalpy of the liquid and vapor fractions of a two phase stream) as a function of pressure and overall composition and enthalpy was developed.

The subroutine YT first determines if a stream is subcooled liquid, superheated vapor or two phase and branches to the appropriate portion of the routine. A subcooled liquid is indicated if the enthalpy of the stream is less than the liquid enthalpy calculated at the saturation temperature for the same pressure and composition. For this case, the secant method is used to iterate on temperature until the calculated enthalpy agrees with the input stream enthalpy.

To check for a superheated vapor condition, it is first necessary to calculate the liquid composition that would be in equilibrium with a saturated vapor at the stream composition and pressure; this allows computation of the saturation temperature. If the stream enthalpy is greater than the enthalpy corresponding to this saturation temperature, a superheated vapor exists and an iteration in temperature is needed. Again, the input and computed enthalpies provide the check for convergence.

If neither of the above conditions is met, the stream is a two phase mixture. In this case, an iteration in liquid composition is carried out. An initial guess for liquid composition is generated between the limits of the stream composition (which would be the composition at a quality of zero) and the equilibrium composition corresponding to the stream pressure and a vapor composition equal to the stream composition (i.e., a quality of unity). For a given guess of liquid composition, the vapor composition and temperature can be found, allowing the computation of the liquid and vapor enthalpies. The vapor quality can then be calculated in terms of both enthalpy and composition:

$$y = \frac{x - x_{liq}}{x_{vap} - x_{liq}} \quad [C-40]$$

$$y = \frac{h - h_{liq}}{h_{vap} - h_{liq}} \quad [C-41]$$

where  $x$  and  $h$  are the overall composition and enthalpy of the stream

and the subscripts liq and vap refer to the liquid and vapor fractions. The iteration proceeds by the secant method until these two quantities agree within a convergence tolerance.

### C.2.5 Table interpolation for P-T-x behavior

The properties for ammonia-water mixtures calculated by means of the Schultz (119) equation of state are thermodynamically consistent and well behaved over wide ranges of temperature and pressure. They proved to be superior in these respects compared to the polynomial fits developed by Jain and Gable (83). (In particular, the accuracy of the Jain and Gable relationships was seriously degraded outside the relatively narrow pressure ranges for which they were developed.) The equation of state approach, however, requires extensive, and often iterative, calculations.

Alternate property routines employing a linear table interpolation technique were developed for the computation of the P-T- $x_{\text{liq}}$ - $x_{\text{vap}}$  behavior. Two-dimensional arrays of saturation temperature and vapor composition were generated from the equation of state relations as functions of pressure and liquid composition. In order to improve the accuracy and reduce the number of required array points, the following variable transformations were used:

$$T^* = 1/(T + 273.15)$$

$$P^* = \ln(P)$$

$$x_{\text{liq}}^* = 2x_{\text{liq}} - x_{\text{liq}}^2$$

$$x_{\text{vap}}^* = \ln(1 - x_{\text{vap}})$$

With these transformations, the P-T-x behavior is reasonably linear

and excellent accuracy is obtained with a 21 by 21 grid of data points covering a liquid composition range of 0.0 to 1.0 and a pressure range of 0.074 to 4.05 MPa. The use of these table interpolation routines reduced the required computing time for the AHP simulation by a factor of four as compared with using the equation of state P-T-x relationships. (The subroutine YT and the routines for enthalpy and specific volume involve three independent variables and are less amenable to a table interpolation approach.)

## APPENDIX D

### TEST DATA FOR THE PROTOTYPE ABSORPTION HEAT PUMP

This appendix contains data for the Arkla prototype AHP obtained during testing at the National Bureau of Standards. In the first phase of testing, the overall steady-state and cyclic performance of the unit was determined. Additional instrumentation was installed to provide more detailed information on the operation of the absorption cycle in the second set of steady-state tests. The stream numbers referenced in the test results are the same as those used in the modeling study and were defined by Figure 4-12. Summaries of test conditions for the three sets of tests are presented in Tables D-1 to D-3. The nomenclature used in these tests is:

COP	coefficient of performance accounting for burner losses and electric input
COP-CY	COP of absorption cycle only
COP-GAS	COP accounting for burner losses only
CYCLIC COP	cyclic coefficient of performance defined by [3-4]
DEW-PT	dewpoint temperature for tests at ambient temperatures below freezing or wet bulb temperature for tests above freezing
FAN	electric power consumed by evaporator fan
GAS	energy content of natural gas consumed by heat pump (based on higher heating value)
H	specific enthalpy
HLF	heating load factor defined by Equation [3-5]

L.O.C.	lack of closure in experimental energy balance
MF	mass flow rate
P	pressure
PLF	part load factor defined by [3-6]
POSITION	fraction of distance between inlet and outlet of evaporator or condenser
QABS	heat transfer rate to load water stream in the absorber
QCOND	heat transfer rate to load water stream in the condenser
QEVAP	heat transfer rate from ambient air in the evaporator
QFHX	heat transfer rate from the combustion products to the strong absorbent stream in the flue gas heat exchanger
QGEN	heat transfer rate from gas flame to the generator
QLOAD	total heat transfer rate to load water stream
X	refrigerant mass fraction
Y	equilibrium vapor quality defined by Equation [4-30]

Table D-1 Summary of ambient and load water conditions for the overall performance steady-state tests of the Arkla AHP

Test number	Ambient	Inlet Load Water	
	Temp (C)	Temp (C)	Flow (1 sec <sup>-1</sup> )
Varying ambient temp:			
SSN7-1	-21.4	40.7	0.373
SSN7-2	-21.2	40.4	0.369
SS05-1	-15.7	40.7	0.374
SS17-1	-8.0	40.4	0.372
SS30-1	-0.9	40.5	0.377
SS40-1	4.7	40.4	0.375
SS47-2	8.3	40.4	0.375
SS47-3	8.8	40.5	0.375
SS47-4	8.2	40.6	0.372
SS47-8	7.2	40.6	0.367
SS60-1	15.5	40.7	0.377
Varying load water temp:			
SSN7-3	-21.8	34.9	0.371
SSN7-4	-21.4	45.6	0.371
SS17-3	-9.2	35.1	0.371
SS17-2	-8.8	43.3	0.369
SS47-5	8.2	35.7	0.371
SS47-6	8.4	44.3	0.371
Varying load water flow:			
SS17-4	-8.8	42.2	0.310
SS17-6	-9.0	40.7	0.315
SS17-5	-8.9	40.6	0.397
SS47-7	8.4	40.5	0.315

Table D-2 Summary of cycle times and ambient and load water conditions for the cyclic testing of the Arkla AHP

Test no.	Cycle times minutes on/off	Ambient Temp (C)	Inlet load water	
			Temp (C)	Flow (l sec <sup>-1</sup> )
slow cycling rate:				
C17-1	12/48	-8.5	40.8	0.377
C47-5	10/90	8.3	40.2	0.362
C47-2	12/48	7.6	40.8	0.369
C47-3	20/20	7.7	40.7	0.367
fast cycling rate:				
C47-1	6/24	7.9	40.6	0.367
C47-4	10/10	7.9	40.4	0.366

Table D-3 Summary of ambient and load water conditions and relative refrigerant charge for the steady-state cycle investigation tests of the Arkla AHP

Test no.	Ambient	Inlet load water			Relative NH <sub>3</sub> charge (kg)
	Temp (C)	Temp (C)	Flow (1 sec <sup>-1</sup> )	fraction of flow to cond	
varying load water temperature and flows:					
AB1702	-9.2	35.5	0.366	0.38	0.0
AB4702	8.4	34.9	0.375	0.37	0.0
AB4705	8.1	35.4	0.340	0.50	0.0
AB1704	-8.9	40.8	0.339	0.33	0.0
AB1701	-8.6	40.5	0.366	0.38	0.0
AB4701	8.3	40.5	0.352	0.49	0.0
AB4704	8.3	40.6	0.282	0.67	0.0
varying refrigerant charge:					
AB1707	-8.9	41.0	0.328	0.50	-0.4
AB1703	-8.7	40.7	0.337	0.50	0.0
AB1705	-8.4	40.6	0.324	0.49	+0.6
AB1706	-9.1	40.7	0.336	0.51	+1.0
AB4708	7.4	40.7	0.330	0.50	-0.4
AB4709	8.7	40.4	0.333	0.49	-0.2
AB4703	8.6	40.8	0.334	0.51	0.0
AB4706	8.0	40.7	0.341	0.50	+0.6
AB4707	8.8	40.6	0.341	0.50	+1.0

## D.1 Overall Performance Steady-State Tests

STEADY STATE TEST NO: SSN7-1  
DATE: 9/ 1/82

TEST CONDITIONS:  
AMBIENT--DRY BULB: -21.4 C DEW PT: -26.0 C  
COOLING WATER--TEMP: 40.7 C TOT FLOW: .373 L/SEC

ENERGY INPUTS:  
GAS: 14.30 KW ELECTRIC: .635 KW

ENERGY OUTPUT  
QLOAD: 12.00 KW

COP: .804 COP-GAS: .839 COP-CY: .993

SYSTEM PRESSURES:  
LOW: .157 MPA HIGH: 2.02 MPA

SYSTEM TEMPERATURES:

STREAM	TEMP (C)	STREAM	TEMP (C)	STREAM	TEMP (C)
2	37.5	16	10.6	21+23	40.5
7	129.6	17	-22.4	22+24	48.3
8	56.6	18	-22.1	25	-21.4
10	72.8	19	-22.5	26	-21.5
14	76.0	20	-22.7	28	64.6

EVAPORATOR TEMPERATURE PROFILE:

POSITION:	TEMP (C):	TEMP (C):	TEMP (C):	OUTLET
.03	-22.1	-22.0	-22.0	-22.5
.33				
.67				

STEADY STATE TEST NO: SSN7-2  
DATE: 9/ 1/82

TEST CONDITIONS:  
AMBIENT--DRY BULB: -21.2 C DEW PT: -26.0 C  
COOLING WATER--TEMP: 40.4 C TOT FLOW: .369 L/SEC

ENERGY INPUTS:  
GAS: 14.29 KW ELECTRIC: .647 KW

ENERGY OUTPUT  
QLOAD: 12.04 KW

COP: .806 COP-GAS: .843 COP-CY: .998

SYSTEM PRESSURES:  
LOW: .159 MPA HIGH: 2.02 MPA

SYSTEM TEMPERATURES:

STREAM	TEMP (C)	STREAM	TEMP (C)	STREAM	TEMP (C)
2	37.5	16	10.8	21+23	40.4
7	129.1	17	-22.2	22+24	48.2
8	56.6	18	-22.0	25	-21.2
10	72.7	19	-22.2	26	-21.3
14	75.8	20	-22.3	28	64.8

EVAPORATOR TEMPERATURE PROFILE:

POSITION:	TEMP (C):	TEMP (C):	TEMP (C):	OUTLET
.03	-22.0	-21.8	-21.9	-22.2
.33				
.67				

## STEADY STATE TEST

NO: SSN7-3

DATE: 9/ 1/82

## TEST CONDITIONS:

AMBIENT--DRY BULB: -21.8 C

DEW PT: 34.9 C

COOLING WATER--TEMP: -26.0 C

TOT FLOW: .371 L/SEC

## ENERGY INPUTS:

GAS: 14.30 KW

ELECTRIC: .647 KW

## ENERGY OUTPUT

QLOAD: 12.54 KW

COP: .839

COP-GAS: .877

COP-CY: 1.038

## SYSTEM PRESSURES:

LOW: .148 MPA

HIGH: 1.77 MPA

## SYSTEM TEMPERATURES:

STREAM	TEMP (C)	STREAM	TEMP (C)	STREAM	TEMP (C)
2	32.7	16	10.5	21+23	34.9
7	122.9	17	-23.5	22+24	43.1
8	51.2	18	-23.0	25	-21.8
10	68.3	19	-23.6	26	-22.3
14	70.0	20	-23.9	28	63.4

## EVAPORATOR TEMPERATURE PROFILE:

POSITION:	.03	.33	.67	OUTLET
TEMP (C):	-23.0	-23.1	-23.1	-23.6

## STEADY STATE TEST

NO: SSN7-4

DATE: 9/ 1/82

## TEST CONDITIONS:

AMBIENT--DRY BULB: -21.4 C

DEW PT: 45.6 C

COOLING WATER--TEMP: -26.0 C

TOT FLOW: .371 L/SEC

## ENERGY INPUTS:

GAS: 14.33 KW

ELECTRIC: .647 KW

## ENERGY OUTPUT

QLOAD: 11.50 KW

COP: .768

COP-GAS: .803

COP-CY: .951

## SYSTEM PRESSURES:

LOW: .164 MPA

HIGH: .88 MPA

## SYSTEM TEMPERATURES:

STREAM	TEMP (C)	STREAM	TEMP (C)	STREAM	TEMP (C)
2	41.9	16	9.7	21+23	45.6
7	139.2	17	-21.4	22+24	53.0
8	62.5	18	-21.3	25	-21.2
10	77.9	19	-21.4	26	-20.8
14	84.0	20	-21.4	28	66.3

## EVAPORATOR TEMPERATURE PROFILE:

POSITION:	.03	.33	.67	OUTLET
TEMP (C):	-21.3	-21.2	-21.2	-21.4

## STEADY STATE TEST

NO: SS05-1

DATE: 7/19/82

## TEST CONDITIONS:

AMBIENT--DRY BULB: -15.7 C

DEW PT: 40.7 C

COOLING WATER--TEMP: -24.0 C

TOT FLOW: .374 L/SEC

## ENERGY INPUTS:

GAS: 14.01 KW

ELECTRIC: .622 KW

## ENERGY OUTPUT

QLOAD: 12.21 KW

COP: .835

COP-GAS: .872

COP-CY: 1.032

## SYSTEM PRESSURES:

LOW: .192 MPA

HIGH: 2.00 MPA

## SYSTEM TEMPERATURES:

STREAM	TEMP (C)	STREAM	TEMP (C)	STREAM	TEMP (C)
2	39.9	16	14.1	21+23	40.7
7	124.8	17	-17.9	22+24	48.2
8	56.4	18	-17.7	25	-15.7
10	72.1	19	-18.0	26	-16.7
14	72.9	20	-18.1	28	61.8

## EVAPORATOR TEMPERATURE PROFILE:

POSITION:	.03	.33	.67	OUTLET
TEMP (C):	-17.7	-17.7	-17.7	-18.0

## STEADY STATE TEST

NO: SS17-1

DATE: 7/15/82

## TEST CONDITIONS:

AMBIENT--DRY BULB: -8.0 C

DEW PT: 40.4 C

COOLING WATER--TEMP: -12.0 C

TOT FLOW: .372 L/SEC

## ENERGY INPUTS:

GAS: 13.93 KW

ELECTRIC: .619 KW

## ENERGY OUTPUT

QLOAD: 13.95 KW

COP: .959

COP-GAS: 1.001

COP-CY: 1.185

## SYSTEM PRESSURES:

LOW: .243 MPA

HIGH: 2.01 MPA

## SYSTEM TEMPERATURES:

STREAM	TEMP (C)	STREAM	TEMP (C)	STREAM	TEMP (C)
2	42.0	16	17.9	21+23	40.4
7	122.3	17	-12.0	22+24	49.1
8	57.0	18	-12.0	25	-8.0
10	73.0	19	-12.2	26	-10.5
14	72.6	20	-11.8	28	27.5

## EVAPORATOR TEMPERATURE PROFILE:

POSITION:	.03	.33	.67	OUTLET
TEMP (C):	-12.0	-12.0	-12.0	-12.2

## STEADY STATE TEST

NO: SS17-2  
DATE: 7/26/82

## TEST CONDITIONS:

AMBIENT--DRY BULB: -8.8 C  
COOLING WATER--TEMP: -18.0 CDEW PT: 43.3 C  
TOT FLOW: .369 L/SEC

## ENERGY INPUTS:

GAS: 13.89 KW

ELECTRIC: .586 KW

## ENERGY OUTPUT

QLOAD: 13.20 KW

COP: .912            COP-GAS: .950            COP-CY: 1.125

## SYSTEM PRESSURES:

LOW: .245 MPA            HIGH: .77 MPA

## SYSTEM TEMPERATURES:

STREAM	TEMP (C)	STREAM	TEMP (C)	STREAM	TEMP (C)
2	44.1	16	17.1	21+23	43.3
7	127.3	17	-12.1	22+24	51.6
8	59.9	18	-12.1	25	-8.9
10	75.4	19	-12.4	26	-10.8
14	76.7	20	-12.1	28	64.1

## EVAPORATOR TEMPERATURE PROFILE:

POSITION:	.03	.33	.67	OUTLET
TEMP (C):	-12.1	-12.1	-12.2	-12.4

## STEADY STATE TEST

NO: SS17-3  
DATE: 7/26/82

## TEST CONDITIONS:

AMBIENT--DRY BULB: -9.2 C  
COOLING WATER--TEMP: -20.0 CDEW PT: 35.1 C  
TOT FLOW: .371 L/SEC

## ENERGY INPUTS:

GAS: 13.98 KW

ELECTRIC: .562 KW

## ENERGY OUTPUT

QLOAD: 14.34 KW

COP: .986            COP-GAS: 1.026            COP-CY: 1.214

## SYSTEM PRESSURES:

LOW: .223 MPA            HIGH: 1.81 MPA

## SYSTEM TEMPERATURES:

STREAM	TEMP (C)	STREAM	TEMP (C)	STREAM	TEMP (C)
2	38.1	16	17.9	21+23	35.1
7	115.5	17	-13.6	22+24	44.1
8	52.3	18	-13.6	25	-9.2
10	69.0	19	-13.9	26	-11.9
14	67.3	20	-13.7	28	61.8

## EVAPORATOR TEMPERATURE PROFILE:

POSITION:	.03	.33	.67	OUTLET
TEMP (C):	-13.6	-13.6	-13.7	-13.9

STEADY STATE TEST  
 NO: SS17-4  
 DATE: 7/26/82

TEST CONDITIONS:  
 AMBIENT--DRY BULB: -8.8 C DEW PT: 42.2 C  
 COOLING WATER--TEMP: -20.0 C TOT FLOW: .310 L/SEC

ENERGY INPUTS:  
 GAS: 13.91 KW ELECTRIC: .581 KW

ENERGY OUTPUT  
 QLOAD: 13.26 KW

COP: .915 COP-GAS: .953 COP-CY: 1.128

SYSTEM PRESSURES:  
 LOW: .245 MPA HIGH: .77 MPA

SYSTEM TEMPERATURES:

STREAM	TEMP (C)	STREAM	TEMP (C)	STREAM	TEMP (C)
2	43.6	16	17.0	21+23	42.2
7	127.1	17	-12.0	22+24	52.2
8	59.7	18	-12.1	25	-8.8
10	75.1	19	-12.3	26	-10.6
14	76.2	20	-11.9	28	66.5

EVAPORATOR TEMPERATURE PROFILE:  
 POSITION: .03 .33 .67 OUTLET  
 TEMP (C): -12.1 -12.1 -12.0 -12.3

STEADY STATE TEST  
 NO: SS17-5  
 DATE: 8/18/82

TEST CONDITIONS:  
 AMBIENT--DRY BULB: -8.9 C DEW PT: 40.6 C  
 COOLING WATER--TEMP: -11.8 C TOT FLOW: .397 L/SEC

ENERGY INPUTS:  
 GAS: 13.99 KW ELECTRIC: .589 KW

ENERGY OUTPUT  
 QLOAD: 14.34 KW

COP: .984 COP-GAS: 1.025 COP-CY: 1.213

SYSTEM PRESSURES:  
 LOW: .240 MPA HIGH: 2.05 MPA

SYSTEM TEMPERATURES:

STREAM	TEMP (C)	STREAM	TEMP (C)	STREAM	TEMP (C)
2	41.8	16	17.4	21+23	40.6
7	123.3	17	-12.5	22+24	49.2
8	57.6	18	-12.6	25	-8.9
10	73.6	19	-12.7	26	-11.0
14	73.7	20	-12.5	28	65.4

EVAPORATOR TEMPERATURE PROFILE:  
 POSITION: .03 .33 .67 OUTLET  
 TEMP (C): -12.6 -12.5 -12.5 -12.7

STEADY STATE TEST NO: SS17-6  
DATE: 8/18/82

TEST CONDITIONS:  
 AMBIENT--DRY BULB: -9.0 C DEW PT: 40.7 C  
 COOLING WATER--TEMP: -11.7 C TOT FLOW: .315 L/SEC

ENERGY INPUTS:  
 GAS: 13.94 KW ELECTRIC: .587 KW

ENERGY OUTPUT  
 QLOAD: 14.17 KW

COP: .975 COP-GAS: 1.016 COP-CY: 1.203

SYSTEM PRESSURES:  
 LOW: .242 MPA HIGH: 2.13 MPA

SYSTEM TEMPERATURES:

STREAM	TEMP (C)	STREAM	TEMP (C)	STREAM	TEMP (C)
2	42.4	16	16.9	21+23	40.7
7	125.7	17	-12.3	22+24	51.5
8	58.9	18	-12.5	25	-9.0
10	74.6	19	-12.5	26	-10.9
14	75.3	20	-12.3	28	65.9

EVAPORATOR TEMPERATURE PROFILE:

POSITION:	TEMP (C):	TEMP (C):	TEMP (C):	OUTLET
.03	.33	.67		
-12.5	-12.3	-12.3	-12.5	

STEADY STATE TEST NO: SS30-1  
DATE: 7/20/82

TEST CONDITIONS:  
 AMBIENT--DRY BULB: -.9 C DEW PT: 40.5 C  
 COOLING WATER--TEMP: -9.0 C TOT FLOW: .377 L/SEC

ENERGY INPUTS:  
 GAS: 13.71 KW ELECTRIC: .581 KW

ENERGY OUTPUT  
 QLOAD: 15.31 KW

COP: 1.072 COP-GAS: 1.117 COP-CY: 1.322

SYSTEM PRESSURES:  
 LOW: .299 MPA HIGH: 2.05 MPA

SYSTEM TEMPERATURES:

STREAM	TEMP (C)	STREAM	TEMP (C)	STREAM	TEMP (C)
2	45.3	16	22.4	21+23	40.5
7	119.2	17	-5.2	22+24	50.0
8	58.2	18	-6.7	25	-.9
10	74.0	19	-6.0	26	-4.7
14	72.7	20	22.1	28	69.4

EVAPORATOR TEMPERATURE PROFILE:

POSITION:	TEMP (C):	TEMP (C):	TEMP (C):	OUTLET
.03	.33	.67		
-6.7	-6.9	-6.9	-6.7	-6.0

## STEADY STATE TEST

NO: SS40-1  
DATE: 7/20/82

## TEST CONDITIONS:

AMBIENT--DRY BULB: 4.7 C      DEW PT: 40.4 C  
COOLING WATER--TEMP: -7.0 C      TOT FLOW: .375 L/SEC

## ENERGY INPUTS:

GAS: 13.54 KW      ELECTRIC: .567 KW

## ENERGY OUTPUT

QLOAD: 15.69 KW

COP: 1.112      COP-GAS: 1.159      COP-CY: 1.372

## SYSTEM PRESSURES:

LOW: .336 MPA      HIGH: 2.08 MPA

## SYSTEM TEMPERATURES:

STREAM	TEMP (C)	STREAM	TEMP (C)	STREAM	TEMP (C)
2	45.5	16	32.3	21+23	40.4
7	115.8	17	16.7	22+24	50.2
8	57.9	18	-3.4	25	4.8
10	73.6	19	5.0	26	.6
14	71.3	20	32.1	28	74.3

## EVAPORATOR TEMPERATURE PROFILE:

POSITION:	.03	.33	.67	OUTLET
TEMP (C):	-3.4	-3.4	1.2	5.0

## STEADY STATE TEST

NO: SS47-2  
DATE: 7/15/82

## TEST CONDITIONS:

AMBIENT--DRY BULB: 8.3 C      DEW PT: 40.4 C  
COOLING WATER--TEMP: 6.9 C      TOT FLOW: .375 L/SEC

## ENERGY INPUTS:

GAS: 13.54 KW      ELECTRIC: .563 KW

## ENERGY OUTPUT

QLOAD: 16.03 KW

COP: 1.137      COP-GAS: 1.184      COP-CY: 1.401

## SYSTEM PRESSURES:

LOW: .351 MPA      HIGH: 2.11 MPA

## SYSTEM TEMPERATURES:

STREAM	TEMP (C)	STREAM	TEMP (C)	STREAM	TEMP (C)
2	45.7	16	34.0	21+23	40.4
7	115.3	17	18.8	22+24	50.5
8	58.1	18	-2.2	25	8.3
10	73.7	19	8.6	26	4.3
14	71.3	20	33.7	28	37.3

## EVAPORATOR TEMPERATURE PROFILE:

POSITION:	.03	.33	.67	OUTLET
TEMP (C):	-2.2	-1.8	9.1	8.6

STEADY STATE TEST NO: SS47-3  
DATE: 7/21/82

TEST CONDITIONS:  
 AMBIENT--DRY BULB: 8.8 C DEW PT: 40.5 C  
 COOLING WATER--TEMP: 4.6 C TOT FLOW: .375 L/SEC

ENERGY INPUTS:  
 GAS: 13.52 KW ELECTRIC: .565 KW

ENERGY OUTPUT  
 QLOAD: 15.83 KW

COP: 1.123 COP-GAS: 1.170 COP-CY: 1.385

SYSTEM PRESSURES:  
 LOW: .352 MPA HIGH: 2.10 MPA

SYSTEM TEMPERATURES:

STREAM	TEMP (C)	STREAM	TEMP (C)	STREAM	TEMP (C)
2	45.9	16	34.1	21+23	40.5
7	115.1	17	19.2	22+24	50.4
8	58.2	18	-2.1	25	8.8
10	73.9	19	9.1	26	4.5
14	71.3	20	33.8	28	76.3

EVAPORATOR TEMPERATURE PROFILE:

POSITION:				OUTLET
TEMP (C):	.03	.33	.67	9.1
	-2.1	-1.9	10.2	

STEADY STATE TEST NO: SS47-4  
DATE: 7/22/82

TEST CONDITIONS:  
 AMBIENT--DRY BULB: 8.2 C DEW PT: 40.6 C  
 COOLING WATER--TEMP: 4.2 C TOT FLOW: .372 L/SEC

ENERGY INPUTS:  
 GAS: 13.51 KW ELECTRIC: .551 KW

ENERGY OUTPUT  
 QLOAD: 15.85 KW

COP: 1.127 COP-GAS: 1.173 COP-CY: 1.388

SYSTEM PRESSURES:  
 LOW: .353 MPA HIGH: 2.11 MPA

SYSTEM TEMPERATURES:

STREAM	TEMP (C)	STREAM	TEMP (C)	STREAM	TEMP (C)
2	46.0	16	34.0	21+23	40.6
7	115.4	17	19.0	22+24	50.6
8	58.3	18	-2.0	25	7.3
10	74.0	19	8.6	26	3.8
14	71.5	20	33.8	28	76.3

EVAPORATOR TEMPERATURE PROFILE:

POSITION:				OUTLET
TEMP (C):	.03	.33	.67	8.6
	-2.0	-2.0	49.4	

STEADY STATE TEST NO: SS47-5  
DATE: 7/22/82

TEST CONDITIONS:  
 AMBIENT--DRY BULB: 8.2 C DEW PT: 35.7 C  
 COOLING WATER--TEMP: 4.3 C TOT FLOW: .371 L/SEC

ENERGY INPUTS:  
 GAS: 13.57 KW ELECTRIC: .545 KW

ENERGY OUTPUT  
 QLOAD: 15.85 KW

COP: 1.123 COP-GAS: 1.168 COP-CY: 1.383

SYSTEM PRESSURES:  
 LOW: .309 MPA HIGH: 1.92 MPA

SYSTEM TEMPERATURES:

STREAM	TEMP (C)	STREAM	TEMP (C)	STREAM	TEMP (C)
2	41.3	16	31.9	21+23	35.7
7	110.5	17	16.3	22+24	45.8
8	53.9	18	-4.8	25	6.1
10	70.2	19	8.6	26	3.6
14	66.7	20	31.2	28	75.1

EVAPORATOR TEMPERATURE PROFILE:  
 POSITION: .03 .33 .67 OUTLET  
 TEMP (C): -4.8 -2.8 9.7 8.6

STEADY STATE TEST NO: SS47-6  
DATE: 7/23/82

TEST CONDITIONS:  
 AMBIENT--DRY BULB: 8.4 C DEW PT: 44.3 C  
 COOLING WATER--TEMP: 4.8 C TOT FLOW: .371 L/SEC

ENERGY INPUTS:  
 GAS: 13.51 KW ELECTRIC: .561 KW

ENERGY OUTPUT  
 QLOAD: 15.72 KW

COP: 1.117 COP-GAS: 1.163 COP-CY: 1.377

SYSTEM PRESSURES:  
 LOW: .384 MPA HIGH: 2.29 MPA

SYSTEM TEMPERATURES:

STREAM	TEMP (C)	STREAM	TEMP (C)	STREAM	TEMP (C)
2	49.7	16	35.7	21+23	44.3
7	120.3	17	21.6	22+24	54.2
8	62.2	18	-.4	25	8.4
10	77.2	19	8.8	26	4.3
14	75.9	20	35.5	28	77.4

EVAPORATOR TEMPERATURE PROFILE:  
 POSITION: .03 .33 .67 OUTLET  
 TEMP (C): -.4 -.2 7.9 8.8

## STEADY STATE TEST

NO: SS47-7  
DATE: 7/23/82

## TEST CONDITIONS:

AMBIENT--DRY BULB:	8.4 C	DEW PT:	40.5 C
COOLING WATER--TEMP:	4.8 C	TOT FLOW:	.315 L/SEC

## ENERGY INPUTS:

GAS:	13.52 KW	ELECTRIC:	.553 KW
------	----------	-----------	---------

## ENERGY OUTPUT

QLOAD: 15.89 KW

COP:	1.129	COP-GAS:	1.175	COP-CY:	1.391
------	-------	----------	-------	---------	-------

## SYSTEM PRESSURES:

LOW:	.363 MPA	HIGH:	1.31 MPA
------	----------	-------	----------

## SYSTEM TEMPERATURES:

STREAM	TEMP (C)	STREAM	TEMP (C)	STREAM	TEMP (C)
2	46.8	16	34.7	21+23	40.5
7	116.8	17	20.2	22+24	52.4
8	59.3	18	-1.5	25	8.4
10	74.8	19	8.8	26	4.1
14	72.8	20	34.5	28	76.4

## EVAPORATOR TEMPERATURE PROFILE:

POSITION:	.03	.33	.67	OUTLET
TEMP (C):	-1.5	-1.4	9.5	8.8

## STEADY STATE TEST

NO: SS47-8  
DATE: 8/ 6/82

## TEST CONDITIONS:

AMBIENT--DRY BULB:	7.2 C	DEW PT:	40.6 C
COOLING WATER--TEMP:	6.1 C	TOT FLOW:	.367 L/SEC

## ENERGY INPUTS:

GAS:	13.61 KW	ELECTRIC:	.565 KW
------	----------	-----------	---------

## ENERGY OUTPUT

QLOAD: 16.39 KW

COP:	1.156	COP-GAS:	1.204	COP-CY:	1.425
------	-------	----------	-------	---------	-------

## SYSTEM PRESSURES:

LOW:	.362 MPA	HIGH:	2.15 MPA
------	----------	-------	----------

## SYSTEM TEMPERATURES:

STREAM	TEMP (C)	STREAM	TEMP (C)	STREAM	TEMP (C)
2	46.9	16	34.2	21+23	40.6
7	116.1	17	19.2	22+24	51.3
8	59.5	18	-1.5	25	7.3
10	75.0	19	7.5	26	3.6
14	72.6	20	33.9	28	76.8

## EVAPORATOR TEMPERATURE PROFILE:

POSITION:	.03	.33	.67	OUTLET
TEMP (C):	-1.5	-1.3	8.2	7.5

## STEADY STATE TEST

NO: SS60-1  
DATE: 7/21/82

## TEST CONDITIONS:

AMBIENT--DRY BULB: 15.5 C      DEW PT: 40.7 C  
COOLING WATER--TEMP: -1.0 C      TOT FLOW: .377 L/SEC

## ENERGY INPUTS:

GAS: 13.38 KW      ELECTRIC: .561 KW

## ENERGY OUTPUT

QLOAD: 15.89 KW

COP: 1.140      COP-GAS: 1.187      COP-CY: 1.405

## SYSTEM PRESSURES:

LOW: .360 MPA      HIGH: 2.13 MPA

## SYSTEM TEMPERATURES:

STREAM	TEMP (C)	STREAM	TEMP (C)	STREAM	TEMP (C)
2	46.1	16	36.4	21+23	40.7
7	115.3	17	23.2	22+24	50.6
8	58.5	18	-1.4	25	15.5
10	74.1	19	15.9	26	11.5
14	71.7	20	36.0	28	78.9

## EVAPORATOR TEMPERATURE PROFILE:

POSITION:	.03	.33	.67	OUTLET
TEMP (C):	-1.4	13.1	16.8	15.9

## D.2 Cyclic Tests

## CYCLIC TEST

NO: C17-1  
DATE: 8/18/82

CYCLE TIMES: 12/48 MINUTES ON/OFF

## TEST CONDITIONS:

AMBIENT--DRY BULB: -8.5 C      DEW PT: -11.7 C  
COOLING WATER--TEMP: 40.8 C      TOT FLOW: .377 L/SEC

## INTEGRATED ENERGY INPUTS PER CYCLE:

GAS: 10.30 MJ      ELECTRIC: .587 MJ

## INTEGRATED CAPACITY PER CYCLE:

QLOAD: 6.11 MJ

CYCLIC COP: .561      PLF: .582      HLF: .123

## SELECTED STREAM CONDITIONS (FOR LAST CYCLE):

TIME*	TEMPERATURE (C)								PRESSURE (MPA)	
	2	8	14	16	18	19	20	22+24	LOW	HIGH
13:29	39.	71.	69.	13.	-6.	3.	29.	27.	.349	.32
13:30	36.	71.	69.	12.	-6.	3.	30.	45.	.359	.39
13:31	17.	38.	68.	21.	-9.	5.	-3.	40.	.338	.57
13:32	22.	22.	63.	26.	-10.	5.	4.	40.	.283	.60
13:33	30.	27.	58.	24.	-12.	8.	-1.	42.	.257	.92
13:34	35.	34.	53.	20.	-14.	11.	-3.	43.	.223	1.30
13:35	38.	40.	49.	8.	-15.	15.	1.	43.	.189	1.67
13:36	40.	46.	50.	5.	-17.	16.	2.	44.	.178	1.87
13:37	41.	50.	54.	15.	-17.	17.	11.	45.	.198	1.93
13:38	43.	53.	58.	20.	-14.	17.	19.	46.	.233	1.93
13:39	43.	55.	63.	15.	-12.	17.	15.	47.	.255	1.96
13:40	42.	57.	67.	16.	-12.	17.	16.	47.	.256	2.00
13:41	42.	58.	70.	19.	-12.	18.	19.	48.	.258	2.02
13:42	42.	59.	72.	19.	-11.	17.	19.	48.	.263	1.99
13:43	43.	57.	70.	10.	-11.	15.	11.	48.	.259	1.77
13:44	43.	54.	67.	-3.	-12.	14.	-2.	46.	.254	1.64
13:45	42.	52.	63.	-5.	-12.	14.	-6.	45.	.257	1.56
13:46	42.	57.	60.	1.	-13.	13.	-2.	44.	.247	1.52

\*UNIT ON: 13:29:59  
BURNER OFF: 13:41:59  
UNIT OFF: 13:45:43

## CYCLIC TEST

NO: C47-1  
DATE: 8/ 5/82

CYCLE TIMES: 6/24 MINUTES ON/OFF

## TEST CONDITIONS:

AMBIENT--DRY BULB: 7.9 C DEW PT: 6.3 C  
COOLING WATER--TEMP: 40.6 C TOT FLOW: .367 L/SEC

## INTEGRATED ENERGY INPUTS PER CYCLE:

GAS: 4.97 MJ ELECTRIC: .316 MJ

## INTEGRATED CAPACITY PER CYCLE:

QLOAD: 3.18 MJ

CYCLIC COP: .601 PLF: .529 HLF: .104

## SELECTED STREAM CONDITIONS (FOR LAST CYCLE):

TIME*	TEMPERATURE (C)								PRESSURE (MPA)	
	2	8	14	16	18	19	20	22+24	LOW	HIGH
11:39	44.	84.	79.	26.	13.	6.	42.	38.	.668	.67
11:40	44.	77.	79.	26.	8.	7.	39.	48.	.524	.79
11:41	40.	47.	75.	34.	0.	8.	15.	43.	.361	.90
11:42	41.	42.	71.	34.	-2.	10.	21.	43.	.278	1.10
11:43	41.	45.	66.	31.	-1.	13.	23.	43.	.197	1.50
11:44	41.	46.	60.	17.	-11.	15.	23.	43.	.190	1.74
11:45	43.	50.	57.	23.	-14.	16.	21.	44.	.228	1.88
11:46	44.	54.	60.	26.	-8.	16.	26.	46.	.302	1.80
11:47	43.	53.	60.	25.	-8.	15.	25.	46.	.292	1.67
11:48	43.	52.	59.	26.	-12.	14.	25.	45.	.248	1.59
11:49	42.	51.	57.	27.	-15.	13.	26.	43.	.233	1.52

\*UNIT ON: 11:39:39  
BURNER OFF: 11:45:39  
UNIT OFF: 11:49:15

## CYCLIC TEST

NO: C47-2  
DATE: 8/ 5/82

CYCLE TIMES: 12/48 MINUTES ON/OFF

## TEST CONDITIONS:

AMBIENT--DRY BULB: 7.6 C      DEW PT: 6.0 C  
COOLING WATER--TEMP: 40.8 C      TOT FLOW: .369 L/SEC

## INTEGRATED ENERGY INPUTS PER CYCLE:

GAS: 10.02 MJ      ELECTRIC: .535 MJ

## INTEGRATED CAPACITY PER CYCLE:

QLOAD: 7.34 MJ

CYCLIC COP: .696      PLF: .619      HLF: .122

## SELECTED STREAM CONDITIONS (FOR LAST CYCLE):

TIME*	TEMPERATURE (C)								PRESSURE (MPA)	
	2	8	14	16	18	19	20	22+24	LOW	HIGH
15: 5	47.	71.	70.	24.	7.	4.	38.	33.	.454	.45
15: 6	43.	71.	69.	24.	6.	4.	40.	49.	.384	.52
15: 7	28.	38.	69.	34.	1.	7.	14.	42.	.309	.76
15: 8	32.	27.	64.	36.	-1.	7.	18.	41.	.255	.79
15: 9	37.	36.	60.	35.	1.	10.	22.	42.	.206	1.11
15:10	39.	41.	56.	30.	-1.	13.	24.	42.	.183	1.47
15:11	41.	45.	52.	20.	-9.	15.	24.	43.	.180	1.72
15:12	42.	49.	53.	23.	-14.	16.	22.	44.	.211	1.84
15:13	42.	52.	56.	24.	-9.	17.	24.	45.	.284	1.90
15:14	41.	53.	61.	19.	-6.	17.	19.	47.	.325	1.95
15:15	42.	55.	64.	21.	-4.	18.	21.	48.	.343	2.01
15:16	43.	56.	66.	24.	-3.	18.	24.	49.	.354	2.05
15:17	44.	57.	67.	28.	-2.	18.	28.	50.	.357	2.08
15:18	45.	57.	68.	31.	-2.	18.	31.	50.	.354	2.06
15:19	46.	56.	67.	31.	-2.	16.	31.	50.	.354	1.84
15:20	45.	54.	64.	29.	-5.	15.	29.	48.	.306	1.71
15:21	44.	53.	61.	28.	-12.	14.	27.	46.	.237	1.63
15:22	43.	59.	59.	29.	-13.	14.	28.	44.	.243	1.62

\*UNIT ON: 15: 5:57  
BURNER OFF: 15:17:57  
UNIT OFF: 15:21:37

## CYCLIC TEST

NO: C47-3

DATE: 8/ 6/82

CYCLE TIMES: 20/20 MINUTES ON/OFF

## TEST CONDITIONS:

AMBIENT--DRY BULB: 7.7 C  
 COOLING WATER--TEMP: 40.7 C

DEW PT: 6.4 C  
 TOT FLOW: .367 L/SEC

## INTEGRATED ENERGY INPUTS PER CYCLE:

GAS: 16.52 MJ

ELECTRIC: .798 MJ

## INTEGRATED CAPACITY PER CYCLE:

QLOAD: 16.64 MJ

CYCLIC COP: .961

PLF: .854

HLF: .413

## SELECTED STREAM CONDITIONS (FOR LAST CYCLE):

TIME*	TEMPERATURE (C)								PRESSURE (MPA)	
	2	8	14	16	18	19	20	22+24	LOW	HIGH
11:29	45.	86.	84.	32.	12.	5.	58.	40.	.637	.64
11:30	45.	85.	83.	32.	10.	6.	59.	55.	.583	.72
11:31	37.	47.	80.	39.	2.	9.	20.	43.	.360	1.02
11:32	40.	39.	75.	37.	-3.	10.	20.	42.	.260	1.11
11:33	40.	44.	69.	33.	1.	13.	24.	42.	.198	1.54
11:34	40.	47.	61.	19.	-11.	15.	23.	43.	.198	1.69
11:35	42.	47.	56.	24.	-14.	16.	23.	44.	.221	1.82
11:36	43.	52.	58.	27.	-10.	17.	27.	45.	.280	1.91
11:37	43.	54.	63.	26.	-6.	17.	26.	47.	.325	1.95
11:38	43.	55.	65.	25.	-3.	17.	26.	48.	.355	1.99
11:39	44.	56.	67.	26.	-3.	18.	26.	49.	.355	2.03
11:40	44.	57.	68.	29.	-2.	18.	29.	50.	.357	2.07
11:41	45.	57.	69.	31.	-2.	18.	31.	50.	.357	2.09
11:42	45.	58.	70.	33.	-2.	19.	32.	51.	.355	2.12
11:43	46.	58.	70.	33.	-2.	19.	33.	51.	.355	2.12
11:44	46.	58.	71.	34.	-2.	19.	33.	51.	.357	2.13
11:45	46.	59.	71.	34.	-2.	19.	33.	51.	.358	2.13
11:46	46.	59.	71.	34.	-2.	19.	34.	51.	.358	2.13
11:47	47.	59.	71.	34.	-2.	19.	34.	51.	.359	2.14
11:48	46.	59.	72.	34.	-2.	19.	34.	51.	.361	2.14
11:49	47.	59.	72.	34.	-1.	19.	34.	51.	.362	2.14
11:50	47.	59.	72.	34.	-1.	18.	34.	51.	.361	2.10
11:51	47.	58.	70.	33.	-2.	16.	33.	50.	.362	1.86
11:52	46.	55.	66.	30.	-4.	15.	30.	49.	.325	1.72
11:53	44.	54.	63.	28.	-10.	14.	28.	46.	.247	1.64
11:54	43.	55.	61.	29.	-13.	14.	28.	44.	.244	1.62

\*UNIT ON: 11:29:56  
 BURNER OFF: 11:49:56  
 UNIT OFF: 11:53:49

## CYCLIC TEST

NO: C47-4  
DATE: 8/ 6/82

CYCLE TIMES: 10/10 MINUTES ON/OFF

## TEST CONDITIONS:

AMBIENT--DRY BULB: 7.9 C      DEW PT: 6.6 C  
COOLING WATER--TEMP: 40.4 C      TOT FLOW: .366 L/SEC

## INTEGRATED ENERGY INPUTS PER CYCLE:

GAS: 8.28 MJ      ELECTRIC: .445 MJ

## INTEGRATED CAPACITY PER CYCLE:

QLOAD: 8.29 MJ

CYCLIC COP: .950      PLF: .845      HLF: .412

## SELECTED STREAM CONDITIONS (FOR LAST CYCLE):

TIME*	TEMPERATURE (C)								PRESSURE (MPA)	
	2	8	14	16	18	19	20	22+24	LOW	HIGH
13: 4	44.	100.	83.	28.	8.	11.	49.	44.	.588	1.28
13: 5	46.	97.	86.	27.	6.	11.	47.	53.	.426	1.32
13: 6	46.	51.	80.	24.	-4.	12.	25.	46.	.301	1.38
13: 7	43.	47.	74.	27.	-4.	13.	25.	43.	.235	1.52
13: 8	42.	51.	66.	22.	-1.	16.	24.	43.	.198	1.80
13: 9	43.	49.	61.	27.	-10.	16.	26.	44.	.269	1.87
13:10	43.	54.	61.	29.	-8.	17.	29.	46.	.299	1.94
13:11	44.	55.	65.	31.	-5.	17.	30.	48.	.332	1.98
13:12	44.	56.	67.	32.	-3.	18.	31.	49.	.346	2.02
13:13	45.	57.	68.	31.	-3.	18.	31.	49.	.358	2.06
13:14	45.	58.	69.	32.	-2.	18.	32.	50.	.360	2.08
13:15	45.	58.	70.	33.	-2.	18.	32.	50.	.360	2.04
13:16	46.	56.	68.	32.	-2.	16.	32.	50.	.358	1.83
13:17	45.	55.	65.	29.	-5.	15.	29.	48.	.309	1.70
13:19	44.	71.	61.	30.	-12.	14.	28.	45.	.269	1.65

\*UNIT ON: 13: 4:51  
BURNER OFF: 13:14:51  
UNIT OFF: 13:18:19

## CYCLIC TEST

NO: C47-5  
DATE: 8/16/82

CYCLE TIMES: 10/90 MINUTES ON/OFF

## TEST CONDITIONS:

AMBIENT--DRY BULB: 8.3 C      DEW PT: 6.6 C  
COOLING WATER--TEMP: 40.2 C      TOT FLOW: .362 L/SEC

## INTEGRATED ENERGY INPUTS PER CYCLE:

GAS: 8.51 MJ      ELECTRIC: .466 MJ

## INTEGRATED CAPACITY PER CYCLE:

QLOAD: 5.04 MJ

CYCLIC COP: .562      PLF: .500      HLF: .050

## SELECTED STREAM CONDITIONS (FOR LAST CYCLE):

TIME*	TEMPERATURE (C)								PRESSURE (MPA)	
	2	8	14	16	18	19	20	22+24	LOW	HIGH
14:24	41.	58.	56.	17.	7.	10.	22.	24.	.540	.53
14:25	39.	58.	56.	17.	7.	10.	22.	42.	.528	.51
14:26	34.	41.	57.	16.	2.	10.	12.	41.	.418	.59
14:27	24.	28.	56.	19.	-3.	14.	19.	41.	.350	.67
14:28	35.	28.	53.	27.	-3.	8.	18.	42.	.273	.95
14:29	38.	36.	50.	30.	-1.	5.	20.	42.	.209	1.31
14:30	39.	42.	48.	24.	0.	5.	22.	42.	.187	1.66
14:31	41.	47.	50.	19.	-13.	7.	19.	44.	.195	1.84
14:32	42.	50.	53.	23.	-10.	11.	23.	45.	.276	1.91
14:33	42.	53.	58.	23.	-6.	10.	24.	47.	.315	1.95
14:34	43.	54.	62.	26.	-4.	9.	26.	48.	.340	1.99
14:35	44.	56.	65.	28.	-3.	9.	28.	49.	.357	2.00
14:36	44.	55.	64.	29.	-3.	8.	28.	49.	.354	1.81
14:37	44.	53.	62.	28.	-6.	8.	27.	47.	.294	1.70
14:38	43.	52.	59.	28.	-13.	8.	27.	45.	.231	1.62
14:39	43.	61.	58.	29.	-14.	8.	28.	44.	.243	1.62

\*UNIT ON: 14:25:0  
BURNER OFF: 14:35:0  
UNIT OFF: 14:38:32

## D.3 Cycle Investigation Tests

## STEADY STATE TEST

NO: AB1701  
DATE: 11/ 3/83

## TEST CONDITIONS:

AMBIENT--DRY BULB: -8.6 C	DEW PT: -17.8 C
COOLING WATER--TEMP: 40.5 C	TOT FLOW: .366 L/SEC
	COND FLOW: .139 L/SEC
AMMONIA CHARGE: .0 KG	

## ENERGY INPUTS:

GAS: 13.71 KW	ELECTRIC--TOTAL: .579 KW
QGEN: 10.24 KW	FAN: .214 KW
QFHX: 1.31 KW	COMB EFF: .843
QEVAP: 3.27 KW	

## ENERGY OUTPUTS:

QLOAD: 14.18 KW	
QCOND: 5.64 KW	QABS: 8.54 KW

ENERGY BAL: QG + QE - QL      L.O.C. = .65 KW = 4.6 %

COP: .993      COP-GAS: 1.035      COP-CY: 1.227

STR	MF (KG/S)	P (MPA)	X	H (KJ/KG)	T (C)	Y
1	.0236	.243	.316	*****	*****	.01
2	.0236	2.137	.317 M	-18.	42.4 M	-.29
3	.0236	2.137	.317	*****	*****	*****
4	*****	2.137	****	*****	*****	****
5	*****	2.137	****	*****	*****	****
6	.0186	2.137	.136	*****	*****	****
7	.0186	2.137	.136	458.	127.1 M	-.12
8	.0186	2.137	.136	142.	58.9 M	-.37
9	.0186	.243	.136	142.	*****	-.06
10	.0186	.243	.136 M	213.	74.8 M	.00
11	*****	2.137	****	*****	*****	****
12	*****	2.137	****	*****	*****	****
13	*****	2.137	****	*****	*****	****
14	.0049	2.137 M	.995	1368.	75.7 M	1.00
15	.0049	2.137	.995	229.	48.5 M	-.02
16	.0049	.718	.995	229.	15.1 M	.14
17	.0049	.718	.995	-65.	-12.2 M	-.11
18	.0049	.243	.995	-65.	-12.3 M	.01
19	.0049	.243	.995	596.	-12.3 M	.51
20	.0049	.243 M	.995	890.	-11.7 M	.73
21	.2270 M				40.5 M	
22	.2270				49.7 M	
23	.1391 M				40.5 M	
24	.1391				50.4 M	
25	1.6261				-8.6 M	
26	1.6261 M				-10.7 M	
27	*****				*****	
28	*****				69.1 M	

## CONDENSER TEMPERATURE PROFILE

POSITION:	INLET	.20	.41	.62	.82	OUTLET
TEMP (C):	75.4	58.1	54.4	52.8	52.0	48.5

## EVAPORATOR TEMPERATURE PROFILE

POSITION:	.03	.19	.33	.48	.67	.85	OUTLET
TEMP (C):	-12.3	-12.1	-12.1	-12.1	-12.2	-12.1	-12.3

NOTE: "M" INDICATES MEASURED QUANTITY  
\*\*\* INDICATES NO INFORMATION

## STEADY STATE TEST

NO: AB1702

DATE: 11/ 3/82

## TEST CONDITIONS:

AMBIENT--DRY BULB: -9.2 C

DEW PT: -17.8 C

COOLING WATER--TEMP: 35.5 C

TOT FLOW: .366 L/SEC

COND FLOW: .139 L/SEC

AMMONIA CHARGE: .0 KG

## ENERGY INPUTS:

GAS: 13.80 KW

ELECTRIC--TOTAL: .561 KW

QGEN: 10.39 KW

FAN: .214 KW

QFHX: 1.24 KW

COMB EFF: .843

QEVAP: 4.00 KW

## ENERGY OUTPUTS:

QLOAD: 14.70 KW

QCOND: 5.76 KW

QABS: 8.94 KW

ENERGY BAL: QG + QE - QL

L.O.C. = .94 KW = 6.4 %

COP: 1.023

COP-GAS: 1.065

COP-CY: 1.263

STR	MF (KG/S)	P (MPA)	X	H (KJ/KG)	T (C)	Y
1	.0218	.228	.330	*****	*****	.01
2	.0218	1.911	.330 M	-42.	38.2 M	-.28
3	.0218	1.911	.330	*****	*****	****
4	*****	1.911	****	*****	*****	****
5	*****	1.911	****	*****	*****	****
6	.0168	1.911	.133	*****	*****	****
7	.0168	1.911	.133	422.	119.3 M	-.13
8	.0168	1.911	.133	121.	53.8 M	-.37
9	.0168	.228	.133	121.	*****	-.07
10	.0168	.228	.133 M	195.	70.4 M	-.02
11	*****	1.911	****	*****	*****	****
12	*****	1.911	****	*****	*****	****
13	*****	1.911	****	*****	*****	****
14	.0050	1.911 M	.997	1359.	69.2 M	1.00
15	.0050	1.911	.997	198.	42.1 M	-.03
16	.0050	.721	.997	198.	15.2 M	.11
17	.0050	.721	.997	-70.	-13.4 M	-.11
18	.0050	.228	.997	-70.	-13.5 M	.01
19	.0050	.228	.997	737.	-13.5 M	.62
20	.0050	.228 M	.997	1004.	-13.2 M	.82
21	.2268 M				35.5 M	
22	.2268				45.2 M	
23	.1388 M				35.5 M	
24	.1388				45.7 M	
25	1.6309				-9.2 M	
26	1.6309 M				-11.8 M	
27	*****				*****	
28	*****				66.9 M	

## CONDENSER TEMPERATURE PROFILE

POSITION: INLET .20 .41 .62 .82 OUTLET  
 TEMP (C): 69.0 52.6 49.5 48.3 47.6 42.1

## EVAPORATOR TEMPERATURE PROFILE

POSITION: .03 .19 .33 .48 .67 .85 OUTLET  
 TEMP (C): -13.5 -13.2 -13.3 -13.3 -13.3 -13.3 -13.5

NOTE: "M" INDICATES MEASURED QUANTITY  
 \*\*\* INDICATES NO INFORMATION

## STEADY STATE TEST

NO: AB1703  
DATE: 11/16/82

## TEST CONDITIONS:

AMBIENT--DRY BULB: -8.7 C      DEW PT: -16.1 C  
 COOLING WATER--TEMP: 40.7 C      TOT FLOW: .337 L/SEC  
 COND FLOW: .167 L/SEC  
 AMMONIA CHARGE: .0 KG

## ENERGY INPUTS:

GAS: 14.02 KW      ELECTRIC--TOTAL: .577 KW  
 QGEN: 10.49 KW      FAN: .220 KW  
 QFHX: 1.31 KW      COMB EFF: .842  
 QEVAP: 2.83 KW

## ENERGY OUTPUTS:

QLOAD: 14.15 KW      QABS: 8.37 KW  
 QCOND: 5.77 KW

ENERGY BAL: QG + QE - QL      L.O.C. = .49 KW = 3.5 %

COP: .969      COP-GAS: 1.009      COP-CY: 1.199

STR	MF (KG/S)	P (MPA)	X	H (KJ/KG)	T (C)	Y
1	.0235	.246	.319	*****	*****	.01
2	.0235	2.101	.319 M	-21.	42.1 M	-.29
3	.0235	2.101	.319	*****	*****	****
4	*****	2.101	****	*****	*****	****
5	*****	2.101	****	*****	*****	****
6	.0184	2.101	.133	*****	*****	****
7	.0184	2.101	.133	463.	127.9 M	-.11
8	.0184	2.101	.133	143.	58.6 M	-.37
9	.0184	.246	.133	143.	*****	-.06
10	.0184	.246	.133 M	214.	74.7 M	-.01
11	*****	2.101	****	*****	*****	****
12	*****	2.101	****	*****	*****	****
13	*****	2.101	****	*****	*****	****
14	.0051	2.101 M	.996	1366.	74.3 M	1.00
15	.0051	2.101	.996	224.	47.5 M	-.03
16	.0051	.768	.996	224.	17.2 M	.12
17	.0051	.768	.996	-64.	-12.0 M	-.11
18	.0051	.246	.996	-64.	-12.1 M	.01
19	.0051	.246	.996	496.	-12.1 M	.43
20	.0051	.246 M	.996	784.	-11.9 M	.65
21	.1703 M				40.7 M	
22	.1703				52.7 M	
23	.1671 M				40.7 M	
24	.1671				49.2 M	
25	1.6634				-8.7 M	
26	1.6634 M				-10.4 M	
27	*****				*****	
28	*****				73.6 M	

## CONDENSER TEMPERATURE PROFILE

POSITION: INLET      .20      .41      .62      .82      OUTLET  
 TEMP (C): 75.7      57.1      53.6      52.1      51.3      47.5

## EVAPORATOR TEMPERATURE PROFILE

POSITION: .03      .19      .33      .48      .67      .85      OUTLET  
 TEMP (C): -12.1      -11.8      -11.9      -11.9      -12.0      -11.9      -12.1

NOTE: "M" INDICATES MEASURED QUANTITY  
 \*\*\* INDICATES NO INFORMATION

## STEADY STATE TEST

NO: AB1704  
DATE: 11/16/82

## TEST CONDITIONS:

AMBIENT--DRY BULB: -8.9 C      DEW PT: -16.1 C  
 COOLING WATER--TEMP: 40.8 C      TOT FLOW: .339 L/SEC  
    COND FLOW: .113 L/SEC  
 AMMONIA CHARGE: .0 KG

## ENERGY INPUTS:

GAS: 14.01 KW      ELECTRIC--TOTAL: .579 KW  
 QGEN: 10.55 KW      FAN: .220 KW  
 QFHX: 1.22 KW      COMB EFF: .840  
 QEVAP: 2.98 KW

## ENERGY OUTPUTS:

QLOAD: 14.17 KW  
 QCOND: 5.43 KW      QABS: 8.74 KW

ENERGY BAL: QG + QE - QL      L.O.C. = .57 KW = 4.1 %

COP: .971      COP-GAS: 1.011      COP-CY: 1.204

STR	MF (KG/S)	P (MPA)	X	H (KJ/KG)	T (C)	Y
1	.0225	.242	.322	*****	*****	.01
2	.0225	2.245	.321 M	-21.	42.1 M	-.30
3	.0225	2.245	.321	*****	*****	****
4	*****	2.245	****	*****	*****	****
5	*****	2.245	****	*****	*****	****
6	.0177	2.245	.137	*****	*****	****
7	.0177	2.245	.137	480.	131.8 M	-.11
8	.0177	2.245	.137	148.	60.4 M	-.38
9	.0177	.242	.137	148.	*****	-.05
10	.0177	.242	.137 M	217.	75.9 M	.00
11	*****	2.245	****	*****	*****	****
12	*****	2.245	****	*****	*****	****
13	*****	2.245	****	*****	*****	****
14	.0048	2.245 M	.996	1365.	76.5 M	1.00
15	.0048	2.245	.996	244.	51.4 M	-.02
16	.0048	.743	.996	244.	16.2 M	.14
17	.0048	.743	.996	-65.	-12.3 M	-.11
18	.0048	.242	.996	-65.	-12.4 M	.01
19	.0048	.242	.996	549.	-12.4 M	.47
20	.0048	.242 M	.996	858.	-12.0 M	.71
21	.2267 M				40.8 M	
22	.2267				50.3 M	
23	.1126 M				40.8 M	
24	.1126				52.6 M	
25	1.6595				-8.9 M	
26	1.6595 M				-10.8 M	
27	*****				*****	
28	*****				74.4 M	

## CONDENSER TEMPERATURE PROFILE

POSITION: INLET .20 .41 .62 .82 OUTLET  
 TEMP (C): 77.9 60.6 56.5 54.9 54.0 51.4

## EVAPORATOR TEMPERATURE PROFILE

POSITION: .03 .19 .33 .48 .67 .85 OUTLET  
 TEMP (C): -12.4 -12.2 -12.2 -12.2 -12.2 -12.2 -12.4

NOTE: "M" INDICATES MEASURED QUANTITY  
 \*\*\* INDICATES NO INFORMATION







## STEADY STATE TEST

NO: AB4701

DATE: 10/28/82

## TEST CONDITIONS:

AMBIENT--DRY BULB: 8.3 C      DEW PT: 5.1 C  
 COOLING WATER--TEMP: 40.5 C      TOT FLOW: .352 L/SEC  
 COND FLOW: .124 L/SEC  
 AMMONIA CHARGE: .0 KG

## ENERGY INPUTS:

GAS: 13.45 KW      ELECTRIC--TOTAL: .569 KW  
 QGEN: 10.22 KW      FAN: .200 KW  
 QFHX: 1.24 KW      COMB EFF: .852  
 QEVAP: 6.56 KW

## ENERGY OUTPUTS:

QLOAD: 16.57 KW  
 QCOND: 5.94 KW      QABS: 10.63 KW

ENERGY BAL: QG + QE - QL      L.O.C. = 1.45 KW = 8.8 %

COP: 1.182      COP-GAS: 1.232      COP-CY: 1.446

STR	MF (KG/S)	P (MPA)	X	H (KJ/KG)	T (C)	Y
1	.0229	.354	.367	*****	*****	.02
2	.0229	2.253	.367 M	-13.	46.0 M	-.25
3	.0229	2.253	.367	*****	*****	****
4	*****	2.253	****	*****	*****	****
5	*****	2.253	****	*****	*****	****
6	.0177	2.253	.179	*****	*****	****
7	.0177	2.253	.179	401.	119.1 M	-.11
8	.0177	2.253	.179	122.	60.0 M	-.35
9	.0177	.354	.179	122.	*****	-.05
10	.0177	.354	.179 M	192.	75.3 M	.00
11	*****	2.253	****	*****	*****	****
12	*****	2.253	****	*****	*****	****
13	*****	2.253	****	*****	*****	****
14	.0053	2.253 M	.997	1354.	73.3 M	1.00
15	.0053	2.253	.997	227.	47.8 M	-.04
16	.0053	1.245	.997	227.	33.1 M	.06
17	.0053	1.245	.997	95.	21.0 M	-.05
18	.0053	.354	.997	95.	-2.3 M	.10
19	.0053	.354	.997	1213.	6.7 M	.96
20	.0053	.354 M	.997	1345.	34.3 M	1.00
21	.2279 M				40.5 M	
22	.2279				51.9 M	
23	.1240 M				40.5 M	
24	.1240				52.2 M	
25	1.6541				8.3 M	
26	1.6541 M				4.2 M	
27	*****				*****	
28	*****				80.7 M	

## CONDENSER TEMPERATURE PROFILE

POSITION: INLET      .20      .41      .62      .82      OUTLET  
 TEMP (C): 73.1      58.8      55.8      54.7      54.0      47.8

## EVAPORATOR TEMPERATURE PROFILE

POSITION: .03      .19      .33      .48      .67      .85      OUTLET  
 TEMP (C): -2.3      \*\*\*\*\*      -2.1      -1.7      7.4      7.7      6.7

NOTE: "M" INDICATES MEASURED QUANTITY  
 \*\*\* INDICATES NO INFORMATION

## STEADY STATE TEST

NO: AB4702  
DATE: 11/ 1/82

## TEST CONDITIONS:

AMBIENT--DRY BULB:	8.4 C	DEW PT:	4.4 C
COOLING WATER--TEMP:	34.9 C	TOT FLOW:	.375 L/SEC
AMMONIA CHARGE:	.0 KG	COND FLOW:	.140 L/SEC

## ENERGY INPUTS:

GAS:	13.48 KW	ELECTRIC--TOTAL:	.545 KW
QGEN:	10.24 KW	FAN:	.198 KW
QFHX:	1.19 KW	COMB EFF:	.848
QEVAP:	6.74 KW		

## ENERGY OUTPUTS:

QLOAD:	16.42 KW	QABS:	10.43 KW
QCOND:	5.98 KW		

ENERGY BAL: QG + QE - QL      L.O.C. = 1.75 KW = 10.7 %

COP: 1.171      COP-GAS: 1.218      COP-CY: 1.437

STR	MF (KG/S)	P (MPA)	X	H (KJ/KG)	T (C)	Y
1	.0213	.309	.371	*****	*****	.01
2	.0213	1.970	.371 M	-39.	40.7 M	-.24
3	.0213	1.970	.371	*****	*****	****
4	*****	1.970	****	*****	*****	****
5	*****	1.970	****	*****	*****	****
6	.0161	1.970	.171	*****	*****	****
7	.0161	1.970	.171	369.	111.7 M	-.13
8	.0161	1.970	.171	99.	54.2 M	-.35
9	.0161	.309	.171	99.	*****	-.07
10	.0161	.309	.171 M	173.	70.4 M	-.01
11	*****	1.970	****	*****	*****	****
12	*****	1.970	****	*****	*****	****
13	*****	1.970	****	*****	*****	****
14	.0051	1.970 M	.998	1348.	66.7 M	1.00
15	.0051	1.970	.998	185.	39.4 M	-.05
16	.0051	1.152	.998	185.	30.4 M	.04
17	.0051	1.152	.998	75.	16.8 M	-.06
18	.0051	.309	.998	75.	-4.9 M	.09
19	.0051	.309	.998	1240.	6.8 M	.98
20	.0051	.309 M	.998	1351.	31.4 M	1.01
21	.2359 M				34.9 M	
22	.2359				45.9 M	
23	.1396 M				34.9 M	
24	.1396				45.5 M	
25	1.6442				8.4 M	
26	1.6442 M				4.1 M	
27	*****				*****	
28	*****				77.7 M	

## CONDENSER TEMPERATURE PROFILE

POSITION:	INLET	.20	.41	.62	.82	OUTLET
TEMP (C):	66.7	52.5	50.0	49.2	48.6	39.4

## EVAPORATOR TEMPERATURE PROFILE

POSITION:	.03	.19	.33	.48	.67	.85	OUTLET
TEMP (C):	-4.9	*****	-4.5	5.2	8.3	7.9	6.8

NOTE: "M" INDICATES MEASURED QUANTITY  
 \*\*\* INDICATES NO INFORMATION

## STEADY STATE TEST

NO: AB4703  
DATE: 11/15/82

## TEST CONDITIONS:

AMBIENT--DRY BULB: 8.6 C      DEW PT: 5.4 C  
 COOLING WATER--TEMP: 40.8 C      TOT FLOW: .334 L/SEC  
 AMMONIA CHARGE: .0 KG      COND FLOW: .169 L/SEC

## ENERGY INPUTS:

GAS: 13.54 KW      ELECTRIC--TOTAL: .549 KW  
 QGEN: 10.23 KW      FAN: .200 KW  
 QFHX: 1.24 KW      COMB EFF: .847  
 QEVAP: 6.63 KW

## ENERGY OUTPUTS:

QLOAD: 16.40 KW  
 QCOND: 6.11 KW      QABS: 10.28 KW

ENERGY BAL: QG + QE - QL      L.O.C. = 1.70 KW = 10.4 %

COP: 1.164      COP-GAS: 1.211      COP-CY: 1.430

STR	MF (KG/S)	P (MPA)	X	H (KJ/KG)	T (C)	Y
1	.0227	.381	.368	*****	*****	.02
2	.0227	2.197	.368 M	-5.	47.6 M	-.24
3	.0227	2.197	.368	*****	*****	****
4	*****	2.197	****	*****	*****	****
5	*****	2.197	****	*****	*****	****
6	.0173	2.197	.173	*****	*****	****
7	.0173	2.197	.173	397.	117.9 M	-.12
8	.0173	2.197	.173	126.	60.2 M	-.35
9	.0173	.381	.173	126.	*****	-.07
10	.0173	.381	.173 M	197.	75.9 M	-.01
11	*****	2.197	****	*****	*****	****
12	*****	2.197	****	*****	*****	****
13	*****	2.197	****	*****	*****	****
14	.0054	2.197 M	.997	1354.	72.2 M	1.00
15	.0054	2.197	.997	216.	45.7 M	-.04
16	.0054	1.323	.997	216.	35.3 M	.05
17	.0054	1.323	.997	93.	20.7 M	-.06
18	.0054	.381	.997	93.	-.4 M	.09
19	.0054	.381	.997	1229.	8.8 M	.97
20	.0054	.381 M	.997	1352.	34.5 M	1.01
21	.1653 M				40.8 M	
22	.1653				55.9 M	
23	.1692 M				40.8 M	
24	.1692				49.6 M	
25	1.6552				8.6 M	
26	1.6552 M				4.4 M	
27	*****				*****	
28	*****				80.7 M	

## CONDENSER TEMPERATURE PROFILE

POSITION: INLET    .20    .41    .62    .82    OUTLET  
 TEMP (C): 73.8    57.7    54.8    53.7    53.0    45.7

## EVAPORATOR TEMPERATURE PROFILE

POSITION: .03    .19    .33    .48    .67    .85    OUTLET  
 TEMP (C): -.4    -.4    -.3    .0    8.6    9.6    8.8

NOTE: "M" INDICATES MEASURED QUANTITY  
 \*\*\* INDICATES NO INFORMATION





## STEADY STATE TEST

NO: AB4706  
DATE: 11/18/82

## TEST CONDITIONS:

AMBIENT--DRY BULB:	8.0 C	DEW PT:	5.0 C
COOLING WATER--TEMP:	40.7 C	TOT FLOW:	.341 L/SEC
		COND FLOW:	.172 L/SEC

AMMONIA CHARGE: .6 KG

## ENERGY INPUTS:

GAS:	13.62 KW	ELECTRIC--TOTAL:	.551 KW
QGEN:	10.29 KW	FAN:	.198 KW
QFHX:	1.25 KW	COMB EFF:	.847
QEVAP:	7.00 KW		

## ENERGY OUTPUTS:

QLOAD:	16.54 KW	QABS:	10.31 KW
QCOND:	6.23 KW		

ENERGY BAL: QG + QE - QL      L.O.C. = 1.99 KW = 12.0 %

COP: 1.167      COP-GAS: 1.214      COP-CY: 1.434

STR	MF (KG/S)	P (MPA)	X	H (KJ/KG)	T (C)	Y
1	.0229	.406	.381	*****	*****	.02
2	.0229	2.220	.380 M	-7.	47.7 M	-.24
3	.0229	2.220	.380	*****	*****	*****
4	*****	2.220	*****	*****	*****	*****
5	*****	2.220	*****	*****	*****	*****
6	.0174	2.220	.185	*****	*****	*****
7	.0174	2.220	.185	382.	115.6 M	-.12
8	.0174	2.220	.185	118.	60.0 M	-.34
9	.0174	.406	.185	118.	*****	-.06
10	.0174	.406	.185 M	190.	75.6 M	-.01
11	*****	2.220	*****	*****	*****	*****
12	*****	2.220	*****	*****	*****	*****
13	*****	2.220	*****	*****	*****	*****
14	.0055	2.220 M	.997	1350.	71.5 M	1.00
15	.0055	2.220	.997	216.	45.6 M	-.05
16	.0055	1.319	.997	216.	35.1 M	.05
17	.0055	1.319	.997	87.	19.5 M	-.07
18	.0055	.406	.997	87.	.8 M	.08
19	.0055	.406	.997	1222.	8.0 M	.96
20	.0055	.406 M	.997	1350.	34.4 M	1.01
21	.1683 M				40.7 M	
22	.1683				55.6 M	
23	.1722 M				40.7 M	
24	.1722				49.6 M	
25	1.6630				8.0 M	
26	1.6630 M				3.6 M	
27	*****				*****	
28	*****				80.6 M	

## CONDENSER TEMPERATURE PROFILE

POSITION:	INLET	.20	.41	.62	.82	OUTLET
TEMP (C):	73.5	57.7	55.0	54.0	53.3	45.6

## EVAPORATOR TEMPERATURE PROFILE

POSITION:	.03	.19	.33	.48	.67	.85	OUTLET
TEMP (C):	.8	.9	.9	.8	1.0	5.2	8.0

NOTE: "M" INDICATES MEASURED QUANTITY  
\*\*\* INDICATES NO INFORMATION



## STEADY STATE TEST

NO: AB4708  
DATE: 11/30/82

## TEST CONDITIONS:

AMBIENT--DRY BULB: 7.4 C      DEW PT: 3.8 C  
 COOLING WATER--TEMP: 40.7 C      TOT FLOW: .330 L/SEC  
    COND FLOW: .166 L/SEC  
 AMMONIA CHARGE: -.4 KG

## ENERGY INPUTS:

GAS: 13.58 KW      ELECTRIC--TOTAL: .532 KW  
 QGEN: 10.16 KW      FAN: .196 KW  
 QFHX: 1.30 KW      COMB EFF: .844  
 QEVAP: 7.07 KW

## ENERGY OUTPUTS:

QLOAD: 15.86 KW      QABS: 9.99 KW  
 QCOND: 5.87 KW

ENERGY BAL: QG + QE - QL      L.O.C. = 2.67 KW = 16.8 %

COP: 1.124      COP-GAS: 1.168      COP-CY: 1.384

STR	MF (KG/S)	P (MPA)	X	H (KJ/KG)	T (C)	Y
1	.0234	.270	.317	*****	*****	.02
2	.0234	2.146	.316 M	17.	49.7 M	-.27
3	.0234	2.146	.316	*****	*****	****
4	*****	2.146	****	*****	*****	****
5	*****	2.146	****	*****	*****	****
6	.0183	2.146	.128	*****	*****	****
7	.0183	2.146	.128	474.	129.9 M	-.12
8	.0183	2.146	.128	169.	63.8 M	-.36
9	.0183	.270	.128	169.	*****	-.06
10	.0183	.270	.128 M	240.	79.8 M	-.01
11	*****	2.146	****	*****	*****	****
12	*****	2.146	****	*****	*****	****
13	*****	2.146	****	*****	*****	****
14	.0051	2.146 M	.994	1382.	79.9 M	1.00
15	.0051	2.146	.994	225.	47.9 M	-.03
16	.0051	1.239	.994	225.	33.1 M	.07
17	.0051	1.239	.994	93.	21.3 M	-.05
18	.0051	.270	.994	93.	-7.5 M	.12
19	.0051	.270	.994	1223.	6.8 M	.97
20	.0051	.270 M	.994	1355.	32.4 M	1.00
21	.1639 M				40.7 M	
22	.1639				55.5 M	
23	.1661 M				40.7 M	
24	.1661				49.4 M	
25	1.6744				7.4 M	
26	1.6744 M				3.0 M	
27	*****				*****	
28	*****				83.2 M	

## CONDENSER TEMPERATURE PROFILE

POSITION: INLET      .20      .41      .62      .82      OUTLET  
 TEMP (C): 81.9      58.9      54.7      52.9      52.2      47.9

## EVAPORATOR TEMPERATURE PROFILE

POSITION: .03      .19      .33      .48      .67      .85      OUTLET  
 TEMP (C): -7.5      -7.1      2.4      6.8      8.0      7.7      6.8

NOTE: "M" INDICATES MEASURED QUANTITY  
 \*\*\* INDICATES NO INFORMATION

## STEADY STATE TEST

NO: AB4709

DATE: 1/ 4/83

## TEST CONDITIONS:

AMBIENT--DRY BULB: 8.7 C  
 COOLING WATER--TEMP: 40.4 C

DEW PT: -1.1 C  
 TOT FLOW: .333 L/SEC  
 COND FLOW: .164 L/SEC

AMMONIA CHARGE: -.2 KG

## ENERGY INPUTS:

GAS: 13.81 KW  
 QGEN: 10.58 KW  
 QFHX: 1.10 KW  
 QEVAP: 6.69 KW

ELECTRIC--TOTAL: .540 KW  
 FAN: .200 KW  
 COMB EFF: .846

## ENERGY OUTPUTS:

QLOAD: 16.77 KW  
 QCOND: 5.85 KW

QABS: 10.92 KW

ENERGY BAL: QG + QE - QL

L.O.C. = 1.60 KW = 9.6 %

COP: 1.169

COP-GAS: 1.214

COP-CY: 1.435

STR	MF (KG/S)	P (MPA)	X	H (KJ/KG)	T (C)	Y
1	.0205	.314	.360	*****	*****	.03
2	.0205	2.166	.359 M	3.	48.9 M	-.24
3	.0205	2.166	.359	*****	*****	****
4	*****	2.166	****	*****	*****	****
5	*****	2.166	****	*****	*****	****
6	.0155	2.166	.153	*****	*****	****
7	.0155	2.166	.153	454.	127.8 M	-.10
8	.0155	2.166	.153	149.	62.7 M	-.35
9	.0155	.314	.153	149.	*****	-.05
10	.0155	.314	.153 M	220.	78.4 M	.00
11	*****	2.166	****	*****	*****	****
12	*****	2.166	****	*****	*****	****
13	*****	2.166	****	*****	*****	****
14	.0050	2.166 M	.994	1382.	80.1 M	1.00
15	.0050	2.166	.994	221.	47.2 M	-.03
16	.0050	1.288	.994	221.	34.4 M	.06
17	.0050	1.288	.994	96.	21.9 M	-.05
18	.0050	.314	.994	96.	-4.4 M	.11
19	.0050	.314	.994	1234.	9.1 M	.97
20	.0050	.314 M	.994	1359.	33.7 M	1.00
21	.1695 M				40.4 M	
22	.1695				56.1 M	
23	.1638 M				40.4 M	
24	.1638				49.2 M	
25	1.6297				8.7 M	
26	1.6297 M				4.4 M	
27	*****				*****	
28	*****				84.0 M	

## CONDENSER TEMPERATURE PROFILE

POSITION:	INLET	.20	.41	.62	.82	OUTLET
TEMP (C):	79.2	58.5	54.9	53.2	52.4	47.2

## EVAPORATOR TEMPERATURE PROFILE

POSITION:	.03	.19	.33	.48	.67	.85	OUTLET
TEMP (C):	-4.4	-4.1	.8	8.6	10.0	9.8	9.1

NOTE: "M" INDICATES MEASURED QUANTITY

\*\*\* INDICATES NO INFORMATION

## APPENDIX E

### COMPUTER PROGRAMS

The computer programs comprising the TRNSYS model for an AHP with chemical storage and the steady-state absorption heat pump simulation program are logged in Tables E-1 and E-2. These programs are written in ASCII Fortran (Fortran 77) and are stored on a magnetic tape on file at the Solar Energy Laboratory; example simulation decks are also included. Listings of these programs or a copy of the tape (written in a 9 track, 1600 bpi, ASCII format) may be obtained at cost by contacting Professor S.A. Klein or the TRNSYS coordinator at the address below.

Solar Energy Laboratory  
University of Wisconsin-Madison  
1500 Johnson Drive  
Madison, Wisconsin 53706 USA

Table E-1	TRNSYS components and related computer programs for the modeling of an absorption heat pump with chemical storage
GCHP-2D	TRNSYS component (TYPE32) for a zero-capacitance generator plus refrigerant storage tank
GCHP-3D	TRNSYS component (TYPE33) for an absorbent storage tank plus zero-capacitance evaporator
GCHPCONT	TRNSYS controller component (TYPE35) for the solar AHP system; includes alternate control strategies discussed in Chapter 2
HX-SW	TRNSYS heat exchange switching component (TYPE36)
TMIXU	calculates the temperature of a two phase, two component mixture in a tank given the total internal energy and volume and component masses
TMIXH	temperature of a liquid mixture given enthalpy and composition
NH3HVAP	enthalpy of ammonia vapor given temperature and vapor dew point temperature
NH3RHOVP	density of ammonia vapor given temperature and pressure
NASCNHMX	enthalpy of NaSCN-NH <sub>3</sub> mixtures given temperature and mass fraction NaSCN
NASCNRLQ	density of liquid NaSCN-NH <sub>3</sub> mixtures as a function of temperature and mass fraction NaSCN
NASCNVPR	vapor pressure of NaSCN-NH <sub>3</sub> mixtures given temperature and composition
NASCNTVP	saturation temperature for NaSCN-NH <sub>3</sub> mixtures given pressure and composition
Note:	units for property routines are kJ kg <sup>-1</sup> , C, kPa, kg m <sup>-3</sup> , and mass fraction absorbent

Table E-2 Computer programs comprising the steady-state absorption heat pump simulation program

The following routines comprise the executive portion of the program:

SS-MAIN2	main program for steady-state simulation; contains pressure (inventory) iteration
SS-INPUT	reads simulation deck
SS-INIT	computes unspecified properties (in simulation deck) for external or tear streams
SS-ITER2	iterates between component subroutines to converge cycle
SS-FEED	supplies appropriate system streams to components as they are called
SS-OUT	uses output streams from most recent component call to reset system stream values
SS-INVEN	sums component inventories to obtain total cycle inventory
SS-PRINT	prints simulation results in tabular form

Component models:

GEN1A	generator modeled as fully-mixed tank with fixed heat input
ABS-6	falling-film absorber
PUMP	constant flow rate solution pump
THROT-2	throttle valve
RECHX-7	general N-stream heat exchanger model employing a finite difference formulation
STRMIX	stream mixer/vapor-liquid separator component
DUMMY	dummy subroutines to satisfy the TYPE8 and TYPE9 subroutine entry points in program unit ITER; additional components would be substituted for those in file DUMMY
CONV-2	convergence component for the iteration of tear streams
HSUB	calculates heat transfer coefficients as a function of local conditions

Table E-2 (continued)

Property routines for ammonia-water mixtures and air:

TSATN } *	saturation temperature of a liquid solution given pressure and refrigerant mass fraction
TSATI2 }	
XLQN } *	saturation refrigerant mass fraction of a liquid solution as a function of temperature and pressure
XLQI2 }	
XLQVN } *	equilibrium composition of a liquid solution given pressure and vapor composition
XLQVI2 }	
XVPN } *	equilibrium composition of vapor given pressure and liquid composition
XVPI2 }	
PSATN } *	saturation vapor pressure as a function of temperature and liquid composition
PSATI2 }	
HLQN	enthalpy of a liquid solution given temperature, composition and pressure
HVFN	enthalpy of vapor given temperature, vapor composition and pressure
CPN	heat capacity of liquid or vapor given temperature, composition and pressure
YTN-2	calculates saturation temperature and quality for a two component mixture (including two phase streams) as a function of overall pressure, composition and enthalpy
VLQN	specific volume of a liquid mixture given temperature, composition and pressure
VVFN	specific volume of vapor given temperature, composition and volume
PDATA	BLOCK DATA for table interpolation property routines

\* Only one of each of these pairs of routines should be linked into the executable element. Program names ending in "I2" employ a table interpolation technique, all others utilize property correlations.

Note: units for the property routines are  $\text{kJ kg}^{-1}$ , C, MPa,  $\text{m}^3 \text{kg}^{-1}$ , and refrigerant mass fraction

## REFERENCES

1. G. Wettermark, "Prospects for Thermochemical Energy Storage," Proceedings, International Seminar on Thermochemical Energy Storage, Stockholm, 1980.
2. P. O'D. Offenhartz, "Chemical Methods of Storing Thermal Energy," Proceedings, Joint Conference of the American and Canadian Sections of ISES, Winnipeg, 1976.
3. L.A. Sarkes, J.A. Nichols and M.S. Menzer, "Gas-Fired Heat Pumps: An Emerging Technology," ASHRAE Journal (1977).
4. International Energy Agency, Heat Pump Systems: A Technology Review, 1982.
5. T.A. Chubb, "Characteristics of  $\text{CO}_2$ - $\text{CH}_4$  Reforming-Methanation Cycle Relevant to the Solchem Thermochemical Power System," Solar Energy, 24, 341 (1980).
6. J.H. McCrary. et al., "An Experimental Study of the  $\text{CO}_2$ - $\text{CH}_4$  Reforming-Methanation Cycle as a Mechanism for Converting and Transporting Solar Energy," Solar Energy, 29 (1982).
7. R.V. Dunkle, "A Method of Solar Air Conditioning," Mechanical and Chemical Engineering Transactions of the Institution of Engineers, Australia, 73 (1965).
8. J.J. Jurinak, J.W. Mitchell and W.A. Beckman, "Open Cycle Desiccant Air Conditioning as an Alternative to Vapor Compression Cooling in Residential Applications," to be published in ASME Journal of Solar Energy Engineering (1984).
9. D.D. Huxtable and D.R. Poole, "Thermal Energy Storage by the Sulfuric Acid-Water System," Proceedings, Joint Conference of the American and Canadian Sections of ISES, Winnipeg, 1976.
10. American Society of Heating, Refrigerating and Air Conditioning Engineers, Handbook and Product Directory, Equipment (1979).
11. A.M. Johnston, "Ammonia/Water Absorption Cycles With Relatively High Generator Temperatures," Solar Energy, 25 (1980).

12. A.M. Johnston and C.H. O'Sullivan, "A Single-Stage Ammonia/Water Absorption Cycle With Integrated Heat Exchange Components," Transactions of the ASME, Journal of Solar Energy Engineering, 102, 42 (1981).
13. M. Taube and M. Furrer, "Opportunities and Limitations for the Use of Ammoniated Salts as Carrier for Thermochemical Energy Storage," Proceedings, International Seminar on Thermochemical Energy Storage, Stockholm, 1980.
14. W.E. Wentworth, "Chemical Heat Pump Reactions Using Metal Salt Ammonia Complexes in Suspensions," Proceedings, International Seminar on Thermochemical Energy Storage, Stockholm, 1980.
15. H. Bjurström and W. Raldow, "The Absorption Process for Heating, Cooling and Energy Storage--An Historical Survey," Energy Research, 5, 43 (1981).
16. M. Goldstein, "Some Physical Chemical Aspects of Heat Storage," Proceedings, UN Conference on New Sources of Energy, 1961.
17. R.M. Buffington, "Qualitative Requirements for Absorbent-Refrigerant Combinations," Refrigeration Engineering, 53, 343 (1949).
18. A.L. Gomez and G.A. Mansoori, "Thermodynamic Equation of State Approach for the Choice of Working Fluids of Absorption Cooling Cycles," Solar Energy, 31, 557 (1983).
19. W.M. Raldow and W.E. Wentworth, "Chemical Heat Pumps--A Basic Thermodynamic Analysis," Solar Energy, 23, 75 (1979).
20. C.C. Hiller, "The Chemical Heat Pump/Chemical Energy Storage System for Solar Heating and Cooling," Sandia Laboratories (1978).
21. R.A. Macriss, "Selecting Refrigerant-Absorbent Fluid Systems for Solar Energy Utilization," ASHRAE Semiannual Meeting, Dallas, 1976.
22. G.A. Mansoori and V. Patel, "Thermodynamic Basis for the Choice of Working Fluids for Solar Absorption Cooling Systems," Solar Energy, 22, 483 (1979).
23. K. Stephan and D. Seher, "Arbeitsgemische für Sorptionswärmepumpen," Ki Klima-Kälte-Heizung (1980).

24. G.C. Blytas and F. Daniels, "Concentrated Solutions of NaSCN in Liquid Ammonia. Solubility, Density, Vapor Pressure, Viscosity, Thermal Conductance, Heat of Solutions and Heat Capacity," Journal of the American Chemical Society, 84, 1075 (1962).
25. S.L. Sargent and W.A. Beckman, "Theoretical Performance of an Ammonia-Sodium Thiocyanate Intermittant Absorption Refrigeration Cycle," Solar Energy, 12, 137 (1968).
26. K.P. Murphy, "Organic Absorption Gas-Fired Residential Heat Pump," Allied Corporation, 1981.
27. J. Trommelmans, E. Van Den Bulck and J. Berghmans, "Factors Influencing the Performance of a Domestic Absorption Heat Pump," Proceedings, International Institute of Refrigeration Meeting, Essen, West Germany, 1981.
28. R. Radermacher, "Working Substance Combinations for Absorption Heat Pumps," PhD thesis, Technical University of Munich, 1981.
29. S. Fujii, et al., "Chemical Reaction Cycles for the Recovery of Low-Level Thermal Energy," Journal of Chemical Engineering of Japan, 10, 224 (1977).
30. L. Lauerhaus, PhD Thesis, Chemical Engineering, University of Wisconsin-Madison, 1978.
31. J.W. Mitchell, Energy Engineering, John Wiley and Sons, 1983.
32. K.P. Murphy and B.A. Phillips, "Development of a Residential Gas Absorption Heat Pump," ASHRAE Transactions, 89 pt 1 (1983).
33. R. deVault, Oak Ridge National Laboratory, Oak Ridge, Tennessee, personal communication, 1982.
34. Arkla Industries, "Solaire 36 Three Ton Absorption Chiller for Solar Air Conditioning," product literature, Evansville, Indiana, 1976.
35. Yazaki Corporation, "Aroace Indirect-Fired Chiller Unit," product literature, Tokyo, Japan, ca. 1979.
36. S.A. Klein, et al., TRNSYS--A Transient Simulation Program," University of Wisconsin-Madison, Engineering Experiment Station Report 38-11 (1981).
37. P. O'D. Offenhartz, "TRNSYS Simulation of Chemical Heat Pumps for Solar Heating, Cooling and Storage," Systems Simulation and Economic Analysis Conference, San Diego, 1980.

38. D.S. Ward, "Solar Absorption Cooling Feasibility," Solar Energy, 22, 259 (1979).
39. J.C. Blinn, "Simulation of Solar Absorption Air Conditioning," MS Thesis, University of Wisconsin-Madison, 1979.
40. L.W. Butz, W.A. Beckman and J.A. Duffie, "Simulation of a Solar Heating and Cooling System," Solar Energy, 16, 129 (1974).
41. R.L. Oonk, W.A. Beckman and J.A. Duffie, "Modeling of the CSU Heating/Cooling System," Solar Energy, 17, 21 (1975).
42. R.M. Lazzarin, "Solar-Assisted Absorption Heat Pump Feasibility," Solar Energy, 26, 223 (1981).
43. P. O'D. Offenhartz, et al., "A Heat Pump and Thermal Storage System for Solar Heating and Cooling Based on the Reaction of Calcium Chloride and Methanol Vapor," Transactions of the ASME, Journal of Solar Energy Engineering, 102, 59 (1980).
44. P. O'D. Offenhartz, et al., "Methanol-Based Heat Pump for Solar Heating, Cooling and Storage, Phase II," EIC Corporation, final report for Sandia contract 18-8423, 1980.
45. E.A. Brundberg, "The Tepidus System for Seasonal Heat Storage and for Cooling," Proceedings, International Seminar on Thermochemical Energy Storage, Stockholm, 1980.
46. D. Tchernev, "Integrated Solar Zeolite Collector," Annual DOE Active Solar Heating and Cooling Contractors' Review Meeting, 1980.
47. J.B. Monnier and M Dupont, "Zeolite-Water Closed Cycle Solar Refrigeration; Numerical Optimisation and Field-Testing," Proceedings, Conference of the American Solar Energy Society, Minneapolis, 1983.
48. G. Ervin, "Solar Heat Storage Based on Inorganic Chemical Reactions," Proceedings, Workshop on Solar Energy Storage Subsystems for the Heating and Cooling of Buildings, Charlottesville, 1975.
49. G. Bauerle, "Studies of Thermal Energy in Inorganic Oxides/Hydroxides," Proceedings, International Seminar on Thermochemical Energy Storage, Stockholm, 1980.
50. Rocket Research Company, "Sulfuric Acid-Water Chemical Energy Storage System," final report for ERDA contract E(04-3)-1185, 1976.

51. E.C. Clark, et al., "Sulfuric Acid and Water Chemical Heat Pump/Chemical Energy Storage System," Rocket Research Company, Phase II final report for DOE contract no EY-76-03-1185, 1978.
52. E.C. Clark and C.C. Hiller, "Sulfuric Acid-Water Chemical Heat Pump/Energy Storage System Demonstration," Proceedings, ASME Winter Annual Meeting, 1978.
53. C.C. Hiller and E.C. Clark, "Development of the Sulfuric Acid-Water Chemical Heat Pump/Chemical Energy Storage System for Solar Heating and Cooling," Proceedings, ISES Conference, Atlanta, 1979.
54. E.C. Clark, et al., "Sulfuric Acid and Water Chemical Heat Pump/Chemical Energy Storage Program," Rocket Research Company, Phase II-A final report for Sandia contract 18-4958, 1978.
55. E.C. Clark and O. Morgan, "Chemical Heat Pumps for Industry," Proceedings, 16th Intersociety Energy Conversion Engineering Conference, Atlanta, 1981.
56. F.A. Jaeger, "Thermal Storage for Solar Cooling Using Paired Ammoniated Salt Reactions," Annual DOE Active Solar Heating and Cooling Contractors' Review Meeting, 1980.
57. F.A. Jaeger and C.A. Hall, "Ammoniated Salt Heat Pump/Thermal Storage System," Proceedings, International Seminar on Thermochemical Energy Storage, Stockholm, 1980.
58. F. Daniels, Direct Use of the Sun's Energy, Yale University Press, 1964.
59. S.L. Grassie and N.R. Sheridan, "Modeling of a Solar-Operated Absorption Air Conditioning System With Refrigerant Storage," Solar Energy, 19, 691 (1977).
60. J.A. Duffie and N.R. Sheridan, "Lithium Bromide-Water Refrigerators for Solar Operation," The Mechanical and Chemical Engineering Transactions of the Institution of Engineers, Australia (1965).
61. P. O'D. Offenhartz, et al., "Analysis of Advanced Thermal Storage Subsystems for Solar Heating and Cooling," EIC Corporation, final report for DOE contract no. EG-77-C-02-4483, 1978.
62. P. O'D. Offenhartz, "TRNSYS Simulation of Chemical Heat Pumps for Solar Heating, Cooling and Storage," Systems Simulation and Economic Analysis Conference, San Diego, 1980.

63. P. O'D. Offenhartz, "TRNSYS Simulation of Chemical Heat Pumps for Solar Heating, Cooling and Storage; Part II: Simulations for Washington, D.C. and Fort Worth, Texas, Including Window Effects," Annual DOE Active Solar Heating and Cooling Contractors' Review Meeting, 1980.
64. M.O. McLinden, "Modeling and Simulation of Chemical Heat Pump Solar Heating Systems," MS thesis, University of Wisconsin-Madison, 1980.
65. M.O. McLinden and S.A. Klein, "Comparison of Chemical Heat Pump and Conventional Solar Heating Systems," Proceedings, Conference of the American Section of ISES, Phoenix, 1980.
66. P. O'D. Offenhartz, "Thermal Storage Studies for Solar Heating and Cooling: Applications Using Chemical Heat Pumps," final report for DOE contract DE-AC02-79CS30428, 1980.
67. R.H. Perry and C.H. Chilton, ed., Chemical Engineers Handbook, 5th ed., McGraw Hill Book Company (1973).
68. C.C. Hiller and E.C. Clark, "Development of the Sulfuric Acid-Water Chemical Heat Pump/Chemical Energy Storage System for Solar Heating and Cooling," Proceedings, ISES Conference, Atlanta, 1979.
69. W.M. Kays and A.L. London, Compact Heat Exchangers, 2nd ed., McGraw-Hill Book Company (1964).
70. J.A. Duffie and W.A. Beckman, Solar Engineering of Thermal Processes, Wiley Interscience (1980).
71. M.O. McLinden and S.A. Klein, "Simulation of an Absorption Heat Pump Solar Heating and Cooling System," Solar Energy, 31, 473 (1983).
72. SOLMET Typical Meteorological Year, Tape Deck 9734, National Oceanic and Atmospheric Administration, Environmental Data Service, National Climatic Center, Asheville, North Carolina (1978).
73. M.O. McLinden, R. Radermacher and D.A. Didion, "A Laboratory Investigation of the Steady State and Cyclic Performance of an Air-to-Water Absorption Heat Pump," Proceedings, Congress of the International Institute of Refrigeration, Paris, 1983.
74. D. Kuhlenschmidt and R.H. Merrick, "An Ammonia-Water Absorption Heat Pump Cycle," ASHRAE Transactions, 89 pt 1 (1983).

75. R.H. Merrick, Arkla Industries, Incorporated, Evansville, Indiana, personal communication, 1982.
76. T.M. Lindsay and D.A. Didion, "Investigation of the Cyclic Performance of a Gas-Fired Absorption Chiller," National Bureau of Standards internal report, 1980.
77. R. Radermacher, S.A. Klein and D.A. Didion, "Investigation of the Part-Load Performance of an Absorption Chiller," ASHRAE Transactions, 89 pt 1 (1983).
78. W. Stephan, Arkla Industries, Incorporated, Evansville, Indiana, personal communication, 1982.
79. W.H. Parken, et al., "Method of Testing, Rating and Estimating the Heating Seasonal Performance of Heat Pumps," National Bureau of Standards, NBSIR 80-2002 (1980).
80. R.A. Macriss, et al., "Physical and Thermodynamic Properties of Ammonia-Water Mixtures," Institute of Gas Technology Research Bulletin No. 34, 1964.
81. National Electrical Manufacturers Association, "Low-Voltage Room Thermostats," NEMA Standards Publication no. DC3-1978 (1972).
82. K. Koenig, G.K. Gable and P.C. Jain, "Computer Analysis of an Aqua-Ammonia Gas-Fired Air Conditioner," Natural Gas Research and Technology Conference, American Gas Association and Institute of Gas Technology, Chicago, 1971.
83. P.C. Jain and G.K. Gable, "Equilibrium Property Data Equations for Aqua-Ammonia Mixtures," ASHRAE Transactions, 77 149 (1971).
84. K.P. Murphy and R.A. Allen, "Development of a Residential Gas-Fired Absorption Heat Pump System: System Computer Simulation, System Seasonal Performance Simulation and System Cost," interim report for ORNL contract 86X-24610C and GRI contract 5014-341-0113 (1982).
85. R.W. Allen, D.K. Anand and E.A. Astiz, "Dynamic Simulation of a Solar-Powered Absorption Cycle," Proceedings, Second Southeastern Conference on Applications of Solar Energy, Baton Rouge, 1976.
86. D.K. Anand, R.W. Allen and E.O. Bazques, "Solar-Powered Absorption Air Conditioning System Performance Predictions Using Stochastic Weather Models," University of Maryland-College Park, Report ORO/4976-77/1 to ERDA, 1977.

87. D.K. Anand, R.W. Allen and B. Kumar, "Transient Simulation of Absorption Machines," Journal of Solar Energy Engineering, 104 197 (1982).
88. P.C. Auh, "Development of Hardware Simulators for Tests of Solar Cooling/Heating Subsystems and Systems: Phase II--Unsteady State Hardware Simulation of Residential Absorption Chiller," Brookhaven National Laboratory, 1979.
89. G.C. Vliet, M.B. Lawson and R.A. Lithgow, "Water-Lithium Bromide Double-Effect Absorption Cooling Analysis," University of Texas at Austin, final report for DOE contract AC03-79SF10540, 1981.
90. G.C. Vliet, et al., "Water-Lithium Bromide Double-Effect Absorption Cooling Cycle Analysis," ASHRAE Transactions, 88 pt 1, 811 (1982).
91. J.W. Andberg and G.C. Vliet, "Design Guidelines for Water-Lithium Bromide Absorbers," ASHRAE Transactions, 89 pt 1 (1983).
92. G. Grossman, "Design Improvements in LiBr Absorption Chillers for Solar Applications," Journal of Solar Energy Engineering, 103, 56 (1981).
93. J.L. Lando, et al., "Solar-Powered Environmental Control Criteria and Realization," Proceedings, International Solar Energy Society Congress, Atlanta, 1979.
94. G. Grossman and K.W. Childs, "Computer Simulation of a Lithium Bromide-Water Absorption Heat Pump for Temperature Boosting," ASHRAE Transactions, 89 pt 1 (1983).
95. G. Grossman and H.P. Blanco, "Conceptual Design and Performance Analysis of Absorption Heat Pumps for Waste Heat Utilization," ASHRAE Transactions, 88 (1982).
96. G. Grossman, "Simultaneous Heat and Mass Transfer in Absorption of Gases in Laminar Liquid Films," Oak Ridge National Laboratory, report ORNL/TM-8366, 1982.
97. G. Grossman, "Simultaneous Heat and Mass Transfer in Absorption/Desorption of Gases in Laminar Liquid Films," Oak Ridge National Laboratory report CONF-820202 (presented at AIChE Winter National Meeting, Orlando), 1982.
98. V.E. Nakoryakov and N.I. Grigor'eva, "Combined Heat and Mass Transfer During Absorption in Drops and Films," Journal of Engineering Physics, 32, 243 (1976).

99. S.C. Kaushik and N.R. Sheridan, "Computer Modelling and Thermodynamic Assessment of an Aqua-Ammonia Absorption Cycle Solar Heat Pump," Building and Environment, 16, 209 (1981).
100. M.M. Elsayed, et al., "Computer Simulation of Solar Cooling," AIChE Symposium Series, 77, no. 210 (1981).
101. S.A. Klein, "A Model of the Steady-State Performance of an Absorption Heat Pump," Internal Report, National Bureau of Standards, 1982.
102. L.B. Evans, "Advances in Process Flowsheeting Systems," Foundations of Computer-Aided Chemical Process Design, Engineering Foundation (1980).
103. R.W.H. Sargent, "A Review of Methods for Solving Nonlinear Algebraic Equations," Foundations of Computer-Aided Chemical Process Design, Engineering Foundation (1980).
104. J.D. Seader, W.D. Seider and A.C. Pauls, "FLOWTRAN Simulation-- An Introduction," Monsanto Company, 1974.
105. L.B. Evans, et al., "ASPEN: An Advanced System for Process Engineering," Computers and Chemical Engineering, 3, 319 (1979).
106. ASPEN User Manual, Massachusetts Institute of Technology, 1982.
107. C.F. Gerald, Applied Numerical Analysis, second edition, Addison-Wesley Publishing Company (1980).
108. N.I. Grigor'eva and V.E. Nakoryakov, "Exact Solution of Combined Heat and Mass Transfer Problem During Film Absorption," Journal of Engineering Physics, 33, 1349 (1977).
109. R.B. Bird, W.E. Stewart and E.N. Lightfoot, Transport Phenomena, John Wiley and Sons, Inc. (1960).
110. J.G. Collier, Convective Boiling and Condensation, second edition, McGraw-Hill Book Company (1981).
111. R. James, "Metering of Steam-Water Two-Phase Flow by Sharp-Edged Orifices," Proceedings, Institution of Mechanical Engineers, 180, 549 (1965), referenced in Collier (109).
112. T.A. Ryan, B.L. Joiner and B.F. Ryan, MINITAB Student Handbook, Duxbury Press (1976).

113. D.F. Rudd and C.C. Watson, Strategies of Process Engineering, John Wiley and Sons (1968).
114. American Society of Heating, Refrigerating and Air Conditioning Engineers, Handbook of Fundamentals (1981).
115. J.L. Threlkeld, Thermal Environmental Engineering, Prentice Hall (1962).
116. G.E.P. Box, W.G. Hunter and J.S. Hunter, Statistics for Experimenters, John Wiley and Sons (1978).
117. G.J. Van Wylen and R.E. Sonntag, Fundamentals of Classical Thermodynamics, second edition, John Wiley and Sons (1976).
118. J.M. Smith and H.C. Van Ness, Introduction to Chemical Engineering Thermodynamics, third edition, McGraw-Hill Book Company (1975).
119. S.C.G. Schultz, "Equations of State for the System Ammonia-Water for Use With Computers," Proceedings, Congress of the International Institute of Refrigeration, Washington, DC, 1971.
120. R.C. Reid, J.M. Prausnitz and T.K. Sherwood, Properties of Gases and Liquids, third edition, McGraw-Hill Book Company, 1977.